Investigating the origins of polyploidy in Barrett's oesophagus and oesophageal adenocarcinoma

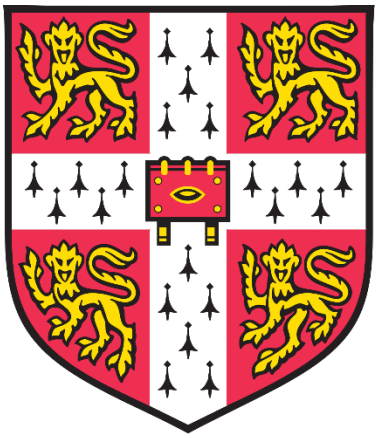

Stacey Jane Scott

303260714

University of Cambridge

Newnham College

September 2019

This dissertation is submitted for the degree of Doctor of Philosophy

Abstracts:

Investigating the origin(s) of polyploidy in Barrett's oesophagus and Oesophageal adenocarcinoma.

Oesophageal adenocarcinoma (OEAC) is preceded by the condition Barrett's oesophagus (BE), in which the stratified squamous mucosa of the oesophagus becomes damaged from exposure to stomach acid, resulting in a transformation into a simple columnar mucosa typical of that of the small intestine. A key step in the progression from BE to OEAC is the acquisition of polyploidy after p53 loss via an unknown genome doubling event. This increase in genomic material is likely to contribute to OEAC evolution and diversification. To identify the origin of polyploidy in OEAC, I analysed mitosis in both BE and OEAC cell lines by time-lapse imaging and immunofluorescence (IF) and found that about 12% of dividing OEAC cells present with an abnormal mitotic phenotype, the most prevalent being a defect in chromosome congression and alignment. Whole genome and RNA sequence analyses of OEAC cell lines indicated numerous copy number changes and gene expression alterations of important inner and outer kinetochore components including genes within the CCAN and KMN networks. These findings were confirmed by the analysis and comparison of the expression and localisation of KMN proteins in OEAC vs. BE cells by IF and quantitative mass spectrometry analysis of immunoprecipitations of KMN components. Finally, I also observed similar chromosome congression defects in OEAC organoids. In sum, my results suggest that subtle changes in the levels of kinetochore proteins are the cause of chromosome congression defects in OEAC cells, which in turn trigger mitotic slippage and polyploidy in OEAC cells.

Identification of factors involved in crosstalk between actin filaments and microtubules.

The eukaryotic cytoskeleton is vital in the control of a number of cellular processes including cell division, maintaining cell shape, establishment of cell polarity, cell motility and cell function. The dynamicity of the cytoskeleton is mediated by actin filaments and microtubules; whilst these structures control different aspects of the cellular behaviour, a cross talk must exist between the two in order to orchestrate a response to stimuli. It is already known that an actin-microtubule cross

talk exists however there is little understanding about the mechanisms and signalling pathways that control this process. Experimental evidence indicates that the addition of actin depolymerising drug Latrunculin-A to cultured *Drosophila* cells results in a rapid change to cell shape, characterised by the formation of long microtubule filled protrusions. RNAi screening of *Drosophila* kinesins revealed a potential role for kinesin heavy chain (KHC), Klp10A and Klp61F in bundle formation; knockdown of these kinesins resulting in the formation of much shorter microtubule bundles compared to controls. As work was being carried out on this screen a study by Jolly *et al.,* (2016) was published outlining a similar line of investigation, in which they had also identified KHC as being involved in microtubule bundle formation following actin depolymerisation. This raised concern regarding the progression of the project and hence the decision was made to cease any further investigation.

Preface:

This thesis is the result of my own work and includes nothing which is the outcome of work done in collaboration except as declared in the Preface and specified in the text. It is not substantially the same as any that I have submitted, or, is being concurrently submitted for a degree or diploma or other qualification at the University of Cambridge or any other University or similar institution except as declared in the Preface and specified in the text. I further state that no substantial part of my dissertation has already been submitted, or, is being concurrently submitted for any such degree, diploma or other qualification at the University of Cambridge or any other University or similar institution except as declared in the Preface and specified in the text. It does not exceed the prescribed word limit for the relevant Degree Committee. For more information on the word limits for the respective Degree Committee.

Acknowledgments:

Foremost I would like to thank my PhD supervisor Dr Pier Paolo D'Avino for giving me the opportunity to carry out my research and for his incredible support throughout. Thanks also needs to be given to Dr Luisa Capalbo for helping and advising me, and for answering all my questions - of which there were many! To the D'Avino lab members past and present, and to the friends I've made along the way I thank you for making my time in Cambridge an enjoyable one.

In addition I thank Professor David Glover and his lab members for their valuable input, advice and feedback on this project, and to Dr Catherine Lindon for her input into the project and for being a great PhD mentor. I also thank my collaborators Professor Rebecca Fitzgerald, Dr Xiaodun Li and the rest of the Fitzgerald lab.

Next, I thank the Medical Research Council and the Department of Pathology for funding this project.

Now for some more personal thanks. I first need to thank my family: Mum, Dad, Emma, Simon and Thomas. I don't think I'd have gotten this far if it wasn't for your support. I appreciate it more than you'll ever know, and I hope I've done you proud. To Nan and Grandad, thank you for your help financially when things were tight, and for always believing I could do it. Yes Nan, I am going to be a Dr, and yes you will get your picture soon.

To my best friends Charmaine and Becky; Thank you for always being there when I needed you, for when I've needed a laugh (or a cry!) and for the years of unwavering friendship. We may not have seen a lot of each other over the past four years, but I promise you there is no getting rid of me now!

Finally to Ian, I would not have gotten through this if it wasn't for you. You are the calm to my storm, and I cannot thank you enough for everything you have done, and continue to do for me, you're the best.

Table of contents:

1. Introduction 16

1.1. Mitosis and the cell cycle 16

1.2. Microtubule and the mitotic spindle 17

1.3. Chromosome segregation and the centromere 20

1.3.1. Eukaryotic chromosomes 20

1.3.2. Chromosome segregation 20

1.3.3. The centromere 21

1.3.4. CENP-A 21

1.4. The kinetochore 22

1.5. The constitutive centromere associated network 25

1.5.1. CENP-B 25

1.5.2. CENP-C 25

1.5.3. CENP- H/I/K and CENP-L/M/N 26

1.5.4. CENP-O/P/Q/R/U 27

1.5.5. CENP-T/W/S/X 27

1.6. The KMN network 28

1.6.1.Knl1 29

1.6.2. The Mis12 complex 29

1.6.3. The Ndc80 complex 31

1.7. The Ska complex 33

1.8. CENP-E 34

1.9. Dynein and the Rod-ZW10-Zwilch (RZZ complex) 34

1.10. The role of cyclin B/Cdk1 in mitotic entry 35

1.11. Monitoring mitosis: the spindle assembly checkpoint and error correction 36

1.11.1. The anaphase promoting complex 36

1.11.2. The spindle assembly checkpoint 39

1.11.3. Kinetochore microtubule attachment error correction 40

1.12. P53 and cancer 42

1.13. Chromosomal instability and aneuploidy 43

1.13.1. Chromosomal instability 44

1.13.2. Aneuploidy and polyploidy 45

1.14. BE and its progression into OEAC 48

1.15. Project aims 54

2. Materials and methods 55

2.1. Tissue culture 55

2.2. Synchronising cells 55

2.2.1. Single thymidine-nocodazole block 55

2.2.2. Palbocyclib nocodazole block 56

2.3. Immunoprecipitation 56

2.3.1. Bead preparation 56

2.3.2. Pull down 56

2.4. Sample preparation for gel electrophoresis 57

2.5. Coomassie staining 57

2.6. Silver staining 57

2.7. Western blot 57

2.8. Mass spectrometry 58

2.9. Fixing cells 58

2.9.1. Pre-extraction 58

2.9.2. Formaldehyde fixation 58

2.9.3. Methanol fixation 58

2.10. Immunostaining 58

2.11. Imaging fixed cells 59

2.12. Quantification of mitosis 59

2.13. Imaging organoids 59

2.14. Time-lapse 59

2.15. Table of primary antibodies used in my experiments 60

2.16. Table of secondary antibodies used in my experiments 61

Results 61

3. Characterisation of cell division defects in BE and OEAC 61

3.1. OEAC cells present with abnormal mitotic phenotypes 62

3.2. OEAC cells do not show high levels of multinucleation 67

3.3 Cells with scattered chromosomes have bipolar mitotic spindles 68

3.4. OEAC cells have a functional mitotic checkpoint 69

3.5. OEAC cells experience mitotic slippage 71

3.6. OEAC organoids have scattered chromosomes 76

4. Kinetochore gene changes and protein expression in BE and OEAC cells 80

4.1. Whole genome sequencing (WGS) of BE and OEAC cell lines and primary tumours shows numerous copy number changes in important kinetochore genes 80

4.1.1. Sequencing of primary tumours 80

4.1.2. Whole genome sequencing of cell lines 91

4.2. Total protein expression of important kinetochore complexes is affected in OEAC cells in accordance with WGS data 93

4.3. OEAC cells showed varied levels of KMN network proteins at their kinetochores suggesting an imbalance within the complex 95

4.4. OEAC cells with scattered chromosomes have a higher percentage of lateral kinetochore microtubule attachments 108

5. Preliminary analysis of protein-protein interaction networks in BE and OEAC 112

5.1. Optimisation of synchronisation methods in BE and OEAC cells 112

5.1.1. CPA 112

5.1.2. FLO and JH-Eso-Ad1 116

5.1.3. RPE1 116

5.2. Investigating the kinetochore interactome in BE and OEAC cells 117

5.2.1 Rapid immunoprecipitation coupled with mass spectrometry 117

5.2.2 Immunoprecipitating Ndc80 for mass spectrometry 120

5.2.3. Mass spectrometry data shows variability between KMN subcomplexes in BE and OEAC cells 122

6. Discussion 126

6.1: BE and OEAC cells present mitotic defects and mitotic slippage 126

6.2: Imbalanced kinetochores drive chromosome mis-segregation via aberrant kinetochore microtubule interactions in OEAC cells 129

6.3: Defective kinetochore microtubule attachments trigger SAC induced mitotic arrest and mitotic slippage in OEAC cells 134

6.4: Scattered chromosomes may be the result of both defective congression and cohesion fatigue? 136

6.5: Conclusions and further perspectives 136

7: Identification of factors involved in cross talk between actin filaments and microtubules 141

7.1: Introduction 141

7.2: Materials and methods 146

7.2.1: *Drosophila* cell culture 146

7.2.2: Testing Lat-A concentrations 146

7.2.3: Fixing cells 146

7.2.4: Immunostaining cells 146

7.2.5: Antibodies 146

7.2.6: Imaging cells 147

7.2.7: Preparation of genomic DNA from DMEL2 cells 147

7.2.8: PCR 147

7.2.9: Production of dsRNA 148

7.2.10: RNAi screen 148

7.2.11: Generating a tubulin GFP cell line 148

7.2.12: Primer design for cloning 148

7.2.13: Insert preparation 149

7.2.14: Vector preparation 149

7.2.15: Ligation 149

7.2.16: Transformation 149

7.3: Results 150

7.3.1: Lower concentrations of Latrunculin A produced a stronger phenotype 150

7.3.2: Generation of a tubulin GFP stable cell line will allow for live imaging of cells treated with Lat-A 152

7.3.3: DMEL2 cells do not require transfection reagents for successful RNAi 153

7.3.4: RNAi of kinesins causes variable projection lengths 154

7.3.5: RNAi of KHC prevents MT sliding and hence the formation of long MT bundles 156

7.4: Discussion 158

7.5: Conclusions 161

8. References 162

List of figures:

1.1: The stages of mitosis and their respective microtubule populations 17

1.2: Structure of the kinetochore 23

1.3: Principles of the spindle assembly checkpoint 38

1.4: Pathways to polyploidy 48

1.5: BE and its progression into OEAC 49

1.6: OEAC displays multiple copy number changes compared to BE 52

1.7: OEAC shows distinct development pathways 54

3.1: Approximately 10% of OEAC cells present with mitotic defects 64

3.2: Defective mitosis in BE and OEAC observed using IF 66

3.3: Less than 1.5% of BE and OEAC cells have multiple nuclei 67

3.4: Up to 15% of OEAC cells have extra centrosomes 70

3.5: BE and OEAC cells are able to sustain a mitotic arrest 71

3.6: CPA and FLO cells show defects in mitosis 73

3.7: JH-Eso-Ad1 cells exhibit mitotic slippage 75

3.8: Scattered chromosomes are present in OEAC organoids 79

4.1: Copy number information for the KMN network in BE and OEAC cells 83

4.2: Copy number information for the CCAN in BE and OEAC cells 85

4.3: Copy number information for the SAC in BE and OEAC cells 87

4.4: Copy number information for the CPC in BE and OEAC cells 88

4.5: Copy number information for the SKA complex in BE and OEAC cells 89

4.6: Copy number information for the protein phosphatases in BE and OEAC cells 91

4.7: Analysis of expression of kinetochore proteins in BE and OEAC cells 94

4.8: Levels of Ndc80 are increased at kinetochores in FLO cells 97

4.9: Levels of Spc24 are not significantly different between BE and OEAC kinetochores 99

4.10: Levels of Dsn1 are significantly lower in dysplastic BE and OEAC kinetochores 100

4.11: Levels of CENP-A is significantly lower at dysplastic BE and OEAC kinetochores 102

4.12: Levels of Aurora B are not significantly different between BE and OEAC kinetochores 103

4.13: Levels of BubR1 are significantly lower in JH-Eso-Ad1 cells 105

4.14: Comparison of kinetochore proteins in each cell line 107

4.15: Kinetochore localisation of Knl1 in BE and OEAC cells 108

4.16: Kinetochore localisation of CENP-C in BE and OEAC cells 109

4.17: Investigating microtubule attachments in BE and OEAC cells 111

5.1: Optimisation of synchronisation methods in BE and OEAC cells 115

5.2: Rapid immunoprecipitation mass spectrometry (RIME) of CENP-C 119

5.3: Immunoprecipitation of Ndc80 in BE and OEAC cells 121

6.1. Flow diagram summarising the findings of this thesis 138

7.1: Investigating the effect of Lat-A on DMEL2 cells 144

7.2: Lat-A is effective at concentrations as low as 0.5 µm 151

7.3: DMEL2 tubulin-GFP cell line 152

7.4: Plasmid map of LifeAct cloned into a pAc5 destination vector 153

7.5: DMEL2 cells do not require transfection reagent for successful dsRNAi knockdown 154

7.6: MT bundles are shorter in KHC knockdown cells 157

7.7: MT bundles are long when DHC is knocked down 158

List of tables:

3.1: Table of cell lines used in my experiments 62

3.2: Table of organoids used in my experiments 77

4.1: Descriptions of copy number status 81

5.1: RIME data for centromere/kinetochore proteins in HeLa cells with and without crosslinking 120

5.2: MS results for the centromere/kinetochore proteins in CPA cells 122

5.3: MS results for the centromere/kinetochore proteins in RPE1 cells 123

5.4: MS results for the centromere/kinetochore proteins in FLO cells 125

5.5: MS results for the centromere/kinetochore proteins in JH-Eso-Ad1 cells 126

7.1: Cell shape change presented by Lat-A treated cells following RNAi knockdown of kinesins 155

List of abbreviations:

APC: Adenomatous polyposis coli

APC/C: Anaphase promoting complex/cyclosome

BE: Barrett's oesophagus

CCAN: Constitutive centromere associated network

CIN: Chromosomal instability

CPC: Chromosomal passenger complex

CN: Copy number

γTuRC: gamma tubulin ring complex

IP: Immunoprecipitation

KMN: Knl1/Mis12/Ndc80 complex network

LC-MS-MS: Liquid chromatography tandem mass spectrometry

LOH: Loss of heterozygosity

MCC: Mitotic checkpoint complex

MI: Mitotic index

MS: Mass spectrometry

MT: Microtubule

NEB: Nuclear envelope breakdown

NGD: Non genome doubled

OEAC: Oesophageal adenocarcinoma

RIME: Rapid immunoprecipitation mass spectrometry of endogenous proteins

RNAi: RNA interference

RZZ: Rod-Zw10-Zwilch complex

SAC: Spindle assembly checkpoint

SNV: Single nucleotide variant

siRNA: Short interfering RNA

WGD: Whole genome doubling

WGS: Whole genome sequencing

1. Introduction

1.1. Mitosis and the cell cycle

The eukaryotic cell cycle is comprised of four stages; G1, S, G2 and M phase (mitosis). G1, also known as the pre-replicative phase, is a gap phase that proceeds DNA synthesis (S phase). In the second gap phase (G2) any damaged DNA is repaired prior to entry into mitosis. The aim of mitosis is to accurately separate the genome to ensure that the two resulting daughter cells inherit an equal and identical compliment of chromosomes (Yanagida 2014).

As reviewed by Scholey and colleagues (2003) mitosis begins at prophase in which the centrosomes duplicate and move towards the poles of the cell to form the bipolar spindle. In this stage the chromatin is condensed into chromosomes, but the nuclear envelope is still intact. Prometaphase is then signified by nuclear envelope breakdown (NEB) which allows the microtubules to capture chromosomes for congression at the metaphase plate. In metaphase the bipolar spindle has fully formed, and the sister chromatids are aligned at the spindle equator facing opposing spindle poles. Upon anaphase onset, cohesion between the sisters is lost allowing them to be moved towards the poles (anaphase A) as the spindle elongates (anaphase B). During anaphase the spindle signals to the cell cortex to define the position and orientation of the contractile ring. Formation of the contractile ring drives furrow ingression as the nuclear envelope reforms around the newly segregated, decondensing chromatids. In telophase the central spindle is formed to drive cytokinesis which is completed once the cleavage furrow is sealed, resulting in the formation of two genetically identical daughter cells (Scholey, Brust-Mascher and Mogilner 2003) (figure 1.1).

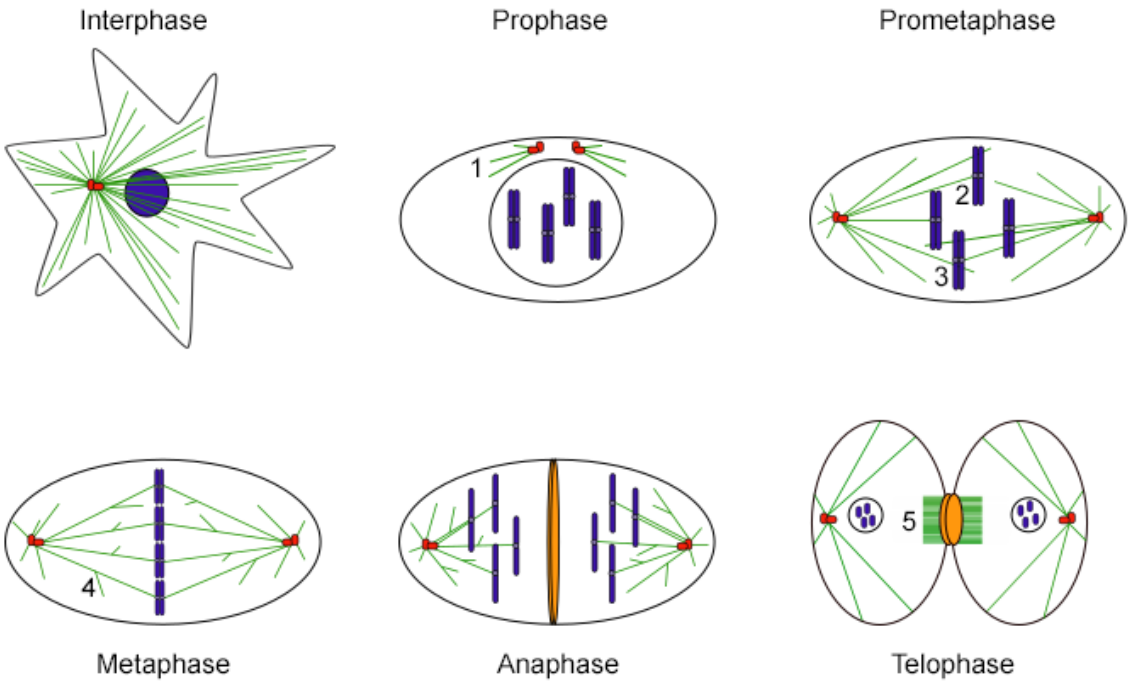

Figure 1.1: The stages of mitosis and their respective microtubule populations. In interphase cells have long microtubule arrays. In prophase astral microtubules form (1). In prometaphase the chromosomes are captured by kinetochore microtubules (2) connecting them to the spindle. The bulk of the spindle is made up of interpolar microtubules (3). In metaphase microtubules are also nucleated by Augmin (4). In anaphase the contractile ring is positioned then, in telophase, the central spindle (5) is formed to drive cytokinesis

1.2. Microtubules and the mitotic spindle

In mitosis the cell must completely reorganise its microtubule cytoskeleton to build the mitotic spindle required to pull apart the sister chromatids, following the severing of the cohesin complexes (Cheeseman 2014, Hirano *et al.,* 2015; Reber and Hyman 2015; Westhorpe and Straight 2014). Central in ensuring accurate chromosome segregation is the mitotic spindle. The spindle is comprised of arrays of microtubules composed of α and β tubulin dimers that form polar filaments; α facing the minus end and β the plus end to establish an intrinsic polarity (Mitchison 1993). The organisation of the mitotic spindle and the dynamics of its microtubules change dramatically throughout the cell cycle in order to generate vastly different microtubule arrays. During interphase, the microtubules are very long, stable polymers whereas

in mitosis they switch, becoming much shorter and highly dynamic (Wiese and Zheng 2000). Within the spindle there are three subpopulations of microtubules: 1) kinetochore microtubules that terminate end on at the outer plate of the kinetochore to facilitate the connection between the spindle and the chromosomes, 2) interpolar microtubules that emerge from the opposing spindle poles to interact in an antiparallel fashion, stabilising the spindle and 3) astral microtubules that extend away from the centrosome into the cytoplasm to assist in the positioning and orientation of the spindle (reviewed in Wittmann, Hyman and Desai 2001) (figure 1.1).

In animal cells the centrosome is considered to be the dominant microtubule organising centre (MTOC) from which microtubules are nucleated (Sanchez and Feldman 2017) via the template model. In this model γ tubulin assembles a ring (γTuRC), forming a template upon which a thirteen protofilament microtubule can be generated (Moritz *et al.,* 1995**;** Zheng *et al.,* 1995; Pereira and Scheibel 1997). Microtubules nucleated by the template model will then attach to a kinetochore via the search and capture mechanism (Mitchison and Kirschner 1984) which occurs as growing ends of microtubules emanate away from the spindle pole towards the chromosomes (Rieder and Alexander 1990). Microtubule nucleation however does not always involve the centrosome. Work carried out in plant cells and *Xenopus laevis* egg extracts showed that microtubules can also be nucleated from chromatin (Heald *et al*. 1996) in which a RanGTP gradient along with the chromosomal passenger complex (CPC) act to regulate a number of spindle assembly factors such as microtubule stabilisers and destabilisers (Carazo-Sales *et al.,* 1999, 2001; Kalab *et al.,* 1999; Ohba *et al.,* 1999; Nachury *et al.,* 2001). Microtubules may also be nucleated by the eight subunit Augmin complex that recruits the γTuRC to the sides of pre-existing microtubules to induce the nucleation of new ones (Goshima *et al.,* 2008**;** Lawo *et al.,* 2009) thus increasing the overall number of spindle microtubules (Goshima *et al.,* 2008).

There are two ways in which a kinetochore can attach to a microtubule; laterally or end on. Lateral attachments occur when a kinetochore binds to the side of a microtubule allowing for initial capture and for kinetochore movement via microtubule motors. Sister kinetochores very rarely attach to the spindle simultaneously; the sister closest to, and facing towards a pole, will attach first

following NEB. Once the sister has attached to the chromosome, it will initiate minus end directed motion towards the pole. As the mono-oriented chromosome is moving towards the pole the attached kinetochore will pick up more microtubule plus ends, forming a kinetochore fibre (K-fibre) (Rieder and Salmon 1998). This attached sister kinetochore will not however acquire its full complement of K-fibres until the chromosome moves towards the spindle equator in metaphase (McEwan *et al.,* 1997). Once the second sister kinetochore has attached to a microtubule from the opposite spindle pole, hence initiating its K-fibre formation, the chromosome will bi-orient and begin to congress to the metaphase plate (Rieder and Salmon 1998).

In the early stages of spindle assembly numerous kinetochore-microtubule attachments can form. Merotelic kinetochore attachments occur when a single kinetochore is attached to microtubules emanating from both spindle poles (Gregan *et al.,* 2011). This type of attachment is frequently observed in the early stages of mitosis and will typically be corrected (Cimini *et al*., 2003; Cimini, Cameron and Salmon 2004), however if merotelic attachments are not corrected they can persist into anaphase, causing chromatids to lag on the mitotic spindle, hindering accurate chromosome segregation. Another incorrect kinetochore-microtubule attachment is the syntellic attachment in which both sister kinetochores will interact with microtubules originating at the same spindle pole (Gregan *et al.,* 2011). If not corrected this type of attachment can result in incorrect numbers of chromosomes being segregated in anaphase, resulting in daughter cells with aneuploid numbers of chromosomes. Kinetochores can also form monotelic attachments, in which one sister kinetochore becomes attached to microtubules from one of the poles whilst the other remains unattached. This is an obligatory step in chromosome alignment and typically happens only briefly (Rieder and Salmon 1998) however if a cell was to progress into anaphase with this type of attachment then both sisters would be segregated to the same pole (Cimini 2008). The spindle assembly checkpoint (SAC) is able to detect monotelic orientations, as the unattached kinetochore will maintain SAC signalling (Rieder *et al.,* 1994, Rieder *et al.,* 1995), as discussed in more detail later in this chapter.

1.3. Chromosome segregation and the centromere

1.3.1. Eukaryotic chromosomes

Eukaryotic genomic DNA is packaged into chromatin and stored in the nucleus. At the onset of mitosis, the nuclear envelope breaks down and chromatin is progressively converted into metaphase chromosomes. On each chromosome a pair of sister kinetochores assemble at its centromeric region, and their bioriented attachment to the mitotic spindle acts as a prerequisite for equal segregation of sister chromatids. The link between the sister chromatids is dissolved in anaphase, allowing them to be pulled to opposing spindle poles. At the end of mitosis the nuclear envelope reassembles around the segregated chromosomes, resulting in two genetically identical daughter cells (reviewed in Hirano 2015).

1.3.2. Chromosome segregation

A single mis-segregation event in a multicellular organism has the potential to lead to lethality, developmental disorders or can contribute to cancer progression (Holland and Cleveland 2009; Gordon, Resio and Pellman 2012). Accurate chromosome segregation requires a number of different factors; the ability to recognise and detect DNA, a physical connection between DNA and other cellular structures mediating their distribution, and force generating mechanisms to drive the spatial movement of DNA to daughter cells (Cheeseman 2014). Duplicated chromatid arms are held together by cohesive forces immediately after they are synthesised until they are ready to be separated in anaphase, thus preventing cells from receiving too few or too many copies of chromosomes (Hirano *et al.,* 2015). Key players in orchestrating accurate chromosome segregation are; cohesin, condensin and the securin-separase complex alongside numerous other kinetochore microtubule destabilisers. In somatic vertebrate cells the cohesin core complex consists of two structural maintenance of chromosome proteins (Smc) Smc1 and Smc3, the kleisin protein Scc1 and either stromal antigen (SA) subunit SA1 or SA2 (Peters, Tedeschi and Schmitz 2008).

As reviewed by Hirano (2015) cohesin starts to associate with chromatin during G1 and establishes sister chromatid cohesion during S phase. During S phase, condensin II will begin to associate with the duplicated chromosome in order to initiate sister chromatid resolution by counteracting cohesin. By prophase the

majority of the cohesin complexes have been released from the chromosome arms and more condensin II is loaded in order to promote early stage chromosome condensation inside the nucleus. When NEB occurs, condensin I in the cytoplasm is granted access to the chromosomes and will further facilitate their condensation. Then, at the onset of anaphase the protease separase cleaves the cohesin subunit scc1/kleisin to promote the segregation of the sisters. Separase is negatively regulated by the protein securin which is a target of the anaphase promoting complex/cyclosome (APC/C). Securin is initially present in the cytoplasm where it binds to separase; the securin-separase complex is maintained when securin is phosphorylated by Cdk1 thus inhibiting its ubiquitination. When held in the securin-separase complex separase is not functional preventing sister chromatid separation (Morgan 2007). To initiate anaphase, securin is dephosphorylated by Cdc14 allowing it to be recognised by the APC/C (discussed later in this chapter) thus targeting it for degradation, resulting in free separase available to target cohesin to initiate chromosome segregation (Morgan 2007; Holt, Krutchinsky and Morgan 2008).

1.3.3. The centromere

The centromere is the point of recognition for the cellular segregation machinery. The centromere will often occupy a single, specific region of the chromosome. Most organisms will present with monocentric centromeres however in rare circumstances a centromere may be built ectopically, resulting in the formation of a neocentromere. Formation of additional centromeres can also occur via chromosomal translocation; in such instances only one of the centromeres will be functional to ensure the assembly of only one kinetochore per chromosome, thus preventing the occurrence of segregation defects (reviewed in Przewloka and Glover 2009). Both prior to and during the early stages of mitosis the centromere recruits kinetochore proteins to provide an attachment site for the spindle microtubules (Westhorpe and Straight, 2014). In the absence of centromeres kinetochore assembly is prevented and so the chromosomes will fail to segregate.

1.3.4. CENP-A

Centromere position is epigenetically defined by the histone related protein CENP-A (Regnier *et al.,* 2005; Liu *et al.,* 2006). For CENP-A to act as a marker it must be structurally distinct from the other chromosomal histones. Deposition of

CENP-A in human somatic cells occurs at different stages of the cell cycle in a tissue and/or organism dependant manner, this generally occurs in two steps; firstly in S phase nucleosomes are removed from the template DNA and loaded on to replicated DNA, during which time CENP-A and all other histones are moved onto the new chromatid. At this stage no new CENP-A is added, so the amount of CENP-A per chromatid following DNA replication is halved (Allshire and Karpen 2008; Ekwall 2007; Mellone 2009). Secondly, in G1 newly synthesised CENP-A is deposited, returning the levels of CENP-A on the chromatids to normal levels (Jansen *et al.,* 2007; Schuh, Lehner and Heidmann 2007).

Centromere assembly of CENP-A requires Mis18 complex and Holliday junction recognition protein (HJURP). HJURP is a CENP-A specific chaperone that binds to soluble CENP-A/histone H4 via the CENP-A-specific sequence within the histone fold domain (Black *et al.,* 2004; Bassett *et al.,* 2012; Yu et al 2015). The interaction between CENP-A and HJURP is required to sustain the long-term function of the centromere (Fachinetti *et al.,* 2013). Mutations or disruptions in CENP-A cause complete failure in centromere and kinetochore formation (Earnshaw and Rothfield 1985; Earnshaw *et al.,* 1986; Palmer *et al.,* 1987; Palmer *et al.,* 1991; Sullivan, Hechenberger and Masri 1994)**.** In a study by Regnier and colleagues (2005) they showed that when CENP-A was depleted in chicken DT40 cells, constitutive centromere associated network (CCAN) components CENP-H, CENP-I and CENP-T, the outer kinetochore Ndc80 complex constituents Nuf2 and Ndc80, the checkpoint protein Mad2 and the kinesin CENP-E were all mis-localised. Following CENP-A depletion, cells typically showed chromosome congression defects and a transient prometaphase delay. A number of these prometaphases presented with one of two phenotypes; cells would either congress the majority of their chromosomes at the spindle equator leaving just a few non-aligned chromosomes, or cells would display the more dramatic phenotype in which chromosomes would randomly disperse over the entire mitotic spindle (Regnier *et al.,* 2005).

1.4. The kinetochore

A group of proteins must assemble on the centromere to facilitate connections to the microtubule; in eukaryotic cells this is the kinetochore (Cheeseman 2014)

(figure 1.2). The kinetochore must be able to carry out three key functions; 1) provide a site of attachment between the chromosomes and the mitotic spindle, 2) coordinate microtubule dynamics allowing the movement of chromosomes along the spindle and 3) generate a “wait” signal preventing anaphase onset until all chromosomes have congressed correctly; this signal is monitored by the SAC which prevents anaphase until correct congression has been achieved. (Jallepalli and Lengauer 2001; Musacchio and Hardwick 2002).

In mitosis the kinetochore is visible by electron microscopy as a trilaminar structure, with pairs of kinetochores sitting back-to-back with one another upon the chromatin (Biggins and Walczak 2003; Cleveland, Mao and Sullivan 2003). This structure is only visible in mitosis, as in interphase the kinetochore appears as a shapeless ball like structure deemed the “pre-kinetochore” that lies next to the heterochromatin (Rieder 1982).

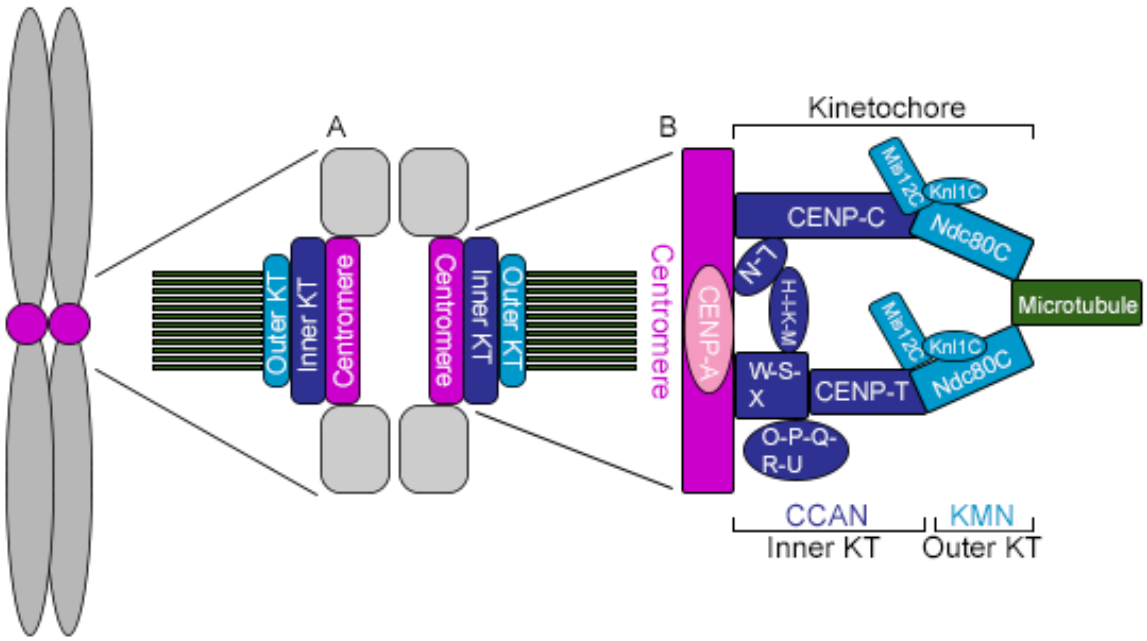

Figure 1.2: Structure of the kinetochore. A) Schematic of a bi-oriented chromosome. Basic kinetochore structure is composed of the centromere, the inner kinetochore and the outer kinetochore (adapted from Przewloka and Glover 2009). B) The major structural components of the kinetochore include the CCAN and the KMN network. The CCAN and the CENP-A nucleosomes make up the chromatin and the inner kinetochore, and targets the KMN network via the independent CENP-C and CENP-T pathways. Microtubule contact is made via direct interaction with the Ndc80 complex of the KMN network.

The kinetochore is a macromolecular structure that requires the coordinated functions of over 100 different protein components (Cheeseman and Desai 2008), each of which are present in multiple copies per centromere. For chromosome movement to occur, the kinetochores must use microtubule interactions to generate forces. In prophase and prometaphase kinetochores are captured by microtubules that then move the chromosome to the centre of the cell ready for segregation. At metaphase, the paired sister chromatids are attached to microtubules that emanate from opposing spindle poles, pushing and pulling forces then act to drive oscillatory chromosome movements and signal the presence of correct attachments. Finally, during anaphase A the kinetochores are pulled by the microtubules towards the spindle poles to segregate the chromosomes (reviewed in Cheeseman 2014). This only occurs if the SAC is satisfied, as kinetochores are the site of mitotic checkpoint activation that prevents anaphase onset if any kinetochores remain unattached (Westhorpe, Fuller and Straight 2015).

Based upon the spatial localisation of its components, the kinetochore can be broken down into two main functional categories that contain two key groups of structural proteins: the inner and the outer kinetochore. The inner kinetochore contains a subset of proteins that binds to chromatin called the constitutive centromere associated network (CCAN), which acts as a bridge between the DNA and the kinetochore, and provides a platform upon which the rest of the kinetochore can assemble. The outer kinetochore is comprised primarily of the large multi-subunit Knl1/Mis12/Ndc80 complex network (KMN network) (Petrovic *et al.,* 2010) which is recruited by the CCAN at the inner kinetochore, to form strong interactions with the mitotic spindle (Cheeseman *et al.,* 2004; Nishino *et al.,* 2013).

1.5. The constitutive centromere associated network (CCAN)

The CCAN (figure 1.2) is composed of sixteen proteins that localise to the centromere for the entire cell cycle (reviewed in Cheeseman and Desai 2008**;** Perpelescu and Fukagawa 2011; Takeuchi and Fukagawa 2012). With interfaces that bind to both centromeric chromatin and the spindle microtubule-binding complex at the outer kinetochore the CCAN functions as the foundation of kinetochore formation (Hara and Fukagawa 2017). With the exception of CENP-B and CENP-O all constituents of the CCAN are essential for chromosome congression and segregation (reviewed in Przewloka and Glover 2009).

1.5.1. CENP-B

The human CENP-B protein is an 80 kDa polypeptide that localises throughout the heterochromatin and the central region of the centromere (Earnshaw and Rothfield 1985; Earnshaw *et al.,* 1987; Cooke, Bernat and Earnshaw 1990; Sullivan and Glass 1991; Pluta *et al.,* 1992). CENP-B is recruited via direct binding to the “CENP-B box” which is a 17 base pair DNA sequence present on human centromeres (Masumoto *et al.,* 1989). Once the centromere has formed, CENP-B appears to be dispensable for centromere function (Westhorpe, Fuller and Straight 2015), and it has been highly debated whether CENP-B is actually essential for mitosis in vertebrate cells. A number of studies (Voullaire *et al.,* 1993; Ohashi *et al.,* 1994; Choo 1997; Depinet *et al.,* 1997; du Sart et al, 1997) have observed stable human neocentromeric markers on chromosomes in cells that are capable of normal mitotic divisions in the absence of CENP-B binding, thus suggesting that, unlike its other CCAN constituents, centromeric CENP-B localisation is not essential for chromosome segregation (Hudson *et al.,* 1998).

1.5.2. CENP-C

CENP-C is a constitutive centromere protein with the capacity to bind to DNA (Saitoh *et al.,* 1992; Yang *et al.,* 1996). CENP-C was the first protein to be confirmed as part of the inner kinetochore through immunoelectron microscopy (Saitoh *et al.,* 1992) and to be shown by antibody microinjection experiments to be required for outer kinetochore assembly (Tomkiel *et al.,* 1994). Therefore, due to its function in recruiting numerous outer kinetochore components, CENP-C has been described as the blue print for kinetochore assembly (Klare *et al.,* 2015).

The CENP-C protein has four domains: The N-terminal region is necessary for the recruitment of the outer kinetochore Mis12 complex (Milks, Moree and Straight 2009; Screpanti *et al.,* 2011), the central region and the “CENP-C motif” are required to target the protein to the centromere (Carroll, Milks and Straight 2010; Song *et al.,* 2002; Milks, Moree and Straight 2009; Tanaka *et al.,* 2009; Heeger *et al.,* 2005), and finally, the C-terminal domain is required for CENP-C dimerization (Cohen *et al.,* 2008). Work in *Drosophila melanogaster* (Przewloka *et al.,* 2011) showed that by ectopically targeting CENP-C away from the centromere, in this case to the centrosome, the KNL1, the Mis12 and the NDC80 complexes of the outer kinetochore were all recruited to this ectopic site. This KMN mis-localisation resulted in cells with chromosome alignment defects typical of defective kinetochores. This would therefore suggest that CENP-C, and specifically its N-terminal region, is sufficient to recruit the KMN network and therefore acts as a primary link between the centromere and kinetochore during mitosis. CENP-C is necessary for chromosome alignment (reviewed in Hara and Fukagawa *et al.,* 2017) and for recruitment of the CENP-H, CENP-I, CENP-K and CENP-M complex, which in turn is required for the centromeric localisation of CENP-T (Westhorpe and Straight, 2014). Therefore in human cells, loss of CENP-C results in the mis-localisation of multiple CCAN components from the centromere including those stated above (Carroll, Milks and Straight 2010; Gascoigne and Cheeseman 2011), thus inducing chromosome alignment defects. It has also been suggested that CENP-C may play a role in the recruitment of factors necessary for the assembly of new CENP-A upon the pre-existing CENP-A as demonstrated by Moree et al (2011). In this study, it was shown that, in the absence of CENP-C, the Mis18 complex subunit Mis18bp1 fails to target to centromeric chromatin, the levels of HJURP are reduced and the assembly of new CENP-A nucleosomes is inhibited (Moree *et al.,* 2011).

1.5.3. CENP-H/I/K and CENP-L/M/N

Purification experiments carried out in chickens (DT40) and in humans (HeLa) identified a set of eleven proteins that constitutively localised to centromeres as part of the CENP-H-I associated complex composed of: CENP-H, CENP-I, CENP-K-CENP-R and CENP-U (Okada *et al.,* 2006) which has been suggested to be required either directly or indirectly for chromosome congression, chromosome alignment, and timely metaphase to anaphase transition (Nishihashi *et al.,* 2002; Foltz *et al.,*

2006; Okada *et al.,* 2006; Izuta *et al.,* 2006; Basilico *et al.,* 2014) (reviewed in Hara and Fukagawa *et al.,* 2017).

CENP-H/I/K, CENP-M and CENP-C have also been implicated in maintaining centromeric chromatin, as their depletion from cells results in defective CENP-A assembly (Okada *et al.,* 2006; Erhardt *et al.,* 2008; Hori *et al.,* 2008; Moree *et al.,* 2011). Both CENP-N and CENP-C directly interact with the CENP-A nucleosome to promote centromere assembly (Carroll *et al.,* 2009). Depletion of CENP-N results in a loss of multiple other centromere components (Foltz *et al.,* 2006; McClelland *et al.,* 2007; Carroll *et al.,* 2009) suggesting that CENP-N is a key centromeric building block, however as the levels of CENP-N decrease in mitosis it may not be necessary for recruiting the kinetochore components (Westhorpe and Straight 2014).

1.5.4. CENP-O/P/Q/R/U

The functions of CENP-O/P/Q/R/U remain largely unclear, however in a study by Hori *et al.,* (2008) time lapse microscopy of DT40 cells with individual CENP-O class (CENP-O/P/Q/R/U) protein depletions revealed that these proteins are required for correct kinetochore function, as indicated by an increased mitotic duration. It has also been reported that CENP-U and CENP-Q associate to form an octamer which has the capability to bind to microtubules in vitro (Amaro *et al.,* 2010) via CENP-U binding to Ndc80 (Hua *et al.,* 2011). However these cells were still able to form kinetochore microtubule attachments, move the chromosomes and progress through the cell cycle suggesting these cells are still viable despite missing CCAN components, and that the CENP-O class of CCAN proteins may not be essential for accurate chromosome segregation. This study also reported that CENP-R appears to be downstream of the other CENP-O class proteins; as when CENP-R was depleted the others were still able to localise. The converse is true when CENP-O/P/Q/U is depleted suggesting that the localisation of these components is interdependent. This would also suggest a separate role for CENP-R independent of the CENP-O/P/Q/R/U complex (Hori *et al.,* 2008).

1.5.5. CENP-T/W/S/X

CENP-T is an extended molecule that spans both the inner and outer regions of the kinetochore (Suzuki *et al.,* 2011). Its C-terminal associates with CENP-W, CENP-S and CENP-X which assemble into dimers (CENP-T/CENP-W) and

tetramers (CENP-S/CENP-X) on the centromere (Hori *et al.,* 2008; Nishino *et al.,* 2012). CENP-T/CENP-W contain histone fold domains that are required for its association with DNA and to target the complex to kinetochores. (Hori *et al.,* 2008). The CENP-T/CENP-W complex also acts as a platform for kinetochore assembly via a long, flexible N-terminal region that binds to the outer kinetochore components, (Gascoigne and Cheeseman 2011; Suzuki *et al.,* 2011). This interaction is sufficient for the recruitment of the outer kinetochore Ndc80 complex via interactions with its Spc24/Spc25 subcomplex, in a manner dependent upon the phosphorylation of CENP-T by Cdk1 (Gascoigne and Cheeseman 2011)**.** CENP-T is capable of recruiting the outer kinetochore complexes independently from other CCAN components. Work from Gascoigne and Cheeseman (2011) and Hori *et al* (2013) demonstrated that ectopically targeting of CENP-T to non-centromeric regions of the chromosome led to kinetochore assembly.

The CENP-T/CENP-W complex associates with the CENP-S/CENP-X complex. CENP-S and CENP-X are conserved kinetochore localising proteins (Perpelescu and Fukagawa 2011) that like CENP-T/CENP-W contain histone fold domains (Amaro *et al.,* 2010). Work presented by Nishino et al (2012) indicated that the association of the CENP-T/CENP-W and CENP-S/CENP-X complexes results in the formation of the DNA supercoiling CENP-T/W/S/X heterotetramer. Disruption in the formation of this heterotetramer caused a dramatic reduction of DNA binding and supercoiling, and resulted in failed kinetochore formation. Hence, this would suggest that the CENP-T/W/S/X complex acts like a nucleosome and possesses functions necessary for kinetochore scaffolding (Nishino *et al.,* 2012).

1.6. The KMN network

The KMN network, comprised of the KNL1, the Mis12 and the Ndc80 complexes, is a crucial constituent of the outer kinetochore region (figure 1.2). The KMN network creates an interface for the association between the kinetochore microtubules and centromeric chromatin (Petrovic *et al.,* 2010), with each microtubule binding site containing from six to eight KMN complexes (Joglekar *et al.,* 2006; Joglekar, Bloom and Salmon 2010; Johnston *et al.,* 2010).

1.6.1. The KNL1 complex

Knl1 interacts with the kinetochore by binding to Nsl1 and Dsn1 of the Mis12 complex (figure 1.2) (Kiyomitsu, Obuse and Yanagida 2007; Cheeseman *et al.,* 2006). The N-terminal domain of Knl1 has been shown to bind to the checkpoint constituents Bub1 and BubR1; depletion of either of these checkpoint proteins or Knl1 displays a similar phenotype**.** The C-terminal region of Knl1 is important for both binding to Mis12 and Knl1 localisation to the kinetochore (Kiyomitsu, Obuse and Yanagida 2007). Knl1 also stably associates with ZWINT to form the Knl1 complex (Desai *et al.,* 2003; Nekrasov *et al.,* 2003; Kiyomitsu, Obuse and Yanagida 2007; Pagliuca *et al.,* 2009; Schittenhelm, Chaleckis and Lehner 2009).

In some species such as *C. elegans,* depletion of Knl1 results in loss of entire kinetochores (Cheeseman *et al.,* 2004), whereas in other species, including human, the loss of Knl1 results in defective kinetochores and chromosome mis-segregation (Cheeseman and Desai, 2008; Przewloka *et al.,* 2007). A study by Przewloka and colleagues showed that in *Drosophila,* RNAi of Knl1 initially causes a scattered chromosome phenotype as a result of chromosome congression failure. This is then followed by a block in cell proliferation and a dramatic decrease in mitotic index. This effect was also observed in human cells however the phenotype was not as pronounced (Przewloka *et al.,* 2007).

1.6.2. The Mis12 complex

The Mis12 complex is comprised of Mis12, Nnf1, Nsl1 and Dsn1 (Euskirchen 2002; Nekrasov *et al.,* 2003), and it is the first to be recruited to the centromere via its interactions with the CCAN and centromeric chromatin. All four components of the Mis12 complex are required for the correct assembly of the complex. As shown in a study by Kline and colleagues, depletion of any one of the subunits via RNAi resulted in a marked reduction of the other three proteins due to altered kinetochore targeting or loss of protein stability. This would therefore suggest that the Mis12 complex proteins are interdependent for both their localisation and stability (Kline *et al.,* 2006).

A study by Goshima et al (2003) revealed that loss of Mis12 negatively impacts the behaviour of the chromosomes. Mis12 RNAi in human cells indicated that, whilst the chromosomes were still capable of congressing upon a bipolar mitotic spindle marked alignment defects were observed, which consisted in the formation

of DNA masses away from the spindle equator. Immunostaining with anti-CENP-C antibodies showed that the DNA masses contained punctate CENP-C signalling, indicating the presence of centromeres and that the masses were mis-aligned chromosomes. Despite this, cells with aberrantly aligned chromosomes were still able to progress through mitosis. Although predominantly abnormal, cells could still be observed in anaphase and telophase with more than 50% of anaphases having lagging chromosomes and telophase cells frequently displayed micronuclei.

Consistent with the notion that depletion of the Mis12 complex affects chromosome alignment, time-lapse microscopy of cells depleted for Dsn1, Nsl1, Nnf1 or Mis12 revealed a mitotic delay in which cells spent around 8 hours in mitosis, whereas in control cells mitosis typically took 1 hour. Cells were observed repeatedly attempting to congress their chromosomes without success, and those that did achieve congression underwent erroneous segregation with abnormal chromatin morphology (Kline *et al.,* 2006). The work in this study agrees with others that also showed that when cells are depleted specifically of Dsn1 they experience a prolonged metaphase delay (Obuse *et al.,* 2004).

It has also been observed that depletion of Mis12 prevents the recruitment of other important kinetochore proteins, causing them to be mis-localised or their levels severely reduced (Cheeseman *et al.,* 2004, Goshima *et al.,* 2003; Kline *et al.,* 2006; Przewloka *et al.,* 2007). Reduced levels of the Mis12 complex correlates with a reduction in the kinetochore accumulation of the Ndc80 complex proteins Ndc80 and Nuf2. This would therefore suggest that the defective chromosome attachments observed in Mis12 depleted cells are actually due to a loss of other outer kinetochore components that are involved in microtubule binding. (Kline *et al.,* 2006).

Loss of Mis12 has also been shown to impact the length of the mitotic spindle; cells depleted of the Mis12 complex typically had longer spindles compared with controls. It has therefore been suggested that mitotic spindle length may be controlled by outer kinetochore proteins, and that loss of these proteins and hence, the generation of an elongated mitotic spindle, affects the ability of the chromosomes to correctly congress and segregate (Goshima *et al.,* 2003).

1.6.3. The Ndc80 complex

The Ndc80 complex comprises four subunits; Spc24, Spc25, Nuf2 and Ndc80, and is a conserved player in forming robust microtubule attachments (DeLuca and Musacchio 2012). The Ndc80 complex has an extended rod shape structure (Ciferri *et al.,* 2005; Wei, Sorger and Harrison 2005), composed of heterodimers Spc24/Spc25 and Nuf2/Ndc80 bound together. The most important function of this complex is microtubule binding (Williams *et al.,* 2007; Przewloka *et al.,* 2007; Ciferri *et al.,* 2005; Bharadwaj, Qi and Yu 2004). Disruption of the Ndc80 complex causes severe defects in the ability of microtubules to attach to chromosomes that leads to extensive mis-segregation (DeLuca *et al.,* 2002; Desai *et al.,* 2003) or even complete failure of chromosome segregation (Wigge *et al.,* 1998; Wigge and Kilmartin 2001). Furthermore, depletion of Ndc80 by RNAi prevents the kinetochore localisation of the kinase multipolar spindle 1 (Mps1), and the checkpoint proteins Mad1 and Mad2 (discussed later in this chapter). However, in spite of these losses, Ndc80 depleted cells are still able to maintain a functional SAC (Martin-Lluesma, Stucke and Nigg 2002) Conversely, overexpression of Ndc80 in human cells increases the incidence of merotelic kinetochore attachments (Diaz-Rodrigues *et al.,* 2008; Ferretti *et al.,* 2010) and has also been suggested to increase the binding capacity of microtubules at the kinetochore, in turn diminishing the efficiency at which erroneous attachments can be corrected (Thompson and Compton 2011).

Localisation of the Ndc80 complex is greatly diminished in cells that are deficient for either CENP-T or Mis12 (Kline *et al.,* 2006, Gascoigne and Cheeseman 2011; Nishino *et al.,* 2012). This observation, in combination with the fact that binding of the Ndc80 complex to CENP-T or Mis12 is mutually exclusive, would indicate the existence of two parallel pathways for the recruitment of the outer kinetochore components (Nishino *et al.,* 2013).

Observations into Nuf2 function at the kinetochore has revealed an important role for this protein in the generation of kinetochore microtubule attachments. Typically Nuf2 associates with the kinetochore from the onset of prophase, just prior to NEB, and will persist there until the end of chromosome segregation. De Luca and colleagues (2002) showed that siRNA depletion of Nuf2 in HeLa cells resulted in cells being blocked in metaphase. These cells entered mitosis normally, but then

arrested; this arrest usually being in conjunction with failed chromosome alignment. This block lasted for approximately 7.5 hours after which the cells developed multiple protrusions and their membranes lost uniformity and eventually the cells died (Mills, Stone and Pittman1999; Zhang and Xu 2002). This would therefore suggest that depleting Nuf2 in HeLa cells results in prolonged metaphase arrest followed by aberrant mitotic exit likely via mitotic catastrophe (mitotic cell death) (Nabha *et al.,* 2002; De Luca *et al.,* 2002).

The Ndc80 complex has a relatively modest intrinsic affinity for microtubule polymers (Cheeseman *et al.,* 2006). Individual complexes fail to remain bound to a shrinking microtubule (Schmidt *et al.,* 2012) however if multiple are present (Joglekar *et al.,* 2006) this could allow the kinetochore to remain associated with the depolymerising microtubule as long as at least one Ndc80 complex is bound.

Microtubule attachment via the kinetochore appears to be facilitated by two main branches: the first involves CENP-C linking the CENP-A nucleosomes (Carroll, Milks and Straight 2010; Kato *et al.,* 2013) to the Mis12 complex (Gascoigne and Cheeseman 2011; Przewloka *et al.,* 2011; Screpanti., 2011) which in turn interacts with the KNL1 and Ndc80 complexes (Cheeseman *et al.,* 2004; Cheeseman *et al.,* 2006; Obuse *et al.,* 2004, Petrovic *et al.,* 2010) and the second involves DNA binding to CENP-T/W/S/X where CENP-T interacts directly with Ndc80 (figure 1.2) (Gascoigne and Cheeseman., 2011; Nishino *et al.,* 2013). As reviewed in Glover and Przewloka (2009) the connection between the KMN, the centromere and the attached K-fibre must be robust enough to withstand the pulling forces generated in anaphase, but also have enough flexibility to allow for the constant polymerisation and depolymerisation of microtubule plus ends. The kinetochore also needs to be able to respond to the regulatory mechanisms that allow for chromosome congression at the metaphase plate. This requires the kinetochore to have the following properties: the ability to signal both correct and incorrect attachments, be able to weaken the bond between the microtubule and the NDC80 complex if an attachment is erroneous and finally the ability to delay anaphase until a full complement of correct bipolar attachments have been established (Przewloka and Glover 2009).

1.7. The Ska complex

The human Ska complex was originally identified as a two subunit complex of Ska1 and Ska2 that were found to localise to spindle microtubules and the kinetochore in a manner dependant on Ndc80 (Hanisch, Sillje and Nigg 2006), then subsequently a third member of the complex (Ska3) was discovered. Ska3 is required for the correct functioning and stability of the Ska complex as a whole (Gaitanos *et al.,* 2009); which is reported to be important for kinetochore-microtubule attachment formation, metaphase alignment, SAC silencing and anaphase chromosome segregation (Daum *et al.,* 2009**,** Gaitanos *et al.,* 2009, Hanisch *et al.,* 2006; Theis *et al.,* 2009, Welburn *et al.,* 2009). A study from Helgeson and colleagues (2018) showed that the Ska complex bears a load on microtubule tips, strengthens the Ndc80 complex based tip attachments and increases the switching dynamics of microtubule tips. It has been suggested that there are multiple models for how the Ska complex may contribute to microtubule coupling strength; firstly, the Ska complex may contribute directly to this coupling (Welburn *et al.,* 2009; Gaitanos *et al.,* 2009; Raaijmakers *et al.,* 2009), secondly the Ska complex may play a more indirect role in kinetochore microtubule coupling by recruiting protein phosphatase 1 (PP1) to the kinetochore rather than bearing microtubule generated forces (Sivakumar *et al.,* 2016) and finally the Ska complex may enhance Ndc80 complex based coupling independently of its own microtubule binding affinity (Kudalkar *et al.,* 2015). Depletion of the Ska complex in vivo generally weakens kinetochore microtubule attachments, thereby diminishing the number of kinetochore microtubule attachments that are resistant to microtubule depolymerising cold treatment (Welburn *et al.,* 2009, Gaitanos *et al.,* 2009, Raaijmakers *et al.,* 2009), thus causing more frequent kinetochore detachments during chromosome congression (Auckland *et al.,* 2017) and relieving the hyper stabilisation of kinetochore microtubule attachments caused by phosphoblocking mutations in the Ndc80 complex (Cheerambathur *et al.,* 2017). The Ska complex is also a target of Aurora B (Chan *et al.,* 2012), Mps1 (Maciejowski *et al.,* 2017) and CDK1 (Zhang *et al.,* 2012) kinases which are thought to regulate its interactions with microtubules and the Ndc80 complex (Helgeson *et al.,* 2018).

1.8. CENP-E

CENP-E is a kinesin with plus end directed microtubule motor activity that localises alongside the dynein/dynactin complex at the fibrous corona. The main role of CENP-E is the recruitment of microtubule plus ends to attachment sites at the outer plate of the kinetochore (Rieder and Salmon 1998), of which there are approximately 20 (Rieder 1982), and to assist in the generation of forces that drive the kinetochores towards the poles (Rieder and Salmon 1998) implicating CENP-E in facilitating and maintaining accurate chromosome congression (Wood *et al.,* 1997; Schaar *et al.,* 1997; Yucel *et al.,* 2000) as part of a kinetochore based signalling pathway ensuring segregation fidelity (Abrieu *et al.,* 2000; Yao *et al.,* 2000). However, loss of CENP-E or the dynein/dynactin complex is not sufficient to fully block the formation of kinetochore microtubules and chromosome movement in mammalian cells (Howell *et al.,* 2001; McEwen *et al.,* 2001).

1.9. Dynein and the Rod-Zw10-Zwilch (RZZ) complex

In early prometaphase, prior to kinetochore occupation by the microtubules, the outermost region of the kinetochore, the corona, expands (Hoffman *et al.,* 2001; Wynne and Funabiki 2016) to generate a larger surface area for lateral microtubule capture by dynein. This attachment drives the transient poleward motion of the chromosomes and accelerates the formation of stable end on attachments facilitated by the Ndc80 complex (Rieder and Alexander 1990; Yang *et al.,* 2007; Vorozhko *et al.,* 2015; Wynne and Funabiki 2015). Once the kinetochore has successfully attached to the microtubules dynein assists in the disassembly of the corona, and in the silencing of the SAC by transporting its components away from the kinetochore towards the spindle poles (Howell *et al.,* 2001; Wojcik *et al.,* 2001). Recruitment of dynein to the kinetochore is dependent upon the three subunit Rod-Zw10-Zwilch (RZZ) complex and the coiled coil protein spindly (Starr *et al.,* 1998; Griffis, Stuurman and Vale 2007; Gassmann *et al.,* 2008; Yamamoto *et al.,* 2008; Chan *et al.,* 2009; Barisic *et al.,* 2010). The RZZ complex has also been shown to be necessary for the recruitment of Mad1/Mad2, which is essential for the activation of the SAC (Buffin *et al.,* 2005; Karess 2005; Kops *et al.,* 2005; Essex *et al.,* 2009). Numerous studies have shown that the RZZ subunits are interdependent for their kinetochore localisation as inhibition of any one of the subunits produces the same

phenotype (Smith, Baker and Gatti 1985; Karess and Glover 1989; Williams and Goldberg 1994; Starr *et al.,* 1997; Scaërou *et al.,* 1999, 2001; Chan *et al.,* 2000; Williams *et al.,* 2003; Gassmann *et al.,* 2008; Wainman *et al.,* 2012). One such phenotype is the formation of anaphase bridges, which have been described as a hallmark of RZZ inhibition in *Drosophila melanogaster* and *Caenorhabditis elegans*; the resulting aneuploidy generated is lethal therefore reinforcing the importance for the RZZ complex in ensuring the fidelity of chromosome segregation (Gama, Pereira and Simões 2017).

1.10. The role of cyclin B/Cdk1 in mitotic entry

Cyclin dependant kinases (Cdks) comprise the conserved machinery driving progression through the cell cycle. Cdks are activated by their association with cyclins in order to control DNA replication and mitosis; these events must be triggered sequentially, with DNA replication occurring prior to mitotic entry (Pagliuca, Collins and Choudhary 2011). Mitotic entry correlates with the activation of the mitotic kinase Cdk1, which must later be inactivated via the ubiquitination-mediated destruction of its associated cyclin B in order to trigger mitotic exit (Rieder and Salmon 1998). Cyclin B/Cdk1 has been described as the “work horse” of mitosis because it phosphorylates numerous different substrates including structural proteins and mitotic regulators (Nigg 1993; Errico *et al* 2010; Pagliuca, Collins and Choudhary 2011). Cyclin B/Cdk1 plays an important role in the restructuring of the mitotic cell, it being implicated in the reshaping of the cytoskeleton, chromosome architecture, to promote NEB and to regulate the timings of anaphase and cytokinesis (Nigg 1991, Nigg et al 1993; Errico et al 2010).

Following NEB, a population of cyclin B1 can be observed at unattached kinetochores (Pagliuca, Collins and Choudhary 2011, Bentley *et al.,* 2007); proteomic analysis performed by Pagliuca and colleagues (2011) showed cyclin B bound to spindle assembly checkpoint components such as Mad1, Mad2, BubR1 and Bub3. Later in mitosis, cyclin B is modified by the anaphase promoting complex/cyclosome via polyubiquitination to promote its degradation by the proteasome (Clute and Pines 1999**;** Hagting *et al.,* 2002; Collin *et al.,* 2013; Dick and Gerlich 2013). This allows sister chromatid separation in anaphase, following which

the levels of cyclin B fall below the threshold required to maintain mitosis and so the cell must exit into the next G1 phase.

1.11. Monitoring mitosis: the spindle assembly checkpoint and error correction

In order to ensure accurate inheritance of the genetic material, the cell has evolved a series of checkpoints to control progression through key cell cycle transitions. These transitions are dependent upon the successful completion of a preceding event (Alfieri, Zhang and Barford 2017). There are two “points of no return” in mitosis; one is in late prophase in which passage through this point leads to NEB and a commitment to mitotic entry, and the other is the metaphase to anaphase transition, when pathways that trigger sister chromatid segregation are activated in order to signal mitotic exit (Rieder and Salmon 1998). The cell cycle is specifically controlled to prevent cells entering mitosis with un-replicated or damaged DNA, and to ensure all chromosomes are correctly aligned and accurately segregated before mitotic exit (Errico *et al.,* 2010).

1.11.1. The anaphase promoting complex

The anaphase promoting complex/cyclosome (APC/C) (Peters et al 1996; Hershko 1999) is a key E3 ubiquitin ligase that controls mitosis (reviewed in Barford 2011, Pines 2011). The APC/C is composed of a 13-subunit core complex (McLean *et al.,* 2011), and its interchangeable coactivators Cdc20 and Cdh1 (Schwab, Lutum and Seufert 1997; Visintin, Prinz and Amon 1997; Kramer *et al.,* 1998). The APC/C subunits can be functionally divided into three classes; the catalytic module, the substrate recognition module and the core complex. The catalytic module is made up of Apc11, which is a RING domain subunit (Gmachl *et al.,* 2000; Leverson *et al.,* 2000; Tang *et al.,* 2001), and the cullin subunit APC2 (Yu *et al.,* 1998; Zachariae *et al.,* 1998; Tang *et al.,* 2001). The substrate recognition module is comprised of the two coactivators (Cdc20 and Cdh1) and Apc10. These two modules are highly conserved and represent key functional subunits, however they only represent a small proportion of the overall APC/C complex; the majority of which is made up of the core subcomplex comprised of seven large scaffolding subunits (Schreiber *et al.,* 2011).

APC/C activity is dependent on its association with its co -activators; Cdc20 and Cdh1. The APC/C is activated early in mitosis during prometaphase at the point

of NEB (figure 1.3) (den Elzen and Pines 2001; Geley *et al.,* 2001; Wolthius *et al*., 2008) and will remain active until late G1, where it maintains a low level of mitotic CDK activity, allowing the replication origins to be reset, ready for the next round of DNA replication in S phase (Irniger and Naysmith 1997; Noton and Diffley 2000). In prometaphase the APC/C ubiquitinates Nek2A and cyclin A (Alfieri, Zhang and Barford. 2017) then during metaphase it targets securin and cyclin B which inhibit the transition into anaphase (Cohen-Fix *et al.,* 1996; Clute and Pines 1999). Reducing the levels of cyclins is vital for the transition from metaphase to anaphase, as CDK activity inhibits the function of separase (Stemmann *et al.,* 2001; Gorr, Boos and Stemmann 2005; Holland and Taylor 2006). After anaphase, the destruction of cyclins continues in order to maintain a low level of Cdk activity necessary for mitotic exit (Clute and Pines 1999; Shirayama *et al.,* 1999; Wasch and Cross 2002; Murray, Solomon and Kirschner 1989; Hagting *et al.,* 2002; van Zon *et al.,* 2010).

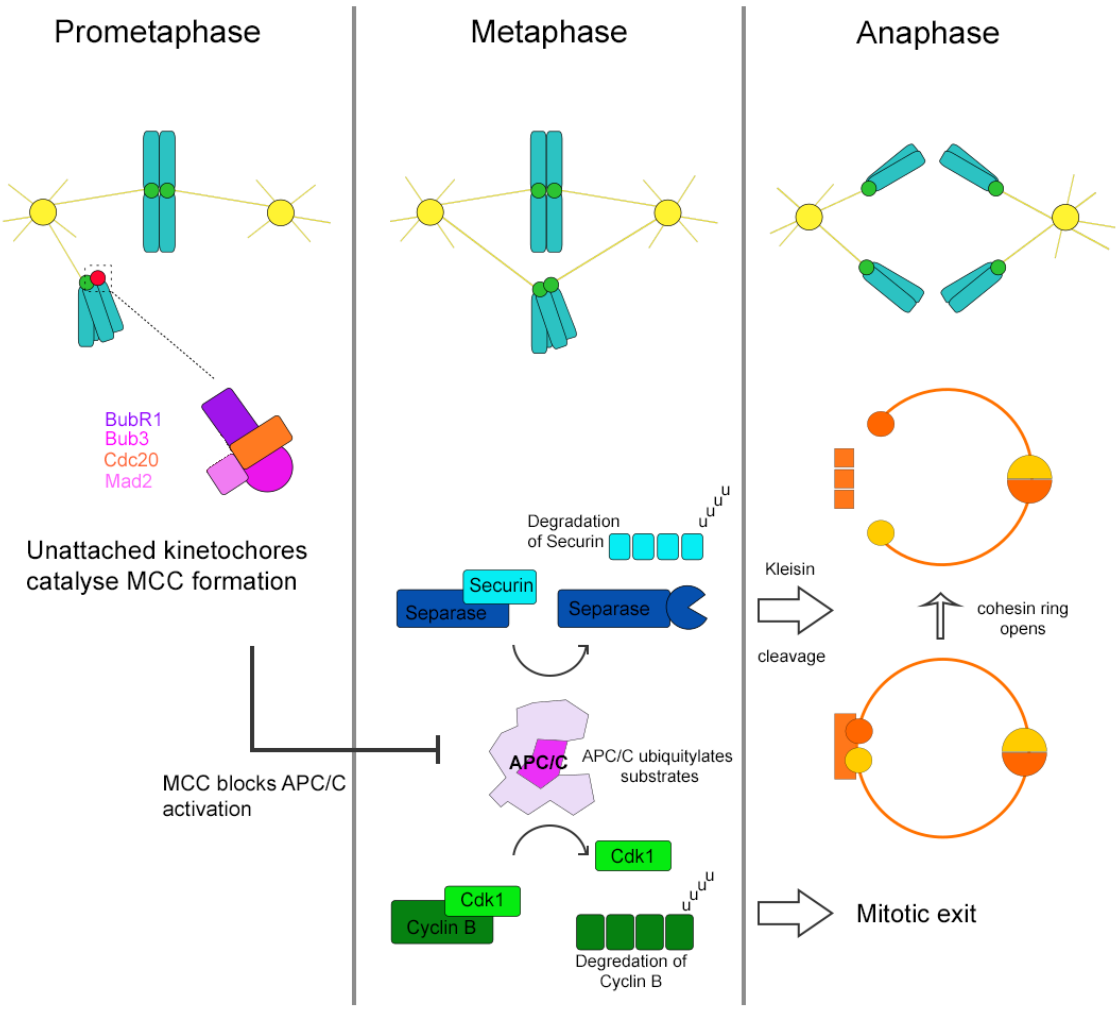

Figure 1.3: Principles of the spindle assembly checkpoint: During prometaphase the unattached kinetochores catalyse the formation of the mitotic checkpoint complex (MCC) composed of BubR1, Bub3, Mad1, Mad2 and Cdc20. Formation of the MCC results in anaphase inhibition. Once in metaphase when all the kinetochores have attached to the mitotic spindle, and the chromosomes are aligned the MCC will prevent any further activation of APC/C via Cdc20. SAC inactivation leads Cdc20 release and APC/C activation which ubiquitylates and degrades cyclin B and securin. Securin degradation frees the kleisin subunit of the cohesin ring, causing it to open and thus allowing the sister chromatids to separate in anaphase. Degradation of cyclin B inactivates Cdk1 resulting in mitotic exit.

The APC/C has also been implicated cancer progression. If the APC/C is inactivated prematurely then this may result in erroneous chromosome segregation (Geley *et al.,* 2001), which, in turn, can result in aneuploidy. Work carried out by Sansregret and Swanton (2017) reported that dysfunctional APC/C activity caused by somatic mutations in cancer cells resulted in prolonged mitoses, suppression of pharmacologically induced chromosome segregation errors and reduced the incidence of naturally occurring lagging chromosomes. Impaired APC/C function was also reported to cause adaptations to the checkpoint component Mps1, which has a highly conserved role in ensuring the proper biorientation of sister chromatids (Liu and Winey 2012), suggesting potential resistance to chemotherapeutic targeting of the SAC (Sansregret and Swanton 2017).

1.11.2. The spindle assembly checkpoint

Just one weakly attached or unattached kinetochore can delay the progression from metaphase to anaphase (reviewed in Wells 1996), as the signal generated can be sufficient to inhibit all APC/C ^{CDC20} activity (reviewed in Barford 2011). Unattached kinetochores recruit the Mad and Bub proteins, and the kinase Mps1. Mad1, Mad2 and Bub1 catalyse the assembly of an APC/C inhibitor (De Antoni *et al.,* 2005) called the mitotic checkpoint complex (MCC) (Sudakin, Chan and Yen 2001). If any unattached kinetochores are detected the SAC will prevent APC/C activation by sequestering Cdc20, inhibiting the progression into anaphase until all kinetochores have established bipolar attachments to the mitotic spindle (Rieder *et al.,* 1995), signalling that the SAC can be “switched-off” allowing cyclin B and securin to be degraded.

The MCC is comprised of Mad1, Mad2, BubR1 and Bub3 tightly bound to Cdc20 (Sudakin, Chan and Yen 2001; Chao *et al.,* 2012). Components of the MCC are recruited in a stepwise fashion starting with the essential kinase Bub1 (Hoyt, Totis and Roberts 1991; Meraldi, Draviam and Sorger., 2004; Perera *et al.,* 2007) which binds early in prophase. This binding is thought to be necessary for the recruitment of the other MCC components (Acquaviva *et al.,* 2004; Vigneron *et al.,* 2004; Howell *et al.,* 2004; Johnson *et al.,* 2004, reviewed in Lara-Gonzalez, Westhorpe and Taylor, 2012) it was reported by Sharp-Baker and Chen (2001) that in *Xenopus* egg extracts depletion of Bub1 prevented the kinetochore localisation of

the other SAC components and the kinetochore motor protein CENP-E. In addition to this observation, depletion of BubR1 also prevented the recruitment of Mad1, Mad2 and CENP-E, and inhibited the localisation of Bub1 (Chen 2002). As Bub1 binding appears to be essential for the recruitment of the other SAC components it has been suggested that it acts as the linker between the SAC and the outer kinetochore (Lara-Gonzalez, Westhorpe and Taylor, 2012).

Mad2 binds to a specific motif of Cdc20 that prevents it from activating the APC/C (Chao *et al.,* 2012; Izawa and Pines 2012). This interaction is stabilised by BubR1 (Lau and Murray 2012), which can have an additional inhibitory effect upon the APC/C by also binding to Cdc20 (Burton and Solomon 2007; Chao *et al.,* 2012). Depletion of either Mad2 or BubR1 results in an accelerated progression through mitosis (Meraldi, Draviam and Sorger 2004), as the degradation of cyclin B and securin is advanced causing it to begin at the onset of NEB (Izawa and Pines 2012).

In a process catalysed by Mps1, the unattached kinetochores have been implicated in the conversion of Mad2 from an open to a closed conformation (Faesen *et al.,* 2017; Ji *et al.,* 2017), in which Mad2 is able to bind to both Cdc20 (Luo *et al.,* 2000; Sironi *et al.,* 2002) and BubR1 (Tipton *et al.,* 2001; Chao et al 2012). Mad2 is recruited to the kinetochore in prometaphase via its interaction with the N-terminal of Mad1 (Chung and Chen 2002; Chen *et al.,* 1998; Chen *et al.,* 1999). The MCC then disappears from the kinetochore when microtubule attachments are formed (Shannon, Canman and Salmon 2002; Chung and Chen 2002; Chen *et al.,* 1998; Chen *et al.,* 1999; Waters *et al.,* 1998).

1.11.3. Kinetochore-microtubule attachment error correction

Correction of erroneous kinetochore microtubule attachments relies on their interaction being reversible, and is reflected in the rate of attachment/detachment dynamics of the K-fibre (Thompson and Compton 2011). As mitosis progresses, the rate of microtubule turn-over at the kinetochore will decrease as their attachment stabilises (Zhai, Kronebusch and Borisy 1995; Cimini *et al.,* 2006; Bakhoum, Genovese and Compton 2009).

Aurora B, along with INCENP, Survivin and Borealin form the chromosomal passenger complex (CPC), so called due to its relocation from the region between the sister kinetochores on duplicated chromatids, the centromere, (Earnshaw and

Rattner 1989) to the central spindle at the metaphase to anaphase transition (reviewed in Ruchaud, Carmena and Earnshaw 2007). Aurora B kinase has a critical role in correcting erroneous microtubule attachments at the kinetochore. This function depends on a spatial gradient set up at the centromere by Aurora B and its antagonistic phosphatase PP1 (Cheeseman 2014). In anaphase, Aurora B moves from the centromere to the microtubules to coordinate cytokinesis (D'Avino, Giansanti and Petronczki 2015). This change in localisation is dependent upon a decline in levels of Cyclin B-Cdk1 kinase activity (Sumara *et al.,* 2007).

Defects in bi-orientation are resolved by Aurora B enriched at the centromeres via a series of feedback loops (Wang *et al.,* 2010; Wang *et al.,* 2011, Yamagishi *et al.,* 2010). Aurora B phosphorylates kinetochore substrates causing non bioriented kinetochore microtubule attachments to detach (Cheerambathur *et al.,* 2013). It is only when microtubule ends are tethered in an end-on fashion to the kinetochore that the growth and shrinkage of the K-fibres can impart their pushing and pulling forces, separating Aurora B from the outer kinetochore components which are de-phosphorylated by PP1, stabilising their interactions with microtubules allowing for chromosome congression (Skibbens, Skeen and Salmon 1993; Cassimeris and Salmon 1991; Mitchison *et al.,* 1986). Aurora B activity has been reported at human kinetochores in the early stages of mitosis (DeLuca, Lens and DeLuca 2011) specifically on kinetochores that are laterally attached (Posch *et al.,* 2010). Aurora B targeted to the kinetochore will detach lateral microtubule attachments prior to end on conversion, whereas Aurora B targeted to the centromere will stabilise the lateral attachments and impede end on conversion. Inhibition of Aurora B or Survivin prevents the recruitment of several kinetochore and SAC proteins such as BubR1, CENP-E and Mad2 (Carvalho *et al.,* 2003; Ditchfield *et al.,* 2003; Hauf *et al.,* 2003; Lens *et al.,* 2003), hence RNAi knock-down of Aurora B has serious implications on kinetochore function (Ditchfield *et al.,* 2003).

Studies from numerous laboratories have shown that the repression of the SAC proteins Bub1 and BubR1, CENP-E and the CPC subunits Aurora B and Survivin all result in the generation of chromosome alignment defects (Ditchfield *et al.,* 2003; Carvalho *et al.,* 2003; Lens *et al.,* 2003; Yao *et al.,* 2000; Johnson *et al.,* 2004). In a study by Johnson *et al* (2004) it was observed that the chromosome alignment defects fell into two categories; in cells depleted of Aurora B, Securin or

BubR1 the chromosomes were observed lying adjacent to the spindle hence indicating microtubule attachment defects. In cases where CENP-E or Bub1 were depleted, cells presented with the majority of chromosomes aligned at the metaphase plate, with a few having not made it to the equator therefore indicating a congression defect.

As expected, depletion of BubR1 also compromises the SAC (Ditchfield *et al.,* 2003). In cells treated with RNAi against BubR1, cells show a reduced metaphase index and an increased number of anaphase cells which typically present one or more lagging chromosomes. However, this phenotype was not observed upon depletion of Bub1, suggesting that loss of this protein does not have an effect on SAC function (Johnson *et al.,* 2004).

1.12. P53 and cancer

As reviewed in Hong et al., (2014) P53 is one of the most frequently mutated tumour suppressor genes in human cancer. Tumour suppressors act as "guardians" that inhibit cell growth pathways and/or induce apoptosis (Vogelstein and Kinzler 2004) to prevent the formation of cancer. Typically, p53 acts as a transcription factor that, as a response to cellular stresses such as DNA damage, hypoxia, nutrient depravation or the activation of oncogenes, can induce cell cycle arrest and subsequent DNA repair, cellular senescence or cell death (ref). If a cell is deficient in p53 it will be able to escape this response resulting in indefinite proliferation, hence p53 plays an important role in the prevention of cancer (Prabhu et al., 2012; Chen et al., 2010). Over 50% of cancer patients will have a somatic mutation in the p53 gene, with around 80% of these being missense mutations of the DNA binding domain. Mutations in the DNA binding domain disrupt the wild type conformation of p53 or will abolish its ability to contact DNA. P53 deficiency in cancer is associated with an increase in genomic instability, metastasis and metabolic adaptation under an unfavourable environment (Hanel and Moll 2012; Vousden and Ryan 2009; Muller et al., 2011); in clinical studies p53 mutations have also been associated with radio and chemotherapeutic resistance, tumour progression and poor patient prognosis (Robles and Harris 2010). In contrast to other tumour suppressor genes, that are commonly truncated or mutated in cancer, the p53 gene is frequently inactivated by just a single mono-allelic missense mutation, and the p53 in its full length form is

often over expressed in human cancer (Brosh and Rotter 2009). Increasing evidence would suggest that p53 mutations not only cause a loss of tumour suppressor function but also results in dominant negative activity over the remaining wild-type allele (Goh et al., 2011). It has been shown in vitro that mutant p53 can inhibit the activity of the wild-type allele thus reducing its ability to bind to p53 responsive elements (Willis et al., 2004). P53 mutations may also result in a "gain-of-function" of oncogenic characteristics (Brosh and Rotter 2009). There are several activities that are involved in this oncogenic activity such as interference with the p53 family proteins p63 and p73 via protein-protein interactions, common in tumours where p53 levels are in excess thus allowing it to bind and inhibit p63 and p73 function (Goh et al., 2011; Jung et al., 2001). Other gain of function examples include regulation of gene transcription of i.e. MDR1, which can lead to drug resistance in p53 expressing cancer cells (Lin et al., 1995), and inhibition of DNA repair pathways which can lead to genomic instability (Song et al., 2007). Through mechanisms such as gene restoration, inhibition of specific p53 interactions, restoration of mutant p53 to wild type or the elimination of mutant genes, p53 is a highly attractive target in cancer therapeutics (Hong et al., 2014).

1.13. Chromosomal instability and aneuploidy

Errors in chromosome segregation can result in chromosomal instability (CIN) and/or aneuploidy. Both CIN and aneuploidy are common cancer features (Chandhok and Pellman 2009; Thompson and Compton 2011), but it is essential to point out that the two are not synonymous. Aneuploidy refers to karyotypic state and denotes chromosome numbers that deviate from the normal diploid number. Some aneuploid cells can have a stable karyotype that is unchanging, like for instance chromosomal syndromes such as Downs syndrome where the only karyotypic change is an additional copy of chromosome 21 (Varetti, Pellman and Gordon., 2014). However, CIN involves the sequential loss or gain of whole (numerical CIN) or fractions of (structural CIN) chromosomes.(Geigl *et al.,* 2008; Cross, Graham and Wright. 2016).

1.13.1. Chromosomal instability

It is believed that numerical chromosomal instability occurs most commonly via erroneous chromosome segregation. In culture, CIN cancer cells can mis-segregate their genome in up to one in every five divisions, whereas in a normal diploid cell line this rate is around one in every hundred divisions (reviewed in Thompson and Compton 2008). It has been suggested that one of the leading causes of CIN via erroneous chromosome segregation is the formation of merotelic attachments between the kinetochore and the microtubule (Ganem, Godinho and Pellman 2009). This type of attachment is not detected by the SAC and so can easily evade detection and proceed into anaphase (Khodjakov *et al.,* 1997; Michel *et al.,* 2001). If a merotelically attached kinetochore proceeds into anaphase and the subsequent telophase, then the resulting progeny will be two aneuploid daughter cells; one with an extra copy of a chromosome and the other missing a copy (Thompson and Compton 2011). Also implicated in the generation of CIN is the presence of extra centrosomes which can arise in a number of ways, either from; cells that fail in cytokinesis, endoreduplication (Ganem, Godinho and Pellman 2009) or when regulation of centrosome duplication is lost (reviewed in Bettencourt-Dias and Glover 2007). In cells with extra centrosomes the architecture of the mitotic spindle is disrupted and spindles with 3 or more poles can arise, an occurrence that has been positively correlated with incidences of CIN in cancer cells (Ghadimi *et al.,* 2000). Segregating chromosomes over a multipolar spindle results in inviable progeny (Kwon *et al.,* 2008; Ganem, Godinho and Pellman *et al.,* 2009) therefore a successful outcome can be achieved by clustering the extra centrosomes to form a bipolar spindle (Quintyne *et al.,* 2005). However these bipolar spindles have a high incidence of merotelic attachments, which at that high a frequency can overwhelm the error correction machinery (Ganem, Godinho and Pellman 2009).

Solid tumours will often contain structural rearrangements that involve multiple chromosomes and break points, cells within the same tumour can also present a varied array of differentially rearranged chromosomes which is a hallmark of structural CIN (Thompson and Compton 2011). Mechanistically, chromosomal gains may alter the transcription dosage of oncogenes (Murugaesu *et al.,* 2015), whilst deletions may act as a second hit removing the remaining good copy of a tumour suppressor gene. This view is concordant with the somatic mutation theory (Soto

and Sonnenschein 2004), however chromosome aberrations are often heterogeneous (Muzny *et al.,* 2012) so disrupting whole chromosomes can in turn affect thousands of genes at once via alterations to the proteome and transcriptome. Therefore, it has been presented that chromosome scale deletions likely act as punctate events that represent dramatic changes in the rate of genome alteration (Cross, Graham and Wright 2016).

CIN is often linked to resistance to chemotherapeutic agents and metastasis (Swanton *et al.,* 2009; Warth *et al.,* 2009) as the frequent chromosomal rearrangements essentially shuffles the genome. These constant genomic changes therefore increase the likelihood of the formation of a karyotype favourable for cancer growth in chemotherapy drugs and hence result in drug resistance and further cancer development (Thompson and Compton 2011).

Catastrophic chromosome aberrations such as chromothripsis (Maher and Wilson 2012; Stephens *et al.,* 2011), otherwise referred to as chromosome shattering, in which chromosomes fragment and reassemble, and chromoplexy, (Baca *et al.,* 2013) where genetic material is scrambled together causing radical and complex genome wide restructuring, are two other ways genome dosage can be altered. These events can either alter the genome by inducing chromosome copy number alterations, by displacing gene promotors and regulators or by mutating coding regions. These events are fairly common occurrences; chromothripsis is believed to be present in 2-3% of all cancers (Stephens *et al.,* 2011) and chromoplexy has been detected in 80% of prostate cancers (reviewed in Cross Graham and Wright 2016).

1.13.2. Aneuploidy and polyploidy

Aneuploidy is a hallmark of cancer that is present in approximately 90% of solid tumours and in over 50% of leukaemia and lymphomas (Beroukhim *et al.,* 2010; Mitelman and Johansson 2013). Two alternate hypotheses have been proposed regarding how aneuploidy leading to cancer can arise. One hypothesis is that aneuploidy initially arises by a gain or loss of one or a few chromosomes which, in turn, can lead to further chromosome instability and transformation (Duesberg and Li 2003; Weaver and Cleveland 2006; Weaver *et al.,* 2007). Weaver *et al.,* (2007) confirmed this hypothesis through the generation of haploinsufficient CENP-E mice;

CENP-E reduction having previously been shown to induce mis-segregation of one or more chromosomes in mitosis due to a partially weakened checkpoint (Saunders *et al.,* 2000; Weaver *et al.,* 2007). However, the alternative suggests that the initial step towards aneuploidy is actually tetraploidy (genome doubling). There are a number of ways that cells can become tetraploid such as cell fusion, mitotic slippage, failure to complete cytokinesis or endoreduplication (figure 1.4) (Holland and Cleveland 2009). These tetraploid cells would then undergo multipolar cell divisions, due to the presence of extra centrosomes, in turn leading to massive chromosome mis-segregation and eventually to the development of the aneuploid, heterogeneous karyotype observed in cancer cells (Storchova and Pellman 2004). This hypothesis was tested by Fujiwara *et al.,* (2005) who transiently blocked cytokinesis in p53 null mouse mammary epithelial cells and showed that the resulting tetraploid cells had an increased frequency of chromosome mis-segregation and were capable of inducing malignant mammary epithelial cancers when injected into nude mice, suggesting that the ability of polyploidy to induce cancer is linked to p53 status. A strongly positive correlation between aneuploidy and mutation of the tumour suppressor gene p53 has also been reported in a number of other studies (De Angelis *et al.,* 1993; Meling *et al.,* 1993; Campomenesi *et al.,* 1998; Duensing and Duensing 2005; Schjolberg *et al.,* 2009) in which they state that p53 mutations often occur before the generation of aneuploidy (Blount *et al.,* 1994) as it is likely that functional p53 would limit the proliferation of aneuploid cells to protect the integrity of the genome (Storchova and Kuffer 2008).

Polyploidy as a first step towards cancer has been raised in a number of other studies for example Nguyen *et al.,* (2005) linked the over expression of Aurora B to polyploidy in mouse mammary epithelial cells. Another example comes from a study by Meraldi and colleagues (2002) showing that Aurora A is frequently over expressed in human cancers, increased levels of which having been linked to cells failing to complete cytokinesis. Aurora A overexpression in the mouse mammary gland has also been shown to increase incidences of tetraploidization, CIN and tumour formation (Wang *et al.,* 2006). With regards to tumour suppressor genes; mutations in the adenomatous polyposis coli (APC) tumour suppressor have been commonly found in human colon cancers, and in mice cancers APC mutations have again been linked to increased rates of cytokinesis failure and the onset of

tetraploidy (Caldwell, Green and Kaplan 2007). Evidence for polyploidization in cancer progression also comes from frequently observed multipolar spindles and amplified centrosomes in many cancer cell types (Ghadami *et al.,* 2000; Lingle *et al.,* 2002; Sato *et al.,* 2001; Saunders *et al.,* 2000). However, polyploidy, whether or not it is the first mutation in cancer, tends not to persist as cancer cells with greater than 90 chromosomes are infrequently observed (Weaver and Cleveland 2006).

Using a long term culture model of colon cancer cells to investigate how genome doubling events affect genome stability over time Dewhurst *et al.,* (2014) reported that cells that survived genome doubling had increased tolerance to chromosome aberrations. They also stated that genome doubling events can act as an independent predictor of poor relapse free survival in the early stage of disease, thus highlighting an important role for the tolerance of genome doubling in driving the evolution of cancer. A number of other studies have also observed tetraploid cells in the transition from premalignant to malignant disease (Galipeau *et al.,*1996, Maley *et al.,* 2006) such is the case for Barrett's oesophagus and oesophageal adenocarcinoma (discussed later in this chapter), suggesting that genome doubling could be a driver of tumorigenesis. Tetraploid sub clones have also been identified at the later stages of cancer development (Gerlinger *et al.,* 2012) and whole genome doubling events have been inferred to occur both before and after copy number alterations across different types of cancer (Nik-Zainal *et al.,* 2012**;** Zack *et al.,* 2013). However, the effect of a whole genome doubling event on CIN and how this could impact genome evolution in cancer cells it yet to be fully explored (Dewhurst *et al.,* 2014).

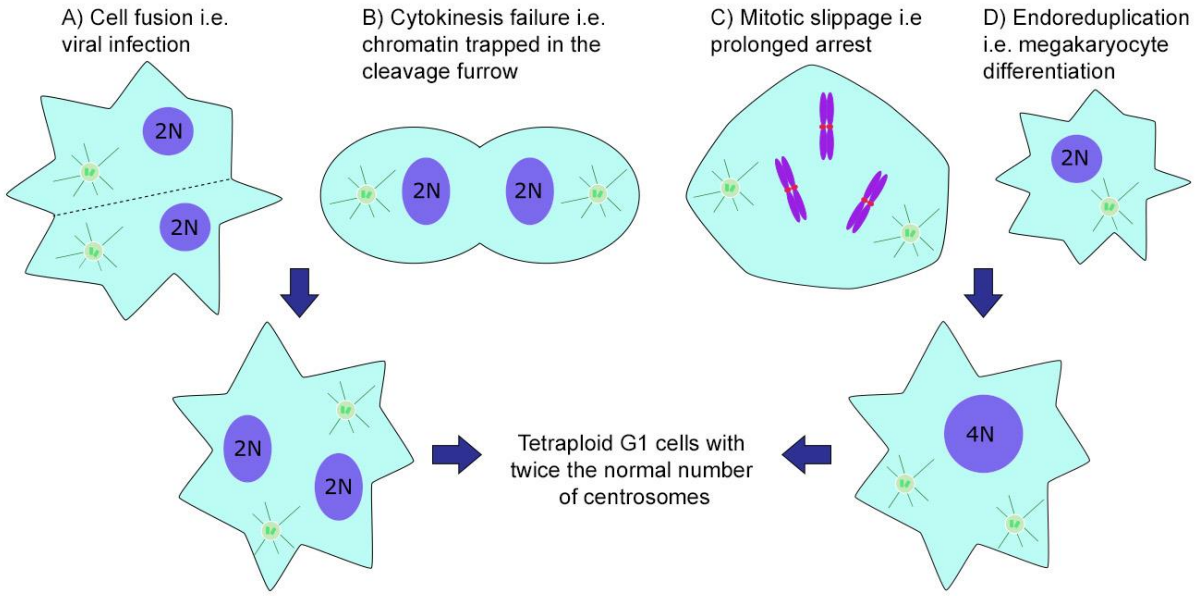

Figure 1.4: Pathways to polyploidy. Cells can become polyploid in a number of ways: A) two cells can fuse together, B) cells can fail to complete cytokinesis, C) they can slip out of mitosis and into the next cell cycle without having completed anaphase, telophase and cytokinesis or they can D) skip mitosis and undergo endoreduplication. In all situations the resulting progeny will have a tetraploid genome with extra centrosomes that will be duplicated in the next cell cycle. Figure adapted from Holland and Cleveland 2009.

1.14. Barrett's oesophagus and its progression into oesophageal adenocarcinoma

Approximately one quarter of all human cancers occur in the gastrointestinal tract making it the most predominant site of cancer development in the human body. Almost all of these cancers are preceded by a pre-malignant condition, with Barrett's oesophagus (BE) being the precursor to oesophageal adenocarcinoma (OEAC) (Kuipers and Spaander 2018). According to cancer research in 2015 around 9200 people were diagnosed with OEAC in the UK, making it the 13th most common adulthood cancer. Frequent exposure of the oesophagus to stomach acid can lead to the development of gastroesophageal reflux disease (GERD). GERD refers to a

spectrum of symptoms that can present from infrequent discomfort to a debilitating condition and is characterised by chronic inflammation of the lining of the lower oesophagus which can lead to BE, which is estimated to exist in 1:100 adults with GERD (Ormsby *et al.,* 2000). BE is typically asymptomatic, the symptoms experienced i.e. acid reflux, upper abdominal pain and heartburn result from GERD. Due to its symptom free presentation, BE is only diagnosable by endoscopy, and is characterised by the transformation of the stratified squamous epithelium of the healthy oesophagus into a simple columnar epithelium typical of that observed in the small intestine (figure 1.5).

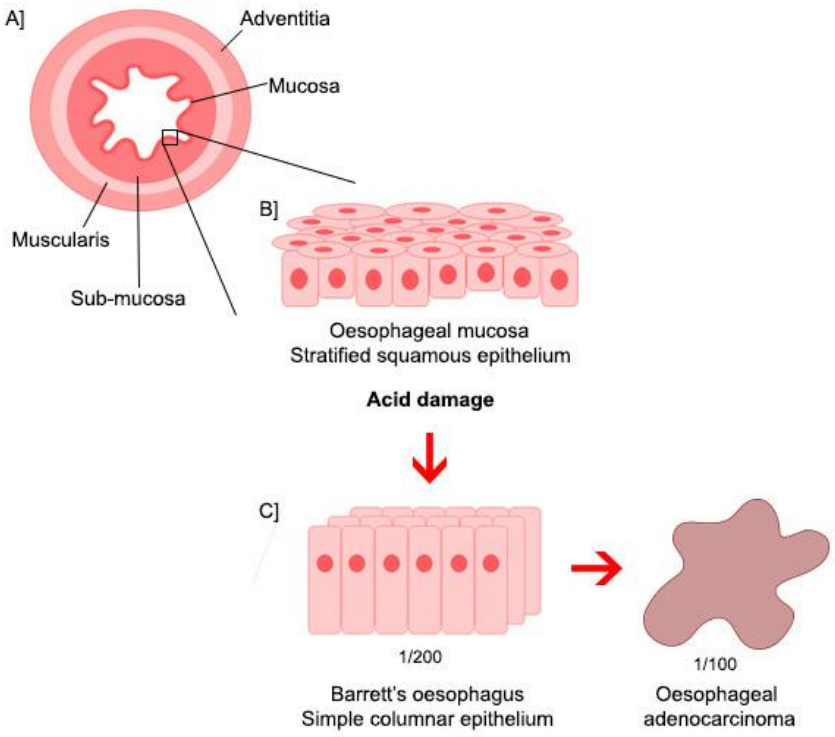

Figure 1.5: BE and its progression into OEAC. A) The human oesophagus is made up of 4 layers; the adventitia, the muscularis, the sub-mucosa and the mucosa. B) The mucosal layer of the oesophagus is lined with a stratified squamous epithelium. These cells can become damaged by frequent exposure to the stomach acid, as a result of gastroesophageal reflux disease (GERD). C) Acid damage to the stratified squamous epithelium can bring about a cellular transformation into a simple columnar epithelium typical of that of the small intestine. This transformation is the main diagnostic feature of BE. Approximately 1/200 people with GERD will develop BE. BE is the precursor lesion to OEAC and around 1/100 cases of BE will progress into OEAC.

It has been reported that GERD may induce alterations in the expression of key developmental transcription factors which results in this transformation, either by causing the mature squamous epithelium to become columnar (transdifferentiation) or by causing immature oesophagus progenitor cells to undergo columnar rather than squamous differentiation (transcommitment) (Burke and Tosh 2012; Wang *et al.,* 2012). Diagnosis of BE occurs when endoscopic investigation shows that the columnar mucosa extends above the gastroesophageal junction which is then further confirmed by biopsy (Spechler 2013). The extent of oesophageal metaplasia, the replacement of one tissue type with another as a result of injury (Burke and Tosh 2012), determines whether BE is classified as long segment (≥ 3 cm) or short segment (< 3 cm) (Sharma *et al.,* 1997). Patients diagnosed with long segment BE typically experience severe GERD with erosive oesophagitis (inflammation of the oesophagus as a result of acid reflux) whereas those with short segment generally do not present any GERD symptoms (Hayeck *et al,* 2010; Taylor and Rubenstein 2010). It is therefore presumed that short segment BE develops as a result of protracted acid reflux involving only the most distal portion of the oesophagus, something which has been reported in those who are otherwise healthy patients (Fletcher *et al.,* 2003).

OEAC develops in the glands that make up the mucosa of the oesophagus, and will typically develop in the lower portion of the oesophagus. Compared to oesophageal squamous cell carcinomas, OEACs are the most common type of oesophageal carcinomas (Cancer research UK 2019). In the absence of dysplasia i.e. the presence of abnormal cells in a tissue, the risk of BE transforming into an invasive cancer is 0.3% per year (Anaparthy and Sharma 2014**,** Desai *et al.,* 2012). BE can progress from a non-dysplastic lesion through intermediate stages of low-grade dysplasia and high-grade dysplasia leading to OEAC formation (Ross-Innes *et al.,* 2015). Dysplasia increases the risk of cancer progression to 10% per year following endoscopic identification (Phoa *et al.,* 2014**;** Shaheen *et al.,* 2009; Rastogi *et al.,* 2008**;** Shaheen *et al.,* 2016). Cases of BE that do progress into cancer if not previously identified endoscopically will typically be diagnosed at an advanced, incurable stage (Stachler *et al.,* 2015).

Through studies of BE, a linear model emerged where early non-dysplastic BE represents a clonal or polyclonal expansion, typically following the inactivation of

tumour suppressor gene CDK2NA (Stachler *et al.,* 2015; Galipeau *et al.,*1999; Li *et al.,* 2014; Li et al 2008; Reid *et al.,* 1996; Wong *et al.,* 2001). Further expansions result in the formation of a clone with inactivated TP53 and other somatic alterations including genome doubling and genomic disruption that lead to malignant transformation (Stachler *et al.,* 2015; Li *et al.,* 2013, Reid *et al.,* 1996).

When OEAC develops, the copy number and heterogeneity of the genome increases such that the spectrum of mutations shown prevent little overlap with its paired BE counterpart, however despite the broad differences in coding mutations the context of said mutations would suggest a common insult underlying the two conditions (Ross-Innes *et al.,* 2015). DNA sequencing of OEAC has revealed a huge mutational burden within this cancer (Weaver *et al.,* 2014; Agrawal *et al.,* 2012; Chong *et al.,* 2013; Dulak *et al.,* 2013). OEAC also presents with distinct mutational signatures (Weaver *et al.,* 2014; Alexandrov *et al.,* 2013) with TP53 being by far the most frequently mutated gene (Chong *et al.,* 2013; Dulak *et al.,* 2013). In a study performed by Agrawal and colleagues (2012) exome sequencing on paired BE and OEAC samples showed that approximately 80% of cancer mutations were already present in the DNA from the adjacent BE epithelium. Furthermore, in a study by Ross-Innes and colleagues (2015) whole genome sequencing (WGS) of paired BE and OEAC samples taken at the same timepoint from 23 OEAC patients with visible BE showed that although BE adjacent to OEACs was found to be highly mutated and contain thousands of single nucleotide variants (SNVs), there were significantly more SNVs in the tumour samples. This study also highlighted a stark contrast between the gene copy number aberrations within the BE samples compared to the OEAC. With the exception of two samples, BE contained very few copy number changes with the vast majority of the genome being diploid, this result was significantly different for that observed in OEAC which showed a range of copy numbers including some highly amplified regions of up to 15-20 copies (figure 1.6).

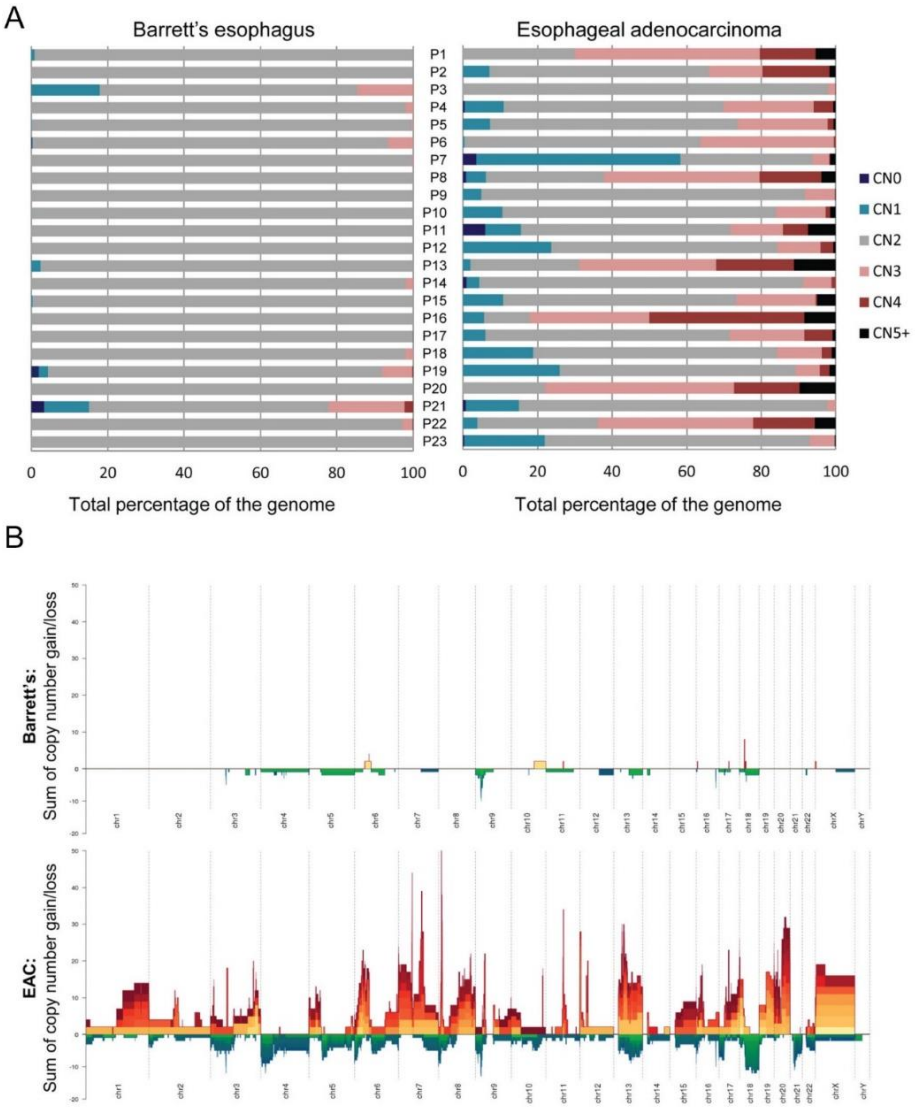

Figure 1.6: OEAC displays multiple copy number changes compared to BE. A) Graphs showing the percentage of the genome at different copy number states for each patient (p) in turn (1-23) for the paired BE (left) and OEAC (right) samples. CN 0/1/2/3/4 = gene copy number of 0/1/2/3/4 CN 5+ = gene copy number of at least 5. B) Stacked mountain plots summarising copy number variation within all of the 23 BE and OEAC samples. Gains of at least two copies on top of the normal copy number are illustrated in yellow-orange-red mountains and deletions by the green-blue valleys. Height and depth of mountains and valleys indicate the summed copy number status across all patients for that region. The colours represent different samples so that the more different colours present, the more samples display that copy number alteration. Figure from Ross-Innes *et al*., 2015

Further evidence for genomic alterations comes from Stachler and colleagues (2015) who presented data from whole exome sequencing of 25 paired BE and OEAC tumours, and from five patients whose paired tumours had been extensively sampled. Their data revealed that amplification of oncogenes typically occurred as a later event in the progression of BE in to OEAC and that TP53 mutation occurred early on. Re-analysis of additional OEAC data also indicated that 62.5% of OEAC's emerged following a genome doubling event, and that tumours with genomic doubling showed different patterns of genomic alterations with more frequent oncogenic amplifications and fewer tumour suppressor inactivations. This data would therefore suggest that many OEACs experience a more direct pathway of progression by which a TP53 mutant cell goes through genome doubling followed by the acquisition of oncogenic amplifications. In whole genome doubled (WGD) samples, 90% of the TP53 mutations were determined to have occurred prior to the doubling event. Whole-genome-doubled (WGD) tumours showed different degrees of ploidy and genomic disruptions to non-WGD tumours however the mutational densities were similar between the two populations. The data from Stachler *et al.,* therefore suggests that the traditional BE progression model combines two pathways for oncogenic transformation (figure 1.7). One pathway appears to involve the gradual, progressive accumulation of losses of tumour suppressor genes, which leads to genomic instability and oncogene amplifications without a previous genome doubling event. However, the majority of OEACs appear to develop following the expansion of a TP53 mutant clone that undergoes genome doubling, with WGD tumours predominantly seen occurring from dysplastic tissues. Genome doubling has been shown to facilitate the acquisition of genomic instability (Fujiwara *et al.,* 2005; Gordon, Resio and Pellman 2012; Dewhurst *et al.,* 2014), and hence tumours that develop following WGD show marked genomic disruption and oncogene amplification. This would therefore suggest that the more practical pathway of transformation of BE into OEAC is likely the one of WGD causing oncogene activation via structural genomic instability, resulting in a large number of copy number alterations (Stachler *et al.,* 2015).

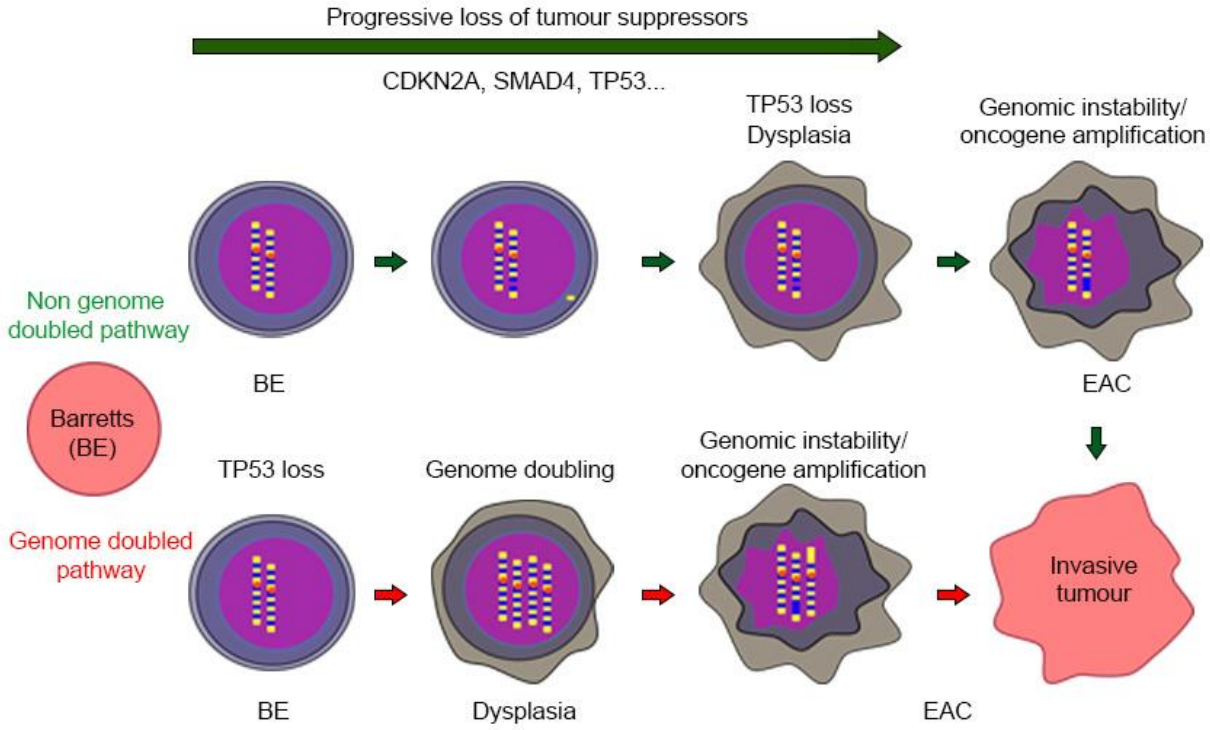

Figure 1.7: OEAC shows distinct development pathways. There are two potential pathways of progression of BE into OEAC. The non-genome-doubled (NGD) pathway involves the gradual accumulation of tumour suppressor gene mutations culminating in a loss of TP53. This is followed by oncogene activation and genomic instability. In the genome-doubled (WGD) pathway of progression loss of TP53 is acquired as a much earlier event. This clone will then undergo genome doubling which again results in oncogene activation, genome instability and the formation of an invasive OEAC tumour. Figure adapted from Stachler et al., 2015.

1.15. Project aims

The aim of this project is investigate the potential origins of genome doubling in BE, with particular focus on mitosis and the identification of mitotic defects in OEAC. In order to explore this I will firstly analyse cell division in BE and OEAC validated cell lines and organoids using immunofluorescence and time-lapse microscopy in order to look for defects in mitosis. Using data from whole genome sequencing I will then compare gene mutations and rearrangements in key cell division factors between BE and OEAC cell lines and in paired BE and OEAC tumours. Next, I will analyse the expression of said cell division factors in BE and

OEAC cell lines via immunofluorescence and western blots; these factors will include mitotic kinases and their substrates, SAC components, centrosomal, centromere, kinetochore and cytokinesis proteins. Finally, using mass spectrometry I will characterise the interactome of key cell division networks and nodes in BE and OEAC cell lines.

2. Materials and methods

2.1. Tissue culture

CPA and CPD cells were cultured in Keratinocyte-SFM supplemented with 2.5 µg prequalified human Epidermal Growth Factor 1-53 (EGF) (Life technologies), 25 mg Bovine Pituitary Extract (BPE) (Life technologies) and 0.5% penicillin/streptomycin (pen/strep) (ThermoFisher). HeLa and FLO cells were cultured in Dulbecco's Modified Eagle Medium (DMEM) (Sigma) supplemented with 10% Fetal Bovine Serum (FBS) (Sigma) and 1% pen/strep (ThermoFisher). JH-Eso-AD1 cells were cultured in Minimum Essential Medium (MEM) (Sigma) supplemented with 10% FBS and 1% pen/strep (ThermoFisher). OE33 and OE19 cells were cultured in Roswell Park Memorial Institute (RPMI) Medium (Life technologies) supplemented with 10% FBS (Sigma) and 1% pen/strep (ThermoFisher). RPE1 cells were cultured in Dulbecco's Modified Eagle Medium Nutrient Mixture F12 (Life technologies) supplemented with 10% FBS (Sigma) and 1% pen/strep (ThermoFisher). All cells were cultured in a humidified atmosphere with 5% CO_2 at 37°C.

2.2. Synchronising cells

2.2.1. Single thymidine nocodazole block

Cells were seeded to an appropriate density (typically 0.9 x 10^7 per T175 flask) then the day after, incubated in 2mM thymidine for 19 hours. Following thymidine treatment cells were washed 3x in PBS + $MgCl_2$ + $CaCl_2$ (Sigma) released into fresh growth medium for 5 hours then incubated in 50 ng/mL nocodazole for 13 hours. Following nocodazole block, mitotic cells were collected via mitotic shake off then centrifuged at 3000 rpm for 3 minutes. Pelleted cells were resuspended in PBS + $MgCl_2$ + $CaCl_2$ and centrifuged at 3000 rpm for 3 minutes, for a total of 5 washes. For a metaphase population cells were released for 30 minutes into fresh growth

medium containing 25 µM MG132, then centrifuged at 3000 rpm for 3 minutes. Pelleted cells were washed as above, all PBS was removed, and the cell pellet was frozen and stored at -80 degrees. For Western blotting, samples are taken at 0 minutes (point at which cells are released into MG132) and at 30 minute time points.

2.2.2. Palbociclib nocodazole block

Cells were seeded as previously described for a single thymidine nocodazole block then incubated with 1 µM Palbociclib for 18 hours. Following this incubation cells were released by washing gently in PBS + $MgCl_2$ + $CaCl_2$ for a total of three washes, then incubated for 8 hours in fresh growth media. Cells were then incubated in 50 ng/mL nocodazole, washed and collected as previously described in the single thymidine nocodazole block protocol.

2.3. Immunoprecipitation

2.3.1. Bead preparation

Protein A and protein G beads (ThermoFisher) were prepared for immunoprecipitation according to manufacturing instructions. 100 µL of beads were vortexed for 10 seconds, then allowed to settle. All supernatant (SN) was removed and replaced with 200 µL PBS 0.1% NP40 containing 1-10 µg of an appropriate antibody. Beads were incubated on a rotating wheel at 4°C overnight.

2.3.2. Pull downs

Synchronised cells were resuspended in 1 mL ice cold extraction buffer (EB) (50 mM HEPES pH7, 100 mM KAc, 50 mM KCl, 2 mM $MgCl_2$, 2 mM EGTA, 5mM DTT, complete protease inhibitor tablet (Roche) 0.1% NP40, 5% glycerol), then homogenised 3x10 seconds. SN was treated with DNase1 for 10 minutes at 37°C then 10 minutes at RT then centrifuged for 15 minutes at 3000 rpm at 4°C. Beads were washed 3 times with 1 mL ice cold EB. Following centrifugation 20 µL was taken for analysis, EB was removed from the beads and replaced with SN then incubated at 4°C on a rotating wheel for 2-4 hours. Following incubation 20 µL of SN was taken for analysis and all remaining SN was replaced with 1 mL ice cold EB. Beads were incubated at 4°C on a rotating wheel for 5 minutes for a total of 5 washes. All contents were removed to a new tube and all EB removed. Beads were then incubated in 1 mL ice cold PBS for 1 minute on ice, the PBS removed and

replaced with 100 µL PBS. 5 µL beads was taken for analysis by Western blot then all PBS removed. Beads were frozen and stored at -80°C prior to MS analysis.

2.4. Sample preparation for gel electrophoresis

Samples were resuspended in an appropriate volume of 1x Laemmli buffer and heated at 100°C for 10 minutes.

2.5. Coomassie staining

Samples were run on a 10% SDS page gel at 100 Volts (V) for 90 minutes. Gels were washed in diH_20 for 5 minutes with shaking, then incubated in Coomassie stain (Generon) for 20-60 minutes with shaking. Gels were washed 3x5 minutes in diH_20 and incubated in gel drying solution (30% MeOH, 5% glycerol) for 20 minutes before sealing in acetate using the Dry-Ease gel drying system (Invitrogen).

2.6. Silver staining

Gels were run as per Coomassie protocol then silver stained using the SilverQuest staining kit (Invitrogen). Gel was incubated in fixing solution (40% ETOH, 10% acetic acid) for 20 minutes then washed in 30% ETOH for 10 minutes. Gel was then incubated in sensitizing solution (30% ETOH, 10% sensitizer) for 10 minutes, washed in 30% ETOH for 10 minutes and water for 10 minutes. Gel was then incubated in staining solution (1% staining reagent) for 15 minutes and washed for a further 1 minute in water. Gel was developed in developing solution (10% developer plus enhancer) for 4-8 minutes until bands had appeared. Stopper solution was then added for 10 minutes, followed by a final 10-minute wash in water. Gel was prepared and dried as per the Coomassie protocol.

2.7. Western blot

Samples were run on an appropriate gel as per Coomassie protocol then transferred onto PVDF membrane (Immobilon-P) at 15V for 1 hour. Membrane was blocked overnight at 4°C in PBS 0.1% tween (PBST) with 5% milk powder. After blocking, membranes were washed once with PBST then incubated in the appropriate primary antibody (in PBST containing 3% BSA (Sigma)) for 2 hours at RT. Membranes were washed 3x5 minutes in PBST, then incubated in the relevant secondary antibody (in PBST plus 1% BSA) for 1 hour at RT. After a further 3x5

minute washes in PBST antibodies were detected using ECL West Pico substrate (ThermoScientific) in the Syngene GBox with GeneSys software.

2.8. Mass spectrometry

RIME was carried out at the Cancer Research UK Cambridge institute by Dr Clive D'Santos.

LC MS-MS was carried out at the Environmental Laboratory of Mass Spectrometry, Institute of Biochemistry and Biophysics, Polish Academy of Sciences. Peptides mixtures were analysed using Nano-Acquity (Waters) LC system and LTQ-FT-Orbitrap mass spectrometer (Thermo Electron Corp., San Jose, CA). Acquired raw data was processed by Mascot Distiller followed by Mascot Search (Matrix Science, London, UK, on-site license) against SwissProt database (June 2015 release) restricted to human sequences by Dr Janusz Debski from IBB PAS.

2.9. Fixing cells

2.9.1. Pre-extraction

Cells seeded on 22x22 mm coverslips were incubated for 5 minutes in pre-extraction buffer (60 mM PIPES pH 7.0, 25 mM HEPES pH 7.0, 10mM EGTA, 4mM $MgSO_4$, 0.5 % Triton) then fixed using one of the following protocols.

2.9.2. Formaldehyde fixation

Coverslips were incubated in 1.5 mL fixing reagent PHEM (3.7% formaldehyde, 60 mM PIPES pH 7.0, 25 mM HEPES pH 7.0, 10 mM EGTA, 4 mM $MgSO_4$) for 12 minutes at RT, then washed in 2 mL PBS for 5 minutes for a total of 3 washes.

2.9.3. Methanol fixation

Coverslips were incubated in 1mL ice cold methanol for 10 minutes at -20 °C, then washed in 2 mL PBS for 5 minutes for a total of 3 washes.

2.10. Immunostaining

Coverslips were blocked for 2 hours at RT in PBT (PBS 5% BSA (Sigma) 0.5% Triton X (Sigma)) then incubated in primary antibody in PBT 1% (PBS 1% BSA 0.1% Triton X) overnight at 4 °C, then washed in 2 mL PBT 1% for a total of 3

washes. Coverslips were then incubated in secondary antibody in PBT 1% for 2 hours at RT then the above wash steps repeated. Coverslips were mounted with Vectashield fluorescent mounting media with DAPI (Vector).

2.11. Imaging fixed cells

Immunostained cells were imaged using a Nikon Eclipse C1si automated microscope (Professor David Glover's lab). A 13 image Z stack was taken at each wavelength, and a composite image created using MetaMorph software. Further image processing was carried out using ImageJ.

2.12. Quantification of mitosis

Cells immunostained for H3 pS10, tubulin and DAPI were counted and scored based on whether they were H3 pS10 positive to indicate mitosis. Mitotic cells were then categorised into prophase/prometaphase, metaphase, anaphase or telophase by eye based upon the organisation of the chromosomes and the mitotic spindle. This was repeated for a minimum of 30 fields of view per coverslip imaged (minimum of three per cell line).

2.13. Imaging organoids

Organoids were fixed with 4% PFA, permeabilized in Triton X-100, quenched with glycine-PBS and then incubated with primary antibodies overnight. Organoids were washed and incubated with appropriate secondary antibody. Nuclei was stained by Vectashield with DAPI. Organoids were imaged by confocal microscope TCS SP5 (Leica), Z stacks were taken at 1-μm intervals through organoids, and images were processed by Volocity image analyze software (Perkin Elmer, version 6.3.0). (Li *et al.,* 2018)

2.14. Time-lapse

Cells were plated on an 8 well μ slide (Ibidi) in their appropriate growth media. Prior to recording media was replaced with Leibovitz's L-15 media (without phenol red) (ThermoFisher), and NucBlue Live Cell Stain ReadyProbes™ reagent was added (Invitrogen). Cells were then incubated in the dark at 37°C for 20 minutes. Cells were imaged on an Olympus IX83 with an LED illuminator (Spectra-X, Lumencor), XY automated stage (ASI) and 37C incubation chamber (Digital Pixel)

controlled using Micromanager Freeware. Images were captured every 5 minutes for 100 frames with 100 ms brightfield and 20 ms Dapi exposures. Further processing was carried out using ImageJ.

2.15 Primary antibodies used in my experiments

Antibody name	Supply
α Actin	Rabbit polyclonal, Sigma A5060
α Astrin	Rabbit polyclonal, Novus NB100-74638
α Aurora B	Mouse monoclonal (AIM-1), BD transduction lab 611082
α BubR1	Rabbit polyclonal, Abcam ab172518
α Cenp-A	Mouse monoclonal, Abcam ab13939
α Cenp-C	Rabbit monoclonal, Abcam ab193666
α Crest	Human polyclonal, Antibodies Inc 15-234, kind gift from the Glover lab.
α Cyclin B1	Mouse monoclonal, clone GNS1, Santa Cruz sc - 245
α Dsn1	Rabbit polyclonal, Sigma SAB2702119
α Gamma tubulin	Mouse, kindly gifted from the Glover lab
α Hec1 (NDC80)	Mouse monoclonal, Santa Cruz sc-515550
α Histone H3 pS10	Rabbit polyclonal, Millipore 06-570
α Knl1	Rabbit, kind gift from Dr Marcin Przewloka (University of Southampton)
α Plk4	Rat, kindly gifted from the Glover lab
α Spc24	Rabbit monoclonal, Abcam ab169786
α Tubulin	Mouse monoclonal, clone DM1A, Sigma T6199

2.16 Secondary antibodies used in my experiments

Name	Information
Goat α Mouse HRP	Jackson laboratories 115-035-003
Goat α Rabbit HRP	Jackson laboratories 111-035-144
Goat α Mouse 488	Molecular Probes A-11001
Goat α Human 488	Invitrogen A-11013
Goat α Rabbit 594	Molecular Probes R37117
Goat α Rat 594	Molecular Probes A-11007

3. Characterisation of cell division defects in BE and OEAC cell lines.

Work from Stachler *et al.,* (2015) revealed the genome-doubled pathway (figure 1.6) as one of the two most probable lines of progression from BE into OEAC. In this pathway, loss of TP53 is closely followed by genome duplication resulting in a polyploid population of cells becoming genomically unstable. The subsequent accumulation of mutations in oncogenes and tumour suppressors then continues to drive these cells into malignant tumour formation. Polyploidy has been reported in a number of solid tumours and their pre-malignancies (Ganem, Storchova and Pellman 2007) and it has been previously reported that there are four key events that can result in genome duplication (figure 1.4). Firstly, two cells may fuse together, this occurrence having been linked usually to viral infection; and whilst approximately 1/5 of all cancer cases can be linked to a viral or bacterial infection (zur Hausen 2006) at present there is no evidence to suggest any infectious implication in BE or OEAC. Cells may also become polyploid through endoreduplication; a process by which the genome is doubled in the absence of M phase. Endoreduplication in cancer has been linked to genome instability however evidence from liver cancer suggests that endoreduplication occurs with the loss of the retinoblastoma tumour suppressor (Rb) resulting in polyploid cells that then proceed to lose p53 (reviewed in Fox and Duronio 2013). However, in OEAC progression polyploidy is predicted to occur after p53 loss therefore suggesting that endoreduplication is an unlikely route to genome doubling in this cancer. Finally, a duplicated genome can arise as a product of defective mitosis, either via failure to complete cytokinesis resulting in binucleate

progeny or a failure to progress past metaphase, termed mitotic slippage. In the latter case, rather than transition from metaphase into anaphase, the cell will sustain a prolonged arrest before decondensing the chromosomes back into a G1 nucleus. Both instances result in the formation of cells with a polyploid number of chromosomes. Given the lack of evidence for both viral infection and endoreduplication in BE and OEAC it can therefore be hypothesised that genome doubling observed in BE and its subsequent OEAC tumour might arise as a result of defective mitosis.

3.1. OEAC cells present with abnormal mitotic phenotypes

As a first step to investigate the potential origins of polyploidy in OEAC it is important to establish how BE and OEAC cells behave in mitosis. I specifically selected a panel of BE and OEAC cells to recapitulate the stages of progression from the pre-malignant condition to the carcinoma, with the H-TERT immortalised retinal pigmented epithelium (RPE1) cells being used as an additional control (Table 3.1).

Cell line	Origin	Ploidy	P53 status
RPE1	Retinal epithelium immortalised with H-TERT	Diploid	Wild type
CPA	BE immortalised with H-TERT	Near diploid	Wild type
CPD	Dysplastic BE immortalised with H-TERT	Near tetraploid	Mutated
FLO	OEAC derived from 68 y/o Caucasian male	Near tetraploid	Mutated
JH-Eso-Ad1	OEAC stage 3 - 66 y/o Caucasian male. Moderately to poorly differentiated	Near tetraploid	Mutated
OE19	OEAC stage 3 - 72 y/o Caucasian male. Moderately differentiated	Near tetraploid	Mutated
OE33	OEAC stage 2 - 73 y/o Caucasian female. Poor differentiation	Near tetraploid	Mutated

Table 3.1: Table of cell lines used in my experiments.

I am using RPE1 as a non-cancerous control, these cells have a diploid genome and a wild type p53. The BE control cell line is CPA, these cells are a near diploid cell line with wild type p53. As an intermediate between BE and OEAC I have the cell line CPD which are a dysplastic BE cell line that have mutated p53 and have a near tetraploid genome. FLO, JH-Eso-Ad1, OE19 and OE33 are derived from OEACs at various stages of progression, all are near tetraploid and have a mutated p53 status.

To visualise mitosis, fixed cells were stained for immunofluorescence with the mitotic marker histone H3 pS10, tubulin and DNA, and then counted to calculate the mitotic index (MI). Both BE and OEAC cells had a lower MI compared to RPE1 cells (6.4% n = 352/5467). CPA, CPD and FLO cells had very similar MI values; 4.4% (n = 312/7103), 4.3% (n = 136/3175) and 4.3% (n = 765/17850) respectively, whereas JH-Eso-Ad1 and OE19 had lower MIs of 3.4% (n = 290/7773) and 2.5% (n = 232/9203) respectively. Only the MI for OE33 cells was comparable to RPE1 with a score of 5.6% (n = 311/5520) (figure 3.1A).

Quantification of cells, then categorised according to their mitotic stage: prophase/prometaphase, metaphase, anaphase or cytokinesis, revealed some interesting differences (figure 3.1B). In the majority of the cell lines the highest percentage of mitotic cells were in prophase; RPE1: 36.4% (n= 128/352), CPA: 54.2% (n = 169/312), CPD: 56.6% (n = 77/136), OE19: 45.7% (n = 106/232) and OE33: 44.4% (n = 138/311). By contrast, in FLO and JH-Eso-Ad1 cells the highest percentage of mitotic cells fell in metaphase with 34.6% of FLO (n = 265/765) (vs 31.5% in prophase (n = 241/765)) and 49.2% JH-Eso-Ad1 (n = 128/260) (vs 26.9% prophase (n = 70/260)) in this stage. This increased percentage of metaphase cells coupled with a low mitotic index indicate that these cells spend longer periods in metaphase possibly because of problems in aligning and/or segregating their chromosomes. Therefore, I investigated whether these cell lines presented specific defects during mitosis. I found that up to 10% of mitotic OEAC cells imaged presented with mitotic defects (figure 3.1C) which could be categorized into the following three phenotypes: lagging chromatin, multipolar spindles/ additional centrosomes and failure in chromosome congression, which I will describe as “scattered chromosomes” (figure 3.1D).

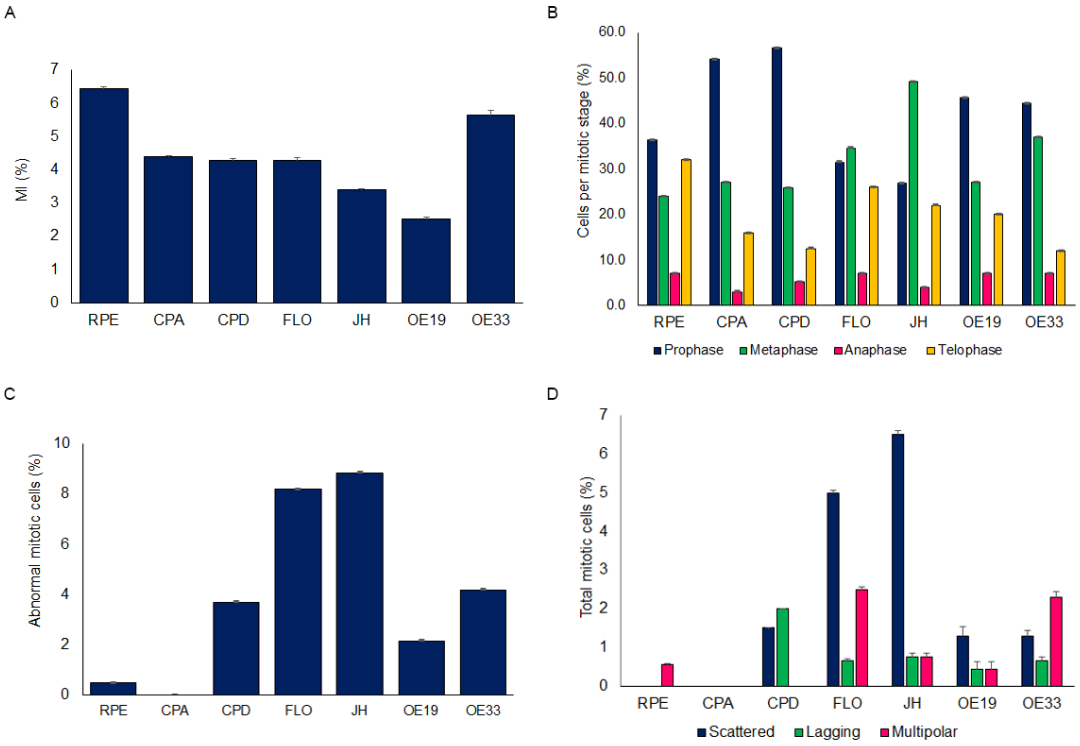

E

	% Mitotic	Prophase	Metaphase	Anaphase	Telophase	% Abnormal	Lagging	Multiple	Scattered
RPE1	6.4	36.9	23.6	7.1	32.4	0.5	0	0.56	0
CPA	4.4	54.2	26.6	3.5	15.7	0	0	0	0
CDP	4.3	56.6	25.7	5.2	12.5	3.7	2.2	0	1.5
FLO	4.3	31.5	34.6	7.2	26.7	8.2	0.7	2.5	5
JH-Eso-AD1	3.4	26.9	49.2	3.9	19.8	8.9	0.8	0.8	6.5
OE19	2.5	45.7	27.2	7.3	19.8	2.2	0.4	0.4	1.3
OE33	5.6	44	37	7	12	4.2	0.6	2.3	1.3

Figure 3.1: Approximately 10% of OEAC cells present with mitotic defects. The percentage of mitotic cells were counted; (A) and categorised by each mitotic stage. (B). The mitotic index counts revealed that approximately 10% of OEAC cells showed abnormalities, (C) which could be categorised into one of three phenotypes: lagging chromatin, multipolar spindles or loss of chromosome organisation over the spindle termed scattered chromosomes: (D). Values from the graphs shown in (E).

Cells with lagging chromatin accounted for 2.2% (n = 3/136) of total mitotic cells in CPD cells, and less than 1% in all other cell lines; RPE1 :0.0%, CPA: 0.0%, FLO: 0.7% (n = 5/765), JH-Eso-Ad1: 0.8% (n = 2/260), OE19: 0.4% (n = 1/232) and OE19: 0.6% (n = 2/311). Similar percentages were recorded for metaphase spindles with additional centrosomes (recorded as multipolar) with 2.5% or fewer total mitotic cells showing this defect; RPE1: 0.6% (n = 2/352), CPA:0.0%, CPD: 0.0%, FLO:

2.5% (n = 19/765), JH-Eso-Ad1: 0.8% (n = 2/260), OE19: 0.4% (n = 1/232) and OE33: 2.3% (n = 7/311). The scattered chromosome phenotype was most prevalent in FLO and JH-Eso-Ad1 cells 5.0% (n = 39/765) and 6.5% (n = 17/260) respectively, and this phenotype was also observed in 1.0% OE33 (n = 3/311) and 0.4% OE19 cells (n = 1/232) as well as the polyploid BE p53 negative cell line CPD (1.5%; n = 2/136). Importantly, this phenotype was not observed in CPA or RPE1 cells, which suggests that it originated after p53 loss and polyploidy. Scattered chromosomes in FLO and JH-Eso-Ad1 cells presented with varying levels of severity; in some cases, the majority of the chromosomes had successfully aligned at the metaphase plate with a few chromosomes remaining at the spindle poles, whereas in other cells there was a complete loss of organisation with chromosomes distributed all over the metaphase spindle (figure 3.2).

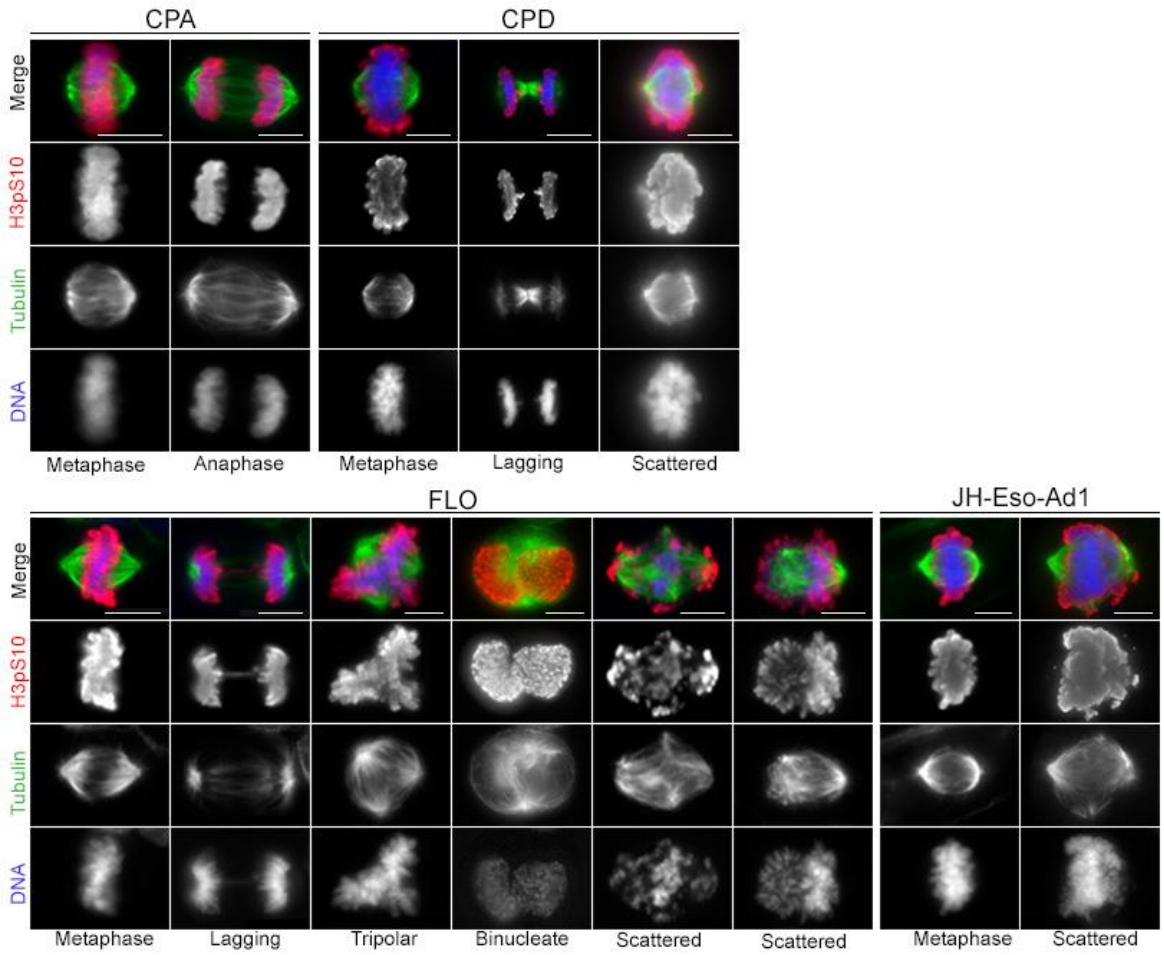

Figure 3.2: Examples of defective mitoses in BE and OEAC cells observed using IF. CPA, CPD, FLO and JH-Eso-Ad1 Cells were fixed and stained for histone H3pS10 (red), tubulin (green) and DNA (blue). Metaphase - chromosomes aligned over a bipolar spindle with no observed defects, anaphase - cells dividing the chromosomes with no observed defects, lagging - lagging chromosomes in anaphase, tripolar - cell dividing with a tripolar spindle, binucleate - cell with two nuclei, scattered - cell in metaphase with scattered chromosomes. Scale bar: 10 µm.

3.2. OEAC cells do not show high levels of multinucleation.

One clear indicator of cytokinesis failure is the presence of cells with multiple nuclei. In order to investigate this as a potential origin of polyploidy in OEAC cells, the number of nuclei in interphase cells was counted from the same slides used to calculate the mitotic index. Neither RPE1 nor CPA had any multinucleate cells (n = 5115 and 7103 respectively), and less than 1.5% of dysplastic BE or OEAC cells had more than one nucleus (CPD = 0.8%; 22/2596, FLO = 0.3%; 51/17799, JH-Eso-Ad1 = 1.4%; 104/8060, OE19 = 0.2%; 12/9191 and OE33 = 0.4%; 19/5501) (figure 3.3). The low percentage of multinucleate cells present in all cell lines would therefore suggest that cytokinesis failure is unlikely to be the predominant route to polyploidy in OEAC.

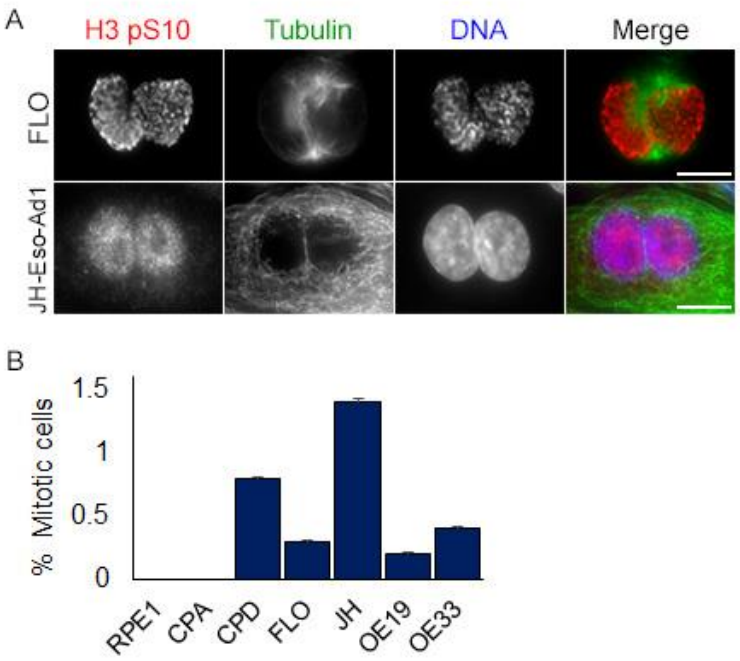

Figure 3.3: Less than 1.5% of BE and OEAC cells have multiple nuclei.
A) Cells were fixed and stained for tubulin, histone H3 ps10 and DNA then the number of cells with multiple nuclei was counted via immunofluorescence. B) Quantification of multinucleate cells across all cell lines. RPE1: 0.0%; CPA: 0.0%; CPD: 0.8%; FLO: 0.3%; JH: 1.4%, OE19: 0.2%; OE33: 0.4%

3.3. Cells with scattered chromosomes have bipolar mitotic spindle

Centrosomes duplicate once every cell cycle to ensure the formation of a bipolar spindle in mitosis (Bornens 2012; Godinho and Pellman 2014), but if a cell fails to complete mitosis the duplicated centrosomes will persist into the next cell cycle. As a result of increased centrosome number, the following mitosis may occur with aberrant, multipolar mitotic spindles (Holland *et al.,* 2012; Marthiens *et al.,* 2013) which in turn can lead to various mitotic defects, including problems in chromosome segregation (Ganem, Godinho and Pellman., 2009, Silkworth *et al.,* 2009). Lopes *et al.,* (2018) investigated if and how centrosome amplification arose in BE and OEAC. They reported that centrosome amplification occurred early on in the progression of BE into cancer, and that this was dependent upon p53 loss. However, the author did not investigate if extra centrosomes caused defects in mitosis. Therefore, I decided to analyse the presence of supernumerary centrosomes in the cell lines I had been working with as some differed from those used in the Lopes study, and whether the presence of extra centrosomes correlated with the chromosome alignment defects observed in OEAC cells. Cells were fixed and stained with antibodies against Plk4 and γ tubulin to mark the centrioles and the respective centrosomes (figure 3.4 A), and analysed and counted by IF (figure 3.4 B).

As expected, the p53 wild-type BE cells (CPA) showed only bipolar spindles with two centrosomes and correctly aligned chromosomes (n = 24) (figure 3.4 B). This was also the case for the dysplastic p53 mutated BE cells (CPD, n = 8). Both FLO and JH-Eso-Ad1 cells had around 10-12% (10.63% n = 6/52 and 10.42% n = 5/48 respectively) of cells with more than two centrosomes, which generated multipolar spindles, but chromosomes congressed normally (figure 3.4). Importantly scattered chromosomes were only observed in cells with two centrosomes and bipolar spindles (FLO: 23.08% n = 12/52 and JH-Eso-Ad1: 14.58% n = 7/33). Together, my results indicate that p53 loss does not immediately cause an increase in centrosome number and multipolar spindles, as is the case of CPD cells. They also show that chromosome misalignment is not linked to the presence of extra centrosomes.

3.4. OEAC cells have a functional mitotic checkpoint.

Having observed cells with mitotic defects it was important to establish whether they had a functional SAC. If the SAC is functional in these cell lines, they should arrest in mitosis in the presence of microtubule depolymerising drugs. BE, OEAC and RPE1 cells were incubated overnight with either 50 ng/ml nocodazole or an equal volume of DMSO as a control, then fixed and stained for DNA, tubulin and histone H3 pS10 to reveal cells in mitosis (figure 3.5 A). Mitotic index counts showed that response to the drug treatment was variable, however all cell lines were able to sustain a mitotic arrest in the absence of microtubules; CPA 1.5% vs 18.7% (n = 41/2659 vs 795/4262; fold increase = 12.5), CPD 1.3% vs 7.8% (n = 17/1327 vs 69/886; fold increase = 6.0), FLO 5.3% vs 56.8% (n = 222/4185 vs 2293/4037; fold increase = 10.7), JH-Eso-Ad1 8.8% vs 36.0% (n = 277/3135 vs 692/1923; fold increase = 4.1) and RPE1 3.0% vs 22.9% (n = 72/2398 vs 356/1555; fold increase = 7.6) of DMSO vs nocodazole treated cells respectively (figure 3.5 B). These results indicate that the spindle assembly checkpoint is functional in all of these cell lines.

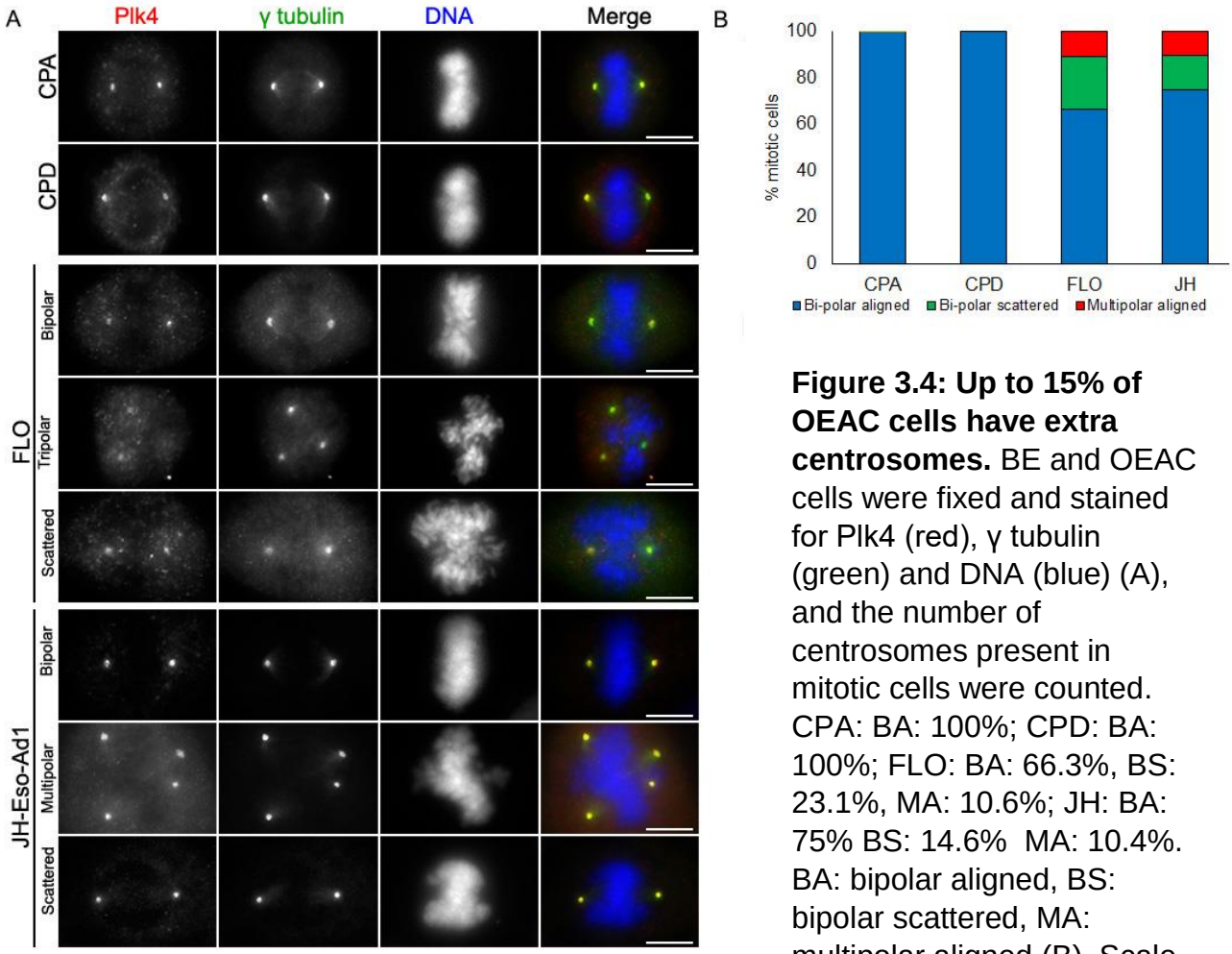

Figure 3.4: Up to 15% of OEAC cells have extra centrosomes. BE and OEAC cells were fixed and stained for Plk4 (red), γ tubulin (green) and DNA (blue) (A), and the number of centrosomes present in mitotic cells were counted. CPA: BA: 100%; CPD: BA: 100%; FLO: BA: 66.3%, BS: 23.1%, MA: 10.6%; JH: BA: 75% BS: 14.6% MA: 10.4%. BA: bipolar aligned, BS: bipolar scattered, MA: multipolar aligned (B). Scale bar 10 μm.

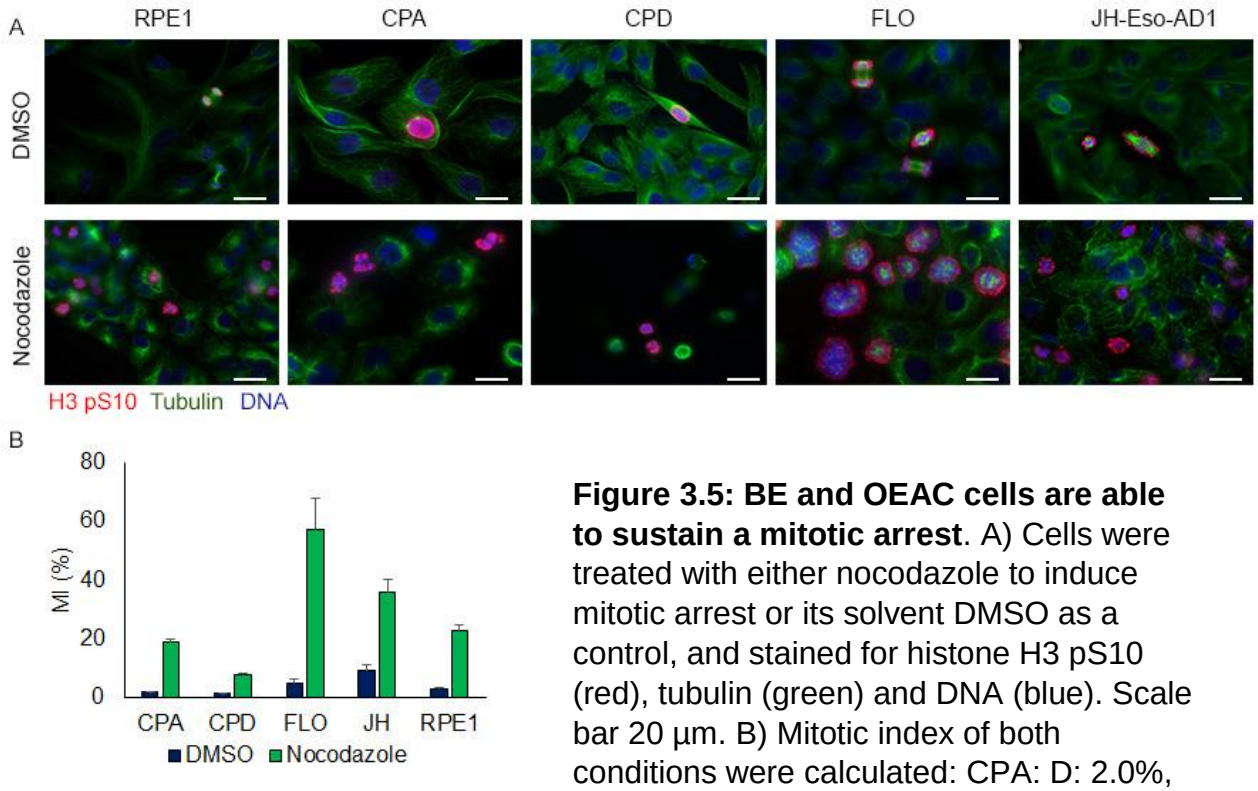

Figure 3.5: BE and OEAC cells are able to sustain a mitotic arrest. A) Cells were treated with either nocodazole to induce mitotic arrest or its solvent DMSO as a control, and stained for histone H3 pS10 (red), tubulin (green) and DNA (blue). Scale bar 20 µm. B) Mitotic index of both conditions were calculated: CPA: D: 2.0%, N: 19.0%; CPD: D: 1.3%, N: 7.8%; FLO: 5.0%, N: 57.0%; JH: D: 9.0%, N: 36.0%; RPE1: D: 3.0%, N: 23.0%. D: DMSO, N: nocodazole.

3.5. OEAC cells experience mitotic slippage

Having observed numerous mitotic defects in both BE and OEAC fixed cells it was important to investigate if and how these defects affected progression through mitosis by time-lapse microscopy. CPA, FLO and JH-Eso-Ad1 cells, we could not film CPD cells because for reasons currently unknown they did not survive in our experimental set up, were treated with a SiR-DNA dye (Cytoskeleton) to visualise chromosomes and then recorded at five-minute intervals for eight to ten-hour periods. Cells were then scored based on their progression through mitosis (figure 3.7 B). As predicted all recorded CPA cells (90.0% n = 27/30) progressed without any defects (figure 3.6 A, supplementary movie 01). A small percentage of CPA cells progressed through mitosis with lagging chromosomes (6.7% n=2/30) (figure 3.6 B, supplementary movie 02) and one cell failed to complete cytokinesis, which is most likely due to recording conditions rather than truly defective mitosis.

Similar to the results observed in the fixed cells 72.% (n = 13/18) of FLO cells divided normally, 5.6% (n = 1/18) divided with multipolar spindles, 11.1% (n = 2/18) had lagging chromosomes (figure 3.6 C, supplementary movie 03) and 11.1% (n = 2/18) experienced mitotic slippage, in which the cells entered G1 of the next cell cycle without having completed M phase (figure 3.7 B). These cells were able to establish a metaphase plate however it appeared less focused than those observed in controls, indicating chromosome congression defects. These cells then spent up to three hours in metaphase with no visible signs of anaphase onset, following which the chromosomes appeared to decondense and a nucleus reformed (figure 3.6 D, supplementary movie 04).

This mitotic slippage was also observed, with even higher frequency, in JH-Eso-Ad1 cells (28.6% n = 2/7) (figure 3.7 B). Cells that failed to progress past metaphase appeared to have congressed their chromosomes at the equator, forming a well-defined metaphase plate, after approximately 30 minutes after NEB. The cells then appeared to remain in this phase for about 90 minutes until the chromosomes began to drift away from this alignment. In one case six hours after the chromosomes began to drift from the metaphase plate, they attempted to realign but this was unsuccessful and, by the end of the recording period (eight hours), the cell had begun to decondense the chromosomes indicating a possible cohesion defect (figure 3.7 A, supplementary movie 05). The final 14.3% (n = 1/7) of JH-Eso-Ad1 cells imaged failed to complete cytokinesis. The n value for the JH-Eso-Ad1 cells is marginally lower than that for the other two cell lines as these cells were incredibly difficult to image. A number of troubleshooting experiments were performed in order to establish optimal conditions for the cells, but the majority of the cell population would die during or even prior to filming for reasons currently unknown. Further testing would need to be carried out to get a more robust sample size for this cell line.

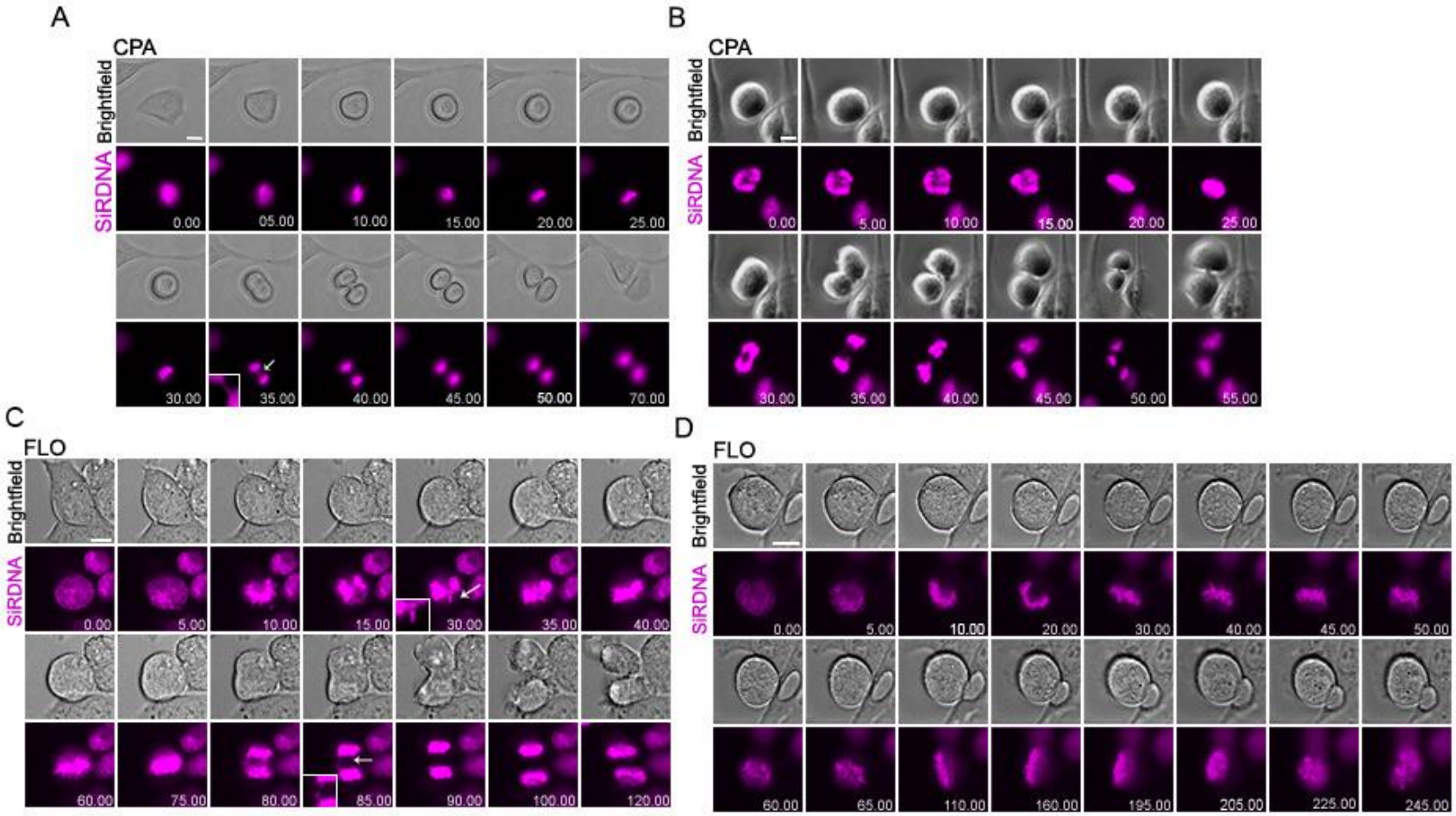

Figure 3.6: CPA and FLO cells show defects in mitosis. CPA and FLO cells were treated with a SiR-DNA dye and imaged via time lapse microscopy. Images were captured at 5 minutes intervals for 8-10 hours. A) Normal mitosis and B) lagging chromosomes (white arrow/insert) in CPA cells. C) Lagging chromosomes and D) cells proceeding into the next G1 phase without completing mitosis (mitotic slippage) in FLO cells.

Scale bar 10 µm

From the movies I also calculated the average length of mitosis and found that OEAC cells took at least twice as long to divide than BE cells. CPA cells took an average of 58 ± 14 minutes, FLO cells 103 ± 31 minutes and JH-Eso-Ad1 212 ± 19 minutes. I also observed that proportionally FLO and JH-Eso-Ad1 cells spent longer from NEB-metaphase than CPA cells (FLO 69 ± 22 minutes 67% of total time in mitosis, JH-Eso-Ad1 147 ± 91 minutes 69% of total time in mitosis and CPA 24 ± 8 minutes 41% of total time in mitosis) (figure 3.7 C). These data would therefore provide further evidence that FLO and JH-Eso-Ad1 cells are spending longer in metaphase, as indicated by the increased proportion of mitosis spent between NEB and anaphase onset, which could be owing to problems in chromosome congression which in turn could lead to mitotic slippage. Note that RPE1 was not used in the time lapse experiments as at this stage I was interested in directly comparing the mitotic profiles of non-dysplastic BE cells and tetraploid OEAC cell lines to establish how the defective mitotic figures effected cell cycle progression.

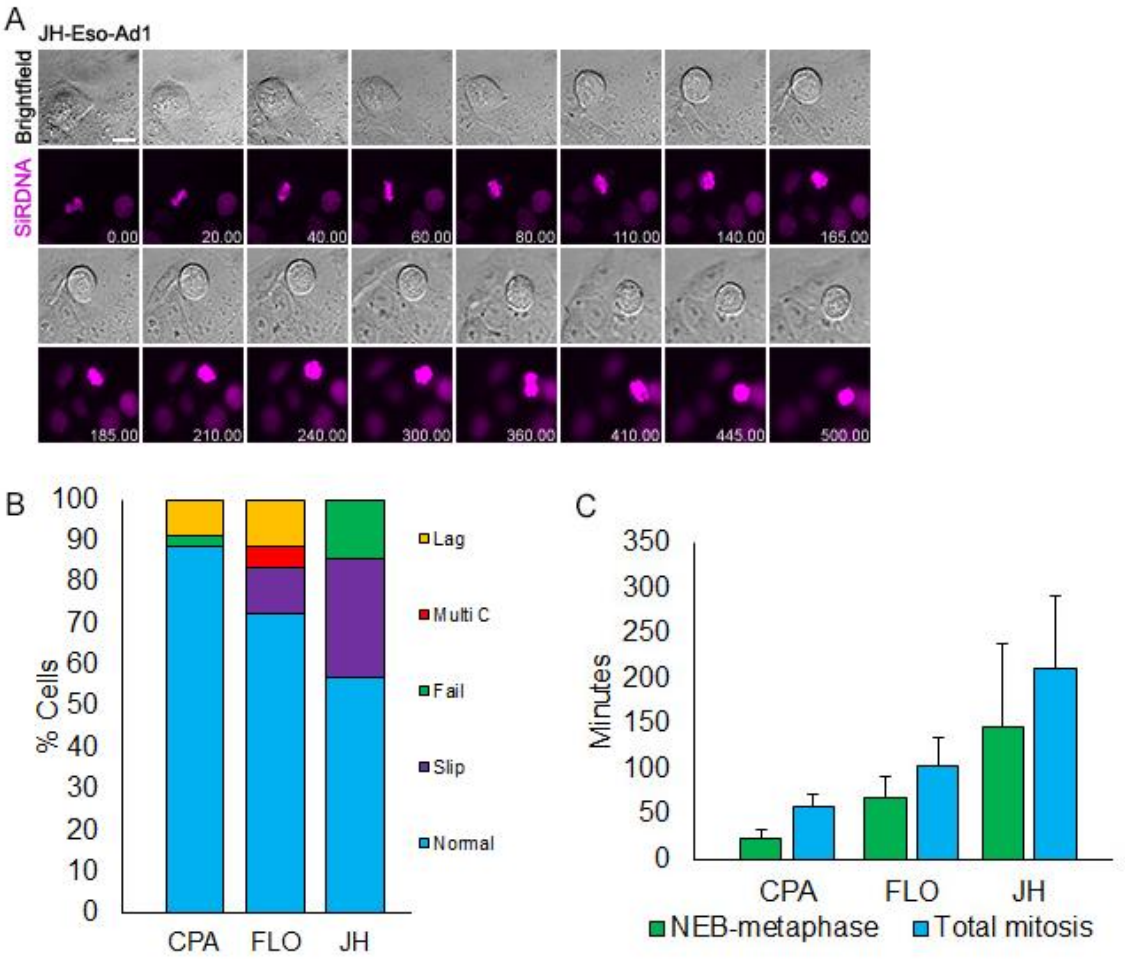

Figure 3.7: JH-Eso-Ad1 cells exhibit mitotic slippage. Cells were recorded as detailed in figure 12. A) Mitotic slippage in JH-Eso-Ad1 cells. B) Mitoses were quantified in CPA, FLO and JH-Eso-Ad1 cells. Lag: lagging chromosomes (L) Multi C: multiple centrosomes (M), fail: cytokinesis failure (F), slip: mitotic slippage (S) and normal: normal bipolar mitosis (N). CPA: L: 8.6%, M: 0.0%, F: 2.9%, S: 0.0%, N: 0.0%; FLO: L: 11.1%, M: 5.6%, F: 0.0%, S: 11.1%, N: 72.2%; JH: L: 0.0%, M: 0.0%, F: 14.3%, S: 28.6%, N: 57.1% C) Duration of mitosis and NEB-metaphase was counted. Total mitosis was counted from the five minute intervals from the first indication of chromosome condensation to the final separation in telophase. Within this the duration from NEB to the first separation of the chromosomes signifying the onset of anaphase to indicate whether cells were experiencing metaphase arrest. Scale bar 10µm. CPA: NEB-Meta: 24 mins, total mitosis: 58 mins; FLO: NEB-Meta: 69 mins, total mitosis 103 mins; JH: NEB-Meta: 147 mins, total mitosis: 212 mins. N values are so low owing to the difficulty in maintaining cells under microscopy conditions, indicating the need for further trouble shooting to achieve a greater sample population.

3.6. OEAC organoids have scattered chromosomes

One current limitation to the study of OEAC is the lack of a model system that accurately represents the primary disease state. A number of 2D cell lines presently exist and these currently make up the most widely used model for OEAC research. However, the main issue with relying on only the cell lines, is that many of them lack the genomic characterisation found in their originating primary tumour and that there is little to no germline data available for these lines (Contino *et al.,* 2016). The cell lines are capable of recapitulating the OEAC tumour to an extent, but culturing them over numerous passages have led them to become unrepresentative with regards to the mutational signature of the original tumour (Contino *et al.,* 2016; Boonstra *et al.,* 2007). Work carried out in the lab of Professor R. Fitzgerald aimed to overcome this issue through the generation of a number of OEAC organoids. The use of organoids as a model system overcomes the limitations of the 2D culture model because of its stability in culture, flexibility in manipulation and faithful representation of the OEAC primary tumour from which it was derived (Li *et al.,* 2018). Therefore, I decided to confirm and further validate my findings from 2D cell lines by investigating whether OEAC organoids presented similar mitotic defects. In collaboration with Dr X. Li from the Fitzgerald lab a number of organoids with various ploidy states (table 3.2) were grown for investigation.

Organoid name	Origin and information
NG088	Normal gastric organoid with wild type p53 and a diploid genome.
277	Derived from 80 y/o female, poorly differentiated. Tetraploid genome. Ploidy of 4.04 indicating this organoid has experienced WGD (WGD threshold is 2.11)
401	Derived from 77 y/o female, poorly differentiated. Aneuploid genome, ploidy of 1.74 (threshold for WGD is 2.19 P53 negative. FISH indicates structural chromosomal instability.
408	Derived from 60 y/o male, moderately differentiated. Aneuploid, Overall ploidy scored 1.94 (threshold for WGD is 1.94) P53 negative.
468	P53 negative. Ploidy status unknown.
423	P53 negative, tetraploid. Ploidy 4.48 indicating this organoid has experienced WGD (WGD threshold is 1.93).

Table 3.2: Table of organoids used in my experiments. NG088 is the control organoid as it's derived from non-cancerous cells from the stomach, the other organoids are all derived from OEAC tumours the majority of which are aneuploid. All cultures are mixed heterogenous populations composed of cells with a variety of changes in chromosome number as well as chromosome rearrangements. For further information on organoid derivation see supplementary information from Li *et al.,* 2018. (Li *et al.,* 2018, Li and Fitzgerald personal communication).

All organoids were grown by Dr X Li, from samples obtained by oesophagectomy and included one derived from healthy gastric tissue. The normal gastric organoid (NG088) showed all the characteristics of the normal glandular epithelium with wild-type sequence p53 expression and mutational sequence and was therefore used as our control organoid (Li *et al.,* 2018). Genome sequencing of the organoids revealed chromosomal amplifications in a number of the samples, with organoids 277 and 401 showing amplifications on chromosome 12, and organoid 408 amplifications on chromosome 20 (Li *et al.,* 2018). Further karyotypic analysis of the organoids also indicated that a number of the cells were aneuploid and that all cultures were composed of mixed heterogeneous populations that had a variety of numerical and structural chromosomal rearrangements (Li *et al.,* 2018). In collaboration with Dr X Li who provided fixed organoid samples, we analysed the

types of mitotic figures present in the organoids by IF staining for tubulin, CREST to mark the centromeres, and DNA (figure 3.8 A). We also tried to stain for NDC80 but unfortunately this antibody could not penetrate the entire organoid. Quantification of the types of mitotic figures showed that 95% of the spindles from normal gastric organoids had bipolar spindles with correctly congressed chromosomes (n=19/20) and only 5% had a multipolar spindle (n=1/20). Similar to the data collected from cell lines, the most prevalent mitotic aberrations were multipolar spindles and scattered chromosomes (figure 3.8 B/C). With the exception of organoid 423, multipolar spindles were present in at least 10% of observed mitoses; 277: 20% (n=4/20), 401: 10% (n=2/20), 408: 30% (n=6/20) and 468: 10% (n=2/20). The incidence of scattered chromosomes was lower than multipolar spindles, but still comparable to the cell line data; 401: 10% (n=2/20), 408: 5% (n=1/20), 468: 5% (n=1/20) and 423: 20% (n=4/20). No scattered chromosomes were observed in organoid 277. The data from this experiment would therefore indicate that the mitotic defects, including scattered chromosomes, can be seen in both primary tumour derived organoid and cell lines.

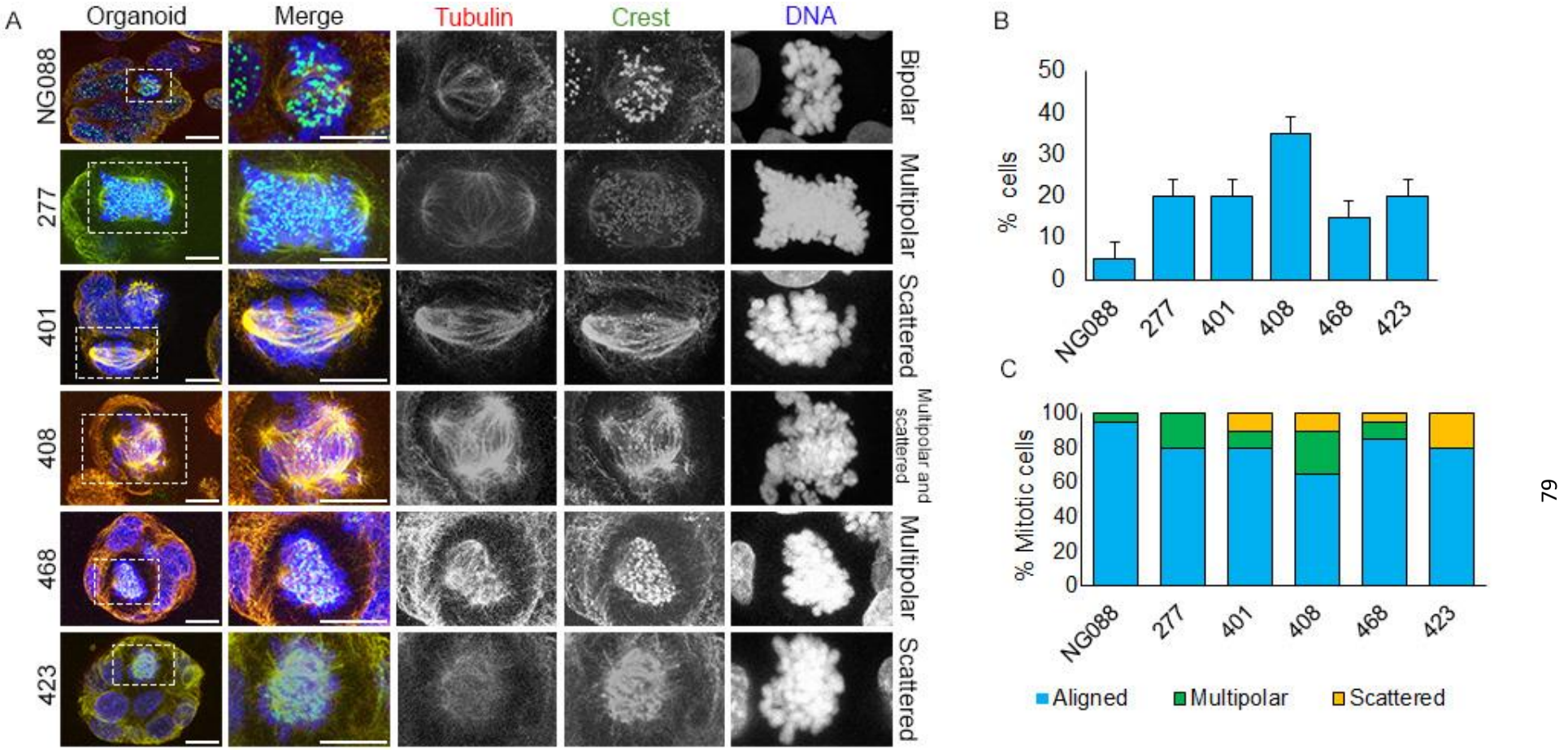

Figure 3.8: Scattered chromosomes are present in OEAC organoids. A) Chromosome alignment in organoids from normal gastric and OEAC origin were fixed and stained for DNA (blue), tubulin (red) and CREST to mark the centromere (green). B) Instance of defective mitoses were counted: NG088: 5%; 277: 20.0%; 401; 20.0%; 408: 35.0%; 468: 15.0%; 423: 20.0% C) Organoids were quantified based on their phenotype: NG088: A: 95.0%, M: 5.0%, S: 0.0%; 277: A: 80.0%, M: 20.0%, S: 0.0%; 401: A: 80.0%, M: 10.0%, S: 10.0%; 408: A: 65.0%, M: 30.0%, S: 5.0%; 468: A: 85.0%, M: 10.0%, S: 5.0%; 423: A: 80.0%, M: 0.0%, S: 20.0%. A: aligned, M: multipolar, S: scattered. Scale bar: 10 µm.

4. Kinetochore gene changes and protein expression in BE and OEAC cells.

4.1. Whole genome sequencing (WGS) of BE and OEAC cell lines and primary tumours shows numerous copy number changes in important kinetochore genes.

Sequencing studies, both exome and whole genome, have shown that OEAC has a high mutational burden (Alexandrov *et al.,* 2014). OEAC has a high number of copy number alterations and large-scale chromosomal rearrangements and many OEACs lack, with the exception of TP53 loss, a clear mutation that could drive oncogenesis (Weaver *et al.,* 2014; Dulak *et al.,* 2013, Nones *et al.,* 2014).

Data presented in the previous chapter would suggest that the potential cause and/or consequence of polyploidy in OEAC cells might be cell division failure due to mitotic slippage, triggered by a prolonged metaphase arrest with chromosome alignment defects. For this reason, and also because RNAi of kinetochore genes caused similar “scattered chromosome” phenotypes, I decided to investigate in more detail the kinetochore genes and protein expression in BE and OEAC cells.

4.1.1. Sequencing of primary tumours

WGS of primary OEAC tumours performed by the Fitzgerald lab has provided information regarding the copy number status of numerous important kinetochore and centromere genes (supplementary tables 01 and 02). The sequencing covered 347 OEAC tumours matched with normal samples and gave information regarding copy numbers that have been categorised by their mutational status (table 4.1).

Copy number category	Criteria
Copy number neutral (CN_neutral); no overall change in copy number.	Minor copy number > 0, relative copy number > -1 but < 1.
Copy number neutral loss of heterozygosity (CN _LOH); cross chromosomal event that has resulted in no overall change in copy number.	Minor copy number = 0, relative copy number > -1 but < 1.
Copy number gain (Gain); gene number has increased.	Minor copy number > 0 and relative copy number > 1.
Copy number gain loss of heterozygosity (Gain_LOH); cross chromosomal event that has led to an overall increase in copy number.	Minor copy number = 0 and relative copy number > 1.
Loss; gene number has decreased	Minor copy number > 0 and relative copy number is < -1.
Hemizygous deletion with loss of heterozygosity (Hemizygous_LOH); only one copy of the chromosome is present.	Minor copy number = 0 and relative copy number is < -1.
Deletion; gene no longer present.	Copy number = 0

Table 4.1: Descriptions of copy number status. Genes have been classed as one of the following: copy number neutral (CN_neutral) in which the overall copy number remains unchanged; copy neutral loss of heterozygosity (LOH) in which LOH occurs with no net change in copy number; copy number gain; copy number gain with LOH ; loss; hemizygous deletions with LOH or deletion. According to the criteria, minor copy number refers to the number of copies of the least frequent allele, i.e. ABB - minor allele A copy number equals 1, and major allele B copy number equals 2, the sum of which giving an overall copy number of 3. The relative copy number equals log2 of total copy number/tumour ploidy.

From the WGS data I extracted copy number information for the KMN complex genes Ndc80, Nuf2, Spc24, Spc25, Mis12, Dsn1, Nnf1, Nsl1 and Knl1 from all pair matched samples (supplementary table 03). Looking at the copy numbers and their status it became clear that the most affected subcomplex of the KMN was the Ndc80 complex. The Ndc80 complex showed the highest percentage of pairs with copy number (CN) loss of heterozygosity (LOH). LOH can be defined as a cross

chromosomal event that results in the loss of an entire gene and its surrounding chromosomal region (Joseph *et al.,* 2014). LOH is a common occurrence in cancer as it can induce the absence of tumour suppressor genes. Up to approximately 30% of pairs featured LOH alongside copy number changes in this complex: Ndc80 27.95% (n = 97/347), Nuf2 10.66% (n = 37/347), Spc24 30.26% (n = 105/347) and Spc25 15.85% (n = 55/347). With regards to the other KMN genes it was clear that the gene that most frequently presented CN neutral LOH was Mis12 as 71.76% (n = 249/347) of the paired samples showed this change (Dsn1 4.03% n = 14/347, Nnf1 4.61% n = 16/347, Nsl1 13.54% n = 47/347 and Knl1 24.50% n = 85/347). Approximately 6% of pairs also reported copy number gains in Ndc80 (n = 22/347) however the greatest frequency of copy number gains was reported for the Mis12 complex subunit Dsn1 (10.37% n = 36/347). 1.73% of pairs reported gains in Nuf2 (n = 3/347), 0.86% in Spc24 (n = 3/347), 0.29% in Spc25 and Nsl1 (n = 1/347), 0.86% in Mis12 (n = 3/347) and 4.61% in Nnf1 (n = 16/347). Hemizygous deletions with LOH and copy number losses occurred much less frequently, only being present for Ndc80 (4.32% n = 15/347), Spc24 (2.02% n = 7/347), Spc25 (0.86% n = 3/347), Mis12 (3.17% n = 11/347) and Knl1 (2.59% n = 9/347). Finally, losses were found in less than 0.3% of pairs for Ndc80, Spc25, Mis12 and Knl1 (all 0.29% n = 1.347) and they were not present in the other KMN genes.

A subset of the CN data can be seen in figure 4.1, in which 20 random pairs were selected in order to illustrate the differences in CN within the KMN network constituents. The graphs illustrate the copy numbers identified in this random data set and shows how many paired samples presented this copy number, i.e. for Ndc80 one pair showed a copy number of one for this gene, and it presented with LOH (coloured yellow). Within these 20 random pairs there have emerged some clear patterns for example; in the Mis12 data set, despite the majority of the pairs (14/20) having a copy number of two for this gene approximately 71% (10/14) presented with LOH. From the data I was also able to identify if any of the genes in the KMN network showed any large increases in copy number and hence found that in the 20 pairs selected for Dsn1 copy numbers ranging from one to thirteen were present, with approximately 35% of the samples reporting a gain (5/14 coloured green). When analysing this data with regard to the KMN as a whole there are pairs that appear to have an entirely balanced KMN with almost all genes having a CN of two

(i.e. pairs LP6008336-DNA_E03 vs 333-DNA_E03 and LP6008031-DNA_A03 vs 032-DNA_E03 see supplementary table 03 for full data set), yet there are also pairs that have extreme CN differences. One example of which CN can be seen in pair LP6005500-DNA_C02 vs 449-DNA_C02; which shows a range of CN from two to eleven with a number of alterations including LOH and gain. This pattern of copy number variation is present in the majority of the sequenced pairs and would therefore provide further evidence for an imbalance in the copy numbers of the kinetochore components in OEACs.

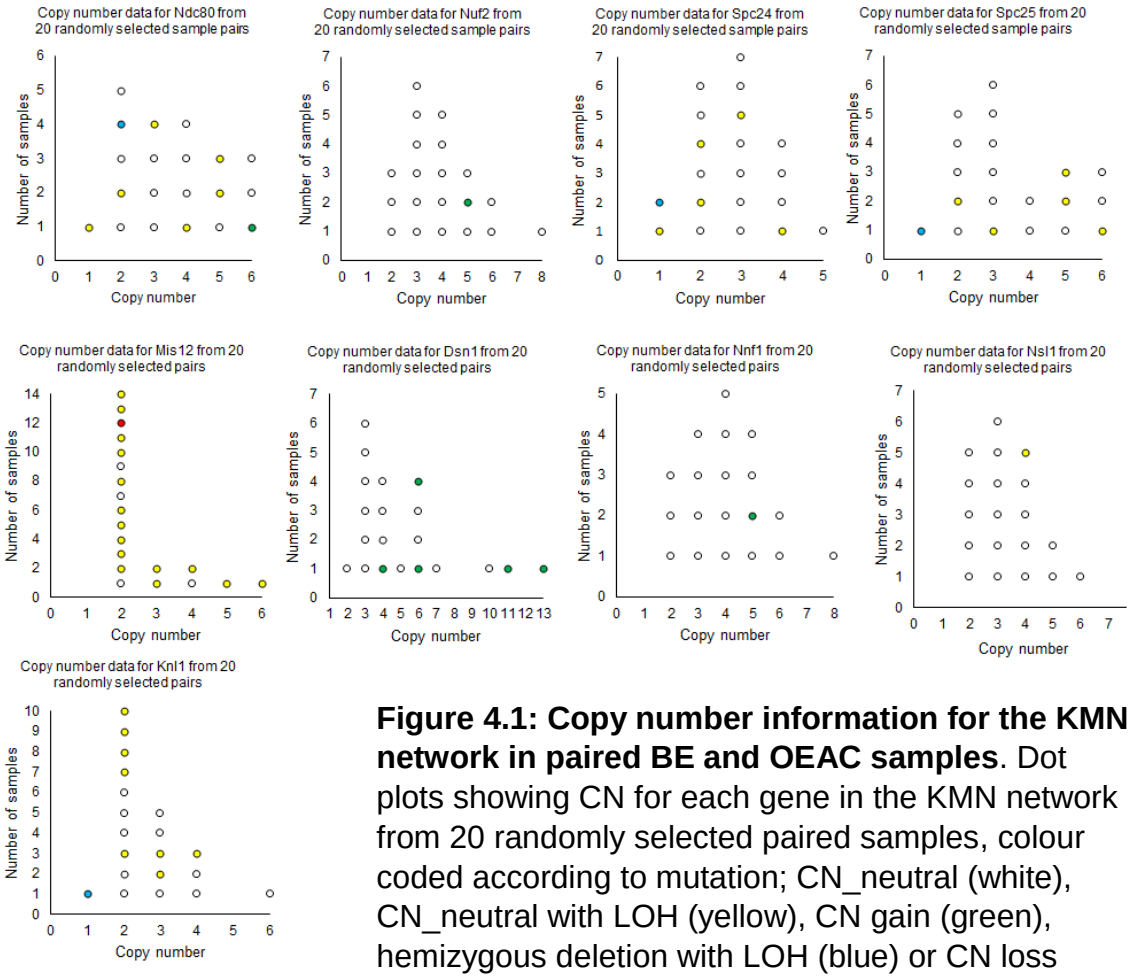

Figure 4.1: Copy number information for the KMN network in paired BE and OEAC samples. Dot plots showing CN for each gene in the KMN network from 20 randomly selected paired samples, colour coded according to mutation; CN_neutral (white), CN_neutral with LOH (yellow), CN gain (green), hemizygous deletion with LOH (blue) or CN loss (red).

From the WGS data I also examined the copy number alterations for the CENP genes including the 16 CCAN subunits, plus the gene encoding motor protein CENP-E and the other CENP genes CENP-F and CENP-V (supplementary table 04). In this data set it is clear that the genes most commonly scored as CN neutral with LOH were the CCAN component CENP-I, and CENP-V along with its related genes CENP-V1 and CENP-V3. CN neutral LOH was present for CENP-I in 59.08% of pairs (n = 205/347), CENP-V in 66.57% (n=231/347), CENP-V1 in 52.74% (n = 183/347) and CENP-V3 in 53.31% of pairs (n = 185/347). CENP-V, -V1 and CENP-V3 also featured in frame deletions in less than one percent of pairs (V/-V1/-V3: 0.58% n=2/347). Unlike in the KMN network, copy number changes featuring hemizygous deletions with LOH occurred in a much higher percentage of the paired samples with, for example, 40.97% of pairs having a hemizygous LOH deletion in CENP-V1.

As I did for the KMN, I selected twenty (different) pairs at random to highlight the variations in the copy number of genes within the CCAN complex (Figure 4.2). Within this data the CN alterations of CENP-I, CENP-V1 and CENP-V3 were again stand out compared to the other CENP genes. In 40% (8/20) of pairs randomly sampled CENP-I had a copy number of 1, of which 62.5% (5/8) presented with a hemizygous deletion and 37.5% (3/8) with LOH. Similarly CENP-V1/V3 (data presented on the same graph) showed that 35% (7/20) of the random pairs had a CN of 1, of which 57% (4/7) had a hemizygous deletion and 43% (3/7) showed LOH. Evidence for genome doubling can be seen in a number of genes in which the majority of samples selected presented with a CN of 4 including: CENP-A (40% 8/20), CENP-B (50% 10/20), CENP-M (40% 8/20), CENP-O (50% 10/20), CENP-Q (35% 7/20) and CENP-X (55% 11/20), however unlike when the copy number was decreased, the majority of these samples were recorded as CN neutral.

Observations of the individual pairs (highlighted in supplementary table 04) there is a pair that features genes that are CN neutral, CN neutral with LOH, genes that have hemizygous deletions with LOH, in-frame deletions and gains and copy numbers that range from 0-7 (pair LP6008334-DNA_F03 vs LP60008335-DNA_B03) indicating a vast number of CN alterations within the CCAN between BE and OEAC. Within these twenty pairs the highest copy number recorded was 10 (pair LP6005690-DNA_C03 vs LP6005689-DNA_C03 CENP-B) however in the whole

data set copy numbers up to 27 could be observed (pair LP6005409-DNA_C01 vs LP6005408-DNA_C01 CENP-Q).

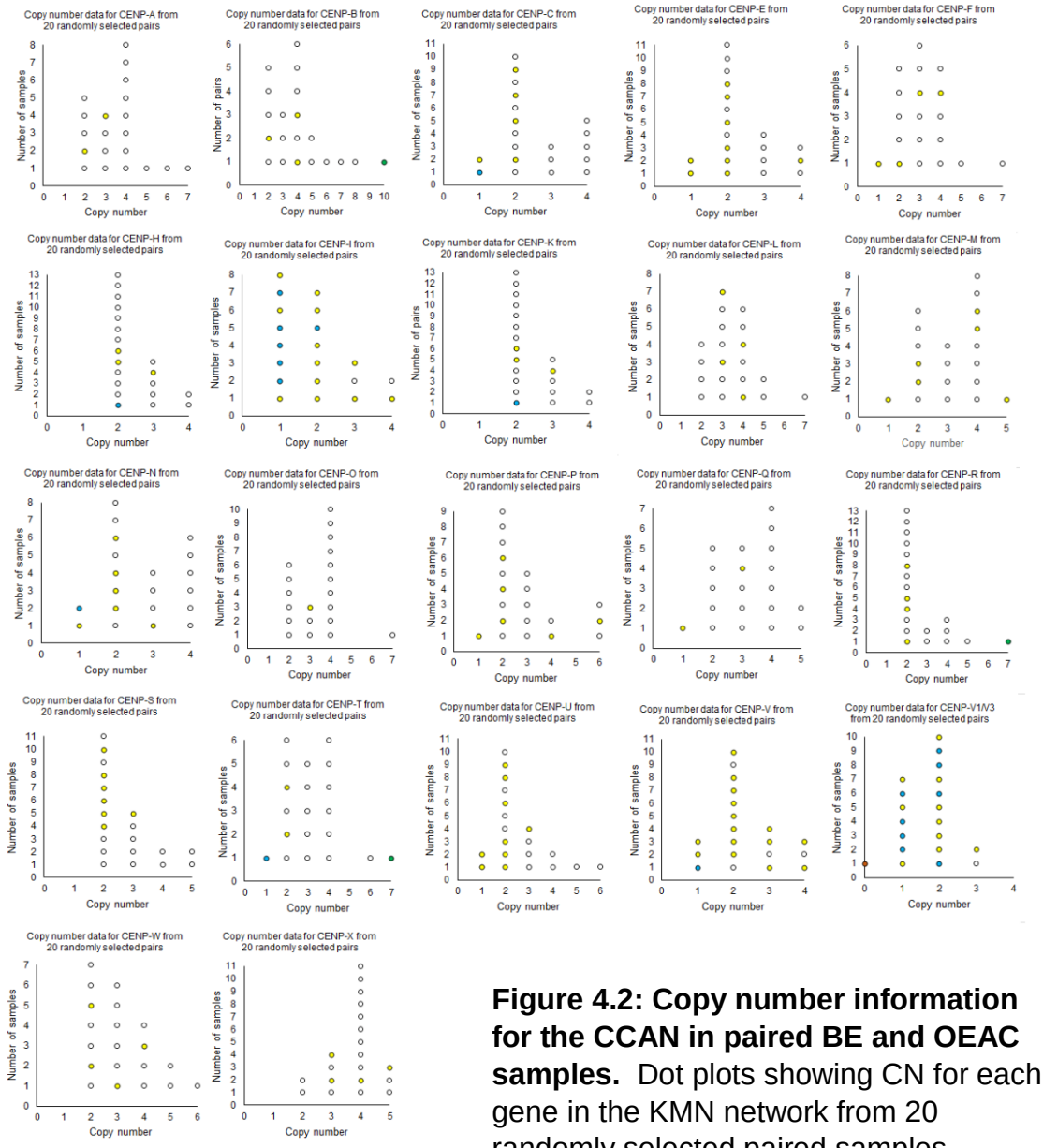

Figure 4.2: Copy number information for the CCAN in paired BE and OEAC samples. Dot plots showing CN for each gene in the KMN network from 20 randomly selected paired samples, colour coded according to mutation; CN_neutral (white), CN_neutral with LOH (yellow), CN gain (green), hemizygous deletion with LOH (blue) or in frame deletion (orange).

I next looked at the sequencing data for the SAC components Mad1, Mad2, Bub1 and BubR1 (supplementary table 05), the CPC subunits Aurora B, Borealin, Survivin and INCENP (supplementary table 06), the Ska complex Ska1, Ska2 and Ska3 (supplementary table 07), then finally I looked at a selection of phosphoprotein phosphatases (supplementary table 08). Starting with the SAC, as per the KMN and the CCAN the most prevalent change was LOH, this affecting 10.1% (35/347) of pairs for Mad1, 36.6% (127/347) for Mad2, 11.8% (41/347) for Bub1, and 27.1% (94/347) for BubR1. Hemizygous deletions in Mad2 were also apparent in 5.2% of pairs. In reference to copy number the highest observed was seen in Mad1 in which one pair had 25 copies (LP6008280-DNA_C01 vs LP600264-DNA_C01 (supplementary table#). Looking at a representative subset of data for the SAC genes (figure 4.3) the majority of pairs selected presented with a CN of 2 (approximately 50% for each gene) however between 20-35% of pairs had a CN of 3 thus indicating potential genomic alterations.

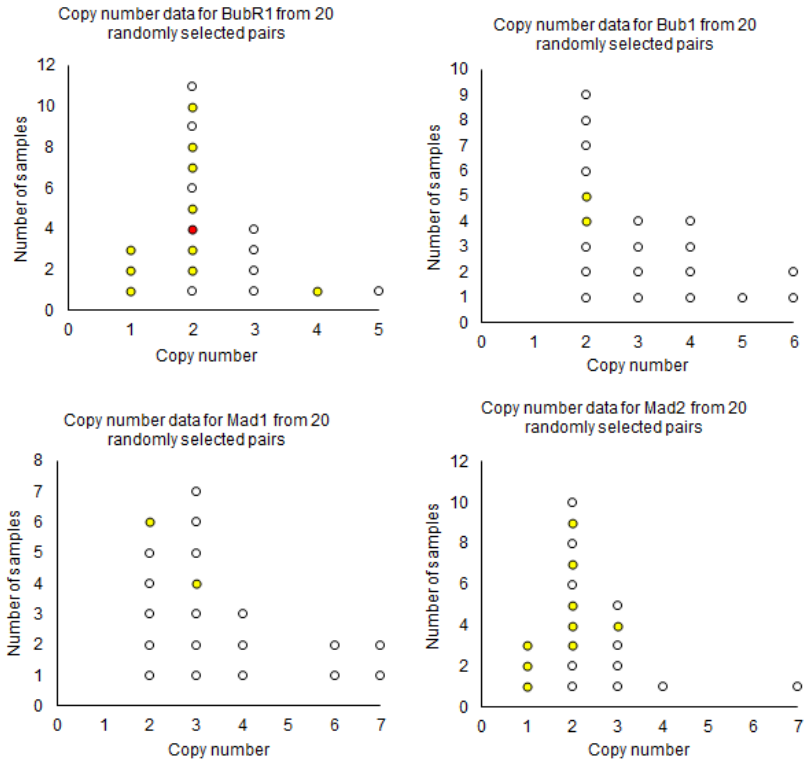

By far the most affected gene of the CPC was Aurora B; LOH was observed for Aurora B in 71.7% (248/347) of pairs sequenced, this being over 3 fold greater

Figure 4.3: Copy number information for the SAC in paired BE and OEAC samples. Dot plots of SAC genes from twenty randomly selected pairs colour coded according to mutation; CN_neutral (white), CN_neutral with LOH (yellow), CN loss (red).

than the percentage LOH observed for the other CPC constituents. Aurora B also showed the highest percentage of hemizygous deletions, this being present in 3.8% (13/347) of all pairs. Other chromosomal aberrations including losses and gains were only observed in approximately 1% of pairs for all four CPC members. Looking at copy number alterations, the highest copy number was observed for Survivin which had been amplified to 69 in pair LP6008031-DNA_F03 vs LP6008032-DNA_H01 (supplementary table 05). The CN information for 20 randomly selected pairs (figure 4.4) showed that despite the genomic alterations i.e. LOH a large percentage of the pairs still had a CN of 2, however for each gene up to 40% of the pairs selected had a CN of 3 (Survivin, 8/20), up to 15% had a CN of 4 (Aurora B and INCENP 3/20)

and up to 20% showed a CN of 5 (Borealin 4/20). This sample would therefore reinforce there being a range of CN alterations in relation to the CPC which could potentially impact its function at the KT.

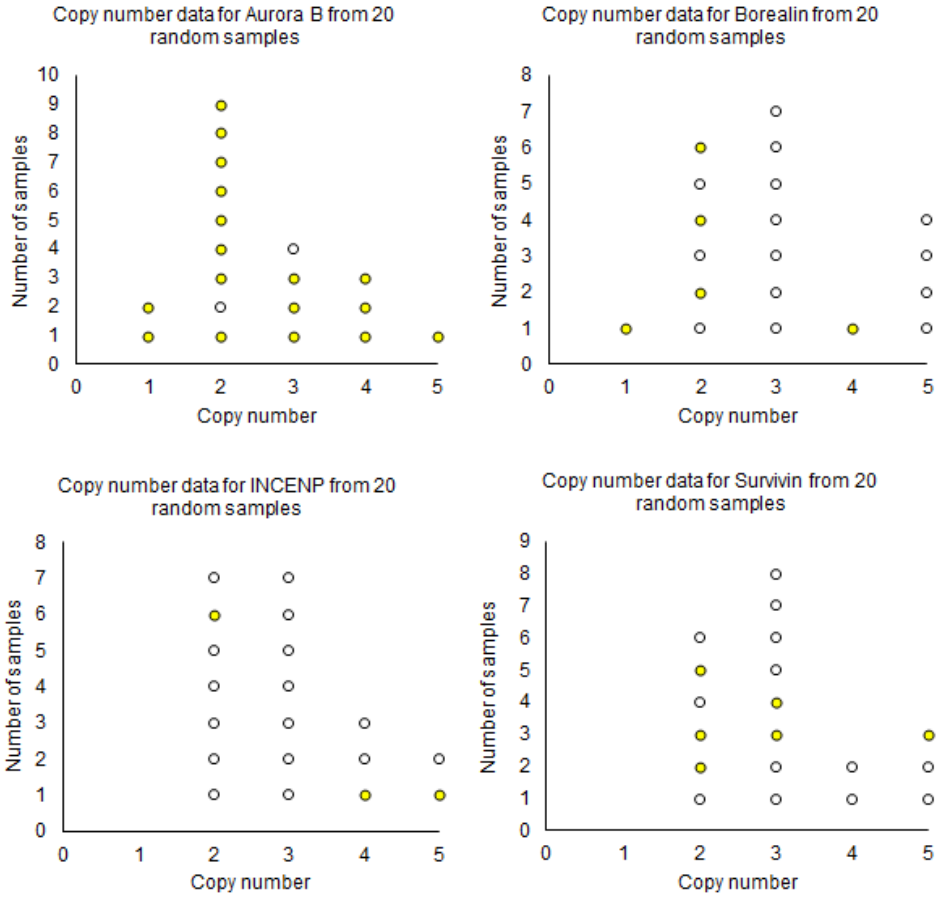

Figure 4.4: Copy number information for the CPC in paired BE and OEAC samples. Copy numbers of CPC genes in twenty randomly selected pairs colour coded according to mutation; CN_neutral (white), CN_neutral with LOH (yellow).

The sequencing data for the MT binding SKA complex (supplementary table 07) indicated that CN aberrations are most prevalent in the SKA1 subunit; 23.9% (83/347) of pairs had a hemizygous deletion and 35.7% (124/345) showed LOH. The instance of LOH was similar for both SKA2 and SKA3 (26.8% 93/347 and 22.8% 79/347 respectively) however hemizygous deletions appeared much less frequently in these subunits (1.4% 5/347 and 1.7% 6/347 respectively). Observations of a subset of the SKA data shows that despite presenting these aberrations 50% (10/20) of the samples had a CN of 2 for SKA1, and between 25-40% of the randomly selected pairs had a CN of 3. Some extreme increases in CN were also observed from this data set with a CN of 7 present for SKA2, 8 for SKA3 and as high as 22 for SKA1 thus indicating that WGD may have occurred in these samples (figure 4.5)

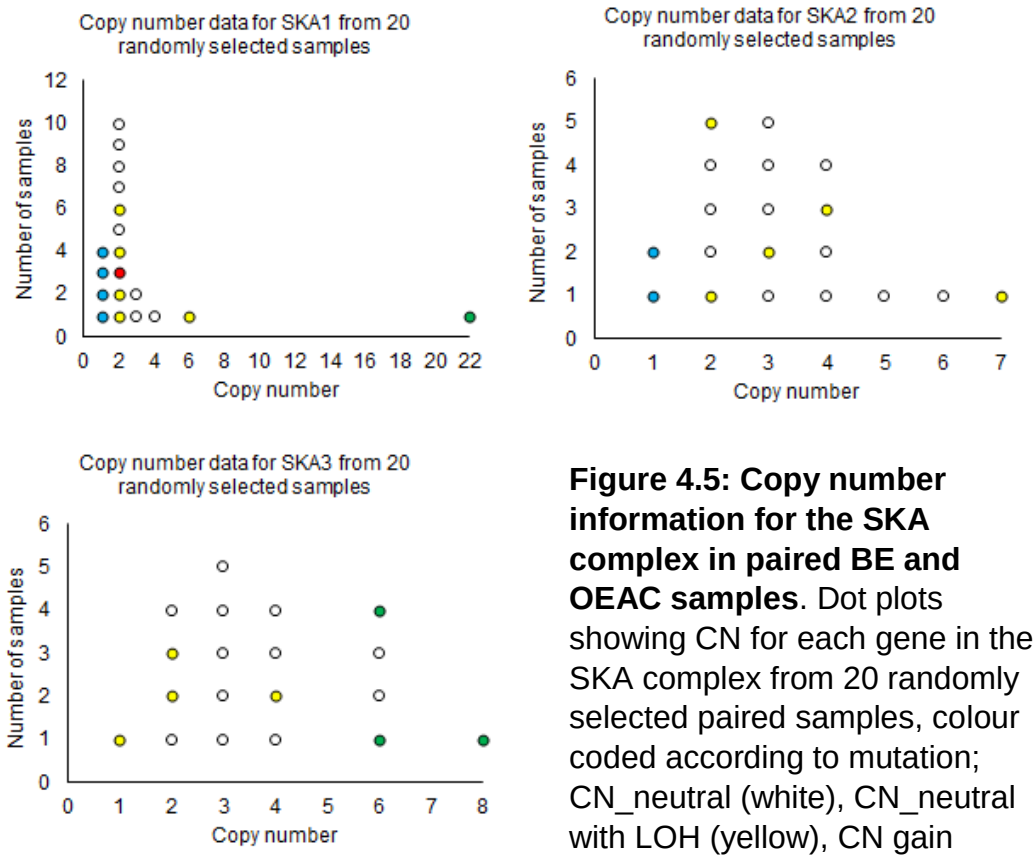

Figure 4.5: Copy number information for the SKA complex in paired BE and OEAC samples. Dot plots showing CN for each gene in the SKA complex from 20 randomly selected paired samples, colour coded according to mutation; CN_neutral (white), CN_neutral with LOH (yellow), CN gain (green), hemizygous deletion with LOH (blue) or CN loss (red).

The most stand out observations from the protein phosphatases were the following seven; protein phosphatase 1 regulatory subunit 1B (PPP1R1B), protein phosphatase 2A 55 KDa regulatory subunit B alpha isoform (PPP2R2A), protein phosphatase 2A 65 KDa regulatory subunit A beta isoform (PPP1R9A/Neurabin 1), protein phosphatase 2A catalytic subunit alpha isoform (PPP2CA), protein phosphatase 2A catalytic subunit beta isoform (PPP2CB), protein phosphatase PP1-beta catalytic subunit (PPP1CA) and protein phosphatase 1 regulatory subunit 16A (PPP1R16A/MYPT3). For these seven LOH was recorded in between 10-36% of pairs, the greatest percentage being seen in PPP2CA. The greatest percentage of gains were present in PPP1R1B (13.6% 67/347) and PPP1R9A (11.2 % 39/347), and hemizygous deletions were most prevalent in PPP2CB (11.5% 40/347) and PPP2R2A (12.4% 43/347). Most interesting about this data set is the extreme copy number alterations, particularly those observed in PPP1R1B, for example pair LP6005334-DNA_H03 vs LP6005333-DNA_H03 had a copy number of 110, pair LP6005690-DNA_B03 vs LP6005777-DNA_A01 copy number 254, pair LP6008051-DNA_A02 vs LP6008050-DNA_E01 copy number 154, pair LP6008051-DNA_E02 vs LP6008050-DNA_A02 copy number 221 and pair LP6008221-DNA_E01 vs LP6008220- DNA_E01 copy number 265 (supplementary table). Extremes in CN can be observed from the random sample data (figure 4.6), whilst up to 60% of samples show a CN of 2 (12/20 PPP2CA) or 3 (20% - 30%) there are instances of CN 11 (PPP1R9A), 13 (PPP1CA) and even more extreme values of 110 and 115 (PPP1R2B).

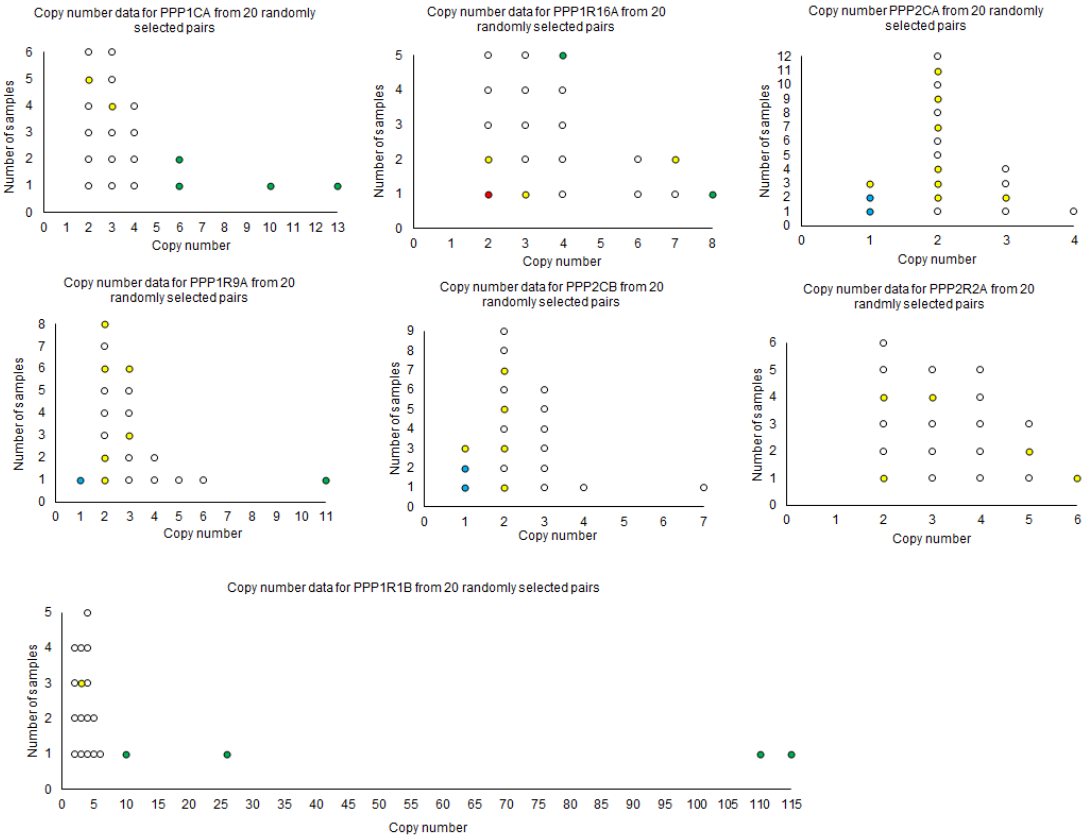

Figure 4.6: Copy number information for a series of protein phosphatases (PPP) in paired BE and OEAC samples. Dot plots of PPP genes in twenty randomly selected pairs colour coded according to mutation; CN_neutral (white), CN_neutral with LOH (yellow), CN gain (green), hemizygous deletion with LOH (blue) or CN loss (red).

4.1.2. WGS of cell lines:

Given that the majority of my experimental work has been carried out in BE and OEAC cell lines it would be valuable to know the mutational background and copy number status of genes relating to the centromere/kinetochore as this information may shed some light on the defective mitoses detailed in chapter one. Whole genome sequencing (WGS) data from BE and OEAC cells was analysed by Juliane Perner from the Fitzgerald lab. This analysis provided information whether a specific centromere/kinetochore gene carried a gain or loss, and the resulting copy number for this gene in dysplastic BE cells (CPD) and OEAC cell lines FLO and JH-Eso-Ad1. (Supplementary figure 03). From this data set it became clear that there wasn't a

consistent trend for gains or losses across the cell lines. Stand out observations from each cell line include a small number of CN gains within the KMN network, coupled with numerous losses within kinetochore/centromere genes in CPD cells. In contrast to this the small number of alterations recorded in FLO cells appeared to be primarily within CCAN genes such as CENP-I and CENP-U, both of which were recorded as having a CN of 1. FLO did also present a small number of amplifications at the KMN and outer kinetochore levels, with Mis12 and Mad1 both being amplified to CN 3. The greatest number of CN alterations were observed in the cell line JH-Eso-AD1, with CN increases and losses observed in a number of the CCAN and KMN subunits. Whilst this data may give an interesting insight into the gene status of the cell lines used in this thesis it is important to note that more details regarding the nature of these changes and the resulting copy number is still required and thus at present the CN analysis of cell lines is purely observational and further sequencing may be required to fully analyse the CN status of KT genes and how these alterations may be affecting the structure and or function of the KT.

In order to widen the investigation into the centromere/kinetochore genes in OEAC cells collaborators from the Fitzgerald lab investigated a large cohort of OEAC samples to look for alterations in genes from the centromere, inner and outer kinetochore. Frankell *et al.,* (2019) accumulated a cohort of 511 genomically characterised OEACs with high quality clinical annotation and associated WGS and RNA sequencing (RNAseq) in cases with sufficient data. From this cohort they reported a total of 11,813,333 single nucleotide variants (SNVs) and small insertions or deletions (InDels), and 134,697 structural variants from the WGS data. From this data set Dr Li extracted and analysed the SNVs and InDels of the kinetochore/ centromere genes. Some of the stand out observations from this data was the presence of 49 mutated cases (47 SNVs and 2 InDels) of PPP1R9A (Neurabin), 25 mutated cases of Clasp1 (24 SNVs and 1 InDel), 24 mutated cases of CENP-F (23 SNVs and 1 InDel) and 14 mutated cases of Rod/Kntc1 (13 SNVs and 1 InDel) (supplementary figure S1) (Frankell *et al.,* 2019, Li and Fitzgerald personal communication).

The sequencing data from the cell lines, paired samples and the wider cohort is encouraging as it indicates copy number alterations within key centromere and kinetochore genes that have the potential to negatively impact the assembly and/or

function of this macromolecular structure. A defective CCAN will affect how the rest of the kinetochore is assembled, and this in combination with copy number alterations within the KMN network could result in the MT binding capability of the kinetochore being impaired. If the kinetochore is unable to successfully bind to the MTs the chromosomes may fail to congress thus resulting in the scattered chromosome phenotype observed in OEAC cells, and hence failure to complete mitosis.

4.2. Total protein expression of important kinetochore complexes is affected in OEAC cells in accordance with WGS data

Having highlighted numerous copy number alterations at the kinetochore of BE and OEAC cells through WGS, I wanted to now investigate whether these changes had any effect on total protein expression. Protein levels of CENP-C, BubR1, Ndc80, Spc24 and Dsn1 were analysed by western blot of cycling cell lysates (figure 4.8 A). Using ImageJ software, the total protein was quantified and then first normalised against a tubulin loading control, and then as a ratio relative to CPA. CPA cells showed no copy number changes in the sequencing and so were used as the control cell line in this experiment (figure 4.8 B). Much like the results of the WGS analysis, the western blots revealed varying levels of protein expression both within the kinetochores of individual cell lines, and comparatively across the cell lines. Compared to CPA, the levels of Ndc80 were increased > 2.5-fold in all cell lines, CPD values being 2.6, FLO 3.6 and JH 5.9 times greater. Similar levels of over-expression relative to CPA were also observed in CPD and FLO cells for the Mis12 complex subunit Dsn1 with CPD showing a 2-fold, FLO a 5-fold and JH-Eso-Ad1 a 2.4 fold increase in protein expression. The levels of Spc24 and CENP-C showed little discrepancy from the controls, the only stand out differences being a 1.58 fold increase in CENP-C in JH cells and a 1.7 fold increase in Spc24 levels in FLO cells. In contrast to these increases in protein expression, BubR1 consistently showed decreased expression with CPD cells scoring 0.29, FLO 0.78 and JH 0.47 compared with CPA cells. Moreover, in CPD cells an additional band was present, indicating possibly either a larger protein or a post translational modification (PTM).

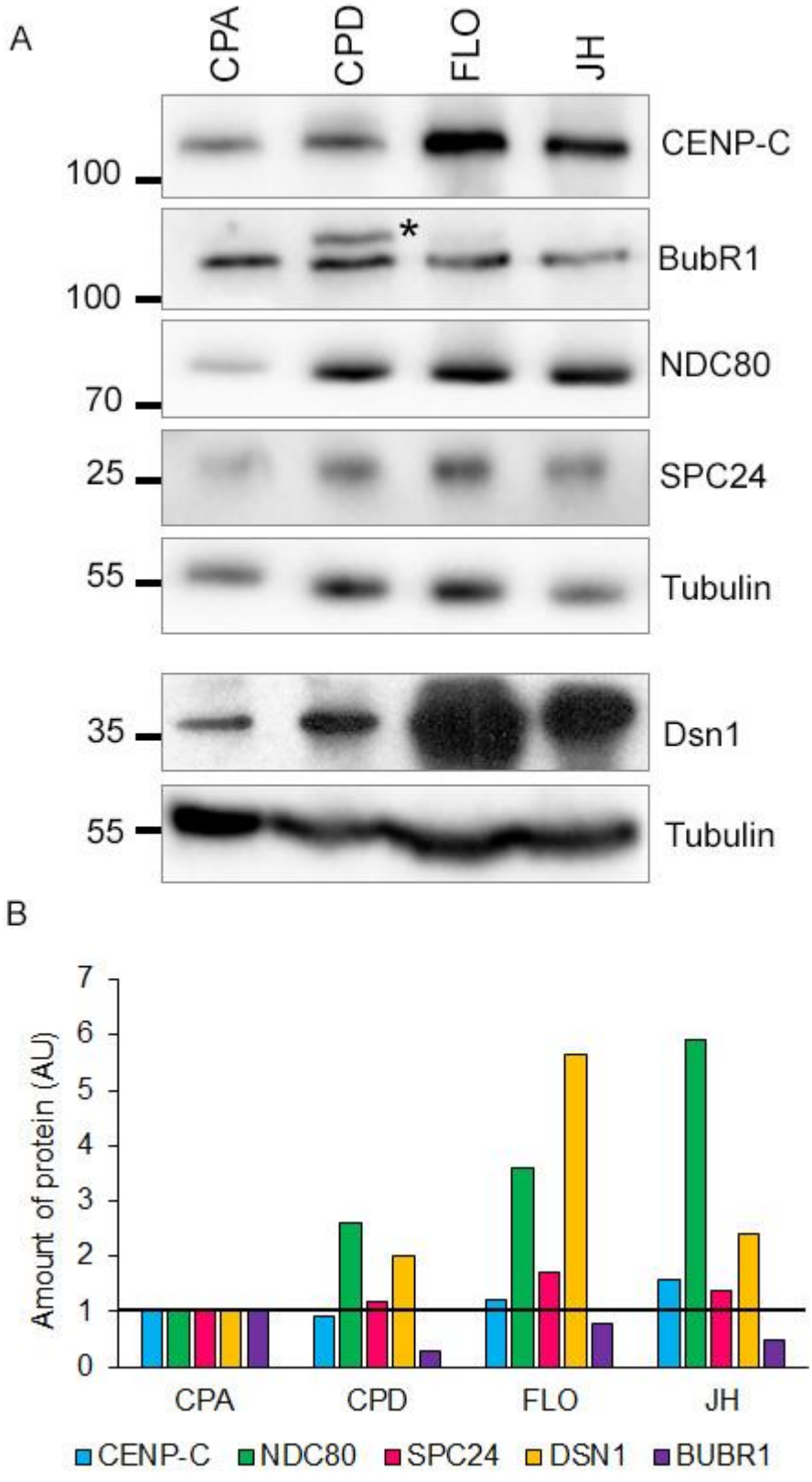
A
CPA
CPD
FLO
JH
100
CENP-C
*
100
BubR1
70
NDC80
25
SPC24
55
Tubulin
35
Dsn1
55
Tubulin
B
Amount of protein (AU)
7
6
5
4
3
2
1
0
CPA
CPD
FLO
JH
CENP-C
NDC80
SPC24
DSN1
BUBR1

Figure 4.7: Analysis of total expression of kinetochore proteins in BE and OEAC cells. A] Western blots showing levels of total protein for inner and outer kinetochore proteins with their respective tubulin loading controls. The numbers to the left of the blots refer to the protein ladder. The asterisk marks an additional band of BubR1 in CPD cells B] Quantification of total protein. Using ImageJ bands were first normalised against the tubulin and then as ratio relative to CPA. Fold change: CENP-C: CPD: 0.90, FLO: 1.20, JH: 1.58; NDC80: CPD: 2.60, FLO: 3.60 JH: 5.90; SPC24: CPD: 1.19, FLO: 1.70, JH: 1.37; DSN1: CPD: 2.02, FLO: 5.65, JH: 2.41; BubR1: CPD: 0.29, FLO: 0.78, JH: 0.47

Interestingly, the data has made it apparent that there are clear imbalances between the Ndc80 complex subunits Ndc80 and Spc24, particularly in the OEAC cell lines as FLO cells were expressing 2x more Ndc80 than Spc24 and JH cells 4.3x more. These differences in expression would therefore re-enforce the concept of an imbalance in kinetochore composition in OEAC cells and highlights areas of interest for further investigation, primarily the Ndc80 complex.

4.3. OEAC cells show varied levels of KMN network proteins at their kinetochores suggesting an imbalance within the complex.

Having shown by western blot that OEAC cells have increased levels of expression of important kinetochore proteins, primarily within the KMN network, I next sought to investigate how this has affected the protein expression at the kinetochore during mitosis. Asynchronous BE and OEAC cells were fixed and stained for immunofluorescence with antibodies against the KMN network proteins Ndc80 (figure 4.9), Spc24 (figure 4.10) and Dsn1 (figure 4.11), the CCAN protein CENP-A (figure 4.12), the CPC protein Aurora B (figure 4.13) or the checkpoint protein BubR1 (figure 4.14), along with CREST as a centromeric control. The kinetochore intensity of the proteins was then calculated using ImageJ software and the following formula: $(I_K - I_B) - (I_C - I_B) / (I_C - I_B)$ which can be simplified to $(I_K - I_B - I_C) / (I_C - I_B)$ which can be further simplified to $(I_K - I_B) / (I_C - I_B)$ where I_K: kinetochore intensity, I_C: CREST intensity and I_B: background intensity.

In accordance with the western blot data the intensity of Ndc80 at the kinetochore in CPD and FLO cells was significantly higher than that observed in CPA cells (figure 4.9 B). However, the levels of Ndc80 at kinetochores of JH-Eso-Ad1 cells was comparable with the CPA controls. I next wanted to understand whether a

difference could be seen when comparing cells with aligned chromosomes vs those with scattered chromosomes. Ndc80 fluorescence intensity measurements at the kinetochores of FLO and JH-Eso-Ad1 indicated a difference in the accumulation of Ndc80 between aligned vs scattered chromosomes in both cell lines, albeit with opposite results (figure 4.9 C). In FLO the cells with scattered chromosomes had significantly lower levels of Ndc80 compared to cells with normally aligned chromosomes, whereas in JH-Eso-Ad1 the Ndc80 intensity was higher when the chromosomes were misaligned.

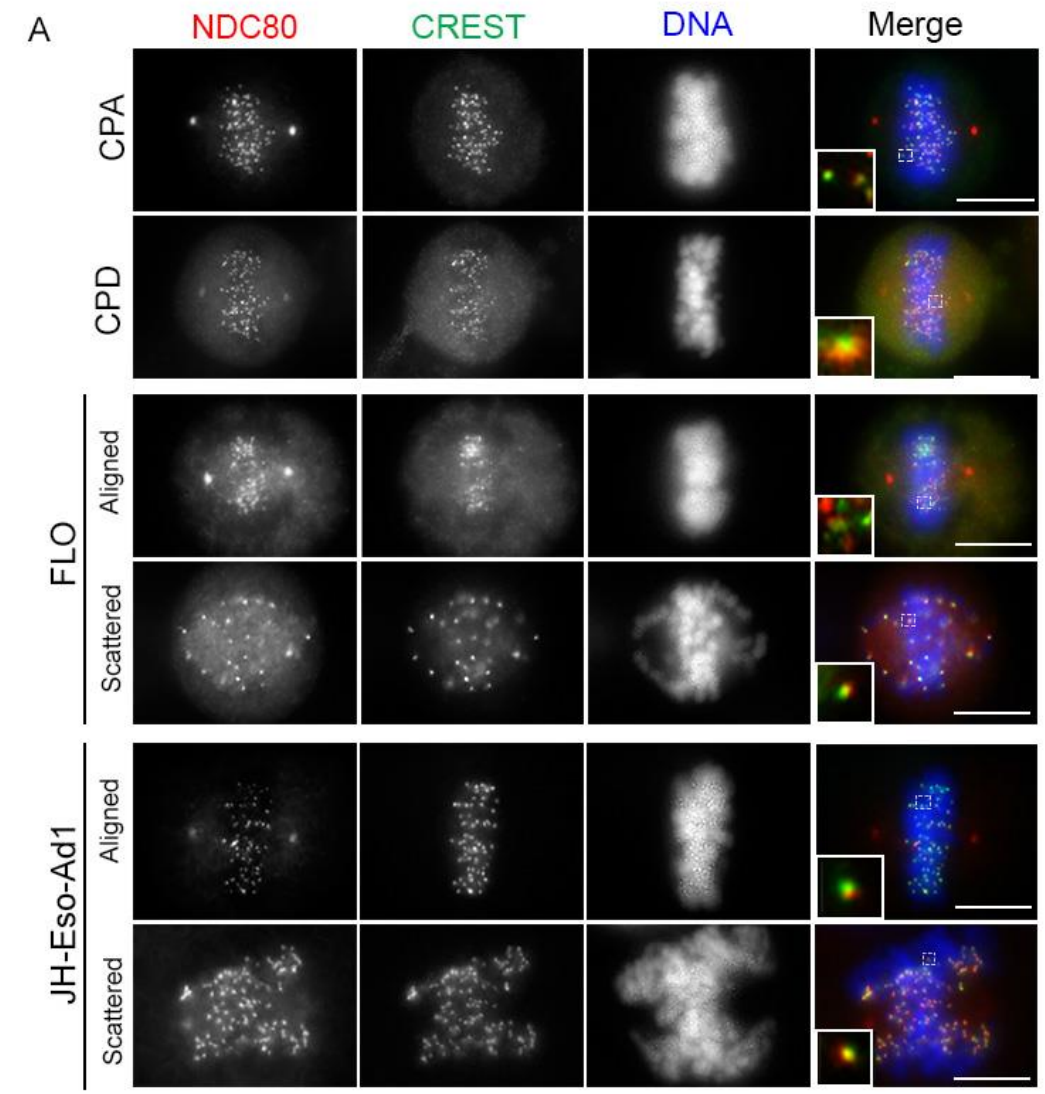
A
NDC80
CREST
DNA
Merge
CPA
CPD
FLO
Aligned
Scattered
JH-Eso-Ad1
Aligned
Scattered

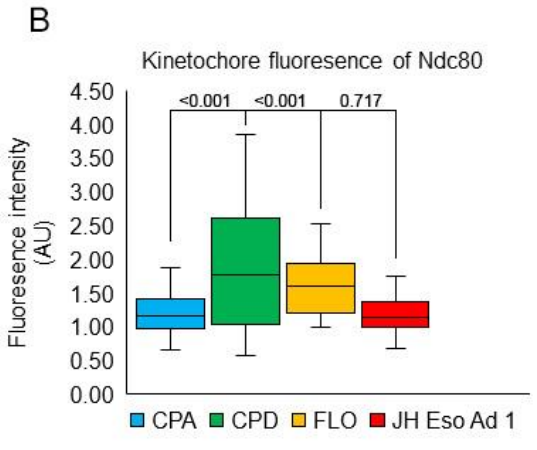
B
Kinetochore fluoresence of Ndc80
Fluoresence intensity (AU)
4.50
4.00
3.50
3.00
2.50
2.00
1.50
1.00
0.50
0.00
<0.001
<0.001
0.717
CPA
CPD
FLO
JH Eso Ad 1

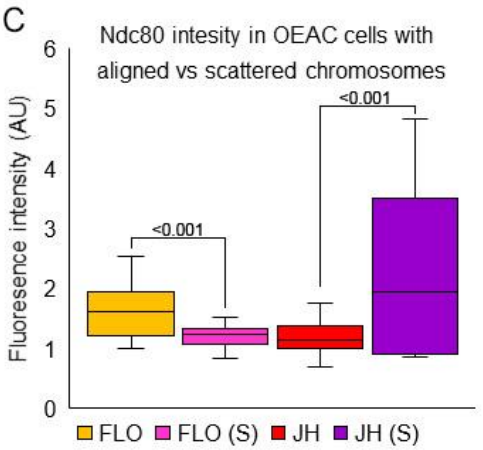
C
Ndc80 intesity in OEAC cells with aligned vs scattered chromosomes
Fluoresence intensity (AU)
6
5
4
3
2
1
0
<0.001
<0.001
FLO
FLO (S)
JH
JH (S)

Figure 4.8: Levels of Ndc80 are increased at kinetochores in FLO cells. A) CPA, CPD, FLO and JH-Eso-Ad1 cells were fixed and stained for Ndc80, Crest and DNA. Inserts show a magnified kinetochore co-stained for Ndc80 and Crest. Scale bar 10 μm. B) Fluorescence intensity of Ndc80 was measured and normalised against CREST (CPA n=60, CPD n=40, FLO n=60, FLO scattered n=15, JH-Eso-Ad1 n=60, JH-Eso-Ad1 scattered n=30. KTs counted from a minimum of 3 different images with at least 5 KTs taken per image). Levels of Ndc80 are significantly increased in the box plots of CPD and FLO cells (*** $p < 0.001$ student's t-test) whereas the box plot for JH-Eso-Ad1 was not significantly different to CPA (0.714 student's t-test) median values: CPA: 1.16, CPD: 1.78, FLO: 1.60, JH: 1.15. C) Comparing levels of Ndc80 in cells with aligned vs scattered chromosomes show significant differences in the cell lines (*** $p < 0.001$ students t-test), median values: FLO aligned: 1.60, FLO scattered: 1.24, JH aligned: 1.15, JH scattered: 1.96.

The results obtained for the Ndc80 complex subunit Spc24 were quite different from those observed for Ndc80. In this case, it was only CPD cells that showed a significant difference in Spc24 levels compared with CPA (figure 4.10B). In contrast with the results seen in western blot analysis, in which CPD showed increased total Spc24 expression, the levels observed at the kinetochore was lower compared to both the control and the OEAC cell lines. Levels of Spc24 in FLO and JH-Eso-Ad1 were not significantly different to controls. Unfortunately, when staining for Spc24 I did not observe any cells with scattered chromosomes and therefore I have not been able to compare the levels of this Ndc80 subunit at kinetochores of aligned vs scattered chromosomes.

The final KMN network protein I investigated was the Mis12 complex subunit Dsn1. Despite western blot analysis indicating increased total protein expression of Dsn1, the results obtained for kinetochore intensity showed the opposite (figure 4.11 B). All three cell lines showed significantly lower levels of Dsn1 at their kinetochores in comparison to CPA. Comparing the intensity of Dsn1 in aligned vs scattered JH cells showed a further decrease in levels when the chromosomes were mis-aligned ($p: 0.77 \times 10^{-11}$) (figure 4.11 C).

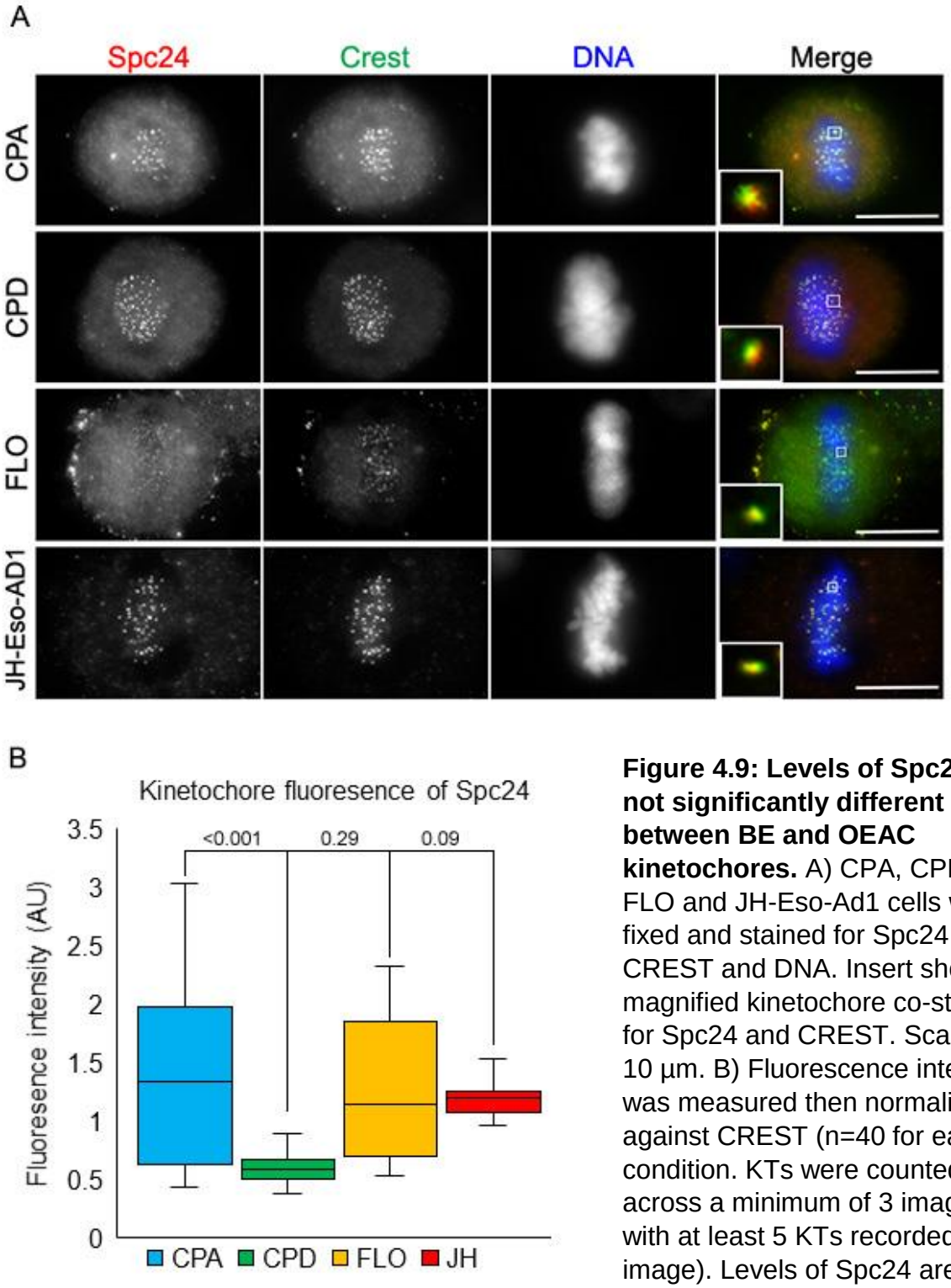

Figure 4.9: Levels of Spc24 are not significantly different between BE and OEAC kinetochores. A) CPA, CPD, FLO and JH-Eso-Ad1 cells were fixed and stained for Spc24, CREST and DNA. Insert shows magnified kinetochore co-stained for Spc24 and CREST. Scale bar 10 µm. B) Fluorescence intensity was measured then normalised against CREST (n=40 for each condition. KTs were counted across a minimum of 3 images with at least 5 KTs recorded per image). Levels of Spc24 are significantly decreased in CPD cells (*** $p < 0.001$ students t-test) but there was no significant difference between CPA and the OEAC lines. Median values: CPA: 1.34, CPD: 0.59, FLO: 1.14, JH: 1.21.

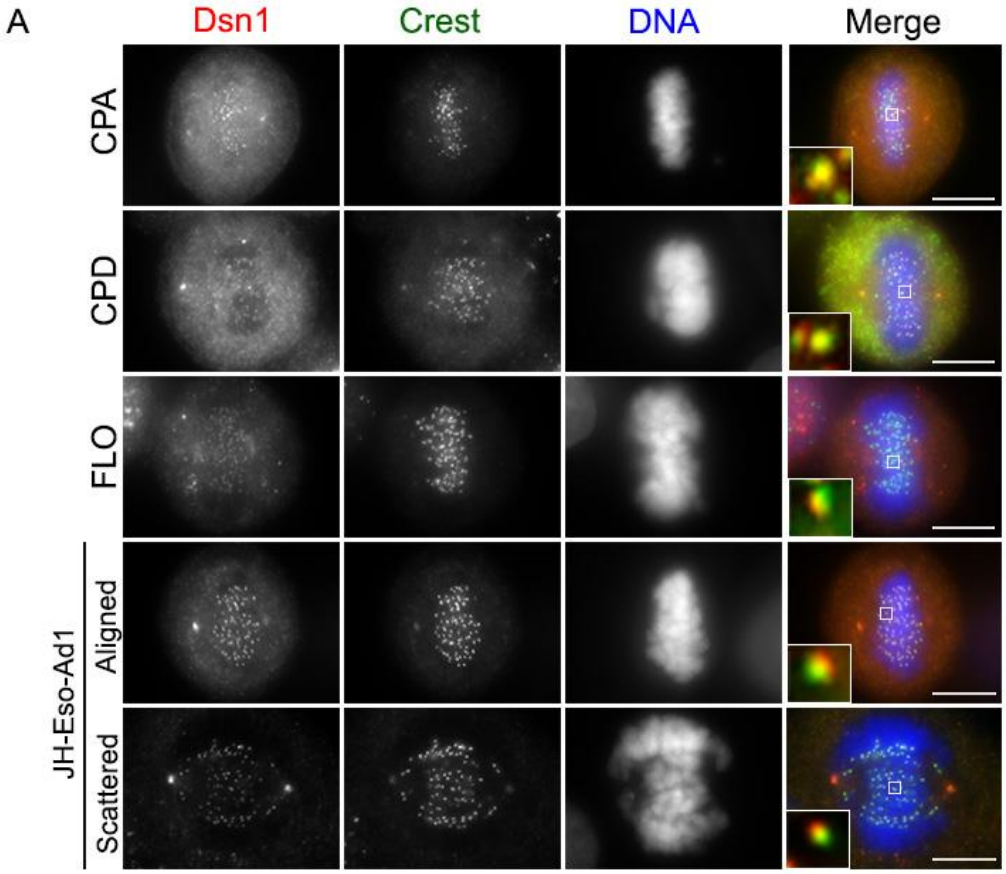
A
Dsn1
Crest
DNA
Merge
CPA
CPD
FLO
JH-Eso-Ad1
Aligned
Scattered

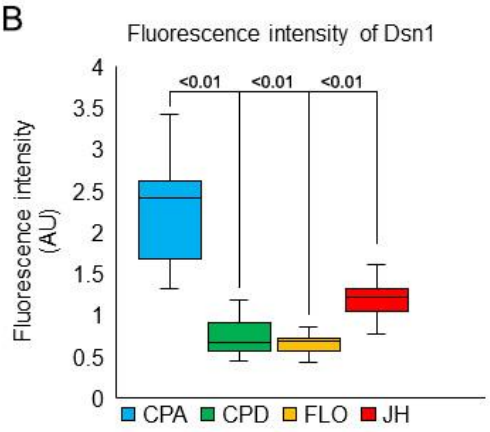
B
Fluorescence intensity of Dsn1
Fluorescence intensity (AU)
<0.01
<0.01
<0.01
CPA
CPD
FLO
JH

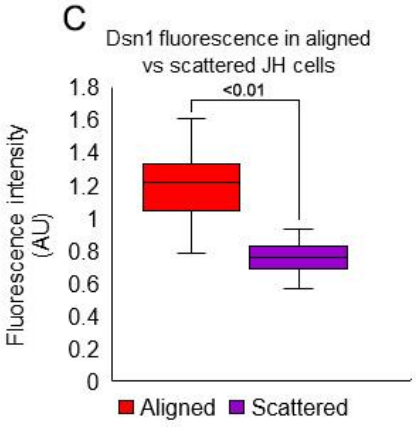
C
Dsn1 fluorescence in aligned vs scattered JH cells
Fluorescence intensity (AU)
<0.01
Aligned
Scattered

Figure 4.10: Levels of Dsn1 are significantly lower in dysplastic BE and OEAC kinetochores. A) CPA, CPD, FLO and JH-Eso-Ad1 cells were fixed and stained for Dsn1, CREST and DNA. Insert shows magnified kinetochore co-stained for Dsn1 and CREST. Scale bar 10 μm. B) Fluorescence intensity was measured then normalised against CREST (CPA n=30, CPD n=25, FLO n=30, JH-Eso-Ad1 n=30, JH—Eso-Ad1 scattered n=15. KTs measured across a minimum of 3 images with at least 5 KTs recorded per image). Levels of Dsn1 are significantly decreased in CPD, FLO and JH-Eso-Ad1 cells (*** $p < 0.001$ students t-test). Median values: CPA: 2.41, CPD: 0.68, FLO: 0.68, JH: 1.21 C) Comparison of Dsn1 intensity in JH-Eso-Ad1 cells with aligned vs scattered chromosomes indicated that Dsn1 levels are significantly reduced when chromosomes are scattered (*** $p < 0.001$ students t-test), median values: aligned: 1.21, scattered: 0.76.

I next looked at the CCAN protein CENP-A (figure 4.12 A). Disrupting CENP-A can have serious consequences for centromere and kinetochore function, so I was interested to observe if there were any differences in the kinetochore intensity of this protein across the cell lines. Like a number of the other proteins, the general pattern observed for CENP-A was a significant decrease in intensity levels in relation to CPA cells (figure 4.12 B). Again when staining for CENP-A I did not observe any cells with scattered chromosomes and thus conclusions regarding differences in CENP-A at kinetochores when chromosomes are scattered cannot be made. The combination of CENP-A and CREST would however produce the same signal therefore the conclusions that could be drawn from this would be minimal.

Given its important role in error correction, I next sought to investigate the levels of Aurora B in BE and OEAC cells. The pattern of kinetochore intensity for Aurora B was remarkably similar to that observed for Spc24 as the only significant difference was observed between CPA and CPD, in which Aurora B levels were significantly lower (figure 4.13 B). However, there was consistency between the levels of Aurora B observed in both FLO and JH-Eso-Ad1 cells; in both cell lines when chromosomes were scattered the levels of Aurora B at the kinetochores were significantly reduced (figure 4.13 C).

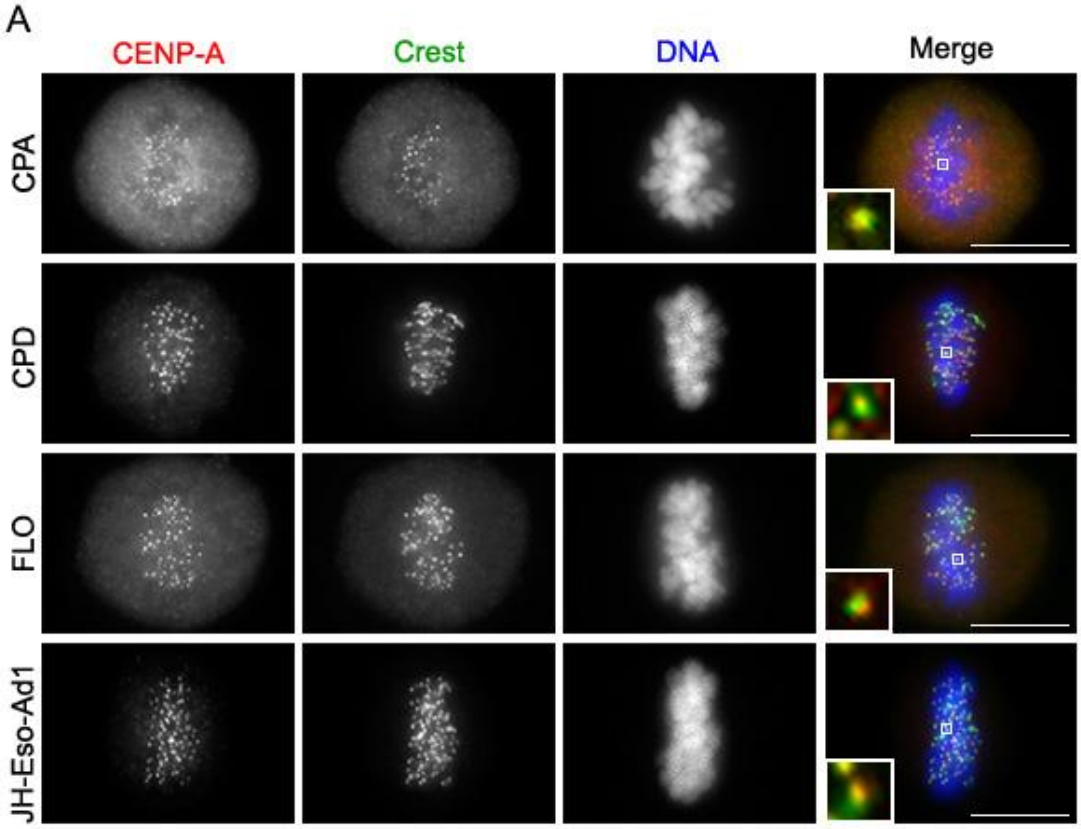

Figure 4.11: Levels of CENP-A are significantly lower at dysplastic BE and OEAC kinetochores. A) CPA, CPD, FLO and JH-Eso-Ad1 cells were fixed and stained for CENP-A, CREST and DNA. Insert shows magnified kinetochore co-stained for CENP-A and CREST. Scale bar 10 µm. B) Fluorescence intensity was measured then normalised against CREST (n=30 for each cell line. KTs were measured from a minimum of 3 images with at least 5. Levels of CENP-A are significantly decreased in CPD, FLO and JH-Eso-Ad1 cells (**/*** $p < 0.01$/ <0.001 students t-test), median values: CPA: 1.75, CPD: 0.38, FLO: 1.19, JH: 0.54

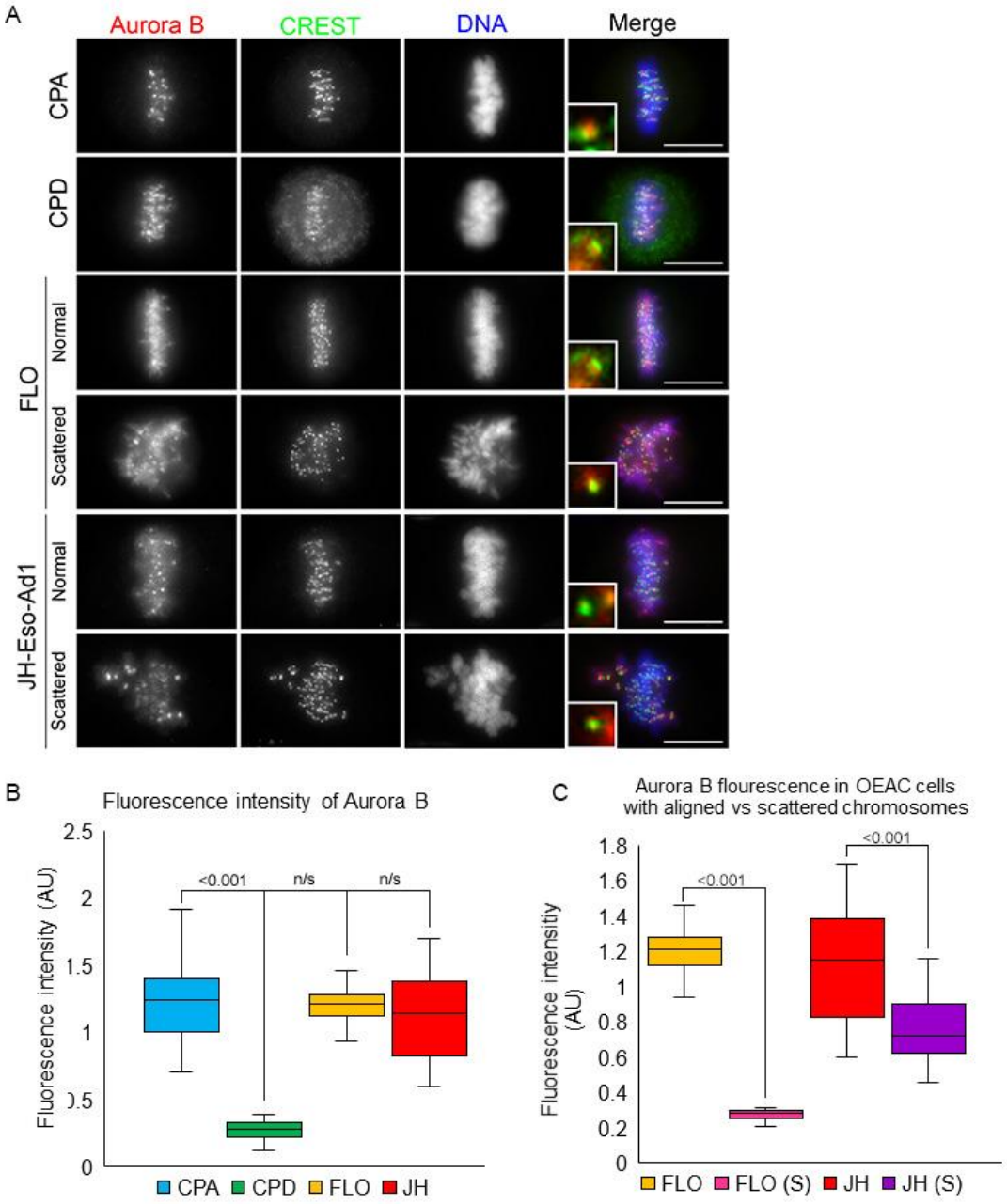
A
Aurora B
CREST
DNA
Merge
CPA
CPD
FLO
Normal
Scattered
JH-Eso-Ad1
Normal
Scattered
B
Fluorescence intensity of Aurora B
Fluorescence intensity (AU)
2.5
2
1.5
1
0.5
0
<0.001
n/s
n/s
CPA
CPD
FLO
JH
C
Aurora B flourescence in OEAC cells
with aligned vs scattered chromosomes
Fluorescence intensity
(AU)
1.8
1.6
1.4
1.2
1
0.8
0.6
0.4
0.2
0
<0.001
<0.001
FLO
FLO (S)
JH
JH (S)

Figure 4.12: Levels of Aurora B are not significantly different between BE and OEAC kinetochores. A) CPA, CPD, FLO and JH-Eso-Ad1 cells were fixed and stained for Aurora B, CREST and DNA. Insert shows magnified kinetochore co-stained for Aurora B and CREST. Scale bar 10 µm. B) Fluorescence intensity measured then normalised against CREST (CPA n=45, CPD n= 30, FLO n=30, FLO scattered n= 15, JH-Eso-Ad1 n=30, JH-Eso-Ad1 scattered n=15, KTs were measured from a minimum of 3 different images with at least 5 KTs recorded per image). Levels of Aurora B are significantly decreased in CPD cells (*** < 0.001students t-test p) but there was no significant difference between CPA and the OEAC lines. Median values: CPA: 1.24, CPD: 0.28, FLO: 1.21, JH: 1.15. C) Levels of Aurora B are significantly lower when chromosomes are scattered in FLO and JH-Eso-Ad1 cells (*** p < 0.001 students t-test). Median values: FLO aligned: 1.21, FLO scattered: 0.28, JH aligned: 1.15, JH scattered: 0.72

Finally I measured the kinetochore intensity of BubR1 in in BE and OEAC cells. Western blot analysis indicated that BubR1 levels decreased in OEAC cells, more so in JH-Eso-Ad1 than FLO, in comparison to CPA (figure 4.14). A similar pattern to this was observed at the kinetochore. The kinetochore intensity of BubR1 in FLO cells was not significantly different to CPA cells however levels in JH-Eso-Ad1 were significantly lower (figure 4.8 B). A decrease in levels was also observed when comparing FLO cell with aligned vs scattered chromosomes. No significant difference was observed between aligned and scattered JH-Eso-Ad1 cells (figure 4.8 C).

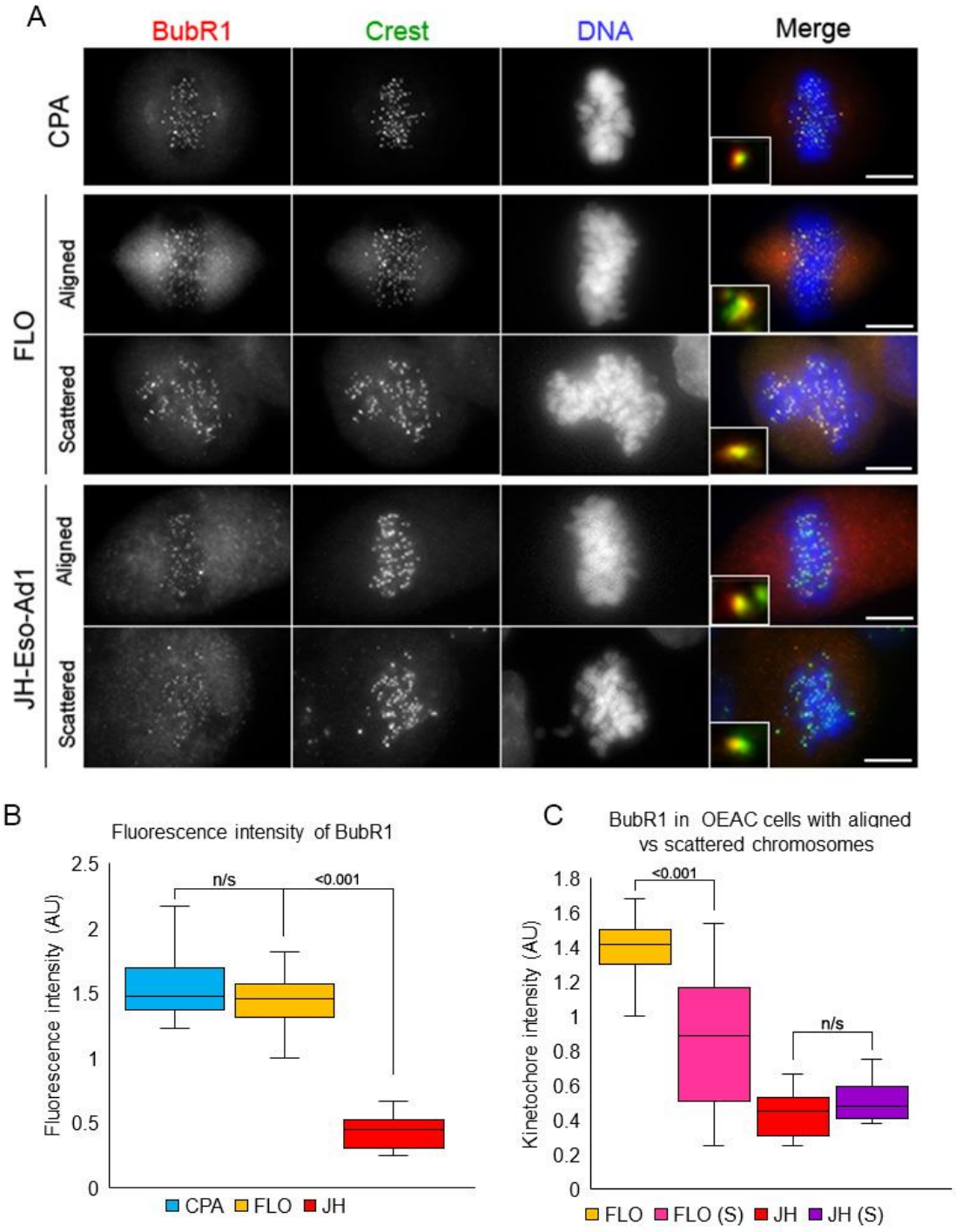
A
BubR1
Crest
DNA
Merge
CPA
FLO
Aligned
Scattered
JH-Eso-Ad1
Aligned
Scattered
B
Fluorescence intensity of BubR1
Fluorescence intensity (AU)
2.5
2
1.5
1
0.5
0
n/s
<0.001
CPA
FLO
JH
C
BubR1 in OEAC cells with aligned vs scattered chromosomes
Kinetochore intensity (AU)
1.8
1.6
1.4
1.2
1
0.8
0.6
0.4
0.2
0
<0.001
n/s
FLO
FLO (S)
JH
JH (S)

Figure 4.13: Levels of BubR1 are significantly lower in JH-Eso-Ad1 cells A) CPA, FLO and JH-Eso-Ad1 cells were fixed and stained for BubR1, CREST and DNA. Insert shows a magnified kinetochore co-stained for BubR1 and CREST. Scale bar 10 μm. B) Fluorescence intensity was measured then normalised against CREST (CPA n=40, FLO n=40, FLO scattered n=30, JH-Eso-Ad1 n=30, JH-Eso-Ad1 scattered n=10, KTs were measured from a minimum of 3 different images with at least 5 KTs recorded per image). Levels of BubR1 are significantly decreased in JH-Eso-Ad1 cells (*** $p < 0.001$ students t-test) but there was no significant difference between CPA and FLO. Median values: CPA: 1.48, FLO: 1.46, JH: 0.45. C) BubR1 levels are significantly lower in FLO cells with scattered chromosomes (*** $p < 0.001$ students t-test) but there is no significant difference between aligned and scattered chromosomes in JH-Eso-Ad1 cells. Median values: FLO aligned: 1.42, FLO scattered: 0.89, JH aligned: 0.45, JH scattered: 0.48. Scale bar 10 μm.

Given my interest in highlighting potential imbalances at the kinetochore, I next compared the kinetochore levels of the above proteins within each cell line. In CPA cells, despite them having no reported copy number alterations, I did observe some significant differences in the intensities of the different proteins (figure 4.15 A). In CPD cells the differences between the kinetochore intensity for each protein was significant, with the most stand out difference being a greatly increased intensity of Ndc80 (figure 4.15 B). A different pattern of kinetochore protein intensity was observed for FLO and JH cells. In FLO the most striking imbalance was seen in the KMN network, with significant differences recorded between all three KMN subunits investigated (figure 4.15 C). By contrast, the level of the KMN network proteins were not significantly different from one another in JH-Eso-Ad1 cells, but CENP-A and BubR1 were lower than the KMN and Aurora B, although they did not significantly differ from one another (figure 4.15D). It is interesting that the profile of the imbalances are quite different from one another yet the resulting consequences, particularly scattered chromosomes, is similar. This may therefore suggest that it requires altered protein expression of a number of kinetochore components to induce the phenotype, and perhaps the more components affected the more severely scattered the chromosomes appear, further investigation is however required to fully understand this notion.

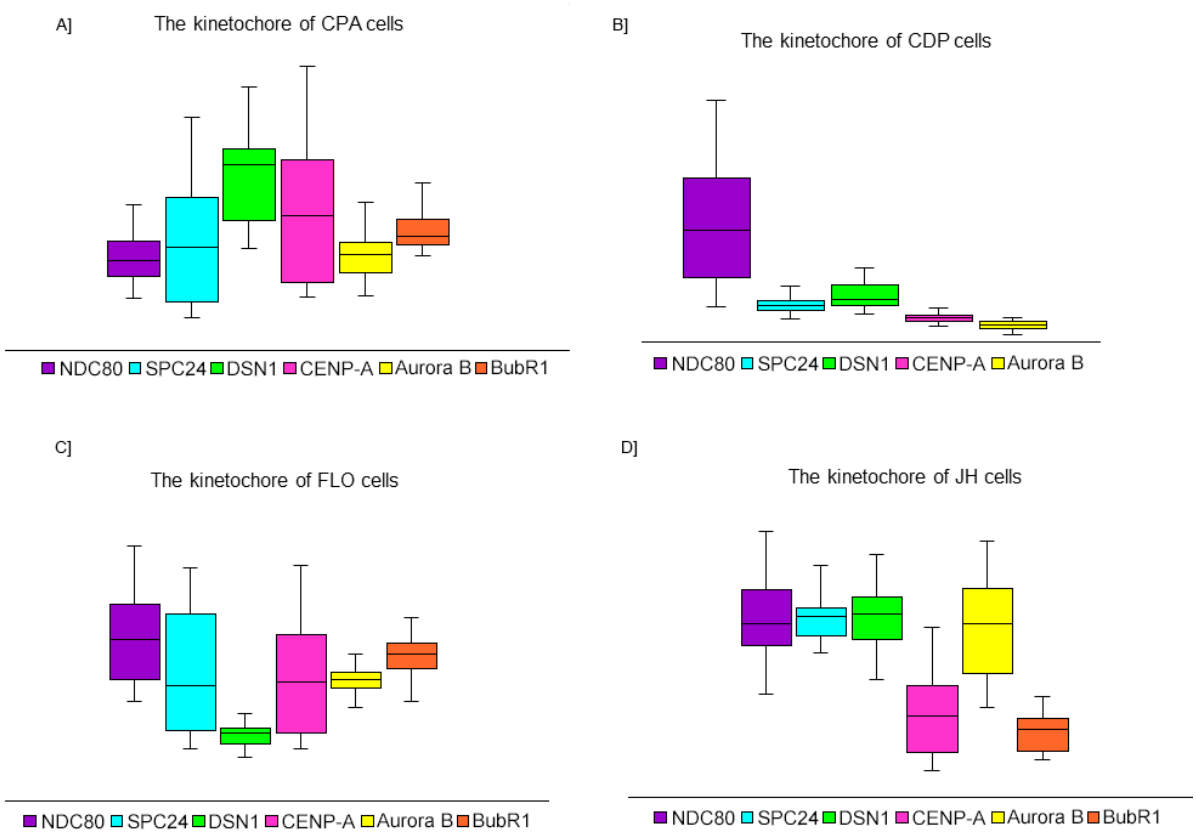

Figure 4.14: Comparison of kinetochore proteins in each cell line. A) CPA B) CPD C) FLO D) JH-Eso-Ad1. Patterns of kinetochore intensities are variable in all cell lines. For p values see supplementary material figure S2.

To get a more complete view of the KMN network as a whole I also tried to quantify the levels of Knl1 in BE and OEAC cells, but unfortunately, I found that the Knl1 antibody would not co-stain with CREST, meaning that these images lacked a centromeric control. As I considered it important to observe the localisation of Knl1 in these cells, particularly those with aligned vs scattered chromosomes, I fixed and stained the cells with antibodies against Knl1 and tubulin to mark the mitotic spindle (figure 4.10). In CPA cells there is a clear kinetochore localisation of Knl1 with very little background cytoplasmic staining, whereas in FLO cells presenting either normally aligned or scattered chromosomes there appears to be a much more cytoplasmic Knl1. This localisation was similar JH-Eso-Ad1 cells, suggesting a potential mis-localisation of Knl1 in OEAC cells.

I had equal difficulties in co-staining for CENP-C and CREST co-stain and thus I again opted to look at CENP-C localisation by staining alongside tubulin (figure 4.11). Like for Knl1, in CPA cells there is a clear CENP-C signal at the kinetochores. FLO cells also showed this kinetochore localisation but again the level of cytoplasmic staining was also increased and in FLO cells with scattered chromosomes there was no distinct CENP-C signal at the kinetochore. In JH-Eso-Ad1 cells CENP-C is visible at the kinetochore, but the signal appears to be reduced and more abundant in the cytoplasm, in comparison to CPA controls.

The data presented in this section has supplemented the notion of a potential imbalance of kinetochore proteins in BE and OEAC cells, specifically in the KMN network, which may result in structural and/or functional deficits to the overall function of this complex and in turn affecting the entire kinetochore.

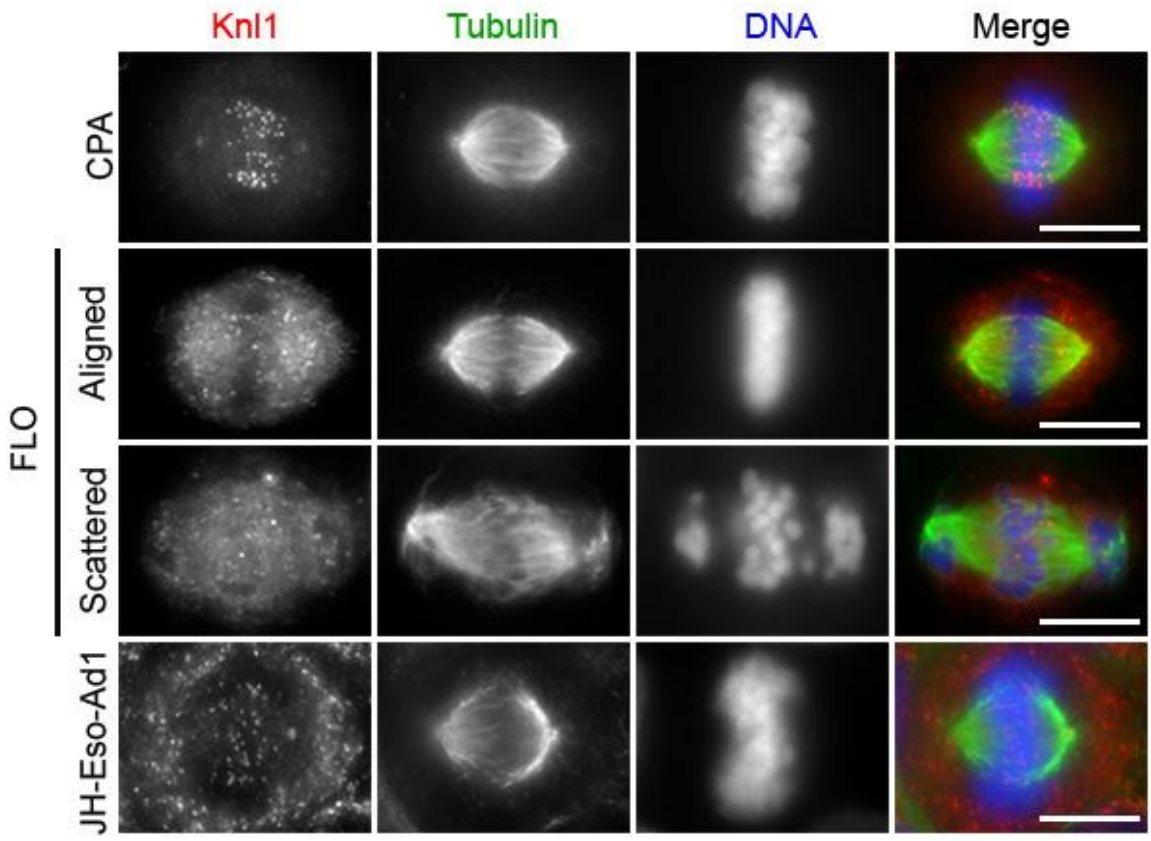

Figure 4.15: Kinetochore localisation of Knl1 in BE and OEAC cells. CPA, FLO and JH-Eso-Ad1 cells were fixed and stained for Knl1, tubulin and DNA. Scale bar 10 µm.

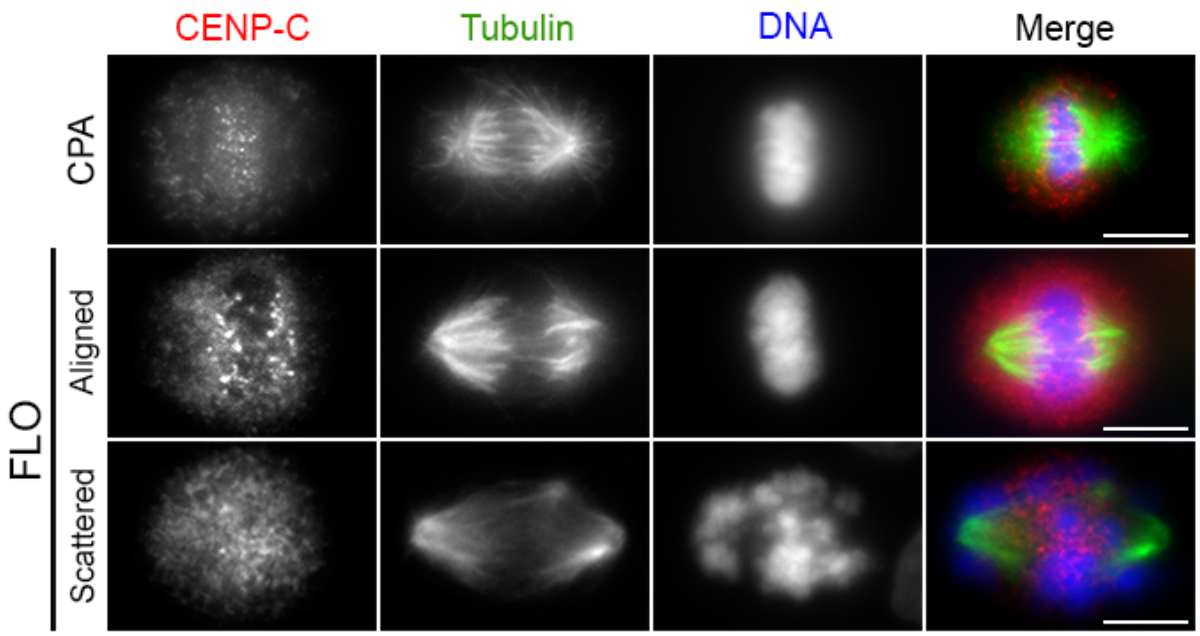

Figure 4.16: Kinetochore localisation of CENP-C in BE and OEAC cells. CPA and FLO cells were fixed and stained for CENP-C, tubulin and DNA. Scale bar 10 µm.

4.4. OEAC cells with scattered chromosomes have a higher percentage of lateral kinetochore-microtubule attachments.

As outlined in the introductory chapter, kinetochores are initially captured laterally on the wall of the microtubule before an end on conversion occurs (Shrestha and Draviam 2013; Alexander and Rieder 1990; Magidson *et al.,* 2011). It is only in this end on conformation that the growth and shrinkage of the K-fibres can impart the pushing and pulling forces required for chromosome congression (Skibbens, Skeen and Salmon 1993; Cassimeris and Salmon 1991; Mitchison *et al.,* 1986). A marker of this conversion is the presence of the Astrin-SKAP complex which is recruited to mature end on kinetochores, the Astrin subunit of this complex being required for the correct metaphase alignment of chromosomes (Shrestha *et al.,* 2017). It has been shown previously that depletion of Astrin delays chromosome congression, alters the spindle architecture and causes premature loss of chromatid cohesion prior to anaphase onset (Thein *et al.,* 2007). To investigate whether the chromosome congression defect observed in OEAC cells was a consequence of kinetochore microtubule attachment errors, and more specifically a failure in converting from lateral to end on attachments, cells were fixed and stained with antibodies against

Astrin and tubulin to visualise the types of kinetochore microtubule attachments (figure 4.18 A). Despite Astrin being described as a marker for mature end on attachments (Shrestha *et al.,* 2017), in both BE and OEAC cells some Astrin signals could be observed lying laterally along the microtubule, in addition to the expected signal at the microtubule end (figure 4.18 B). As I was able to observe both lateral and end on attachments, I quantified the number of these attachments present in each cell line to compare between aligned and mis-aligned chromosomes. In all cell lines in which chromosomes had successfully congressed to the metaphase plate, less than 13% of kinetochores appeared laterally attached (CPA 6% n = 6/100, FLO 9% n = 9/100 and JH-Eso-AD1 12.5% n = 5/40). The percentage of lateral attachments in cells with scattered chromosomes was increased to 18-20% in both cell lines (FLO n = 18/100 and JH-Eso-Ad1 n = 2/10) (figure 4.18 C). This data suggest that a problem in converting from lateral to end on attachments could be affecting chromosome congression in OEAC cells.

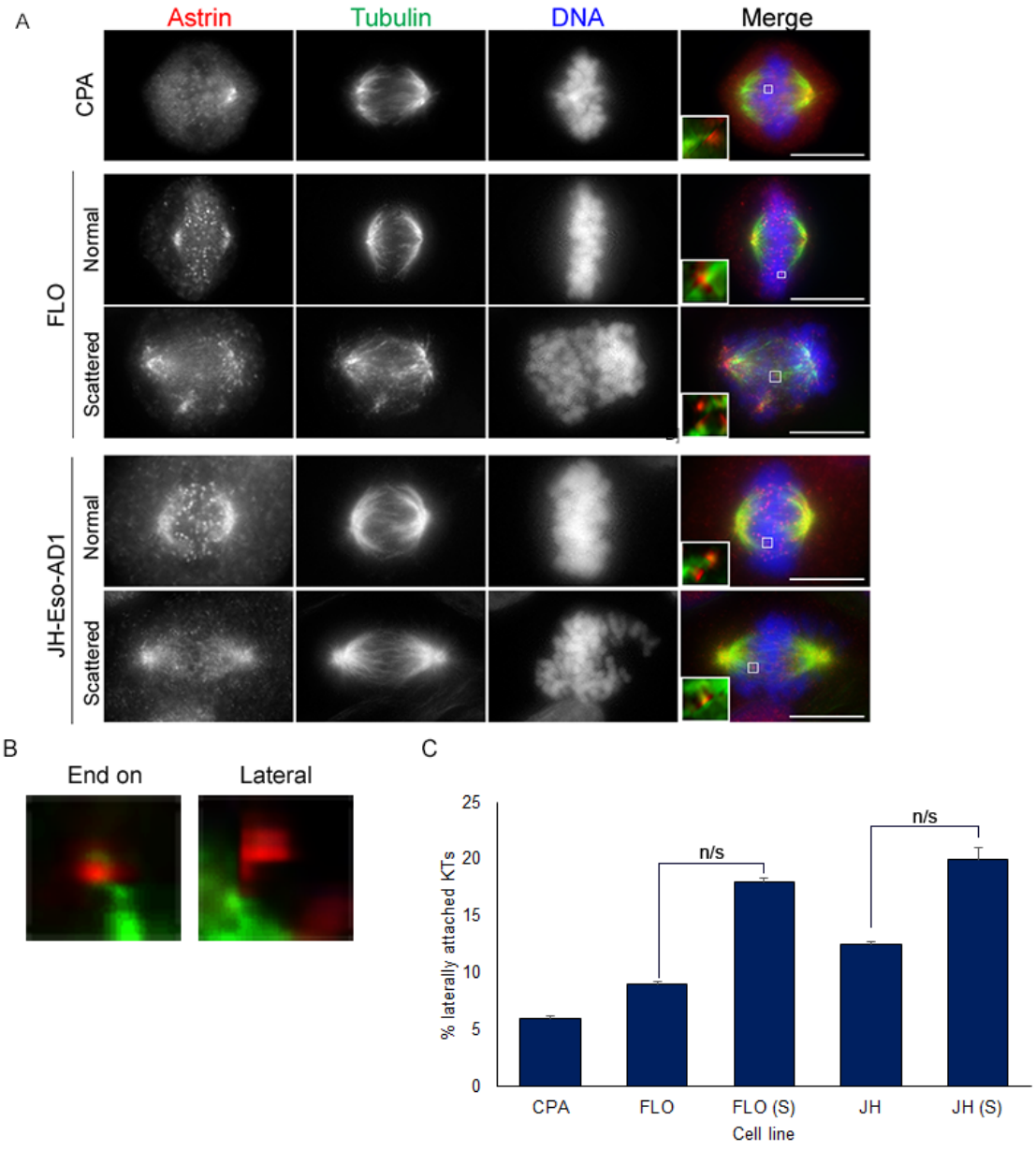

Figure 4.17: Investigating microtubule attachments in BE and OEAC cells. A] CPA. FLO and JH-Eso-Ad1 cells were fixed and stained for Astrin (red), tubulin (green) and DNA (blue). Insert shows zoom of Astrin localisation at the kinetochore. Scale bar 10 µm. B] Example of an end on vs laterally attached kinetochore. C] Quantification of lateral vs end on attachments shows that cells with scattered chromosomes have a higher percentage of laterally attached kinetochores: CPA: 6% n=6/100, FLO 9% n=9/100,, FLO scattered (S): 18% n=18/100, JH: 12.5% n=5/40, JH scattered (S): 20% n=2/10. These differences are not significant (possibly owing to the low sample number in each condition).

5. Preliminary analysis of protein-protein interaction networks

The findings presented in chapter 4 led me to hypothesise that an imbalance in the amount of kinetochore proteins might be responsible for the chromosome alignment defects observed in OEAC cells. To investigate this possibility in a comprehensive and quantifiable manner, I decided to test whether it would be possible to characterise the kinetochore protein-protein interaction networks (interactome) in BE and OEAC cell lines.

5.1. Optimisation of synchronisation methods for BE and OEAC cells.

In order to maximise the yield of kinetochore proteins that could be obtained by immunoprecipitation for mass spectrometry (MS) analysis BE and OEAC cells needed to be synchronised into M phase. As no synchronisation protocol had been published for this, a series of troubleshooting experiments were required in order to find a protocol that would be the most effective in generating a mitotic cell population, specifically increased in metaphase cells.

5.1.1. CPA

The first protocol trialled with all the cell lines was the combination of a single thymidine treatment to arrest cells at G1/S followed by a nocodazole block to halt the cells in mitosis. Cells were incubated in thymidine for 19 hours and then following washout were released for 5 hours before being subjected to incubation in nocodazole for 13 hours. After nocodazole treatment, cells were collected via mitotic shake off and released for approximately 30-40 minutes (depending on the cell line) to obtain a metaphase population.

Unfortunately, only a small fraction of the CPA cells appeared to respond to this treatment (visually rounding up, indicating mitosis) and were very resistant to mitotic shake off, making collecting only mitotic cells incredibly challenging. To investigate why the synchronisation failed, CPA cells were treated with either thymidine or nocodazole to study how each drug affected the cells. Cells treated with thymidine only became very stressed and a number of the cells were dead by the end of the incubation period. The cells that survived the treatment showed no visibly dividing cells, suggesting they had all responded to the thymidine. Western blot analysis of these cells showed no cyclin B was present in these cells (figure 5.1 A),

which is expected, as cyclin B is virtually absent at the G1/S transition. However, in conflict with the cyclin B signal thymidine treated cells also presented a 1.3-fold increase in Histone H3 pS10 compared to unsynchronised CPA cells, which would suggest an M phase population. These results were inconclusive as to whether thymidine was able to successfully arrest CPA cells at the G1/S boundary.

I did in parallel, experiments that showed that nocodazole treatment of CPA cells was able to enrich the population of mitotic cells five-fold. Therefore, I wanted to establish at what point following nocodazole washout these cells exited mitosis in order to identify an appropriate release interval for obtaining a metaphase population. Following a 13-hour nocodazole treatment cells were released for 0, 20, 40 or 60 minutes and then fixed and stained for DNA, tubulin and Histone H3 pS10. Mitotic index counts indicated that at 0 minutes 15% of the cells were in mitosis, this then slightly increased to 16% at 20 minutes, 17% at 40 minutes, to finally drop to 3% at 60 minutes which is comparable to unsynchronised controls, indicating that at 60 minutes cells had now exited mitosis (figure 5.1 B). Based on this data, collecting cells at around 30-40 minutes after nocodazole release should be sufficient to obtain a small metaphase population of CPA cells.

Having confirmed that only a small population of CPA cells arrested in mitosis using nocodazole alone, I decided to try another cell cycle inhibitor, instead of thymidine to further increase the yield of mitotic cells. I opted to try palbocyclib, an inhibitor of CDK4/6, to arrest cells in G1. Cells were incubated in palbocyclib for 18 hours, then released for 8 hours before being treated with nocodazole as previously described. Following this procedure, the yield of mitotic cells did increase, and western blotting for Histone H3 pS10 indicated that the cells had been successfully arrested in mitosis (figure 5.1 C).

Whilst testing the palbocyclib/nocodazole synchronisation in CPA, I noticed that the cells appeared to respond better to the treatment when seeded at low densities. To test whether the starting density had an effect on the result of the synchronisation, I plated cells at different confluences: 20%, 25%, 30%, 40%, 60% and 80%. I then carried out the synchronisation procedure as described above and then fixed and stained the cells for DNA, tubulin and Histone H3 pS10 to calculate the mitotic index. At 20% confluency the cells failed to respond to the

synchronisation (mitotic index 1%), but just a 5% increase in cell density led to a mitotic index of 47%. At 30% confluency the mitotic index rose again to 54% and this level was maintained at 40% and 60% confluency, with mitotic index scores reaching 46% and 51% respectively. However, when the starting confluency was increased to 80% the mitotic index dropped to 25%. Based on this, I was able to establish that the maximum starting density for CPA cells when using palbocyclib and nocodazole is 60% in order to achieve a mitotic population of approximately 50% (figure 5.1 D).

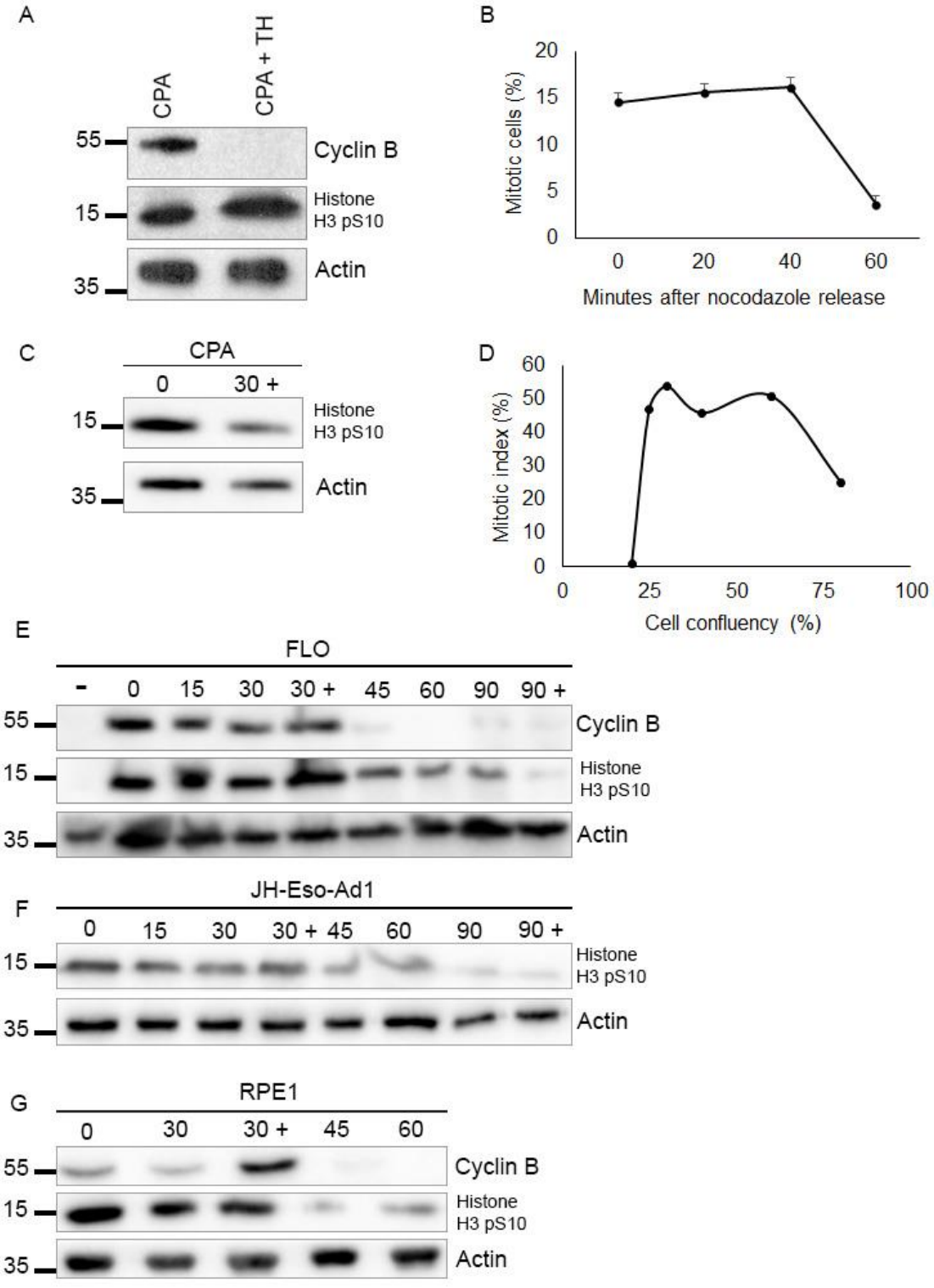
A
CPA
CPA + TH
55
Cyclin B
15
Histone
H3 pS10
35
Actin
B
Mitotic cells (%)
20
15
10
5
0
0
20
40
60
Minutes after nocodazole release
C
CPA
0
30 +
15
Histone
H3 pS10
35
Actin
D
Mitotic index (%)
60
50
40
30
20
10
0
0
25
50
75
100
Cell confluency (%)
E
FLO
-
0
15
30
30 +
45
60
90
90 +
55
Cyclin B
15
Histone
H3 pS10
35
Actin
F
JH-Eso-Ad1
0
15
30
30 +
45
60
90
90 +
15
Histone
H3 pS10
35
Actin
G
RPE1
0
30
30 +
45
60
55
Cyclin B
15
Histone
H3 pS10
35
Actin

Figure 5.1: Optimisation of synchronisation methods in BE and OEAC cells. A) Synchronisation of CPA cells using thymidine (+TH) compared with unsynchronised controls (CPA). B) Nocodazole washout in CPA cells. Cells were fixed at the specified time points and the mitotic index was counted. 0 mins MI: 14.6%, 20 mins MI: 15.6%, 40 mins MI: 16.2%, 60 mins MI: 3.6% C) Synchronising CPA cells with palbocyclib and nocodazole. + indicates a 20 minute incubation in MG132. D) Effect of confluency was tested for cells synchronised with palbocyclib and nocodazole. Cells were plated at different densities prior to synchronisation and then after incubating with nocodazole, were fixed and stained to quantify the mitotic index. 20% confluent MI: 1%, 25% confluent MI: 47%, 30% confluent MI: 54%, 40% confluent MI: 46%, 60% confluent MI: 51%, 80% confluent MI: 25%. E/F/G) time course synchronisations of FLO (E), JH-Eso-Ad1 (F) and RPE1 (G). FLO and JH-Eso-Ad1 cells were synchronised with thymidine and nocodazole, RPE1 with palbocyclib and nocodazole. Numbers indicate the minutes post release from nocodazole. +30 indicates a 20 minute MG132 incubation and +90 indicates a 15 minute incubation in RO3306.

5.1.2. FLO and JH-Eso-Ad1:

The FLO and JH-Eso-Ad1 cell lines readily responded to a standard single thymidine/nocodazole synchronisation. Western blot analysis of FLO cell lysates collected at 15-minute intervals for the first hour after release and then at 90 minutes showed that the cells reached metaphase after 30 minutes as indicated by the high levels of both cyclin B and histone H3 pS10, which were maintained by the presence of the proteasome inhibitor MG132 for 20 minutes. The cyclin B signal almost disappeared after 45 minutes suggesting the cells had entered anaphase. The histone H3 pS10 signal was greatly reduced by 90 minutes and almost completely abolished after the addition of the CDK1 inhibitor RO3306, indicating that after this time the cells have exited mitosis and were in G1 (figure 5.1 E). A similar result was observed in JH-Eso-Ad1 cells. Again, at 30 minutes both with and without MG132 the levels of histone H3 pS10 were high and then steadily declined towards the 90-minute mark (figure 5.1 F).

5.1.3. RPE1:

RPE1 cells also failed to respond to the single thymidine/nocodazole synchronisation, and therefore I opted to try synchronising them with palbocyclib. Like CPA, RPE1 cells responded well to the combination of palbocyclib and

nocodazole, and a large mitotic population could be obtained. Western blot analysis of lysates again showed that the levels of both cyclin B and H3ps10 were highest after 30 minutes in the presence of MG132. The levels of cyclin B dropped to almost undetectable levels at 45 minutes and levels of H3ps10 were greatly reduced at the 45 and 60-minute time points. This would therefore suggest that palbocyclib and nocodazole is a suitable drug combination for synchronising RPE1 cells and that after 30 minutes a metaphase population (enhanced by the addition of MG132) can be achieved (figure 5.1 G).

5.2. Investigating the kinetochore interactome in BE and OEAC cells.

5.2.1. Rapid immunoprecipitation coupled with mass spectrometry.

In order to further investigate the kinetochore composition in OEAC cells, I next sought to use mass spectrometry to examine the interactome of key kinetochore proteins in BE and OEAC cells. To this goal, I decided to use a technique called Rapid Immunoprecipitation Mass spectrometry of Endogenous protein (RIME), which works by crosslinking proteins with formaldehyde to stabilise the complexes that can then be immunoprecipitated using an antibody against a specific bait protein (figure 5.2 A). By purifying and analysing the proteins within a complex, important insights into the structure, function and biological relevance of interactions can be obtained (Mohammed *et al.,* 2016). As a proof of principle experiment, I first tried RIME using HeLa cells with the CCAN protein CENP-C as bait because this protein acts as the platform for the assembly of the outer kinetochore (Przewloka *et al.,* 2011). HeLa cells were synchronised into metaphase using a single thymidine/ nocodazole block and released in the presence of MG132. Prior to collection cells were treated with formaldehyde and the resulting protein extracts were used in immunoprecipitation experiments with magnetic beads conjugated to either an anti CENP-C antibody or generic, non-specific IgG as a control. To compare the overall yield of proteins achieved with crosslinking, an experiment without crosslinking was also carried out. Western blot analysis of the immunoprecipitated samples (figure 5.2 B) indicated the presence of CENP-C in the starting cell lysates and after IP with the CENP-C antibody, whereas no CENP-C was detected on beads conjugated to IgG only. This result indicated that CENP-C had been successfully pulled down, this result further confirmed by silver staining

(figure 5.2 C). These samples were sent for analysis by mass spectrometry in collaboration with Dr Clive D'Santos (CRUK Cambridge institute). The MS results, a subset of which can be seen in table 5.1**,** were somewhat encouraging as they confirmed that CENP-C had been pulled down (albeit with a low score) along with a number of other KMN and CCAN proteins including the entire Ndc80 complex, but only after crosslinking. These results also showed that the yield of proteins was increased when cells were treated with formaldehyde, thus providing a better coverage of the kinetochore proteins present in the sample. Having had some success with RIME in HeLa cells, I moved onto OEAC cells, starting with FLO cells because they showed a high percentage of chromosome alignment defects and could be readily synchronised. Western blot analysis (figure 5.2 D) and silver stain analysis (figure 5.2 E) suggested that CENP-C had been immunoprecipitated in both cross-linked and un-cross-linked samples, but MS analysis did not identify the bait protein, or any of the CCAN or KMN network proteins. Multiple repeats of this experiment led to the same results, indicating that using RIME in FLO cells with CENP-C as a bait was not a suitable technique.

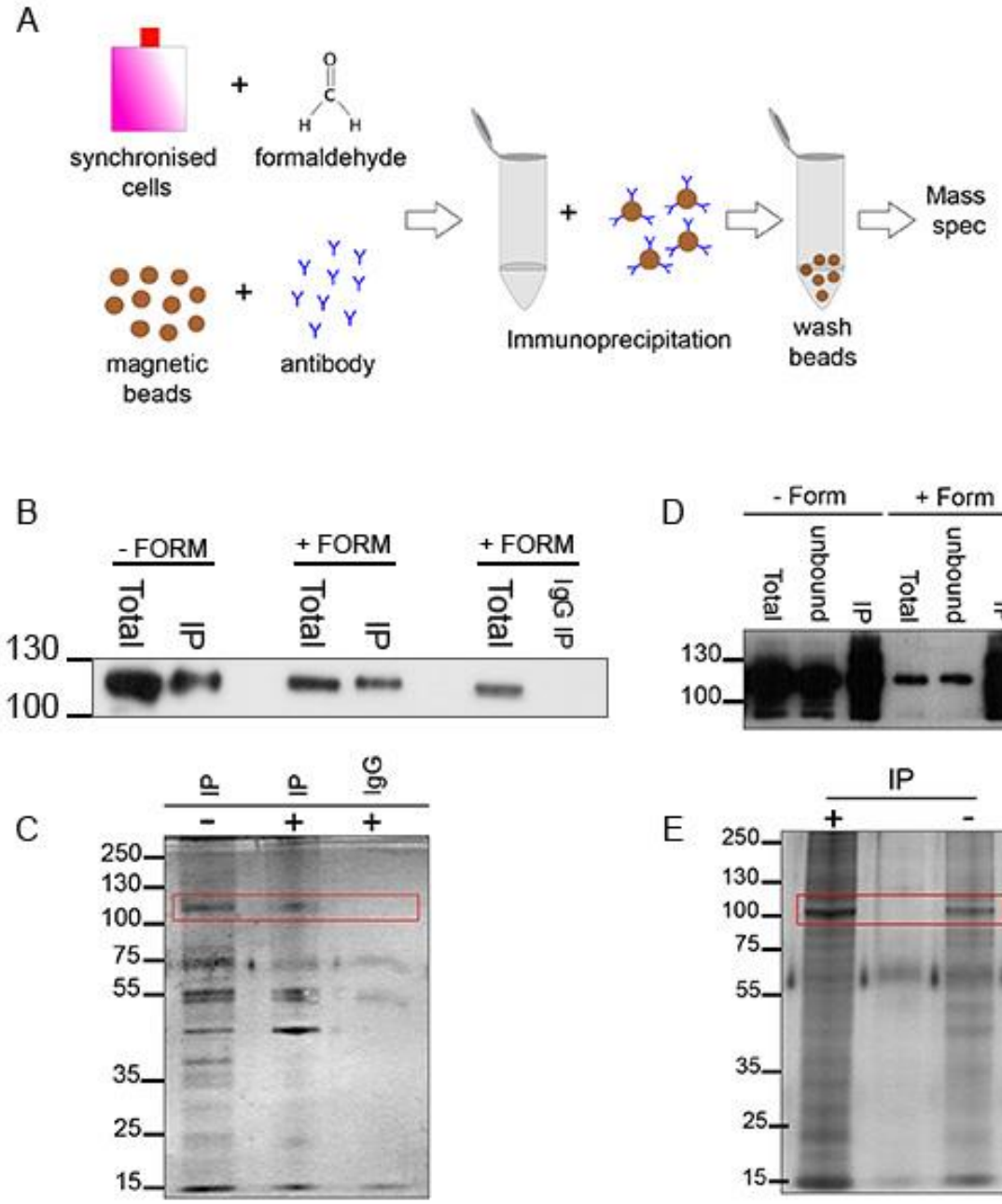

Figure 5.2: Rapid immunoprecipitation mass spectrometry (RIME) of CENP-C. A) Overview of experimental procedure. Synchronised cells are treated with formaldehyde then mixed with magnetic beads that have been conjugated to antibodies targeting the bait protein. Following a 4 hour incubation the beads are washed and then analysed via MS. B) Western blot and C) silver stain of CENP-C immunoprecipitation with (+ form) and without (- form) crosslinking in HeLa and D) western blot and E) silver stain of CENP-C immunoprecipitation with (+form) and without (- form) crosslinking. Numbers to left of blots indicate protein ladder sizes. Total refers to starting supernatant, unbound refers to supernatant not bound to beads and IP refers to beads following immunoprecipitation. Red box indicates CENP-C band.

	+ formaldehyde		- formaldehyde	
Name	**Score**	**Peptides**	**Score**	**Peptides**
CENP-F	149.09	47	4.20	1
CENP-V	17.05	4	2.58	-
INCENP	16.71	4	6.72	-
Spc24	11.98	3	3.95	1
Nuf2	10.34	3	-	-
Aurora B	4.15	2	2.22	1
Spc25	3.20	1	-	-
Nsl1	2.62	1	-	-
ZWINT	2.61	1	-	-
CENP-E	2.39	1	-	-
CENP-C	1.98	1	20.82	8
Ndc80	1.96	1	-	-

Table 5.1: RIME data for centromere/kinetochore proteins in HeLa cells with and without crosslinking. Proteins are sorted based on score in the crosslinked samples. Yellow- CCAN, blue - CPC, green - KMN and violet - RZZ

5.2.2. Targeting Ndc80 for immunoprecipitation yields the entire KMN network

The sequencing data and western blot analysis presented in the previous chapters indicated that Ndc80 was overexpressed in OEAC cell lines suggesting that Ndc80 could be a more suitable bait for immunoprecipitation than CENP-C. As part of the KMN, Ndc80 should co-precipitate with the entire network along with members of the CCAN, as Ndc80 is known to be recruited by CENP-C and CENP-T (Gascoigne and Cheeseman 2011; Suzuki *et al.,* 2011). I also decided to eliminate the formaldehyde treatment because crosslinking can often generate very large complexes that may make the identification of the bait protein and its close partners more difficult. I opted to use a different facility equipped with more sensitive machines for liquid chromatography tandem mass spectrometry (LC MS-MS). Immunoprecipitations were performed using magnetic beads conjugated to either an anti-Ndc80 antibody or purified IgG as a control and protein extracts from metaphase synchronised BE, OEAC and RPE1 cells. For each pulldown, the presence of Ndc80 was confirmed by western blot (figure 5.3 A, B, C and D) and silver stain (figure 5.3 E), in particular the silver stain of the IP with FLO cells showed a number of different bands with sizes matching those of proteins of the KMN and CCAN. These results were very encouraging and promising, suggesting that a detailed analysis and

comparison of the kinetochore interactomes in BE and OEAC cells lines was feasible.

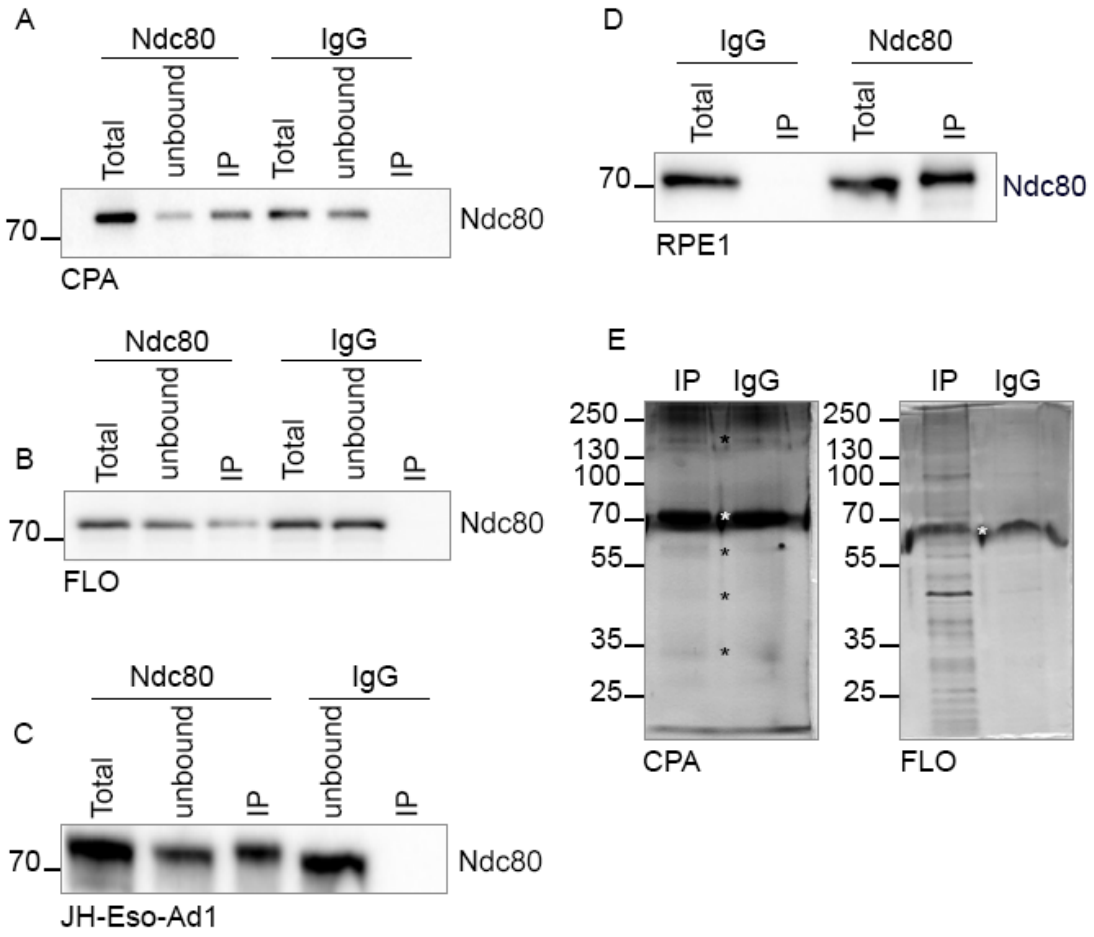

Figure 5.3: Immunoprecipitation of Ndc80 in BE and OEAC cells. Western blots of A) CPA, B) FLO, C) JH-Eso-Ad1 and D) RPE1 immunoprecipitations, and E) silver stain analysis for CPA and FLO beads. Numbers to the left of the blots refer to the sizes of the protein ladder. Total refers to whole cell lysate prior to bead incubation, unbound refers to supernatant removed from beads following incubation and IP refers to beads bound to bait protein. Ndc80 lanes are taken from immunoprecipitations using beads conjugated to Ndc80 and IgG lanes are from beads conjugated to purified IgG.

5.2.3. Mass spectrometry data shows variability between KMN subcomplexes in BE and OEAC cells.

The CPA cells were chosen as our reference for pre-cancerous cells, but unfortunately the MS results indicated that the IPs with these cells required further optimisation because the bait protein was only detected in one of the three pulldown experiments and had a very low MASCOT score (hereafter referred to as score) and few peptide hits (score 171, peptides 5). In the data set CPA_02, only the Ndc80 complex proteins Spc24 (score 162, peptides 3) and Nuf2 (score 47, peptides 2) were identified and in CPA_03 the only KMN/CCAN protein found was Knl1 (score 31 peptides 1) (table 5.2) (for full data set see supplementary material).

	CPA_01			CPA_02			CPA_03	
	Score	Peptides		Score	Peptides		Score	Peptides
Ndc80	171	5	Spc24	162	3	Knl1	31	1
Spc24	158	3	Nuf2	47	2			
Nuf2	112	4						
CENP-I	49	2						
ZWINT	39	1						

Table 5.2: MS results for the centromere/kinetochore proteins in CPA cells. Proteins in each repeat have been sorted by score. Green - Ndc80 complex, yellow - CENP/CCAN, Knl1 complex.

As an alternative to CPA, I decided to employ the non-transformed RPE1 cell line (for full data set see supplementary material). In RPE1 cells Ndc80 was identified in two separate IPs with near identical scores (score 1462, peptides 42 vs score 1416, peptides 47) (table 5.3) comparable to the most successful scores obtained with FLO cells (table 5.4). However, there was a significant difference between the two replicates. In only one of the repeats (RPE_01) all the four subunits of the Ndc80 complex were identified whereas in the other (RPE_02) just a few KMN/CCAN proteins were found. Additionally, only one of the Mis12 complex proteins was pulled down in RPE_01 (Nsl1; score 33 and 1 peptide). The CPC proteins - Aurora B, INCENP and Borealin - the motor protein CENP-E, and the checkpoint protein Bub3 also had very low scores and only one peptide hit.

	RPE1_01			RPE1_02	
	Score	Peptides		Score	Peptides
Ndc80	1462	42	Ndc80	1416	47
Nuf2	867	24	INCENP	65	1
Spc24	699	13	Knl1	41	1
Spc25	399	11	CENP-V	38	1
ZWINT	181	3			
Aurora B	160	3			
INCENP	65	1			
Knl1	53	1			
CENP-E	51	1			
Borealin	51	1			
Bub3	38	1			
Nsl1	33	1			

Table 5.3: MS results for the centromere/kinetochore proteins in RPE1 cells. Proteins in each repeat have been sorted by score. Green - Ndc80 complex, violet - Knl1 complex, pink - CPC, yellow - CENP/CCAN, red - SAC and blue - Mis12 complex.

The results achieved for the FLO IPs were very good (table 5.4) (for full data set see supplementary material). All members of the Ndc80 complex were identified in three out of four repeats (Nuf2 was not detected in experiment FLO_02) and a similar result was observed for the Mis12 complex (Dsn1 was not present in experiment FLO_02). The KMN network protein Knl1 was present in all four experiments along with its associated protein Zwint (not found in experiment FLO_02). Additionally, the CENP proteins CENP-V, CENP-I and CENP-E were found in two of the repeats (experiment FLO_02: CENP- V and CENP-E, and FLO_03: CENP-I) along with some of the CPC proteins. Having obtained some more consistent results with this cell line, I tried to understand whether any imbalances amongst kinetochore components could be observed, by preliminarily comparing the protein scores of the KMN components. Although this does not represent a rigorous quantitative MS method, it could still give some semi-quantitative indications about possible differences in the amount of these proteins. As expected, the bait Ndc80 consistently scored the highest (FLO_01: score 1835, peptides 54; FLO_02: score 810 peptides 30; FLO_03 score 1948, peptides 59 and FLO_04: score 1858,

peptides 44). In half of the repeats the second highest scoring Ndc80 complex protein was Nuf2 (FLO_03: score 1074, peptides 33 and FLO_04: score 1446, peptides 35) while in the other half it was Spc24 (FLO_01: score 1835, peptides 54 and FLO_02: score 560, peptides 13). Spc25 was consistently the lowest scoring Ndc80 complex protein (FLO_01: score 325, peptides 8; FLO_02: score 265, peptides 6; FLO_03: score 526, peptides 13 and FLO_04: score 675, peptides 14). As the Ndc80 complex is formed of stoichiometric amounts of the heterodimers of Ndc80/Nuf2 and Spc24/Spc25 it would be expected that these proteins should present similar scores. However, this was not the case, particularly for the Spc24/Spc25 heterodimer, in which Spc24 consistently scored higher than Spc25 and had more peptides, with in some cases more than 2-fold difference. There was less discrepancy in the scores of the Mis12 complex proteins as in the majority of cases the scores were all relatively similar, with the exception of Dsn1 in experiment FLO_03, which had a score over 2-fold higher than its other partners (score 273, peptides 10). Notably, the overall scores for the Mis12 complex, whilst more consistent across the repeated experiments and all four subunits, were much lower than those for the Ndc80 complex. The values for Knl1 were the most inconsistent across all four repeats (FLO_01: score 452, peptides 14; FLO_02: score 254, peptides 8; FLO_03 score 161, peptides 8 and FLO_04 score 121, peptides 4). In three out of the four repeats Zwint was also present, scoring very similarly in each repeat (Table 5.4).

	FLO_01			FLO_02	
	Score	Peptides		Score	Peptides
Ndc80	1835	54	Ndc80	810	30
Spc24	981	19	Spc24	560	13
Nuf2	849	23	Spc25	265	6
Knl1	452	14	Knl1	254	8
Spc25	325	8	Nsl1	72	2
ZWINT	150	5	INCENP	63	1
Nsl1	127	6	Pmf1	61	1
Dsn1	124	4	Mis1	59	2
Aurora B	115	2	CENP-V	50	1
Pmf1	99	2	CENP-E	35	2
Mis12	96	4			
Borealin	88	2			
	FLO_03			FLO_04	
	Score	Peptides		Score	Peptides
Ndc80	1948	59	Ndc80	1858	44
Nuf2	1074	33	Nuf2	1446	35
Spc24	848	23	Spc24	1112	17
Spc25	526	13	Spc25	675	14
Dsn1	273	10	Nsl1	252	3
Knl1	161	8	ZWINT	143	2
ZWINT	139	6	Pmf1	125	2
Nsl1	128	4	Knl1	121	4
Mis12	114	3	Dsn1	70	2
Pmf1	82	2	Mis12	50	1
CENP-I	30	1			

Table 5.4 MS results for the centromere/kinetochore proteins in FLO cells. Proteins in individual repeats are sorted by score. Green - Ndc80 complex, violet - Knl1 complex, blue - Mis12 complex, pink - CPC and yellow - CENP/CCAN.

The MS data for the IPs using the JH-Eso-Ad1 cell line yielded far fewer hits compared to FLO cells (Table 5.5) (for full data set see supplementary material). Again, as predicted, Ndc80 was the highest scoring protein in all three repeats (JH_01: score 490, peptides 19; JH_02: score 333, peptides 11 and JH_03: score 667, peptides 23), and the rest of the Ndc80 complex co-precipitated with the bait protein in almost all IPs, with the only exception of Spc24 in experiment JH_02. Like for FLO cells, Spc25 was consistently the lowest scoring protein of the Ndc80

complex (JH_01: score 39, peptides 1; JH_02: score 103 peptides, 2 and JH_03: score 182, peptides 4). When comparing the scores across the repeats and within the complexes, the results were highly variable and the scores considerably lower than those obtained with FLO cells (for full MS results see supplementary materials).

	JH _01			JH _02			JH _03	
	Score	Peptides		Score	Peptides		Score	Peptides
Ndc80	490	19	Ndc80	333	11	Ndc80	667	23
Nuf2	395	9	Nuf2	173	5	Spc24	515	6
Spc24	382	5	Spc25	103	2	Nuf2	361	12
Spc25	39	1				Spc25	182	4
CENP-I	1	1				ZWINT	87	1

Table 5.5 MS results for the centromere/kinetochore proteins in JH-Eso-Ad1 cells. Proteins from individual repeats are sorted by score. Green - Ndc80 complex, yellow - CENP/CCAN, violet - Knl1 complex.

In summary the results presented in this chapter indicate it is possible to synchronise BE and OEAC cells and to specifically in FLO cells, isolate and characterise the entire KMN network along with some CCAN components by using Ndc80 as bait in IP-MS experiments. Furthermore, an initial qualitative analysis of these data suggests a possible imbalance amongst components within the outer kinetochore. However, it is important to point out that these results are simply indicative because using MASCOT scores and number of peptides is not a valid method to properly quantify the amounts of proteins by MS, and further troubleshooting is currently required to ensure the reproducibility of these results. Nevertheless, the experiments presented here provide the basis for future optimisations that would ultimately lead to a more rigorous quantitative MS analysis, using for example tandem mass tag (TMT) MS, to properly characterise differences in the composition and post translational modifications of the kinetochore proteins.

6. Discussion

6.1. BE and OEAC cells present mitotic defects and mitotic slippage.

The overarching aim of my project was to identify the origin(s) of polyploidy in BE and OEAC cells. Polyploidy is known to propagate chromosomal instability (CIN)

and accelerate cancer heterogeneity and evolution (Dewhurst *et al*., 2014; Fujiwara *et al.,* 2005; Gordon, Resio and Pellman 2012). Therefore, the identification of the molecular basis underpinning genome doubling in OEAC is crucial to both understanding the evolution of a very heterogeneous cancer like OEAC and designing new tools for its diagnosis therapy.

My first observations of mitoses in BE and OEAC cells revealed a series of mitotic defects including multipolar spindles, lagging chromosomes and scattered chromosomes, which would suggest that genome doubling following loss of p53 occurs as a result of defective cell division. Interestingly, a lower incidence of some of these mitotic defects were observed in dysplastic p53-mutated BE cells (CPD) and a very few abnormal mitoses were found in BE cells containing WT p53 (CPA) (figure 3.1 C/D and figure 3.7 B).

CPA cells have been classified as having a near diploid genome (table 3.1); despite there being no observed mitotic defects in fixed cells (figure 3.1 and figure 3.2) analysis by time lapse microscopy revealed that approximately 10% of non-dysplastic CPA cells had lagging chromosomes in anaphase (figure 3.7 B) and in the tetraploid p53-mutated dysplastic BE cell line CPD, lagging chromosomes were observed in approximately 2% of fixed cells (figure 3.1 D). Lagging chromosomes are typically a result of merotelic kinetochore microtubule attachments. Merotelic attachments are common in early mitosis and are usually repaired prior to anaphase. However, if these attachments are left unrepaired, they can go unnoticed by the SAC, resulting in loss or gain of chromosomes and consequently the formation of aneuploid daughter cells. When examining mitosis by time lapse microscopy in CPA cells I did not observe any mitotic delay (figure 3.6 B and figure 3.7 C) or chromosome alignment defects. However, merotelically attached kinetochores are capable of accurately congressing to the metaphase plate (Cimini *et al*., 2003; Cimini, Cameron and Salmon 2004) and do not cause a SAC induced metaphase delay (Cimini, Cameron and Salmon 2004; Cimini 2007), which is consistent with the lack of these phenotypes in this cell line. As lagging chromosomes results in aneuploid daughter cells, it can induce a modest increase in the rate of further chromosome mis-segregation (Nicholson et al., 2015).These results suggest the possibility that these initial mis-segregation defects in pre-cancerous BE cells, in combination with p53 loss, might be the original cause of genomic instability, which

in turn could lead to further mis-segregation and in extreme cases prevent completion of mitosis and hence whole genome doubling.

Polyploidy can originate either through the inability of a cell to complete cytokinesis or via mitotic slippage. Mitotic slippage is a phenomenon in which cells can proceed to the G1 phase of the next cell cycle without dividing their DNA (Orth et al., 2008; Ganem, Storchova and Pellman 2007; Topham and Taylor 2013; Meek 2000), whereas cytokinesis failure occurs when the two daughter cells fail to segregate, such as when lagging chromosomes become trapped in the cleavage furrow, resulting in its regression and preventing abscission. As stated above, time lapse microscopy of CPA cells did reveal a small number of cells dividing with lagging chromosomes however this did not lead to cytokinesis failure in most of the cases. Only one cell failed to complete cytokinesis but, as discussed earlier (chapter 3.5), this was most likely the result of cellular stresses brought about by microscopy conditions. This, in combination with a low percentage of multinucleate cells (a clear readout of cytokinesis failure), both in BE and OEAC cells leads me to conclude that the most likely primary route leading to polyploidy in these cells is mitotic slippage (figure 3.3).

A current model for the origin of CIN in cancer cells is based on the increase of merotelic attachments caused by the presence of additional centrosomes (Ganem, Godinho and Pellman 2009). Additional centrosomes can be advantageous to cancer cells through the facilitation of CIN, but increased centrosome number does also increase the potential for multipolar divisions and inviable progeny, thereby stunting overall tumour growth (Kwon et al., 2008). In a recent study of centrosome amplification in BE and OEAC, Lopes and colleagues (2018) reported that centrosome amplification could be observed as early as the metaplastic stage of BE, and that amplification significantly increased with progression into dysplasia and loss of p53. With this in mind, I would have expected to see increased numbers of centrosomes in CPA and CPD cells when compared to a non-cancerous epithelial control (RPE1), however this was not the case. I observed no centrosome amplification in either BE cell line. Lack of centrosome amplification in CPA cells could be explained both by the presence of WT p53, as p53 is known to suppress centrosome amplification, and by the lack of mitotic defects in these cells. However, it was surprising to find that there was no significant increase of supernumerary

centrosomes in CPD cells (figure 10), considering the mitotic defects (i.e. lagging and scattered chromosomes) observed in this cell line (figure 3.1 D). Lopes *et al* (2018) also reported that the incidence of centrosome amplification decreased in OEAC, but my results showed the opposite (figure 3.4), which never the less falls into line with one of their concluding remarks that centrosome amplification is dynamic, context dependant and has different consequences in the progression of BE into OEAC (Lopes *et al.,* 2018). Possible explanations for these discrepancies include the use of different BE and OEAC cell lines and/or different sensitivity of the cells to experimental manipulation. Based on the frequency of defects observed in CPD and OEAC cells (figure 3.1 C and D), I would predict that in CPA cells defective mitosis should be apparent in approximately 0.3% of the total cell population, which suggests that a very large number of cells (>300) would need to be imaged to enable observation of these defects in just one or two cells. As it was challenging to culture both CPA and CPD cells under microscopy conditions, further optimisation is required to achieve accurate results regarding mitotic progression and the potential for centrosome amplification in these cell lines. As cells will often cluster additional centrosomes into a bipolar arrangement (Ring, Hubble and Kirschner 1982; Brinkley 2001; Nigg 2002) to prevent multipolar divisions, another limitation to the experiments is the fact the majority of the observations come from fixed cells, or in live cells lacking centrosomal markers. Therefore, I could not assess whether multipolar divisions in OEAC cells would cluster their supernumerary centrosomes to generate viable progeny. Further investigation using centriole and pericentriolar matrix (PCM) markers in live cell imaging would be necessary to properly understand the impact of extra centrosomes in the progression of BE into OEAC.

In conclusion, my results provide compelling evidence that would suggest that mitotic defects and polyploidy potentially originate from mitotic slippage caused by defective chromosome attachments in both dysplastic BE and OEAC cells.

6.2. Imbalanced kinetochores drive chromosome mis-segregation via aberrant kinetochore-microtubule interactions in OEAC cells.

The most prevalent mitotic defect observed in OEAC cells was the presence of scattered chromosomes, which likely indicates chromosome congression failure which is typically caused by defective kinetochores. Given that kinetochores play a

critical role in mitosis, structural and/or functional alterations to kinetochore and centromere genes have been widely implicated in the promotion of chromosome mis-segregation and aneuploidy (Cimini and Degrassi 2005; Yuen, Montpetit and Hieter 2005). Analysis of kinetochore gene structure and expression in paired BE and OEAC samples using WGS coupled with analysis of kinetochore protein expression via western blot and IF, revealed a number of chromosomal aberrations and abnormal expression and/or localisation of numerous important constituents of the inner and outer kinetochore.

Total protein analysis by western blot indicated that the outer kinetochore protein Ndc80 is overexpressed in dysplastic BE and OEAC cells, a phenomenon that has only previously been described in brain, liver, breast and lung cancers (Pérez de Castro, de Cárcer and Malumbres 2007). Ferretti et al., (2010) showed that increase in total Ndc80 translated into increased accumulation of this protein at the kinetochore in human colorectal carcinoma (Hct116), colorectal adenocarcinoma (HT29), osteosarcoma (U2OS) and cervix adenocarcinoma (HeLa). This led the authors to speculate that increased accumulation of Ndc80, as part of the Ndc80 complex, might influence the interaction between kinetochores and microtubules. I similarly found that in OEAC cells, when the total Ndc80 expression is increased, the ratio of Ndc80 at the kinetochores compared to the centromeric marker CREST increased accordingly when compared to non-malignant controls. This similarity could indicate a common mechanism for the establishment of CIN in both cell types, something that I will also discuss later in this chapter.

It is well known that dysplastic BE and OEAC cells have mutated p53, but there is no evidence that this transcription factor regulates Ndc80 expression, which has been instead linked to the retinoblastoma tumour suppressor gene (pRb) (Ferretti *et al.,* 2010). pRb has also been linked to the altered transcription of a number of other mitotic proteins (Iovino *et al.,* 2006; Amato *et al.,* 2006). It is therefore possible that progressive loss of tumour suppressors like p53 and RB, a mechanism reported in the non-genome doubled pathway of OEAC progression (Stachler *et al.,* 2015), could trigger Ndc80 overexpression in BE cells, which would in turn impact kinetochore assembly and chromosome congression. In the early stages of mitosis, Ndc80 phosphorylation by Aurora B reduces its microtubule binding affinity to correct improper kinetochore microtubule attachments (Biggins *et*

al., 1999; Tanaka *et al.,* 2002; Cimini et al., 2006; Cheeseman 2006; DeLuca 2006). As the cell proceeds into metaphase, this phosphorylation is reduced to allow for correct bipolar kinetochore microtubule attachments to be stabilised (Caldas, DeLuca and DeLuca 2013). At this stage, Aurora B activity is counteracted by protein phosphatase 1 (PP1) and protein phosphatase 2A (PP2A) (Foley, Maldonado and Kapoor 2011; Suijkerbiyk *et al.,* 2003; Kruse *et al.,* 2013). My observations indicated that CPD cells have significantly reduced levels of Aurora B at the kinetochores (figure 4.7 B), which is in line with the sequencing data that highlighted a deletion in Aurora B in this cell line. Aurora B levels were also reduced in OEAC cells containing scattered chromosomes (figure 4.7 C). Together, these findings lead to the hypothesis that a combination of reduced Aurora B and Ndc80 overexpression could result in low Ndc80 phosphorylation and the formation of hyperstable kinetochore microtubule attachments. If these attachments are erroneous, this would impair the formation of bipolar attachments and have a detrimental effect on mitotic progression. As explained previously, merotelic attachments, in which both sister kinetochores are attached to microtubules from the same pole (Kwon et al., 2008), are hyperstabilised this could induce mitotic arrest because of lack of adequate tension between the sister kinetochores. A prolonged mitotic arrest would then likely result in mitotic slippage and consequent formation of polyploid cells.

Another player that may be involved in the disruption of forming adequate kinetochore microtubule attachments in BE and OEAC cells is the KMN network constituent Knl1. Knl1 has been reported to be essential for efficient kinetochore microtubule attachment dynamics through BubR1 mediated targeting of Aurora B (Caldas *et al*., 2013). It also has a role in counteracting Aurora B directly via PP1 and indirectly via PP2A, and the Knl1 mediated recruitment of BubR1 and Bub1 is known to promote Aurora B localisation and activity respectively (Lampson and Kapoor 2005; Kiyomitsu, Obuse and Yanagida 2007; Suijkerbiyk et al., 2012; Kruse et al., 2013). Loss of Knl1 has been reported to affect the entire kinetochore (Cheeseman *et al.,* 2004): firstly it abolishes the Aurora B phosphorylation of Ndc80 and the Mis12 complex protein Dsn1, preventing the proper regulation of kinetochore microtubule attachments (Caldas *et al.,* 2013); and secondly, it was shown in *Drosophila* that RNAi of Knl1 caused scattered chromosomes due to congression failure, followed by a block in cell proliferation, an effect also observed in human cells, although not as

pronounced (Przewloka *et al.,* 2007). Finally, it has been shown that when Knl1 is depleted the inter kinetochore distances of bioriented chromosomes were significantly increased, indicating either hyperstable kinetochore microtubule interactions or weakened sister chromatid cohesion (DeLuca *et al.,* 2006; Stevens *et al.,* 2011; Caldas *et al.,* 2013), a phenomenon that will also be discussed in more detail later in this chapter. Unfortunately, I was unable to obtain quantifiable results for total protein and kinetochore levels of Knl1 as the antibody was not suitable for western blot, and would not readily co-stain with the CREST antibody. However, the sequencing analyses showed the presence of numerous chromosomal aberrations, including LOH and hemizygous deletions in OEAC patient samples (table 4.2), and similar results were also found in the cell lines (figure 4.1). Furthermore, immunofluorescence microscopy indicated a potential Knl1 mis-localisation in cells with scattered chromosomes, highlighting a potential defect that could contribute to the chromosome alignment defects observed in OEAC cells.

One of the stand-out observations from the WGS of paired BE and OEAC samples was the incidence of chromosomal aberrations in CENP-V (table 4.3). Very little is known about the role of CENP-V in cancer. A study from Tadeu *et al.,* (2008) reported that CENP-V depletion in HeLa cells resulted in defects in chromosome alignment, lagging chromosomes in anaphase, destabilisation of the CPC and cytokinesis failure, all of which I have observed in BE and OEAC cells. Interestingly, the study also found that when CENP-V was depleted in HeLa cells this corresponded to a clear reduction in the levels of Aurora B, and caused it to localise abnormally to the axis between the chromosome arms (Tadeu *et al.,* 2008). Whilst CENP-V has not been previously reported to be affected in OEAC, WGS of paired BE and OEAC samples from patients indicated that the majority of the OEAC samples had hemizygous deletions in the CENP-V gene, which were also found in genome sequencing of the OEAC cell lines (figure 4.1). It is interesting that the gene encoding the CPC component Aurora B, as mentioned earlier, also presents similar deletions in the cell lines and high frequency of copy number loss in paired BE and OEAC patient samples. It could therefore be suggested that loss of CENP-V could cause Aurora B mis-localisation thereby affecting its role in error correction. IF analyses indicated a reduced level of Aurora B at the kinetochore in CPD cells and in cells with scattered chromosomes, both of which could be attributed to a reduction in

the levels of CENP-V. IF and western blot analysis of CENP-V in BE and OEAC cells could help understand if deletions in this gene affect total protein expression and its localisation to kinetochores.

The CCAN constituent CENP-I was also significantly affected by copy number alterations, as highlighted by the WGS of both the paired samples and the OEAC cell lines (table 4.3). CENP-I is known to be required for the localisation of CENP-F, Mad1 and Mad2 to the kinetochore, and depletion of CENP-I in HeLa cells generates the following three major phenotypes: (i) cell cycle progression delays, in which cells are reported to be delayed in G2 phase; (ii) a high incidence of mitotic cells in which chromosomes have monopolar attachments; and (iii) a defective mitotic checkpoint, probably as a secondary effect through reduced localisation of Mad2 at kinetochores (Liu *et al.,* 2003). Relating this back to my data, it could be argued that, if as expected CENP-I copy number alterations affect its expression and/or localisation to the kinetochore, this might be responsible for inducing the SAC induced mitotic delay in OEAC cells, which in turn would induce mitotic slippage and polyploidy.

One of the most overexpressed genes highlighted in the sequencing data was PPP1R1B, otherwise known as DARPP-32. DARPP-32 is a recognised neuronal protein, and is a potent inhibitor of the cell cycle regulatory enzyme protein phosphatase 1 (PP1) (Bibb *et al.,* 1999; Greenguard 2001). Amplification of DARPP-32 and its truncated isoform t-DARPP has been previously shown in 68% of gastric cancers (Belkhiri, Zhu and El-Rifai 2016), and several studies have also indicated its over expression in cancers of the breast, prostate, colon and oesophagus - specifically in 30% of cases of oesophageal squamous cell carcinoma (El-Rifai *et al.,* 1998; El-Rifai *et al.,* 2001; Christenson, Denny and Kane 2015; Vangamudi *et al.,* 2010; Gu, Walainy and Kane 2009; Wang *et al.,* 2005; Ebihara *et al.,* 2004). A study by Mukherjee *et al.,* (2010) demonstrated that in human gastric adenocarcinoma tissues DARPP-32 is over expressed in the early stages of gastric tumorigenesis, suggesting that this event may participate to the transition of intestinal metaplasia and progression into adenocarcinoma. The data presented in this study in combination with my findings would therefore indicate PPP1R1B as another potential driver for BE progression into OEAC, however the effect of PPP1R1B overexpression at the kinetochore and how this may impact mitosis is yet to be elucidated.

Further evidence for an imbalanced kinetochore in OEAC cells can be drawn from the mass spectrometry data shown in tables 5.2 - 5.5 in which in all the cell lines examined I noticed a clear difference between the abundance of the proteins within each complex of the KMN network. This data, together with the results from the protein expression and IF image analyses, support the theory that a defective kinetochore might be responsible for impeding successful chromosome congression and inducing mis-segregation, mitotic failure and polyploidy.

6.3. Defective kinetochore microtubule attachments trigger SAC induced mitotic arrest and mitotic slippage in OEAC cells.

As touched upon previously in this chapter, the data I have collected suggests that the kinetochore microtubule attachments might be compromised due to imbalances in kinetochore components and/or their regulation by phosphorylation. Investigations into kinetochore microtubule attachments using Astrin as a marker indicated that OEAC cells may have a problem in converting from the initial lateral attachment to the end-on configuration (figure 4.12), thus preventing the generation of the forces required to drive chromosome congression, which would explain the scattered chromosome phenotype observed in these cells.

Another recognised cause of aneuploidy is a defective mitotic checkpoint. My experiments indicated that both BE and OEAC cells possessed a functional SAC, but WGS and western blot analyses of individual SAC components showed changes to copy number and protein expression levels (figure 4.2 and table 4.4), which may act to enhance or diminish SAC activity whilst allowing it to retain some functionality. Mutations in SAC genes are rarely found in cancer (Sansregret and Swanton 2017), but there have been reports that overexpression of SAC components in mice resulted in the development of aneuploid tumours, thus leading to the proposal that a hyperstabilised SAC can lead to CIN (Sotillo *et al.,* 2007; Kato *et al.,* 2011). Up-regulation of Ndc80 has also been linked to SAC hyperactivation in mouse embryonic fibroblasts (MEFs) and tumour formation in various tissues (Diaz-Rodrigues *et al.,* 2008). Furthermore, Mad2 overexpression has been observed in tetraploid cells and shown to contribute to the over-stabilisation of kinetochore microtubule interactions, suggesting that it might be another potential candidate driving CIN (Hernando *et al.,* 2004; Sotillo *et al.,* 2007; Kabeche and Compton 2012).

In contrast with this, the WGS data from paired BE and OEAC tumour samples and of the cell lines suggest that Mad2 may actually be under-expressed, as deletions and consequent LOH occurred frequently in both BE and OEAC; this loss of Mad2, in combination with reduced expression of CCAN components, may be one of the factors involved in the generation of the scattered chromosome phenotype.

The expression of BubR1 in BE and OEAC cells should also be considered when discussing potential SAC deficiency in OEAC. Western blot analysis of total protein extracts indicated BubR1 was under-expressed in dysplastic BE and OEAC cells (figure 4.8 B), and IF showed that significantly less BubR1 was recruited to the kinetochores in the JH-Eso-Ad1 cell line (figure 4.8). Interestingly, FLO cells with scattered chromosomes also had significantly less BubR1 in comparison to their aligned counterparts. This data could therefore indicate that BubR1 under-expression may impair either SAC function or the regulation of kinetochore microtubule attachments (Lampson and Kapoor 2005; Malureanu *et al.,* 2009). As BubR1 appears to be under-expressed in cells that are already polyploid, and in those with scattered chromosomes, it is possible that reduced levels of BubR1 might contribute to chromosome segregation defects by preventing accurate regulation of kinetochore microtubule attachments. This, in turn, would allow merotelic and syntellic attachments to go unnoticed by the SAC and result in defective chromosome congression and/or segregation. BubR1 has been previously linked to aneuploidy; a number of mouse studies in mutants carrying hypomorphic alleles of BubR1 showed that a reduced protein expression made the mice more prone to aneuploidy (Baker *et al.,* 2004; Matsumoto *et al.,* 2007; Baker *et al.,* 2008). My data showed that the SAC is still functional in BE and OEAC cells because they were able to sustain a mitotic arrest after depolymerisation of microtubules (figure 3.5). However, it cannot be excluded that slight alterations to the copy number of SAC components could simply weaken, rather than completely inactivate, the checkpoint. This could allow some defective attachments to go unnoticed, resulting in lagging chromosomes and aneuploidy.

6.4. Scattered chromosomes maybe the result of both defective congression and cohesion fatigue.

Another question raised from my data is whether the scattered chromosome phenotype occurs because of chromosome congression failure or as a result of cohesion fatigue following a prolonged metaphase delay. Cohesion fatigue can be defined as the asynchronous separation of chromatids that have been arrested or delayed in metaphase, with cells often remaining locked in mitosis for some time after the chromatids have separated (Gorbsky 2013). In a study by Sapkota *et al.,* (2008) it was reported that the rates of cohesion fatigue reflect a dynamic balance between the spindle pulling forces and resistance to separation by inter chromatid cohesion. Massive separation of chromatids in cohesion fatigue would likely result in inviable progeny and it was found that a short mitotic delay combined with a partial chromosome separation is more likely to predispose cells to chromosome mis-segregation (Sapkota *et al.,* 2008). In my time-lapse experiments, I noticed that in some OEAC cells the time taken to initially congress the chromosomes was similar to that of control cells and it was only after the metaphase plate was formed that I began to notice metaphase delays and problems in maintaining chromosome alignment (figure 3.6 C and D, figure 3.7A supplementary movies). This would therefore suggest that the spread of the chromosomes over the mitotic spindle might also be the result of cohesion fatigue induced by the mitotic delay. Further investigations using live imaging of cells with microtubule spindle fluorescent markers, such as SiR-tubulin, are needed to clarify whether the scattered chromosome phenotype is caused by erroneous congression or cohesion fatigue. The possibility of a combination of the two should also be considered, as defective congression due to erroneous attachments could also trigger the initial metaphase delay responsible for the cohesion fatigue.

6.5. Conclusions and future perspectives

To conclude, based on the findings presented in this thesis, I would like to hypothesise that p53 loss in premalignant BE cells, with or without prior aneuploidy caused by chromosome segregation errors, could promote CIN which in turn would lead to imbalances in kinetochore assembly and/or regulation. Alterations such as increased expression of Ndc80 and/or reduced levels of Aurora B, Knl1 and BubR1

would lead to increased stability of kinetochore microtubule attachments, including incorrect ones like merotelic and syntellic attachments, which would ultimately result in chromosome congression and/or segregation defects. These defects would generate aneuploidy and polyploidy, propagate CIN and drive evolution and diversification of OEAC (figure 6.1).

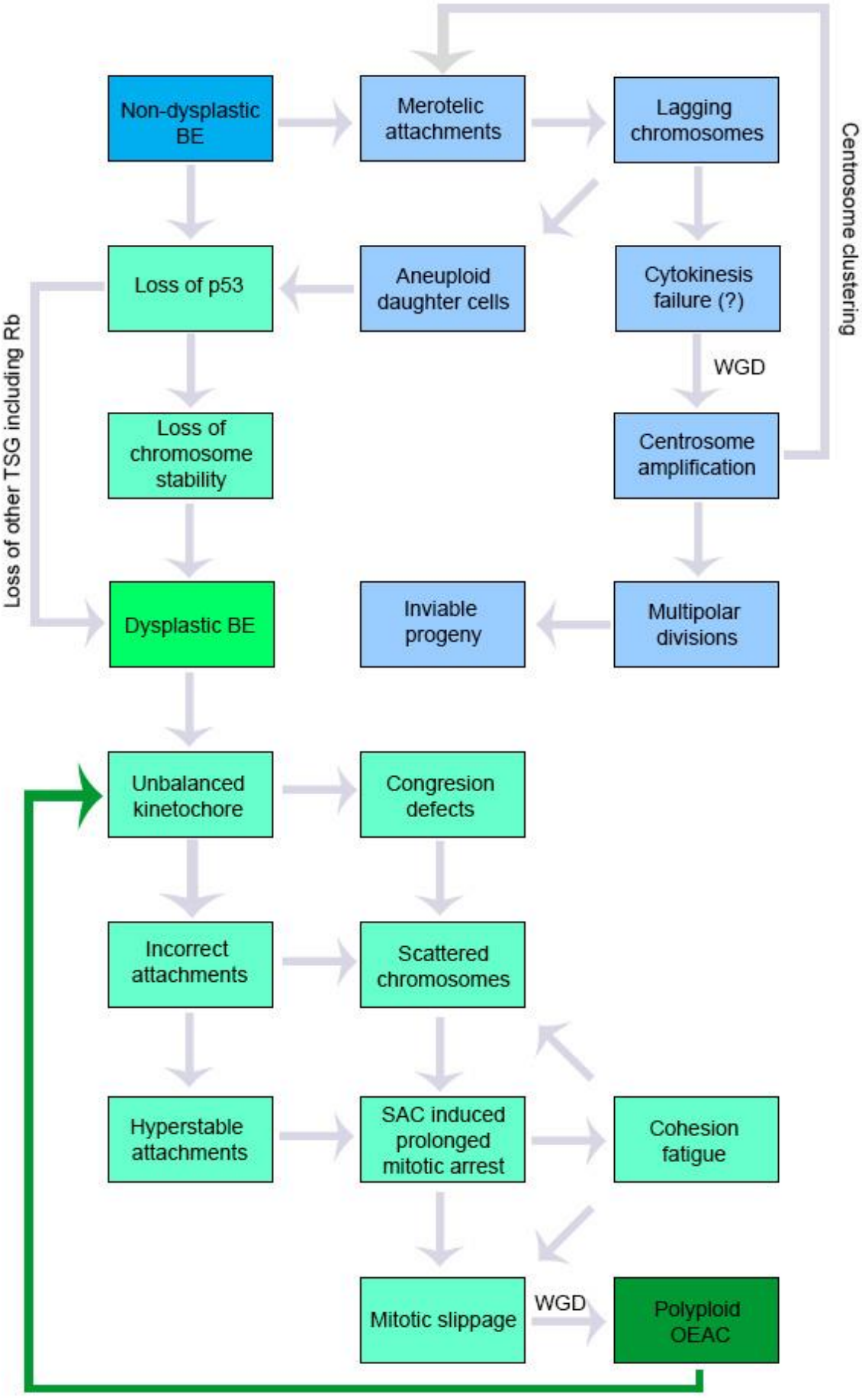
Non-dysplastic BE
Merotelic attachments
Lagging chromosomes
Centrosome clustering
Loss of p53
Aneuploid daughter cells
Cytokinesis failure (?)
WGD
Loss of chromosome stability
Centrosome amplification
Loss of other TSG including Rb
Dysplastic BE
Inviable progeny
Multipolar divisions
Unbalanced kinetochore
Congresion defects
Incorrect attachments
Scattered chromosomes
Hyperstable attachments
SAC induced prolonged mitotic arrest
Cohesion fatigue
Mitotic slippage
WGD
Polyploid OEAC

Figure 6.1 Flow diagram summarising the findings of this thesis. Starting at near diploid non dysplastic BE (dark blue) the diagram details the series of events that may result to the formation of the near diploid genome prior to loss of p53. Following loss of p53 cells become chromosomally unstable and become dysplastic (light green). Due to defective segregation and CIN these cells develop kinetochore imbalances that lead to defective kinetochore microtubule attachments, hyper stabilisation, congression defects, mitotic arrest, mitotic slippage and whole genome doubling leading to polyploid OEAC (dark green) these OEAC cells then re-enter the cycle (dark green arrow) as a consequence of polyploidy to maintain their near tetraploid genome.

The information I have presented does however still leave the question of whether the mitotic defects observed in OEAC cells are a cause or a consequence of polyploidy and subsequent CIN. This is a classic chicken and egg question that has never been resolved in the field of cancer cell biology. As the greatest percentage of mitotic defects were observed in polyploid cell lines this would suggest that they are likely a consequence of chromosome instability and/or polyploidy. However it could still be argued that they are the cause of further chromosome segregation defects by propagating CIN. The presence of chromosome mis-alignments in aneuploid OEAC organoids (figure 3.8) could also support the hypothesis that defective mitoses are the cause of CIN. The fact that segregation errors and the potential for failed mitosis were present in a small present in a small percentage of cells with a near diploid p53 positive genome (figure 3.7 B) would also suggest that, in the early onset of OEAC progression, aberrant chromosome segregation and defective mitosis is the route to triggering whole genome doubling and CIN.

The future perspectives of this project would be to firstly further investigate the incidence of defective mitosis using live imaging to assess how the cells behave in the next cell cycle following mitotic slippage. By imaging with additional markers such as tubulin for the mitotic spindle, or centrosome components, I could gain better insights into how chromosome congression and segregation are defective in the different cell lines and organoids. Further investigation into the genes highlighted by the sequencing studies to have copy number alterations may also add further clarification to how whole genome doubling may be triggered and maintained in BE and OEAC cells. Finally, another important perspective of this project would be to test whether kinetochore formation or regulation in CPA cells would trigger genome

doubling via defective mitosis. It could be possible to over and under express components of the inner and outer kinetochore in CPA cells after mutating p53 and test if this induces the cell division defects observed in OEAC cells and whether these cells progress normally through subsequent mitoses or become polyploid and chromosomally unstable. Another complimentary approach could be to alter the phosphorylation status of kinetochore components in the same p53-deficient CPA cells by treating, for example, with Aurora B inhibitors.

It would also be interesting to investigate whether the presence of mitotic defects observed in OEAC cells and organoids could help in the diagnosis and therapy of OEAC. For a long time, chromosome segregation has been a target in cancer therapy by utilising antimitotic drugs such as the microtubule poisons taxanes and vinca alkaloids. Despite having been used for many years, the non-specific nature of these drugs can lead to many toxic side effects (Herman *et al.,* 2015). More recently, drug treatments have been developed that target Aurora B or the kinesin Eg5, but these inhibitors target all dividing cells and thus have poor performance outcomes in clinical trials (Cheung *et al.,* 2009; Talapatra *et al.,* 2013). The poor performance of these drugs has been reported to be likely caused by the fact that by targeting these mitotic master regulators required in healthy cells, they are reducing the therapeutic window and efficacy of the treatment. It has therefore come to light that the next generation of antimitotic chemotherapy drugs should aim at targeting specific mitotic defects that are already present in cancer cells (Herman *et al.,* 2015). The data presented in a number of studies, including mine in this thesis, would suggest that Ndc80 could be a potential target in chemotherapy. A recent study by Ferrara and colleagues (2018) focused on using Ndc80 as an anticancer agent in cell lines derived from osteosarcoma, breast and cervical cancers, and reported some interesting results in relation to the data I have presented here. Their study reported that induction of massive aneuploidy should exert a substantial anticancer effect, and that targeting the interaction between Ndc80 and microtubules would induce chromosome segregation defects in cancer cells through the inhibition of kinetochore microtubule attachment error correction, which is a phenotype that I have observed in OEAC (figure 3.1 C and D). A previous study from the same authors showed that when kinetochores retained excess levels of Ndc80, they formed persistent lateral microtubule attachments (Mattiuzo *et al.,* 2011), again a

phenotype I observed in OEAC cells (figure 12.4). The study also reported that these laterally attached kinetochores recruited the plus end microtubule depolymerase kinesin 13/MCAK and the K-fibre stabiliser HURP, and preferentially retained the microtubule motor CENP-E (Mattiuzo *et al.,* 2011). In contrast to what I observed in OEAC cells, Ferrara *et al.,* (2018) showed that mitotic arrest and segregation errors lead to cell death via mitotic catastrophe, whereas my time lapse experiments indicated that the cells did not die after mitotic slippage (figure 3.6 and 3.7), or at least not immediately after exiting mitosis. This difference could be explained by the fact that Ndc80 overexpression isn't as pronounced in my OEAC cell lines as in other cell lines and therefore the effects were not so dramatic. Perhaps, if I could overexpress Ndc80 further in these cells they may not be able to survive the resulting cell division defects and aneuploidy.

In conclusion, one of the most significant novel findings presented in this thesis is that Ndc80 is overexpressed in OEAC and this might be at least one of the driving factors that promotes erroneous chromosome segregation and mitotic arrest, leading then to mitotic slippage and polyploidy. This in turn could induce further copy number alterations of kinetochore genes and consequent imbalances of protein complexes at the kinetochore, thereby propagating CIN. My results also indicate that measuring the level of expression of Ndc80 and other kinetochore components in OEAC may help to classify this highly heterogeneous cancer and aid in the design of better targeted antimitotic cancer therapies.

7. Identification of factors involved in the cross-talk between actin filaments and microtubules

7.1. Introduction

The cytoskeleton is a highly dynamic structure that controls a number of different cellular functions including; cell shape, polarity, motility and function. Alterations to the cytoskeleton have been linked to a number of different diseases and developmental defects in humans, including; skeletal muscle and cardio myopathies, neurodegenerative diseases, neurodevelopmental disorders and cancer (Breuss and Keays 2014; Li *et al.,* 2014; O'Connor and Chen 2013; Ouderkirk and Krendel 2014; Rubenstein and Wen 2014; Stroud *et al.,* 2014). One of the most pathologically dramatic changes associated with the dysfunction of the cytoskeleton

is the gain of invasiveness seen in tumour cells, resulting in the transition to a malignant cancer (O'Connor and Chen 2013; Ouderkirk and Krendel 2014).

The cytoskeleton is composed of three different structural elements; intermediate filaments, actin filaments and microtubules (MTs). MTs are dynamic polymers of α and β tubulin (Li *et al.,* 2012) heterodimers; the head to tail association of the heterodimers results in the formation of a protofilament, 13 of which associate to form the hollow cylindrical structure of the MT (Amos and Klug 1974). In interphase, MTs are responsible for processes such as intracellular transport and maintenance of cellular architecture (Hughes *et al., 2008*), and as the cell progresses into mitosis, MTs are primarily responsible for ensuring accurate chromosome segregation (Karsenti 1993) via the formation of the mitotic spindle. MTs undergo a process termed dynamic instability in which rapid cycles of polymerisation and depolymerisation are transitionally repeated through events known as rescue and catastrophe. In terms of energy this a very costly process, however the fact that it is evolutionarily conserved would indicate its incredible biological importance (Desai and Mitchison 1997).

The actin cytoskeleton plays a crucial role in a number of processes, including the formation of lamellapodia, stress fibres and focal adhesions (Bailly and Condeelus 2002). Actin is an ATPase and ATP hydrolysis is essential for the transition from monomeric G-actin to filamentous F-actin. The actin filament is asymmetric; actin monomers join the filament at the barbed (plus end) fast growing end in an ATP bound state, and leaves the filament at the pointed (minus end) in the ADP bound state. This action of addition and loss of G-actin monomers results in the dynamic process of actin treadmilling (Lee and Dominguez 2010).

Whilst actin and MTs control different aspects of cellular behaviour, a cross talk must exist between the two filaments to mediate a response to stimuli. Our current knowledge of actin-MT cross talk is limited, with very few molecules and pathways that are involved in this cross talk having been identified. One molecule known to be involved in actin-MT cross talk is the GTPase activating protein (GAP) RacGAP1. RacGAP1 is a component of the centralspindlin complex that plays a key role in promoting assembly of the actomyosin contractile ring (White and Glotzer 2012). RacGAP1 is transported to MT plus ends by the other centralspindlin

component, the kinesin MKLP1/KIF23, where it binds to and activates the Rho guanine nucleotide exchange factor (GEF) Ect2.This interaction stimulates the activity of the small GTPase RhoA resulting in the assembly and contraction of actomyosin filaments at the cleavage site (Kamijo *et al.,* 2006; Lee *et al.,* 2004; Su, Takaki and Petronczki., 2011; Yüce, Piekny and Glotzer., 2005). In this example, MT polymerisation induces an actin response, however MT depolymerisation can also impact actin dynamics. Depolymerisation of MTs disrupts the polarity of the actin cytoskeleton, promoting the formation of stress fibres and focal adhesions (Bershadsky *et al.,* 1996), through the actions of the protein GEF-H1. GEF-H1 is held inactive by its association with the MT motor protein dynein, however when MTs are disassembled, GEF-H1 is released and free to activate Rho-A, promoting stress fibre formation (Meiri *et al.,* 2012). This evidence indicates that signalling is responsible for MT actin cross talk, but also highlights that our knowledge of the specific mechanisms and signalling pathways involved in mediating this actin – MT cross talk remains poor.

A few studies have indicated that the addition of actin depolymerising drug Latrunculin – A (Lat-A) to *Drosophila* cells induces the formation of long MT bundle filled arrays (D'Avino *et al.,* 2008; Eggert *et al.,* 2004; Kiger *et al.,* 2003). Lat-A is able to rapidly, specifically and reversibly disrupt the actin cytoskeleton (Spector *et al.,* 1983). In comparison to cytochalasin-D, another potent actin depolymeriser, the mechanism of action of Lat-A appears much simpler (Moreton, Ayscough and McLaughlin 2000); Lat-A only interacts with actin monomers, preventing them from repolymerising into actin filaments (Coué *et al.,* 1987). Actin depolymerisation seems to have little effect on the polarity of MTs (Magdalena, Millard and Machesky 2003) however it does appear to impact MT targeting. MTs are guided by actin stress fibres towards cell matrix adhesion sites (Krylyshkina *et al.,* 2003). When actin is depolymerised, these sites can no longer be generated and MTs are not correctly targeted (Doherty and McMahon. 2008).

An initial investigation into this cell shape change has been carried out by my supervisor Dr D'Avino (figure 7.1). *Drosophila* DMEL2 cells treated with Lat-A rapidly formed long MT filled projections. The same change in shape also being observed when cells were treated with Lat-A combined with the proteasome inhibitor MG132 (Figure 7.1 B). MG132 alone had no effect on cell morphology which suggests that

protein degradation results in the formation of MT projections following actin depolymerisation. Treatment with the PP1/PP2 phosphatase inhibitor Okadaic acid (OA) resulted in the formation of cellular blebs associated with concentric actin foci, which would suggest unregulated actin contraction most likely due to the inhibition of PP1 myosin phosphatase. Treatment with OA and Lat-A combined (Figure 7.1 C) produced a slightly different cellular response; under these conditions fewer bundles formed and those that did were shorter than those observed when Lat-A was added alone. Together, these results indicate that it is a series of phosphorylation/dephosphorylation events mediating the formation of long MT bundles when actin is depolymerised.

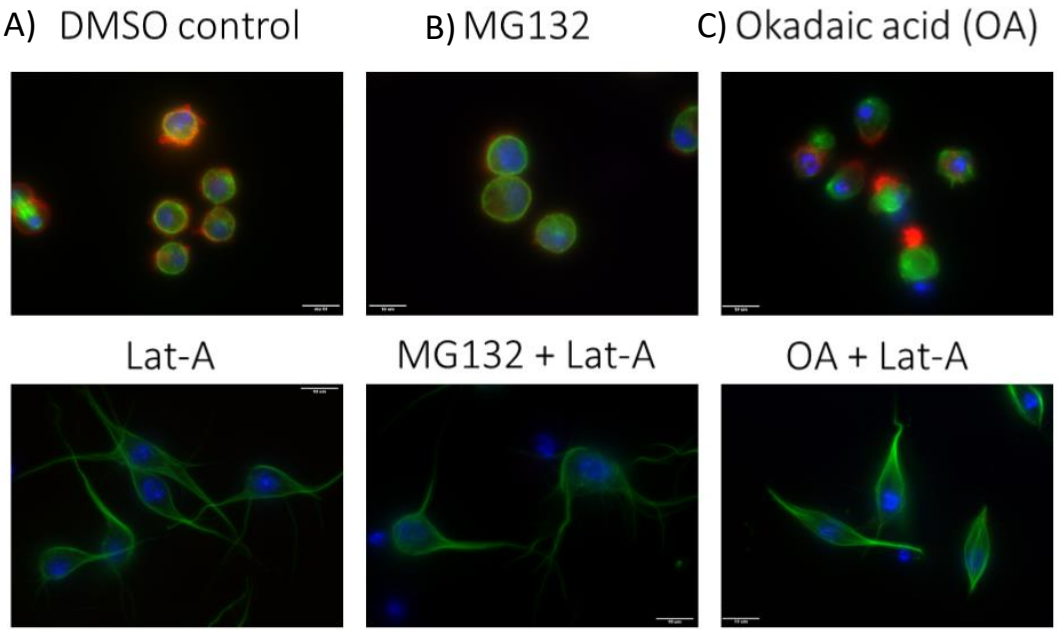

Figure 7.1 investigating the effect of Lat-A on DMEL2 cells

DMEL2 cells were treated with 20 µM Lat-A, 25µM MG132, or 25 nM OA, and with a combination of Lat-A and MG132 or OA, DMSO was used as a control. Cells were then fixed and stained for tubulin (green), actin (red) and DNA (blue). MG132 had no effect on cell morphology both with and without Lat-A, however OA alone caused cell blebbing and when combined with Lat-A fewer, shorter MT bundles. This would suggest that the change in cell shape is due to a series of phosphorylation/dephosphorylation events.

Scale bar 10µm

The aim of my project is to identify factors and pathways that are involved in cell shape change induced by actin disassembly in cultured cells, by means of targeted RNAi screens in *Drosophila* cells. The change in cell shape observed after actin depolymerisation was also observed in HeLa S3 cells, although the response was much less prominent than in DMEL2 cells. This indicates that this cell shape change is conserved, and that DMEL cells offer a more suitable model to investigate this process, allowing changes to be observed using simple light microscopy. Moreover, *Drosophila* cells are advantageous because (i) the *Drosophila* genome is much less redundant than the human genome and (ii) the response to RNA interference (RNAi) is also more powerful and with less risk of off target results.

The project plan is to knockdown by RNAi all kinases, phosphatases and MT associated proteins (MAPs) in the *Drosophila* genome. These RNAi depleted cells will then be treated with Lat-A. If a specific kinase, phosphatase or MAP is required for the formation of MT filled projections, its depletion should lessen or prevent Lat-A induced MT bundle formation. 615 proteins will be analysed in total; 228 kinases (Bettencourt-Dias *et al.,* 2004), 117 phosphatases (Chen *et al.,* 2007) and 270 MAPs (Hughes *et al.,* 2008). Screens will be carried out in duplicate in 96 well plates, with three different interfering RNAs being pooled into a single well with subsequent initial observations being made by light microscopy. Positive samples will be re-analysed by individual gene knockdown using two distinct interfering RNAs, coupled with immunostaining to visualise MTs. Further analysis of proteins that appear to have a function in Lat-A induced shape changes and MT bundle formation will then be GFP tagged allowing for their dynamics after Lat-A treatment to be observed using time-lapse microscopy. As a final step, the dynamics and interactome of a subset of positive proteins pre and post Lat-A treatment can be characterised via GFP-Trap (ChromoTek) tagging and affinity purification coupled with mass spectrometry (AP-MS).

7.2. Materials and methods:

7.2.1. *Drosophila* cell culture

DMEL2 cells were cultured in Express Five serum free (SF) media (Gibco – Life technologies) containing 1% penicillin/streptomycin.

7.2.2. Testing Lat-A concentrations

DMEL2 cells were plated 3 x 10^6 in 6 well plates in 2 mL Express 5 serum free media and allowed to adhere for 1 hour. Cells were then incubated with 20 µM, 10 µM, 1µM or 0.5 µM Lat-A (Abcam) or 4 µL DMSO for 1 hour. For fixing, cells were re plated onto 22x22 mm glass coverslips and allowed to adhere for 1 hour.

7.2.3. Fixing cells

Cells were fixed using a formaldehyde fixing reagent (3.7% formaldehyde, 60 mM PIPES pH 7.0, 25 mM HEPES pH 7.0, 10 mM EGTA, 4 mM $MgSO_4$ made to desired volume with ddH_2O), for 12 minutes at room temperature. Following incubation, all fixing reagent was removed, and coverslips were washed 3 x 5 minutes with 1 mL PBS. Following the final wash, fresh PBS was added, and cells stored at 4°C.

7.2.4. Immunostaining cells

All PBS was removed, and cells were blocked in PBT (PBS, 0.5% triton x 100, 3% BSA) for 2 hours. After blocking cells were incubated overnight at 4°C with an appropriate primary antibody in PBT (PBS, 0.1% triton 100 x, 1% BSA). After incubation coverslips were washed 3 x 5 minutes with PBT, then incubated with an appropriate secondary antibody in PBT for 2 hours at 4°C, then washed 3 x 5 minutes with PBT. Coverslips were then mounted with Vectashield fluorescent mounting media with DAPI (Vector).

7.2.5. Antibodies

Primary - mouse α tubulin DM1A (Sigma), rabbit α Pavarotti GM2 (Glover lab – Department of Genetics, University of Cambridge), mouse α lamin T47, mouse α PLK1 (Santa Cruz Biotechnology)

Secondary - goat α mouse 488 (Molecular probes), goat α rabbit 594 (Molecular probes), phalloidin (Invitrogen)

7.2.6. Imaging cells

Immunostained cells were imaged using a Nikon Eclipse C1si automated microscope. A 13 image Z stack was taken at each wavelength, and a composite image created using MetaMorph software. Further image processing was carried out using ImageJ.

7.2.7. Preparation of genomic DNA from DMEL2 cells

$1.3x10^7$ DMEL2 cells were pelleted and re-suspended in 200µL Buffer A (dH_2O, 100mM Tris-HCL pH 7.5, 100mM EDTA, 100mM NaCl, 0.5% SDS). Another 200µL Buffer A was added, then the cells were incubated at 65°C for 30 minutes. 800µL of LiCl/KAc solution (1:2.5 5M KAc: 6M LiCl) was added, then the cells were incubated on ice for 10 minutes. Cells were then spun at 16,000rpm for 15 minutes at room temperature, and 1mL of supernatant was transferred to a clean 1.5mL tube. 600µL of isopropanol was added to the supernatant, it was mixed and then spun at 16,000rpm for 15 minutes at room temperature. Supernatant was aspirated, the pellet washed with 70% ethanol and left to dry. The pellet was re-suspended in 150µL TRIS.

7.2.8. PCR

Kinase sequences required for dsRNA production were amplified using PCR. The following reaction mix was set up; 10µL 5x GoTaq Flexi buffer (Promega), 5µL $MgCl_2$ (Promega), 1µL 10mM DNTPs, 0.5µL upstream primer, 0.5µL downstream primer, 1µL template DNA, 0.25µL GoTaq hot start DNA polymerase (Promega), 31.75µL dH_2O. PCR was run on the following setting; 95°C for 2 minutes, 35 cycles of 95°C for 30 seconds, 55°C for 30 seconds and 72°C for 1 minute, then 72°C for 10 minutes and held at 4°C. Samples were then run on a 1% agarose gel (80V for 1 hour). Positive samples were excised from the gel using a Qiagen gel extraction kit as according to the manufacturer's instructions.

7.2.9. Production of dsRNA

dsRNA was produced from excised PCR fragments using the T7 Ribomax™ Express RNAi system (Promega) according to the manufacturer's instructions. 10µL of each sample was run on a 1% agarose gel (80V for 1 hour). dsRNA concentration was assessed via nanodrop.

7.2.10. RNAi screen

For the RNAi screen, DMEL2 cells were plated 1.5 x 10^6 in 200 µL Express 5 SF media, in 24 well plates. Cells were allowed to adhere for 1 hour, then 2 µg of dsRNA was added to the well with a further 600 µL Express 5 SF media. Cells were left to incubate with the dsRNA for 72 hours, following which all media was removed from the cells and replaced with 200 µL fresh media containing 10 µM Lat-A. Cells were incubated with Lat-A for 1 hour then all observations were made by eye using a light microscope.

7.2.11. Generating a tubulin GFP cell line

DMEL 2 cells were plated in a 6 well plate 3 x 10^6 in Express 5 SF media and allowed to adhere for 1 hour. 15 µL FuGENE HD transfection reagent (Promega) was added directly into the following solution; 3.0 µg tubulin GFP plasmid, 0.3 µg pCoBlast, made up to 10 µL sterile water. The transfection mix was vortexed for 1-2 seconds to mix, then incubated for 15 minutes at room temperature. Transfection mixture was then added dropwise to cells. After 48 hours' incubation at 37°C Blasticidin was added to cells to a final concentration of 20 µg/ mL. When the well reached confluency cells were transferred into a T25 flask and allowed to grow to over confluency. When this stage is reached cells were transferred into a T75 flask until over confluent. Cells were then split into 3 T75 flasks and labelled "passage 1". Cells were kept in 20 µg/mL Blasticidin throughout.

7.2.12. Primer design for cloning

Primers were designed against the FusionRed-LifeAct-7 plasmid (Addgene), with the addition of restriction sites for Not1 (New England Biolabs) and PmeI (New England Biolabs). Primer sequences -

Forward 5'TACCTTGCGGCCGCGATCCGCTAGCGCCACCATG

Reverse 5’ GACCACTACCTCCATTTACTCAAATTTGTCACGT

7.2.13. Insert preparation

To amplify the region of interest from the FusionRed-LifeAct-7 plasmid the following PCR reaction was set up; 38.5 µL dH_2O, 10 µL Phusion buffer (Thermo), 2 µL $MgCl_2$ (Thermo), 1 µL DNTPs, 1 µL forward primer, 1 µL reverse primer, 1 µL FusionRed-LifeAct-7 template, 0.5 µL Phusion (Thermo). The PCR reaction was run on the following programme; 98°C for 30 seconds, 25 cycles of: 98°C for 10 seconds, 55°C for 30 seconds and 72°C for 30 seconds, followed by a 10-minute extension at 72°C and a final hold at 4°C. Sample was then run on a 1% agarose gel to check the size, then purified from the gel using a Qiagen gel extraction kit as according to the manufacturer’s instructions.

7.2.14. Vector preparation

5 µL of pAc5.1/V5-Tap vector was digested with 2 µL Not1 and 1 µL PmeI in 5 µL Cutsmart buffer (New England Biolabs) and 37 µL dH_2O. DNA yield was checked on a 1% agarose gel then excised as before. Vector ends were then dephosphorylated using shrimp alkaline phosphatase (SAP); sample was made up to 50 µL with phosphatase buffer, then 1 µL of SAP was added and the sample incubated for 30 minutes at 37°C, another 1 µL SAP was then added and the sample incubated for a further 30 minutes at 37°C. Sample was then incubated at 65°C for 15 minutes to deactivate the SAP.

7.2.15. Ligation

Ligation was carried out in a 20 µL total reaction volume containing 2 µL T4 ligase buffer (Promega), a 3:1 molar ratio of insert to vector and 1 µL T4 ligase (Promega). The ligation reaction was incubated at 4°C for a minimum of 24 hours.

7.2.16. Transformation

5 µL of ligated plasmid was transformed into 50 µL DH5α competent cells (Invitrogen). pAc5.1/v5-tap-LifeAct plasmids were harvested from 2 mL bacterial cultures formed from single colonies grown on LB carbenicillin agar plates, using a QIAprep Spin Miniprep Kit (Qiagen). Restriction digests using Not1 and PmeI and 1% gel electrophoresis was carried out to select positive colonies. Selected positives

were re-transformed into DH5α competent cells and harvested from 100 mL bacterial cultures grown on LB carbenicillin plates using a QIAprep Spin Midiprep kit (Qiagen).

7.3. Results

7.3.1. Lower concentrations of Latrunculin-A produced a stronger phenotype

In a study by Coúe *et al.,* (1987) it was stated that Lat-A is effective at depolymerising actin at concentrations as low as 0.1-1 µM in cultured cells. Previous experiments have shown that in DMEL2 cells a clear MT bundling phenotype is observed when using Lat-A at 20 µM, but the effect of lower Lat-A concentrations have not been tested. Therefore, prior to screening I investigated the range of Lat-A concentrations that could be used to achieve the desired phenotype visible under light microscopy. DMEL2 cells were exposed to either 20 µM, 10 µM, 1 µM or 0.5 µM Lat-A, or its solvent DMSO as a control, for 1 hour and observed under light microscopy. Cells were then fixed and stained to detect actin and MTs (Figure 7.2).

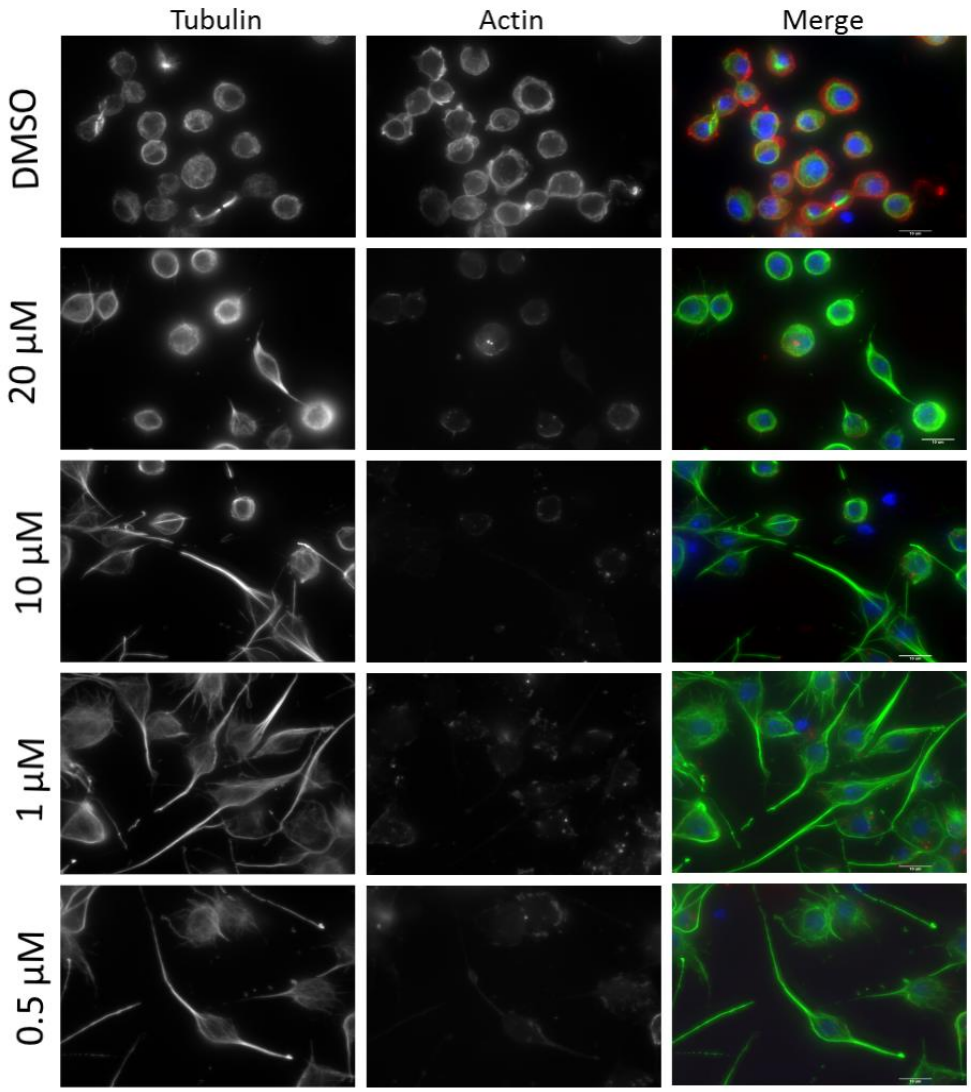

Figure 7.2 - **Lat-A is affective at concentrations as low as 0.5 µM.**

DMEL2 cells were treated with either 20 µM, 10 µM, 1 µM or 0.5 µM Lat-A for 1 hour and then fixed and stained to detect tubulin (green), actin (red) and DNA (blue). DMSO was used as a control.

Scale bar - 10 µm

When treated with 20 µM Lat-A cells should produce long MT filled projections (Figure 7.2), however in this instance the majority of cells have failed to do so. At 10 µM, 1 µM and 0.5 µM there is a clear MT bundle phenotype present however, at 10 µM the actin depolymerisation appeared most successful. Based upon this I decided to use 10 µM Lat-A for future experiments.

7.3.2. Generation of a tubulin-GFP stable cell line will allow for live imaging of cells treated with Lat-A

In order to visualise the dynamics of rapid MT bundle formation observed after actin depolymerisation, I decided to generate a DMEL2 cell line stably expressing GFP-tagged tubulin and Fusion-Red tagged actin. I first generated a DMEL2 tubulin-GFP cell line via transfection with a tubulin-GFP plasmid. Cells were then fixed and stained for DNA, and imaged to see if GFP was being expressed (Figure 7.3).

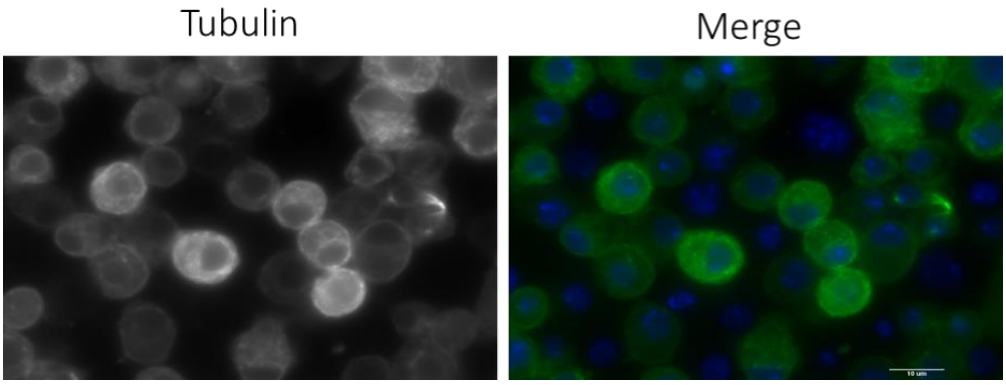

Figure 7.3: DMEL2-Tubulin GFP cell line. DMEL2 cells transfected with a tubulin GFP plasmid were fixed and stained for DNA (blue) Scale bar 10 µm.

It is evident that the majority of cells expressed tubulin GFP. I then attempted to generate a cell line expressing both GFP tubulin and Fusion red Actin. Firstly, I cloned the FusionRed-LifeAct-7 sequence into a pAc5.1/V5-Tap *Drosophila* destination vector (Figure 7.4) which could then be transfected alongside tubulin GFP into DMEL2; however, at present I am yet to achieve any positive colonies.

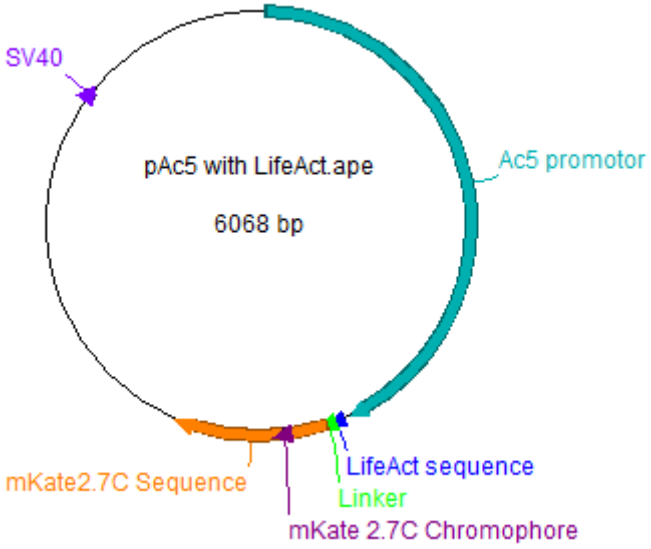

Figure 7.4 – Plasmid map of LifeAct cloned into a pAc5 destination vector. Primers containing restriction enzyme sequences for Not1 and Pme1 were designed to insert the desired LifeAct sequence into the pAc5 vector. Image not representative of the full cassette, for full information visit Addgene website.

7.3.3. DMEL2 cells do not require transfection reagents for successful RNAi

Before carrying out the entire screen, to optimise the efficiency of dsRNA transfection I tested two methods using RNAi against Pavarotti (Figure 7.5). Pavarotti is the *Drosophila* kinesin member of centralspindlin (Minestrini, Harley and Glover 2003); Pavarotti RNAi causes cytokinesis failure resulting in the formation of binucleate cells (Kiger *et al.,* 2003). RNAi is triggered in *Drosophila* cells by incubating with short (~100bp) double strand RNA (dsRNA) against the target gene. Cells were plated in 6 well plates incubated with both Pavarotti dsRNA and transFAST™ transfection reagent, or Pavarotti dsRNA alone. As a control cells were incubated with kanamycin dsRNA and transFAST™. All samples were left to incubate for 3 days and then cells were fixed and stained for lamin, actin and DNA. In the kanamycin controls cells were unaffected by both the presence of the transfection reagent or the dsRNA. In both Pavarotti RNAi samples, the cells appeared larger and binucleate. This indicates that the RNAi knockdown of Pavarotti

has been successful both in the presence and absence of transfection reagent. Based on this result all future RNAi knockdowns featured in this report have been carried out without transfection reagent.

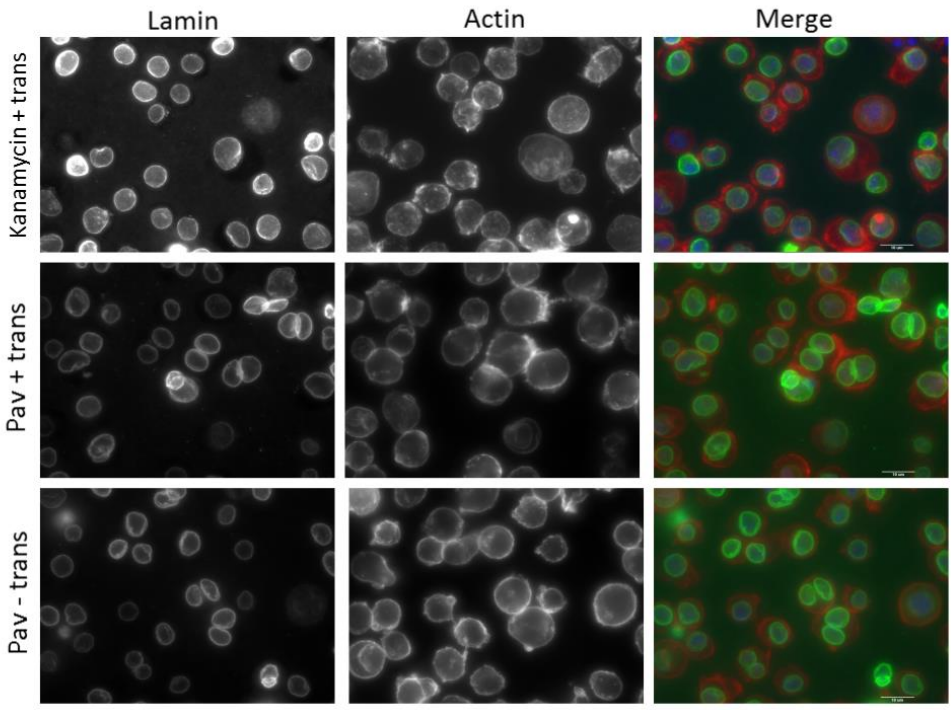

Figure 7.5 - DMEL 2 cells do not require transfection reagent for successful dsRNAi knockdown. RNAi against Pavarotti was performed both with and without transfast transfection reagent. Cells were incubated for 3 days then fixed and stained for lamin (green), actin (red) and DNA (blue). RNAi against kanamycin (with transfast) was used as a control. Scale bar 10µm.

7.3.4. RNAi of kinesins causes variable projection lengths

The first family targeted in my RNAi screen was the MT associated kinesin motors. *Drosophila* have 26 kinesin genes and I could successfully produce 24 dsRNA's out of the 26 kinesins, and for dynein heavy chain. DMEL2 cells were plated in a 24 well plate and incubated with dsRNA for 3 days, cells were then treated with Lat-A for 1 hour and finally observed using a light microscope. The resulting phenotypes were categorised as either long, as seen in wild type cells (Figure 7.2) or short in comparison (Table 7.1)

Name	Phenotype
Cenp-Ana (cana)	Long MT projections
Cenp-Meta (cmet)	Long MT projections
Costa (cos)	Long MT projections
CG10845	Long MT projections
Dynein heavy chain (DHC)	Long MT projections
Kinesin family member 3C (Kif3C)	Long MT projections
Kinesin family member 19A (Kif19A)	Long MT projections
Kinesin family member 59C (Kif59C)	Long MT projections
Kinesin heavy chain (KHC)	Increased cell size Long and short MT projections
Kinesin heavy chain 73 (KHC73)	Increased cell size Short MT projections
Kinesin like protein 10A (Klp10A)	Cell death Long and short MT projections
Kinesin like protein 3A (Klp3A)	Cell death
Kinesin like protein 31E (Klp31E)	Long MT projections
Kinesin like protein 38B (Klp38B)	Long and short MT projections
Kinesin like protein 53D (Klp53D)	Long MT projections
Kinesin like protein 54D (Klp54D)	Cell death Short MT projections
Kinesin like protein 61F (Klp61F)	Cell death Short projections No projections
Kinesin like protein 64D	Short MT projections
Kinesin like protein 67A	Long MT projections
Kinesin like protein 68D	Long MT projections
Kinesin like protein 98A	Short MT projections
Non-claret disjunctional	Long MT projections
No distributive disjunction	Long MT projections
Pavarotti	Increased cell size Long MT projections
Subito	Long MT projections

Table 7.1 - **Cell shape change presented by Lat-A treated cells following RNAi knockdown of kinesins**. MT bundles have been categorised as either long (blue) or short (red) long referring to those observed in the wild type and short indicating the presence of bundles visibly shorter than the WT. Some cells showed a mixed phenotype (purple) and one sample showed total cell death (green).

16/25 (64%) of the samples presented the normal long MT projections after Lat-A (blue), 6/25 (24%) showed MT bundles that were much shorter compared to wild type (no dsRNA) (red) and controls (kanamycin dsRNAi). 2/25 (Klp10A and Klp38B) (8%) presented both long and short MTs at the point of observation (purple) and 1/25 (4%) wells showed total cell death (Klp3A) (green).

7.3.5. RNAi of KHC prevents MT sliding and hence the formation of long MT bundles

Jolly *et al* (2010) reported that RNAi of kinesin heavy chain (KHC), but not dynein heavy chain (DHC) or kinesin -1 light chain (KLC) eliminated lateral MT movements, and reported that, in the presence of actin depolymerising drug cytochalasin-D, the MT network appeared straight and absent of any lateral movement. This study also suggested that KHC might be the kinesin responsible for mediating the sliding of MT filaments against one another, driving the formation of the long MT bundles observed in cells treated with cytochalasin- D (Jolly *et al.,* 2010). In my RNAi screen, knockdown of KHC resulted in the formation of larger cell bodies coupled with shorter MT projections, rather than them being entirely absent. In order to take a closer look at the projections formed under my conditions, the KHC knockdown and Lat-A treatment was repeated and cells were fixed and stained for tubulin, actin and DNA (Figure 7.6). This experiment showed that, whilst in agreement with the literature actin depolymerisation did reduce the length of the MT bundles; in the majority of cases, cells were still able to produce the long bundles as in controls.

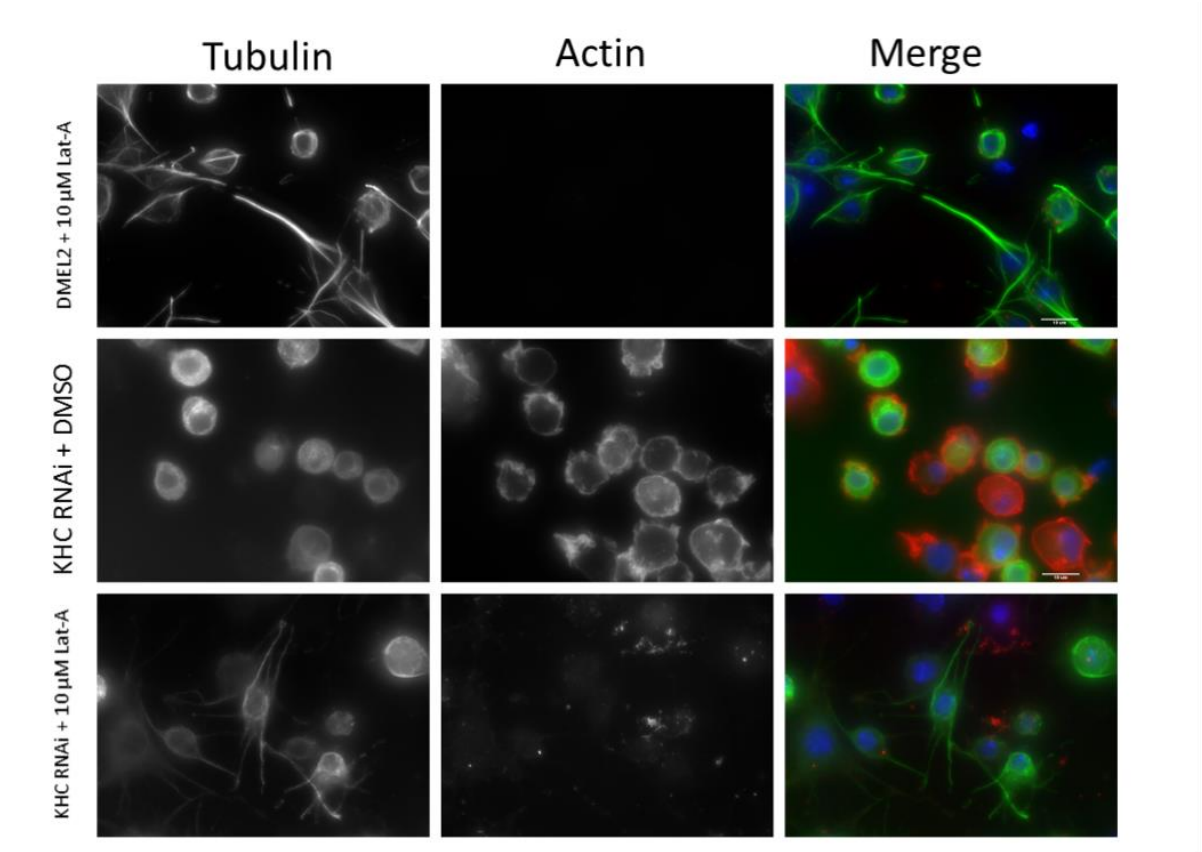

Figure 7.6 - MT bundles are shorter in KHC knockdown cells.

Cells were transfected with KHC dsRNA, treated for 1 hour with 10 µM Lat-A, then fixed and stained for tubulin (GFP) actin (red) and DNA (blue). In control cells addition of Lat-A resulted in total actin depolymerisation, and the production of long MT filled processes. In the KHC knockdown cell bodies appear larger in both treated and untreated populations. When treated with 10 µM Lat-A cells appeared to produce a combination of short projections and long projections comparable to controls.

Scale bar 10 µM.

In a subsequent study published very recently, Jolly *et al.,* (2016) reported that knockdown of DHC caused cells to produce much longer MT bundle filled processes. However, in my condition DHC RNAi did not (Figure 7.7). The MT bundles produced when actin was depolymerised is very similar to controls rather than being abnormally long as described by Jolly *et al.,* (2016).

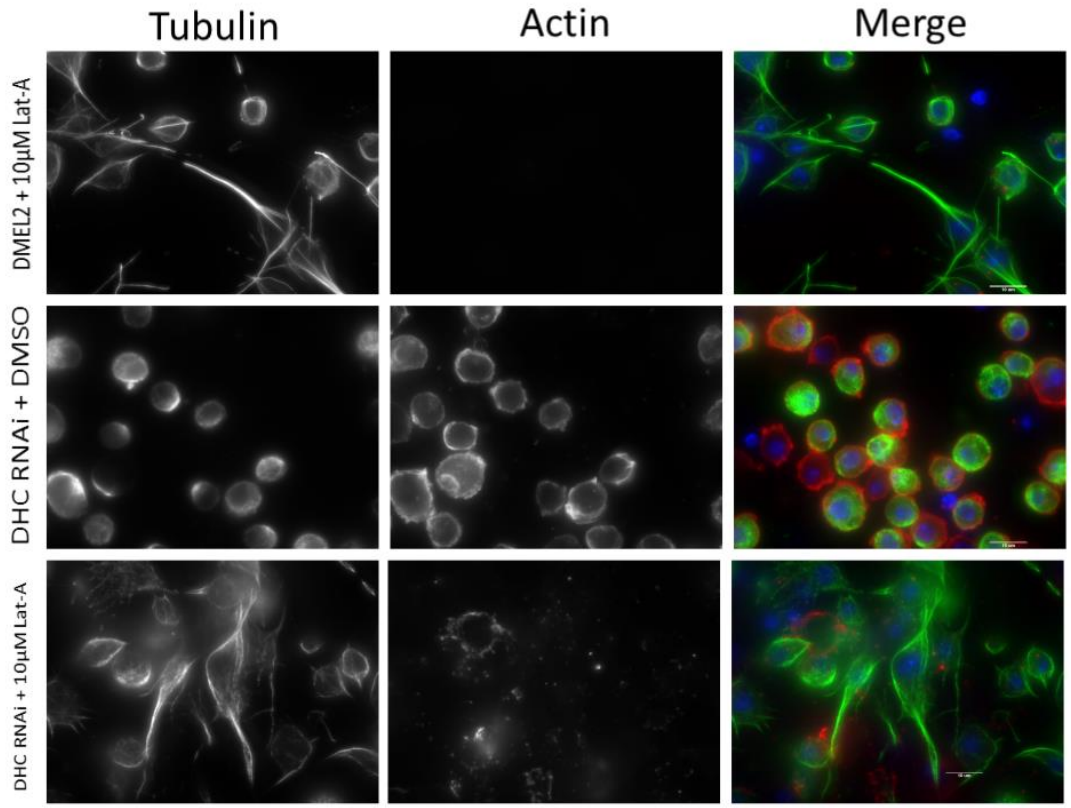

Figure 7.7 - MT bundles are long when DHC is knocked down.

In control cells the addition of Lat-A resulted in total actin depolymerisation and the production of long MT filled processes. In the DHC knockdown cells there was no obvious difference in cellular morphology, and when treated with Lat-A long MT bundles comparable to controls were formed.

Scale bar 10 µM.

7.4. Discussion

The results of the initial RNAi screen of the kinesin family in DMEL2 cells indicated that only a few kinesins are required for the Lat-A induced cell shape change. In a small number of cases cells formed much shorter MT processes. KHC73, Klp61F, Klp64D and Klp98A RNAi cells were only able to produce short MT processes following treatment with Lat-A. KHC73 is one of the four kinesin 3 family members found in *Drosophila*, and is required for the correct orientation of the mitotic spindle. KHC73 undergoes rapid progressive movement and is able to generate forces comparable with kinesin-1 (Huckaba *et al.,* 2011), but despite this similarity to kinesin 1 (KHC), KHC73 is not well characterised. The plus end directed MT motor

KHC is well known for its function in cargo transport (Melkov *et al.,* 2015) and amongst its other cellular roles, has been reported to be involved in mediating cytoplasmic MT-MT sliding (Jolly *et al.,* 2010). In a recent RNAi screens carried out by Jolly *et al.,* (2010, 2016) to identify factors involved in MT bundle formation it was shown that in *Drosophila* S2 cells knockdown of KHC eliminated MT sliding in interphase, therefore when cells were treated with actin depolymerising drug cytochalasin –D MT bundles and processes failed to form. In contrast to this my results indicated that Lat-A treatment of DMEL2 cells following KHC RNAi resulted in the formation of both long and short MT bundles, rather than a complete absence. As some short bundles were observed in this condition it is possible that the dsRNA knockdown of KHC was incomplete, so cells retained some of their MT sliding capabilities and so were still able to produce some long MT processes. The similarity between the expected cell shape change for KHC RNAi and that observed for KHC-73 could indicate a possible functional similarity between these two kinesins with regard to MT-MT sliding in interphase cells. One other possibility could be down to plating method used. Jolly *et al.,* (2016) plated their cells on concanavalin -A (con-A) coated coverslips, whereas I plated directly onto the glass. Con-A stimulates DMEL cells to flatten; within one hour cells lose their rounded appearance and spread out, making them more amenable to microscopy (Buster *et al.,* 2010). This could therefore increase the severity of the cell shape change by encouraging cell spreading.

Previous RNAi screens of kinesins in *Drosophila* S2 cells reported that knockdown of Klp61F resulted in the formation of monopolar spindles, spindle defects and spindle collapse (Goshima and Vale 2003). In the RNAi screen presented here, knockdown of Klp61F caused partial cell death prior to Lat-A treatment, and in cells treated with Lat-A MT bundles formed were either short or entirely absent. This result is consistent with the role of Klp61F in the elongation of the bipolar mitotic spindle via the crosslinking of interpolar MTs, exerting an outward force on the spindle poles (Goshima and Vale 2003). These outward pulling forces are generated by cortical dynein which is thought to slide astral MTs relative to cortical actin as part of the sliding filament mechanism (Kwon and Scholey 2004., McIntosh, Hepler and von Wie., 1969). Based on this evidence, it is likely that in my experiments, the loss of both Klp61F and cortical actin is preventing MT sliding from

occurring and thus the cell is unable to produce the characteristic long MT filled processes observed following actin depolymerisation. Klp61F RNAi would also result in spindle collapse and mitotic arrest, hence the high degree of cell death observed prior to Lat-A treatment in this condition.

Klp64D, part of the kinesin 2 subfamily, is a plus end directed motor involved in organelle transport (Miki, Okada and Hirokawa 2005), neuron projection morphogenesis (Sepp *et al.,* 2008) and cilia assembly (Sarpal *et al.,* 2003). The human homologue of Klp64D, Kif3A, has also been linked to plus end directed MT sliding activity in vivo as part of a complex with Kif3B (Yamazaki *et al.,* 1995). In my screen, when cells were treated with dsRNAi against Klp64D and Lat-A the MT bundles produced were not as characteristically long, which could be a result of a loss of MT sliding function normally mediated by Klp64D.

At present there is limited knowledge of the cellular function of Klp98A in *Drosophila*, however a structural similarity with human Kif16B suggests a potential role in endosome transport (Flybase Curators 2008). RNAi of Klp98A followed by Lat-A treatment resulted in the formation of short MT bundles, which could suggest a potential role in MT sliding or bundling for this protein.

Rather than just the characteristic long MT bundles typically observed following Lat-A treatment, KHC, Klp10 and Klp38B RNAi cells presented a combined long and short MT bundle cell shape change. The result presenting in Klp10A RNAi cells was somewhat unexpected. Klp10A is member of the kinesin 1 family of motor proteins, known for being a MT destabiliser (Desai *et al.,* 1999). Consistent with this function previous RNAi screens of this protein have reported that in the absence of Klp10A cells produce very long spindle and astral MTs (Goshima and Vale, 2003). Therefore, it was surprising to see the numerous short projections alongside the characteristic long bundles seen in Lat-A treated controls. Klp10A RNAi also resulted in partial cell death; this is likely due to the requirement for Klp10A in the correct formation and assembly of a bipolar mitotic spindle (Goshima and Vale. 2003), without which can result in cells arresting in mitosis.

RNAi of Klp38B also resulted in the formation of both long and short MT bundles. Klp38B has a role in chromatid condensation and segregation (Alphey *et al.,* 1997), and also acts as a plus end directed MT motor (Sharp *et al.,* 2000). Whilst there is no

evidence to suggest that Klp38B has a role in MT bundle formation, the formation of these short bundles alongside the longer bundles could suggest a potential implication for its role as a motor protein in this process.

There is also the possibility that the short projections observed in both Klp10A and Klp38B RNAi may continue to grow over a prolonged treatment period; the bundles may be slower to form rather than simply being short, however experimentation would be required to fully assess this.

A cell shape change could not be observed for Klp3A as RNAi of this protein caused total cell death. Klp3A is a known chromokinesin with a role in mitotic spindle assembly and organisation (Moutinho- Pereira *et al.,* 2013; Kwon and Scholey 2004). A previous RNAi screen in *Drosophila* S2 cells reported that RNAi of Klp3A resulted in chromosome misalignment (Goshima and Vale 2003) which has the potential to result in mitotic arrest and cell death. Based on what is known about the function of Klp3A it would seem unlikely that this protein would be involved in the cross talk between actin and MTs, however to fully assess this a different experimental approach would be required.

7.5. Conclusions

It has been previously demonstrated that when actin is depolymerised by Lat-A cells form long projections filled with MT bundles. Preliminary testing of different Lat-A concentrations showed that this change of cell shape can occur when cells are treated with as low as 0.5 µM for one hour. Treating cells with Lat-A following RNAi of kinesin family members generated some surprising results, some of which was in contrast with published literature. In the majority of cases the cells were still able to produce these long MT bundles in the absence of a certain kinesin however there were instances in which the projections failed to form as seen in controls. Based on these preliminary observations there are a few potential candidates for follow up investigation, however the RNAi screen published by Jolly *et al.,* (2016) has also begun to highlight some potential proteins involved in facilitating actin and MT cross talk. In a similar experimental set up to the one presented here, Jolly *et al.,* performed a genome wide RNAi screen in *Drosophila* S2 cells to look for factors involved in MT bundle formation following actin depolymerisation with Cytochalasin-D. Their screen identified a number of long and short MT bundle formation hits, and

whilst their results predominantly highlighted neuronal proteins, they also identified proteins such as KHC, Klp10A and the RhoGef Pebble (human Ect2). The Jolly et al (2016) presented a very similar experimental design to the one I have been using, and hence have published part of the results obtained in my screen. The results from both the 2010 and the 2016 study have potential for further experiments future publications that would be in competition with the work I plan to do during my PhD therefore this project will not be continued.

8. References

Abrieu, A. *et al.* (2000) 'CENP-E as an essential component of the mitotic checkpoint in vitro.', *Cell*. 102(6), pp. 817–826.

Acquaviva, C. *et al.* (2004) 'The anaphase promoting complex/cyclosome is recruited to centromeres by the spindle assembly checkpoint.', *Nature cell biology*. 6(9), pp. 892–898.

Agrawal, N. *et al.* (2012) 'Comparative genomic analysis of esophageal adenocarcinoma and squamous cell carcinoma.', *Cancer discovery*, 2(10), pp. 899–905.

Alexander, S. P. and Rieder, C. L. (1991) 'Chromosome motion during attachment to the vertebrate spindle: initial saltatory-like behavior of chromosomes and quantitative analysis of force production by nascent kinetochore fibers.', *The Journal of cell biology*. 113(4), pp. 805–815.

Alexandrov, L. B. *et al.* (2013) 'Signatures of mutational processes in human cancer.', *Nature*. 500(7463), pp. 415–421.

Alfieri, C., Zhang, S. and Barford, D. (2017) 'Visualizing the complex functions and mechanisms of the anaphase promoting complex/cyclosome (APC/C).', *Open biology*. 7(11).

Allshire, R. C. and Karpen, G. H. (2008) 'Epigenetic regulation of centromeric chromatin: old dogs, new tricks?', *Nature reviews. Genetics*. 9(12), pp. 923–937.

Alphey, L. *et al.* (1997) 'KLP38B: A mitotic kinesin-related protein that binds PP1', *Journal of Cell Biology*, 138(2), pp. 395–409.

Amaro, A. C. *et al.* (2010) 'Molecular control of kinetochore-microtubule dynamics and chromosome oscillations.', *Nature cell biology*. 12(4), pp. 319–329.

Amato, A. *et al.* (2009) 'RNAi mediated acute depletion of retinoblastoma protein (pRb) promotes aneuploidy in human primary cells via micronuclei formation.', *BMC cell biology*. 10, p. 79.

Amos, L. and Klug, a (1974) 'Arrangement of subunits in flagellar microtubules.', *Journal of cell science*, 14(3), pp. 523–549.

Anaparthy, R. and Sharma, P. (2014) ‘Progression of Barrett oesophagus: role of endoscopic and histological predictors.’, *Nature reviews. Gastroenterology & hepatology*. 11(9), pp. 525–534.

Arnaud, L., Pines, J. and Nigg, E. A. (1998) ‘GFP tagging reveals human Polo-like kinase 1 at the kinetochore/centromere region of mitotic chromosomes.’, *Chromosoma*. 107(6–7), pp. 424–429.

Auckland, P. *et al.* (2017) ‘Congressing kinetochores progressively load Ska complexes to prevent force-dependent detachment.’, *The Journal of cell biology*. 216(6), pp. 1623–1639.

Baca, S. C. *et al.* (2013) ‘Punctuated evolution of prostate cancer genomes.’, *Cell*. 153(3), pp. 666–677.

Bailly, M. and Condeelis, J. (2002) ‘Cell motility : insights from the backstage’, 4(December), pp. 292–294.

Baker, D. J. *et al.* (2004) ‘BubR1 insufficiency causes early onset of aging-associated phenotypes and infertility in mice.’, *Nature genetics*. 36(7), pp. 744–749.

Baker, D. J. *et al.* (2008) ‘Opposing roles for p16Ink4a and p19Arf in senescence and ageing caused by BubR1 insufficiency.’, *Nature cell biology*. 10(7), pp. 825–836.

Bakhoum, S. F., Genovese, G. and Compton, D. A. (2009) ‘Deviant kinetochore microtubule dynamics underlie chromosomal instability.’, *Current biology : CB*. 19(22), pp. 1937–1942.

Barford, D. (2011) ‘Structural insights into anaphase-promoting complex function and mechanism.’, *Philosophical transactions of the Royal Society of London. Series B, Biological sciences*. 366(1584), pp. 3605–3624.

Barisic, M. *et al.* (2010) ‘Spindly/CCDC99 is required for efficient chromosome congression and mitotic checkpoint regulation.’, *Molecular biology of the cell*. 21(12), pp. 1968–1981.

Bassett, E. A. *et al.* (2012) ‘HJURP uses distinct CENP-A surfaces to recognize and to stabilize CENP-A/histone H4 for centromere assembly.’, *Developmental cell*. 22(4), pp. 749–762.

Basilico, F. *et al.* (2014) ‘The pseudo GTPase CENP-M drives human kinetochore assembly.’, *eLife*. 3, p. e02978.

Belkhiri, A., Zhu, S. and El-Rifai, W. (2016) ‘DARPP-32: from neurotransmission to cancer.’, *Oncotarget*. 7(14), pp. 17631–17640.

Bentley, A. M. *et al.* (2007) ‘Distinct sequence elements of cyclin B1 promote localization to chromatin, centrosomes, and kinetochores during mitosis.’, *Molecular biology of the cell*. 18(12), pp. 4847–4858.

Beroukhim, R. *et al.* (2010) ‘The landscape of somatic copy-number alteration across human cancers.’, *Nature*. 463(7283), pp. 899–905.

Bershadsky, a *et al.* (1996) 'Involvement of microtubules in the control of adhesion-dependent signal transduction.', *Current biology : CB*, 6(10), pp. 1279–1289.

Bettencourt-Dias, M. *et al.* (2004) 'Genome-wide survey of protein kinases required for cell cycle progression.', *Nature*, 432(7020), pp. 980–7.

Bettencourt-Dias, M. and Glover, D. M. (2007) 'Centrosome biogenesis and function: centrosomics brings new understanding.', *Nature reviews. Molecular cell biology*. 8(6), pp. 451–463.

Bharadwaj, R., Qi, W. and Yu, H. (2004) 'Identification of two novel components of the human NDC80 kinetochore complex.', *The Journal of biological chemistry*. 279(13), pp. 13076–13085.

Bibb, J. A. *et al.* (1999) 'Phosphorylation of DARPP-32 by Cdk5 modulates dopamine signalling in neurons.', *Nature*. 402(6762), pp. 669–671.

Biggins, S. *et al.* (1999) 'The conserved protein kinase Ipl1 regulates microtubule binding to kinetochores in budding yeast.', *Genes & development*. 13(5), pp. 532–544.

Biggins, S. and Walczak, C. E. (2003) 'Captivating capture: how microtubules attach to kinetochores.', *Current biology : CB*. England, 13(11), pp. R449-60.

Black, B. E. *et al.* (2004) 'Structural determinants for generating centromeric chromatin.', *Nature*. 430(6999), pp. 578–582.

Blount, P. L. *et al.* (1994) '17p allelic losses in diploid cells of patients with Barrett's esophagus who develop aneuploidy.', *Cancer research*. 54(9), pp. 2292–2295.

Boonstra, J. J. *et al.* (2007) 'Molecular biological challenges in the treatment of esophageal adenocarcinoma.', *Expert review of gastroenterology & hepatology*. 1(2), pp. 275–286.

Bornens, M. (2012) 'The centrosome in cells and organisms.', *Science (New York, N.Y.)*. 335(6067), pp. 422–426.

Breuss, M. and Keays, D. A. (2014) 'Microtubules and neurodevelopmental disease: the movers and the makers.', *Advances in experimental medicine and biology*, 800, pp. 75–96.

Brinkley, B. R. (2001) 'Managing the centrosome numbers game: from chaos to stability in cancer cell division.', *Trends in cell biology*. 11(1), pp. 18–21.

Brosh, R. and Rotter, V. (2009) 'When mutants gain new powers: news from the mutant p53 field', *Nat Rev Cancer*, 9(10), pp. 701–713.

Buffin, E. *et al.* (2005) 'Recruitment of Mad2 to the kinetochore requires the Rod/Zw10 complex.', *Current biology : CB*. 15(9), pp. 856–861.

Burke, Z. D. and Tosh, D. (2012) 'Barrett's metaplasia as a paradigm for understanding the development of cancer.', *Current opinion in genetics & development*. 22(5), pp. 494–499.

Burton, J. L. and Solomon, M. J. (2007) ‘Mad3p, a pseudosubstrate inhibitor of APCCdc20 in the spindle assembly checkpoint.’, *Genes & development*. 21(6), pp. 655–667.

Buster, D. W. *et al.* (2010) ‘Preparation of Drosophila S2 cells for light microscopy.’, *Journal of visualized experiments : JoVE*, (40), pp. 1–5.

Cahill, D. P. *et al.* (1999) ‘Characterization of MAD2B and other mitotic spindle checkpoint genes.’, *Genomics*. 58(2), pp. 181–187.

Caldas, G. V, DeLuca, K. F. and DeLuca, J. G. (2013) ‘KNL1 facilitates phosphorylation of outer kinetochore proteins by promoting Aurora B kinase activity.’, *The Journal of cell biology*. 203(6), pp. 957–969.

Caldwell, C. M., Green, R. A. and Kaplan, K. B. (2007) ‘APC mutations lead to cytokinetic failures in vitro and tetraploid genotypes in Min mice.’, *The Journal of cell biology*. 178(7), pp. 1109–1120.

Campomenosi, P. *et al.* (1998) ‘p53 mutations and DNA ploidy in colorectal adenocarcinomas.’, *Analytical cellular pathology : the journal of the European Society for Analytical Cellular Pathology*. 17(1), pp. 1–12.

Cancerresearchukorg. 2019. Cancer Research UK. [Online]. [10 September 2019]. Available from: https://www.cancerresearchuk.org/

Carazo-Salas, R. E. *et al.* (1999) ‘Generation of GTP-bound Ran by RCC1 is required for chromatin-induced mitotic spindle formation.’, *Nature*. 400(6740), pp. 178–181.

Carazo-Salas, R. E. *et al.* (2001) ‘Ran-GTP coordinates regulation of microtubule nucleation and dynamics during mitotic-spindle assembly.’, *Nature cell biology*. 3(3), pp. 228–234.

Carroll, C. W. *et al.* (2009) ‘Centromere assembly requires the direct recognition of CENP-A nucleosomes by CENP-N.’, *Nature cell biology*. 11(7), pp. 896–902.

Carroll, C. W., Milks, K. J. and Straight, A. F. (2010) ‘Dual recognition of CENP-A nucleosomes is required for centromere assembly.’, *The Journal of cell biology*. 189(7), pp. 1143–1155.

Carvalho, A. *et al.* (2003) ‘Survivin is required for stable checkpoint activation in taxol-treated HeLa cells.’, *Journal of cell science*. 116(Pt 14), pp. 2987–2998.

Cassimeris, L. and Salmon, E. D. (1991) ‘Kinetochore microtubules shorten by loss of subunits at the kinetochores of prometaphase chromosomes.’, *Journal of cell science*. 98 (Pt 2), pp. 151–158.

Castillo, L. *et al.* (2004) ‘Pharmacological background of EGFR targeting’, *Annals of Oncology*, pp. 1007–1012.

Chan, G. K. *et al.* (2000) ‘Human Zw10 and ROD are mitotic checkpoint proteins that bind to kinetochores.’, *Nature cell biology*. 2(12), pp. 944–947.

Chan, Y. W. *et al.* (2009) ‘Mitotic control of kinetochore-associated dynein and spindle orientation by human Spindly.’, *The Journal of cell biology*. 185(5), pp. 859–874.

Chan, Y. W. *et al.* (2012) ‘Aurora B controls kinetochore-microtubule attachments by inhibiting Ska complex-KMN network interaction.’, *The Journal of cell biology*. 196(5), pp. 563–571.

Chandhok, N. S. and Pellman, D. (2009) ‘A little CIN may cost a lot: revisiting aneuploidy and cancer.’, *Current opinion in genetics & development*. 19(1), pp. 74–81.

Chao, W. C. H. *et al.* (2012) ‘Structure of the mitotic checkpoint complex.’, *Nature*. 484(7393), pp. 208–213.

Cheerambathur, D. K. *et al.* (2013) ‘Crosstalk between microtubule attachment complexes ensures accurate chromosome segregation.’, *Science (New York, N.Y.)*.342(6163), pp. 1239–1242.

Cheeseman, I. M. *et al.* (2004) ‘A conserved protein network controls assembly of the outer kinetochore and its ability to sustain tension.’, *Genes & development*. 18(18), pp. 2255–2268.Cheeseman, I. M. *et al.* (2006) ‘The conserved KMN network constitutes the core microtubule-binding site of the kinetochore.’, *Cell*. 127(5), pp. 983–997.

Cheeseman, I. M. and Desai, A. (2008) ‘Molecular architecture of the kinetochore-microtubule interface.’, *Nature reviews. Molecular cell biology*. 9(1), pp. 33–46.

Cheeseman, I. M. (2014) ‘The kinetochore.’, *Cold Spring Harbor perspectives in biology*. 6(7), p. a015826.

Chen, R. H. *et al.* (1998) ‘Spindle checkpoint protein Xmad1 recruits Xmad2 to unattached kinetochores.’, *The Journal of cell biology*. 143(2), pp. 283–295.

Chen, R. H. *et al.* (1999) ‘The spindle checkpoint of budding yeast depends on a tight complex between the Mad1 and Mad2 proteins.’, *Molecular biology of the cell*. 10(8), pp. 2607–2618.

Chen, R.-H. (2002) ‘BubR1 is essential for kinetochore localization of other spindle checkpoint proteins and its phosphorylation requires Mad1.’, *The Journal of cell biology*. 158(3), pp. 487–496.

Chen, F. *et al.* (2007) ‘Multiple Protein Phosphatases Are Required for Mitosis in Drosophila’, *Current Biology*, 17(4), pp. 293–303.

Chen, F., Wang, W. and El-Deiry, W. S. (2010) ‘Current strategies to target p53 in cancer.’, *Biochemical pharmacology*. 80(5), pp. 724–730.

Cheung, C. H. A. *et al.* (2009) ‘Aurora kinase inhibitors in preclinical and clinical testing.’, *Expert opinion on investigational drugs*. 18(4), pp. 379–398.

Christenson, J. L., Denny, E. C. and Kane, S. E. (2015) ‘t-Darpp overexpression in HER2-positive breast cancer confers a survival advantage in lapatinib.’, *Oncotarget*. 6(32), pp. 33134–33145.

Chong, I. Y. *et al.* (2013) 'The genomic landscape of oesophagogastric junctional adenocarcinoma.', *The Journal of pathology*. 231(3), pp. 301–310.

Choo, K. H. (1997) 'Centromere DNA dynamics: latent centromeres and neocentromere formation.', *American journal of human genetics*. 61(6), pp. 1225–1233.

Chung, E. and Chen, R.-H. (2002) 'Spindle checkpoint requires Mad1-bound and Mad1-free Mad2.', *Molecular biology of the cell*., 13(5), pp. 1501–1511.

Ciferri, C. *et al.* (2005) 'Architecture of the human ndc80-hec1 complex, a critical constituent of the outer kinetochore.', *The Journal of biological chemistry*. 280(32), pp. 29088–29095.

Cimini, D. *et al.* (2003) 'Merotelic kinetochore orientation occurs frequently during early mitosis in mammalian tissue cells and error correction is achieved by two different mechanisms.', *Journal of cell science*. 116(Pt 20), pp. 4213–4225.

Cimini, D., Cameron, L. A. and Salmon, E. D. (2004) 'Anaphase spindle mechanics prevent mis-segregation of merotelically oriented chromosomes.', *Current biology : CB*. 14(23), pp. 2149–2155.

Cimini, D. and Degrassi, F. (2005) 'Aneuploidy: a matter of bad connections.', *Trends in cell biology*. 15(8), pp. 442–451.

Cimini, D. *et al.* (2006) 'Aurora kinase promotes turnover of kinetochore microtubules to reduce chromosome segregation errors.', *Current biology : CB*. 16(17), pp. 1711–1718.

Cimini, D. (2007) 'Detection and correction of merotelic kinetochore orientation by Aurora B and its partners.', *Cell cycle.* 6(13), pp. 1558–1564.

Cimini, D. (2008) 'Merotelic kinetochore orientation, aneuploidy, and cancer.', *Biochimica et biophysica acta*. 1786(1), pp. 32–40.

Cleveland, D. W., Mao, Y. and Sullivan, K. F. (2003) 'Centromeres and kinetochores: from epigenetics to mitotic checkpoint signalling.', *Cell*. 112(4), pp. 407–421.

Clute, P. and Pines, J. (1999) 'Temporal and spatial control of cyclin B1 destruction in metaphase.', *Nature cell biology*. 1(2), pp. 82–87.

Cohen, R. L. *et al.* (2008) 'Structural and functional dissection of Mif2p, a conserved DNA-binding kinetochore protein.', *Molecular biology of the cell*., 19(10), pp. 4480–4491.

Cohen-Fix, O. *et al.* (1996) 'Anaphase initiation in Saccharomyces cerevisiae is controlled by the APC-dependent degradation of the anaphase inhibitor Pds1p.', *Genes & development*. 10(24), pp. 3081–3093.

Collin, P. *et al.* (2013) 'The spindle assembly checkpoint works like a rheostat rather than a toggle switch.', *Nature cell biology*. 15(11), pp. 1378–1385.

Contino, G. *et al.* (2016) 'Whole-genome sequencing of nine esophageal adenocarcinoma cell lines.', *F1000Research*. 5, p. 1336.

Cooke, C. A., Bernat, R. L. and Earnshaw, W. C. (1990) 'CENP-B: a major human centromere protein located beneath the kinetochore.', *The Journal of cell biology*. 110(5), pp. 1475–1488.

Cooper, J. E. (1983) 'NH4'-N-that', 5932(February), pp. 1–4.

Coué, M. *et al.* (1987) 'Inhibition of actin polymerization by latrunculin A', *FEBS Letters*, 213(2), pp. 316–318.

Cross, W. C., Graham, T. A. and Wright, N. A. (2016) 'New paradigms in clonal evolution: punctuated equilibrium in cancer.', *The Journal of pathology*. 240(2), pp. 126–136.

Curators, F. (2008) 'Assigning Gene Ontology (GO) terms by sequence similarity in FlyBase.'

Dai, J. *et al.* (2005) 'The kinase Haspin is required for mitotic histone H3 Thr 3 phosphorylation and normal metaphase chromosome alignment.', *Genes & development*. 19(4), pp. 472–488.

Dai, J., Sullivan, B. A. and Higgins, J. M. G. (2006) 'Regulation of mitotic chromosome cohesion by Haspin and Aurora B.', *Developmental cell*. 11(5), pp. 741–750.

Daum, J. R. *et al.* (2009) 'Ska3 is required for spindle checkpoint silencing and the maintenance of chromosome cohesion in mitosis.', *Current biology : CB*. 19(17), pp. 1467–1472.

D'Avino, P. P. *et al.* (2008) 'Interaction between Anillin and RacGAP50C connects the actomyosin contractile ring with spindle microtubules at the cell division site.', *Journal of cell science*, 121(Pt 8), pp. 1151–8.

D'Avino, P. P., Giansanti, M. G. and Petronczki, M. (2015) 'Cytokinesis in animal cells.', *Cold Spring Harbor perspectives in biology*. 7(4), p. a015834. De Antoni, A. *et al.* (2005) 'The Mad1/Mad2 complex as a template for Mad2 activation in the spindle assembly checkpoint.', *Current biology : CB*. 15(3), pp. 214–225.

De Angelis, P. *et al.* (1993) 'P53 expression is associated with a high-degree of tumor DNA aneuploidy and incidence of p53 gene mutation, and is localized to the aneuploid component in colorectal carcinomas.', *International journal of oncology*. 3(2), pp. 305–312.

DeLuca, J. G. *et al.* (2002) 'hNuf2 inhibition blocks stable kinetochore-microtubule attachment and induces mitotic cell death in HeLa cells.', *The Journal of cell biology*. 159(4), pp. 549–555.

DeLuca, J. G. *et al.* (2006) 'Kinetochore microtubule dynamics and attachment stability are regulated by Hec1.', *Cell*. 127(5), pp. 969–982.

DeLuca, K. F., Lens, S. M. A. and DeLuca, J. G. (2011) 'Temporal changes in Hec1 phosphorylation control kinetochore-microtubule attachment stability during mitosis.', *Journal of cell science*. 124(Pt 4), pp. 622–634.

DeLuca, J. G. and Musacchio, A. (2012) 'Structural organization of the kinetochore-microtubule interface.', *Current opinion in cell biology*. 24(1), pp. 48–56.

den Elzen, N. and Pines, J. (2001) ‘Cyclin A is destroyed in prometaphase and can delay chromosome alignment and anaphase.’, *The Journal of cell biology*. 153(1), pp. 121–136.

Depinet, T. W. *et al.* (1997) ‘Characterization of neo-centromeres in marker chromosomes lacking detectable alpha-satellite DNA.’, *Human molecular genetics*. 6(8), pp. 1195–1204.

Desai, A. and Mitchison, T. J. (1997) ‘Microtubule polymerization dynamics.’, *Annual review of cell and developmental biology*, 13, pp. 83–117.

Desai, A. *et al.* (1999) ‘Kin I kinesins are microtubule-destabilizing enzymes’, *Cell*, 96(1), pp. 69–78.

Desai, A. *et al.* (2003) ‘KNL-1 directs assembly of the microtubule-binding interface of the kinetochore in C. elegans.’, *Genes & development*. 17(19), pp. 2421–2435.

Desai, T. K. *et al.* (2012) ‘The incidence of oesophageal adenocarcinoma in non-dysplastic Barrett’s oesophagus: a meta-analysis.’, *Gut*, 61(7), pp. 970–6.

Dewhurst, S. M. *et al.* (2014) ‘Tolerance of whole-genome doubling propagates chromosomal instability and accelerates cancer genome evolution.’, *Cancer discovery*. 4(2), pp. 175–185.

Diaz-Rodriguez, E. *et al.* (2008) ‘Hec1 overexpression hyperactivates the mitotic checkpoint and induces tumor formation in vivo.’, *Proceedings of the National Academy of Sciences of the United States of America*. 105(43), pp. 16719–16724.

Dick, A. E. and Gerlich, D. W. (2013) ‘Kinetic framework of spindle assembly checkpoint signalling.’, *Nature cell biology*. 15(11), pp. 1370–1377.

Ditchfield, C. *et al.* (2003) ‘Aurora B couples chromosome alignment with anaphase by targeting BubR1, Mad2, and Cenp-E to kinetochores.’, *The Journal of cell biology*. 161(2), pp. 267–280.

Doherty, G. J. and McMahon, H. T. (2008) ‘Mediation, Modulation, and Consequences of Membrane-Cytoskeleton Interactions’, *Annual Review of Biophysics*, 37(1), pp. 65–95.

Duesberg, P. and Li, R. (2003) ‘Multistep carcinogenesis: a chain reaction of aneuploidizations.’, *Cell cycle*. 2(3), pp. 202–210.

Duensing, A. and Duensing, S. (2005) ‘Guilt by association? p53 and the development of aneuploidy in cancer.’, *Biochemical and biophysical research communications*. 331(3), pp. 694–700.

Dulak, A. M. *et al.* (2013) ‘Exome and whole-genome sequencing of esophageal adenocarcinoma identifies recurrent driver events and mutational complexity.’, *Nature genetics*, 45(5), pp. 478–86.

du Sart, D. *et al.* (1997) ‘A functional neo-centromere formed through activation of a latent human centromere and consisting of non-alpha-satellite DNA.’, *Nature genetics*. 16(2), pp. 144–153.

Earnshaw, W. C. and Rothfield, N. (1985) ‘Identification of a family of human centromere proteins using autoimmune sera from patients with scleroderma.’, *Chromosoma*. 91(3–4), pp. 313–321.

Earnshaw, W. *et al.* (1986) ‘Three human chromosomal autoantigens are recognized by sera from patients with anti-centromere antibodies.’, *The Journal of clinical investigation*. 77(2), pp. 426–430.

Earnshaw, W. C. *et al.* (1987) ‘Molecular cloning of cDNA for CENP-B, the major human centromere autoantigen.’, *The Journal of cell biology*. 104(4), pp. 817–829.

Earnshaw, W. C. and Rattner, J. B. (1989) ‘A map of the centromere (primary constriction) in vertebrate chromosomes at metaphase.’, *Progress in clinical and biological research*. 318, pp. 33–42.

Ebihara, Y. *et al.* (2004) ‘DARPP-32 expression arises after a phase of dysplasia in oesophageal squamous cell carcinoma.’, *British journal of cancer*. 91(1), pp. 119–123.

Eggert, U. S. *et al.* (2004) ‘Parallel chemical genetic and genome-wide RNAi screens identify cytokinesis inhibitors and targets’, *PLoS Biology*, 2(12).

Ekwall, K. (2007) ‘Epigenetic control of centromere behaviour.’, *Annual review of genetics*. 41, pp. 63–81.

El-Rifai, W. *et al.* (1998) ‘Consistent genetic alterations in xenografts of proximal stomach and gastro-esophageal junction adenocarcinomas.’, *Cancer research*. 58(1), pp. 34–37.

El-Rifai, W. *et al.* (2001) ‘Genetic differences between adenocarcinomas arising in Barrett’s esophagus and gastric mucosa.’, *Gastroenterology*. 121(3), pp. 592–598.

Erhardt, S. *et al.* (2008) ‘Genome-wide analysis reveals a cell cycle-dependent mechanism controlling centromere propagation.’, *The Journal of cell biology*. 183(5), pp. 805–818.

Errico, A. *et al.* (2010) ‘Identification of substrates for cyclin dependent kinases.’, *Advances in enzyme regulation*. 50(1), pp. 375–399.

Essex, A. *et al.* (2009) ‘Systematic analysis in Caenorhabditis elegans reveals that the spindle checkpoint is composed of two largely independent branches.’, *Molecular biology of the cell*. 20(4), pp. 1252–1267.

Euskirchen, G. M. (2002) ‘Nnf1p, Dsn1p, Mtw1p, and Nsl1p: a new group of proteins important for chromosome segregation in Saccharomyces cerevisiae.’, *Eukaryotic cell*. 1(2), pp. 229–240.

Fachinetti, D. *et al.* (2013) ‘A two-step mechanism for epigenetic specification of centromere identity and function.’, *Nature cell biology*. 15(9), pp. 1056–1066.
Faesen, A. C. *et al.* (2017) ‘Basis of catalytic assembly of the mitotic checkpoint complex.’, *Nature*. 542(7642), pp. 498–502.

Ferrara, M. *et al.* (2018) ‘Small molecules targeted to the microtubule-Hec1 interaction inhibit cancer cell growth through microtubule stabilization.’, *Oncogene*. 37(2), pp. 231–240.

Ferretti, C. *et al.* (2010) ‘Expression of the kinetochore protein Hec1 during the cell cycle in normal and cancer cells and its regulation by the pRb pathway.’, *Cell cycle (Georgetown, Tex.)*. 9(20), pp. 4174–4182.

Foley, E. A., Maldonado, M. and Kapoor, T. M. (2011) ‘Formation of stable attachments between kinetochores and microtubules depends on the B56-PP2A phosphatase.’, *Nature cell biology*. 13(10), pp. 1265–1271.

Foltz, D. R. *et al.* (2006) ‘The human CENP-A centromeric nucleosome-associated complex.’, *Nature cell biology*. 8(5), pp. 458–469.

Fox, D. T. and Duronio, R. J. (2013) ‘Endoreplication and polyploidy: insights into development and disease.’, *Development (Cambridge, England)*. 140(1), pp. 3–12.

Fletcher, J. *et al.* (2003) ‘Barrett’s esophagus evokes a quantitatively and qualitatively altered response to both acid and hypertonic solutions.’, *The American journal of gastroenterology*. 98(7), pp. 1480–1486.

Frankell, A. M. *et al.* (2019) ‘The landscape of selection in 551 esophageal adenocarcinomas defines genomic biomarkers for the clinic.’, *Nature genetics*. 51(3), pp. 506–516.

Fujiwara, T. *et al.* (2005) ‘Cytokinesis failure generating tetraploids promotes tumorigenesis in p53-null cells.’, *Nature*. 437(7061), pp. 1043–1047.

Gaitanos, T. N. *et al.* (2009) ‘Stable kinetochore-microtubule interactions depend on the Ska complex and its new component Ska3/C13Orf3.’, *The EMBO journal*. 28(10), pp. 1442–1452.

Galipeau, P. C. *et al.* (1996) ‘17p (p53) allelic losses, 4N (G2/tetraploid) populations, and progression to aneuploidy in Barrett’s esophagus.’, *Proceedings of the National Academy of Sciences of the United States of America*. 93(14), pp. 7081–7084.

Galipeau, P. C. *et al.* (1999) ‘Clonal expansion and loss of heterozygosity at chromosomes 9p and 17p in premalignant esophageal (Barrett’s) tissue.’, *Journal of the National Cancer Institute*. 91(24), pp. 2087–2095.

Gama JB, Pereira C, Simões PA, *et al*. Molecular mechanism of dynein recruitment to kinetochores by the Rod-Zw10-Zwilch complex and Spindly. *J Cell Biol*. 2017;216(4):943–960.

Ganem, N. J., Godinho, S. A. and Pellman, D. (2009) ‘A mechanism linking extra centrosomes to chromosomal instability.’, *Nature*. 460(7252), pp. 278–282.

Ganem, N. J., Storchova, Z. and Pellman, D. (2007) ‘Tetraploidy, aneuploidy and cancer.’, *Current opinion in genetics & development*. 17(2), pp. 157–162.

Gascoigne, K. E. and Cheeseman, I. M. (2011) ‘Kinetochore assembly: if you build it, they will come.’, *Current opinion in cell biology*. 23(1), pp. 102–108.

Gassmann, R. *et al.* (2008) ‘A new mechanism controlling kinetochore-microtubule interactions revealed by comparison of two dynein-targeting components: SPDL-1 and the Rod/Zwilch/Zw10 complex.’, *Genes & development*. 22(17), pp. 2385–2399.

Geigl, J. B. *et al.* (2008) ‘Defining “chromosomal instability”.’, *Trends in genetics : TIG*. 24(2), pp. 64–69.

Geley, S. *et al.* (2001) ‘Anaphase-promoting complex/cyclosome-dependent proteolysis of human cyclin A starts at the beginning of mitosis and is not subject to the spindle assembly checkpoint.’, *The Journal of cell biology*. 153(1), pp. 137–148.

Gerlinger, M. *et al.* (2012) ‘Intratumor heterogeneity and branched evolution revealed by multiregion sequencing.’, *The New England journal of medicine*. 366(10), pp. 883–892.

Ghadimi, B. M. *et al.* (2000) ‘Centrosome amplification and instability occurs exclusively in aneuploid, but not in diploid colorectal cancer cell lines, and correlates with numerical chromosomal aberrations.’, *Genes, chromosomes & cancer*. 27(2), pp. 183–190.

Gmachl, M. *et al.* (2000) ‘The RING-H2 finger protein APC11 and the E2 enzyme UBC4 are sufficient to ubiquitinate substrates of the anaphase-promoting complex.’, *Proceedings of the National Academy of Sciences of the United States of America*. 97(16), pp. 8973–8978.

Godinho, S. A. and Pellman, D. (2014) ‘Causes and consequences of centrosome abnormalities in cancer.’, *Philosophical transactions of the Royal Society of London. Series B, Biological sciences*. 369(1650).

Goh, A. M., Coffill, C. R. and Lane, D. P. (2011) ‘The role of mutant p53 in human cancer.’, *The Journal of pathology*. 223(2), pp. 116–126.

Golsteyn, R. M. *et al.* (1994) ‘Cell cycle analysis and chromosomal localization of human Plk1, a putative homologue of the mitotic kinases Drosophila polo and Saccharomyces cerevisiae Cdc5.’, *Journal of cell science*. 107 Pt 6, pp. 1509–1517.

Gorbsky, G. J. (2013) ‘Cohesion fatigue.’, *Current biology : CB*. 23(22), pp. R986–R988.

Gordon, D. J., Resio, B. and Pellman, D. (2012) ‘Causes and consequences of aneuploidy in cancer.’, *Nature reviews. Genetics*. 13(3), pp. 189–203.

Gorr, I. H., Boos, D. and Stemmann, O. (2005) ‘Mutual inhibition of separase and Cdk1 by two-step complex formation.’, *Molecular cell*. 19(1), pp. 135–141.

Goshima, G. and Vale, R. D. (2003) ‘The roles of microtubule-based motor proteins in mitosis: Comprehensive RNAi analysis in the Drosophila S2 cell line’, *Journal of Cell Biology*, 162(6), pp. 1003–1016.

Goshima, G. *et al.* (2003) ‘Human centromere chromatin protein hMis12, essential for equal segregation, is independent of CENP-A loading pathway.’, *The Journal of cell biology*.160(1), pp. 25–39.

Goshima, G. *et al.* (2008) ‘Augmin: a protein complex required for centrosome-independent microtubule generation within the spindle.’, *The Journal of cell biology*. 181(3), pp. 421–429.

Gregan, J. *et al.* (2011) ‘Merotelic kinetochore attachment: causes and effects.’, *Trends in cell biology*. 21(6), pp. 374–381.

Griffis, E. R., Stuurman, N. and Vale, R. D. (2007) ‘Spindly, a novel protein essential for silencing the spindle assembly checkpoint, recruits dynein to the kinetochore.’, *The Journal of cell biology*. 177(6), pp. 1005–1015.

Gu, L., Waliany, S. and Kane, S. E. (2009) ‘Darpp-32 and its truncated variant t-Darpp have antagonistic effects on breast cancer cell growth and herceptin resistance.’, *PloS one*. 4(7), p. e6220.

Hagting, A. *et al.* (2002) ‘Human securin proteolysis is controlled by the spindle checkpoint and reveals when the APC/C switches from activation by Cdc20 to Cdh1.’, *The Journal of cell biology*. 157(7), pp. 1125–1137.

Hanel, W. and Moll, U. M. (2012) ‘Links between mutant p53 and genomic instability.’, *Journal of cellular biochemistry*. 113(2), pp. 433–439.

Hanisch, A., Sillje, H. H. W. and Nigg, E. A. (2006) ‘Timely anaphase onset requires a novel spindle and kinetochore complex comprising Ska1 and Ska2.’, *The EMBO journal*. 25(23), pp. 5504–5515.

Hara, M. and Fukagawa, T. (2017) ‘Critical Foundation of the Kinetochore: The Constitutive Centromere-Associated Network (CCAN).’, *Progress in molecular and subcellular biology*., 56, pp. 29–57.

Hauf, S. *et al.* (2003) ‘The small molecule Hesperadin reveals a role for Aurora B in correcting kinetochore-microtubule attachment and in maintaining the spindle assembly checkpoint.’, *The Journal of cell biology*. 161(2), pp. 281–294.

Hayeck, T. J. *et al.* (2010) ‘The prevalence of Barrett’s esophagus in the US: estimates from a simulation model confirmed by SEER data.’, *Diseases of the esophagus : official journal of the International Society for Diseases of the Esophagus*. 23(6), pp. 451–457.

Heald, R. *et al.* (1996) ‘Self-organization of microtubules into bipolar spindles around artificial chromosomes in Xenopus egg extracts.’, *Nature*. 382(6590), pp. 420–425.

Heeger, S. *et al.* (2005) ‘Genetic interactions of separase regulatory subunits reveal the diverged Drosophila Cenp-C homolog.’, *Genes & development*. 19(17), pp. 2041–2053.

Helgeson, L. A. *et al.* (2018) ‘Human Ska complex and Ndc80 complex interact to form a load-bearing assembly that strengthens kinetochore-microtubule attachments.’, *Proceedings of the National Academy of Sciences of the United States of America*. 115(11), pp. 2740–2745.

Herman, J. A. *et al.* (2015) ‘Molecular pathways: regulation and targeting of kinetochore-microtubule attachment in cancer.’, *Clinical cancer research : an official journal of the American Association for Cancer Research*. 21(2), pp. 233–239.

Hernando, E. *et al.* (2004) 'Rb inactivation promotes genomic instability by uncoupling cell cycle progression from mitotic control.', *Nature*. 430(7001), pp. 797–802.

Hershko, A. (1999) 'Mechanisms and regulation of the degradation of cyclin B.', *Philosophical transactions of the Royal Society of London. Series B, Biological sciences*. 354(1389), pp. 1571–1576.

Hoffman, D. B. *et al.* (2001) 'Microtubule-dependent changes in assembly of microtubule motor proteins and mitotic spindle checkpoint proteins at PtK1 kinetochores.', *Molecular biology of the cell*. 12(7), pp. 1995–2009.

Holland, A. J. and Cleveland, D. W. (2009) 'Boveri revisited: chromosomal instability, aneuploidy and tumorigenesis.', *Nature reviews. Molecular cell biology*. 10(7), pp. 478–487.

Holland, A. J. and Taylor, S. S. (2006) 'Cyclin-B1-mediated inhibition of excess separase is required for timely chromosome disjunction.', *Journal of cell science*. 119(Pt 16), pp. 3325–3336.

Holland, A. J. *et al.* (2012) 'The autoregulated instability of Polo-like kinase 4 limits centrosome duplication to once per cell cycle.', *Genes & development*. 26(24), pp. 2684–2689.

Holt, L. J., Krutchinsky, A. N. and Morgan, D. O. (2008) 'Positive feedback sharpens the anaphase switch.', *Nature*. 454(7202), pp. 353–357.

Hong, B. *et al.* (2014) 'Targeting tumor suppressor p53 for cancer therapy: strategies, challenges and opportunities.', *Current drug targets*. 15(1), pp. 80–89.

Hori, T. *et al.* (2008) 'CENP-O class proteins form a stable complex and are required for proper kinetochore function.', *Molecular biology of the cell*. 19(3), pp. 843–854.

Hori, T. *et al.* (2013) 'The CCAN recruits CENP-A to the centromere and forms the structural core for kinetochore assembly.', *The Journal of cell biology*. 200(1), pp. 45–60.

Howell, B. J. *et al.* (2000) 'Visualization of Mad2 dynamics at kinetochores, along spindle fibers, and at spindle poles in living cells.', *The Journal of cell biology*. 150(6), pp. 1233–1250.

Howell, B. J. *et al.* (2001) 'Cytoplasmic dynein/dynactin drives kinetochore protein transport to the spindle poles and has a role in mitotic spindle checkpoint inactivation.', *The Journal of cell biology*. 155(7), pp. 1159–1172.

Howell, B. J. *et al.* (2004) 'Spindle checkpoint protein dynamics at kinetochores in living cells.', *Current biology : CB*. 14(11), pp. 953–964.

Hoyt, M. A., Totis, L. and Roberts, B. T. (1991) 'S. cerevisiae genes required for cell cycle arrest in response to loss of microtubule function.', *Cell*. 66(3), pp. 507–517.

Hingorani, S. R. *et al.* (2005) 'Trp53R172H and KrasG12D cooperate to promote chromosomal instability and widely metastatic pancreatic ductal adenocarcinoma in mice', *Cancer Cell*, 7(5), pp. 469–483.

Hirano, T. (2015) ‘Chromosome Dynamics during Mitosis.’, *Cold Spring Harbor perspectives in biology*. 7(6).

Hua, S. *et al.* (2011) ‘CENP-U cooperates with Hec1 to orchestrate kinetochore-microtubule attachment.’, *The Journal of biological chemistry*. 286(2), pp. 1627–1638.

Huckaba, T. M. *et al.* (2011) ‘Kinesin-73 is a processive motor that localizes to Rab5-containing organelles’, *Journal of Biological Chemistry*, 286(9), pp. 7457–7467.

Hudson, D. F. *et al.* (1998) ‘Centromere protein B null mice are mitotically and meiotically normal but have lower body and testis weights.’, *The Journal of cell biology*. 141(2), pp. 309–319.

Hughes, J. R. *et al.* (2008) ‘A microtubule interactome: Complexes with roles in cell cycle and mitosis’, *PLoS Biology*, 6(4), pp. 785–795.

Iovino, F. *et al.* (2006) ‘RB acute loss induces centrosome amplification and aneuploidy in murine primary fibroblasts.’, *Molecular cancer*. 5, p. 38.

Irniger, S. and Nasmyth, K. (1997) ‘The anaphase-promoting complex is required in G1 arrested yeast cells to inhibit B-type cyclin accumulation and to prevent uncontrolled entry into S-phase.’, *Journal of cell science*. 110 (Pt 1, pp. 1523–1531.

Izawa, D. and Pines, J. (2012) ‘Mad2 and the APC/C compete for the same site on Cdc20 to ensure proper chromosome segregation.’, *The Journal of cell biology*. 199(1), pp. 27–37.

Izuta, H. *et al.* (2006) ‘Comprehensive analysis of the ICEN (Interphase Centromere Complex) components enriched in the CENP-A chromatin of human cells.’, *Genes to cells : devoted to molecular & cellular mechanisms*. 11(6), pp. 673–684.

Jallepalli, P. V and Lengauer, C. (2001) ‘Chromosome segregation and cancer: cutting through the mystery.’, *Nature reviews. Cancer*. 1(2), pp. 109–117.

Jansen, L. E. T. *et al.* (2007) ‘Propagation of centromeric chromatin requires exit from mitosis.’, *The Journal of cell biology*. 176(6), pp. 795–805.

Ji, Z. *et al.* (2017) ‘A sequential multi-target Mps1 phosphorylation cascade promotes spindle checkpoint signaling.’, *eLife*. 6.

Joglekar, A. P. *et al.* (2006) ‘Molecular architecture of a kinetochore-microtubule attachment site.’, *Nature cell biology*. 8(6), pp. 581–585.

Joglekar, A. P., Bloom, K. S. and Salmon, E. D. (2010) ‘Mechanisms of force generation by end-on kinetochore-microtubule attachments.’, *Current opinion in cell biology*. 22(1), pp. 57–67.

Johnson, V. L. *et al.* (2004) ‘Bub1 is required for kinetochore localization of BubR1, Cenp-E, Cenp-F and Mad2, and chromosome congression.’, *Journal of cell science*. 117(Pt 8), pp. 1577–1589.

Johnston, K. *et al.* (2010) 'Vertebrate kinetochore protein architecture: protein copy number.', *The Journal of cell biology*. 189(6), pp. 937–943.

Jolly, A. L. *et al.* (2010) 'Kinesin-1 heavy chain mediates microtubule sliding to drive changes in cell shape.', *Proceedings of the National Academy of Sciences of the United States of America*, 107(27), pp. 12151–6.

Jolly, A. L. *et al.* (2016) 'A Genome-wide RNAi Screen for Microtubule Bundle Formation and Lysosome Motility Regulation in Drosophila S2 Cells.', *Cell reports*. 14(3), pp. 611–620.

Joseph, C. G. *et al.* (2014) 'Association of the autoimmune disease scleroderma with an immunologic response to cancer.', *Science* 343(6167), pp. 152–157.

Jung, M. S. *et al.* (2001) 'p53 and its homologues, p63 and p73, induce a replicative senescence through inactivation of NF-Y transcription factor.', *Oncogene*. 20(41), pp. 5818–5825.

Kabeche, L. and Compton, D. A. (2012) 'Checkpoint-independent stabilization of kinetochore-microtubule attachments by Mad2 in human cells.', *Current biology : CB*. 22(7), pp. 638–644.

Kamijo, K. *et al.* (2006) 'Dissecting the role of Rho-mediated signaling in contractile ring formation.', *Molecular biology of the cell*, 17(1), pp. 43–55.

Kalab, P., Pu, R. T. and Dasso, M. (1999) 'The ran GTPase regulates mitotic spindle assembly.', *Current biology : CB*. 9(9), pp. 481–484.

Karess, R. E. and Glover, D. M. (1989) 'rough deal: a gene required for proper mitotic segregation in Drosophila.', *The Journal of cell biology*. 109(6 Pt 1), pp. 2951–2961.

Karess, R. (2005) 'Rod-Zw10-Zwilch: a key player in the spindle checkpoint.', *Trends in cell biology*. 15(7), pp. 386–392.

Karsenti, E. (1993) 'Microtubule dynamics: severing microtubules in mitosis.', *Current biology : CB*. 3(4), pp. 208–210.

Kato, T. *et al.* (2011) 'Overexpression of MAD2 predicts clinical outcome in primary lung cancer patients.', *Lung cancer*. 74(1), pp. 124–131.

Kato, H. *et al.* (2013) 'A conserved mechanism for centromeric nucleosome recognition by centromere protein CENP-C.', *Science*. 340(6136), pp. 1110–1113.

Khodjakov, A. *et al.* (1997) 'Chromosome fragments possessing only one kinetochore can congress to the spindle equator.', *The Journal of cell biology*. 136(2), pp. 229–240.

Kiger, A. A. *et al.* (2003) 'A functional genomic analysis of cell morphology using RNA interference.', *Journal of biology*, 2(4), p. 27.

Kiyomitsu, T., Obuse, C. and Yanagida, M. (2007) 'Human Blinkin/AF15q14 is required for chromosome alignment and the mitotic checkpoint through direct interaction with Bub1 and BubR1.', *Developmental cell*. 13(5), pp. 663–676.

Klare, K. *et al.* (2015) 'CENP-C is a blueprint for constitutive centromere-associated network assembly within human kinetochores.', *The Journal of cell biology*. 210(1), pp. 11–22.

Kline, S. L. *et al.* (2006) 'The human Mis12 complex is required for kinetochore assembly and proper chromosome segregation.', *The Journal of cell biology*. 173(1), pp. 9–17.

Kops, G. J. P. L. *et al.* (2005) 'ZW10 links mitotic checkpoint signalling to the structural kinetochore.', *The Journal of cell biology*. 169(1), pp. 49–60.

Kramer, E. R. *et al.* (1998) 'Activation of the human anaphase-promoting complex by proteins of the CDC20/Fizzy family.', *Current biology : CB*. 8(22), pp. 1207–1210.

Kruse, T. *et al.* (2013) 'Direct binding between BubR1 and B56-PP2A phosphatase complexes regulate mitotic progression.', *Journal of cell science*. 126(Pt 5), pp. 1086–1092.

Krylyshkina, O. *et al.* (2003) 'Nanometer targeting of microtubules to focal adhesions', *Journal of Cell Biology*, 161(5), pp. 853–859.

Kudalkar, E. M. *et al.* (2015) 'Regulation of outer kinetochore Ndc80 complex-based microtubule attachments by the central kinetochore Mis12/MIND complex.', *Proceedings of the National Academy of Sciences of the United States of America*. 112(41), pp. E5583-9.

Kuipers, E. J. and Spaander, M. C. (2018) 'Natural History of Barrett's Esophagus.', *Digestive diseases and sciences*. 63(8), pp. 1997–2004.

Kwon, M. and Scholey, J. M. (2004) 'Spindle mechanics and dynamics during mitosis in Drosophila', *Trends in Cell Biology*, pp. 194–205.

Kwon, M. *et al.* (2008) 'Mechanisms to suppress multipolar divisions in cancer cells with extra centrosomes.', *Genes & development*. 22(16), pp. 2189–2203.

Lampson, M. A. and Kapoor, T. M. (2005) 'The human mitotic checkpoint protein BubR1 regulates chromosome-spindle attachments.', *Nature cell biology*. 7(1), pp. 93–98.

Lara-Gonzalez, P., Westhorpe, F. G. and Taylor, S. S. (2012) 'The spindle assembly checkpoint.', *Current biology : CB*. 22(22), pp. R966-80.

Lau, D. T. C. and Murray, A. W. (2012) 'Mad2 and Mad3 cooperate to arrest budding yeast in mitosis.', *Current biology : CB*. 22(3), pp. 180–190.

Lawo, S. *et al.* (2009) 'HAUS, the 8-subunit human Augmin complex, regulates centrosome and spindle integrity.', *Current biology : CB*. 19(10), pp. 816–826.

Lee, J. S. *et al.* (2004) 'MgcRacGAP regulates cortical activity through RhoA during cytokinesis', *Experimental Cell Research*, 293(2), pp. 275–282.

Lee, K. S. *et al.* (2014) 'Mechanisms underlying Plk1 polo-box domain-mediated biological processes and their physiological significance.', *Molecules and cells*. 37(4), pp. 286–294.

Lee, S. H. and Dominguez, R. (2010) 'Regulation of actin cytoskeleton dynamics in cells.', *Molecules and cells*, pp. 311–325.

Lens, S. M. A. *et al.* (2003) 'Survivin is required for a sustained spindle checkpoint arrest in response to lack of tension.', *The EMBO journal*. 22(12), pp. 2934–2947.

Leverson, J. D. *et al.* (2000) 'The APC11 RING-H2 finger mediates E2-dependent ubiquitination.', *Molecular biology of the cell*. 11(7), pp. 2315–2325.

Li, H. *et al.* (2014) 'Rho GTPases and cancer', *BioFactors*, pp. 226–235.

Li, W. *et al.* (2012) 'Reconstitution of dynamic microtubules with drosophila XMAP215, EB1, and sentin', *Journal of Cell Biology*, 199(5), pp. 849–862.

Li, X. *et al.* (2008) 'Single nucleotide polymorphism-based genome-wide chromosome copy change, loss of heterozygosity, and aneuploidy in Barrett's esophagus neoplastic progression.', *Cancer prevention research*. 1(6), pp. 413–423.

Li, X. *et al.* (2014) 'Temporal and spatial evolution of somatic chromosomal alterations: a case-cohort study of Barrett's esophagus.', *Cancer prevention research*. 7(1), pp. 114–127.

Li, X. *et al.* (2018) 'Organoid cultures recapitulate esophageal adenocarcinoma heterogeneity providing a model for clonality studies and precision therapeutics.', *Nature communications*. 9(1), p. 2983.

Lin, J., Teresky, A. K. and Levine, A. J. (1995) 'Two critical hydrophobic amino acids in the N-terminal domain of the p53 protein are required for the gain of function phenotypes of human p53 mutants.', *Oncogene*. 10(12), pp. 2387–2390.

Lingle, W. L. *et al.* (2002) 'Centrosome amplification drives chromosomal instability in breast tumor development.', *Proceedings of the National Academy of Sciences of the United States of America*. 99(4), pp. 1978–1983.

Liu, S.-T. *et al.* (2003) 'Human CENP-I specifies localization of CENP-F, MAD1 and MAD2 to kinetochores and is essential for mitosis.', *Nature cell biology*. 5(4), pp. 341–345.

Liu, S.-T. *et al.* (2006) 'Mapping the assembly pathways that specify formation of the trilaminar kinetochore plates in human cells.', *The Journal of cell biology*. 175(1), pp. 41–53.

Liu, D. *et al.* (2010) 'Regulated targeting of protein phosphatase 1 to the outer kinetochore by KNL1 opposes Aurora B kinase.', *The Journal of cell biology*. 188(6), pp. 809–820.

Liu, X. and Winey, M. (2012) 'The MPS1 family of protein kinases.', *Annual review of biochemistry*. 81, pp. 561–585.

Llamazares, S. *et al.* (1991) 'polo encodes a protein kinase homolog required for mitosis in Drosophila.', *Genes & development*. 5(12A).

Lopes, C. A. M. *et al.* (2018) 'Centrosome amplification arises before neoplasia and increases upon p53 loss in tumorigenesis.', *The Journal of cell biology*. 217(7), pp. 2353–2363.

Luo, X. *et al.* (2000) 'Structure of the Mad2 spindle assembly checkpoint protein and its interaction with Cdc20.', *Nature structural biology*. 7(3), pp. 224–229.

Maciejowski, J. *et al.* (2017) 'Mps1 Regulates Kinetochore-Microtubule Attachment Stability via the Ska Complex to Ensure Error-Free Chromosome Segregation.', *Developmental cell*. 41(2), pp. 143-156.e6.

Magdalena, J., Millard, T. H. and Machesky, L. M. (2003) 'Microtubule involvement in NIH 3T3 Golgi and MTOC polarity establishment.', *Journal of cell science*, 116, pp. 743–756.

Magidson, V. *et al.* (2011) 'The spatial arrangement of chromosomes during prometaphase facilitates spindle assembly.', *Cell*. 146(4), pp. 555–567.

Maher, C. A. and Wilson, R. K. (2012) 'Chromothripsis and human disease: piecing together the shattering process.', *Cell*. 148(1–2), pp. 29–32.

Maley, C. C. *et al.* (2006) 'Genetic clonal diversity predicts progression to esophageal adenocarcinoma.', *Nature genetics*. 38(4), pp. 468–473.

Malureanu, L. A. *et al.* (2009) 'BubR1 N terminus acts as a soluble inhibitor of cyclin B degradation by APC/C(Cdc20) in interphase.', *Developmental cell*. 16(1), pp. 118–131.

Marthiens, V. *et al.* (2013) 'Centrosome amplification causes microcephaly.', *Nature cell biology*. 15(7), pp. 731–740.

Martin-Lluesma, S., Stucke, V. M. and Nigg, E. A. (2002) 'Role of Hec1 in spindle checkpoint signalling and kinetochore recruitment of Mad1/Mad2.', *Science*. 297(5590), pp. 2267–2270.

Masumoto, H. *et al.* (1989) 'A human centromere antigen (CENP-B) interacts with a short specific sequence in alphoid DNA, a human centromeric satellite.', *The Journal of cell biology*. 109(5), pp. 1963–1973.

Matsumoto, T. *et al.* (2007) 'Aging-associated vascular phenotype in mutant mice with low levels of BubR1.', *Stroke*. 38(3), pp. 1050–1056.

Mattiuzzo, M. *et al.* (2011) 'Abnormal kinetochore-generated pulling forces from expressing a N-terminally modified Hec1.', *PloS one*. 6(1), p. e16307.

McClelland, S. E. *et al.* (2007) 'The CENP-A NAC/CAD kinetochore complex controls chromosome congression and spindle bipolarity.', *The EMBO journal*. 26(24), pp. 5033–5047.

McEwen, B. F. *et al.* (1997) 'Kinetochore fiber maturation in PtK1 cells and its implications for the mechanisms of chromosome congression and anaphase onset.', *The Journal of cell biology*. 137(7), pp. 1567–1580.

McEwen, B. F. *et al.* (2001) 'CENP-E is essential for reliable bioriented spindle attachment, but chromosome alignment can be achieved via redundant mechanisms in mammalian cells.', *Molecular biology of the cell*. 12(9), pp. 2776–2789.

McIntosh, J. R., Hepler, P. K. and Van Wie, D. G. (1969) 'Model for Mitosis', *Nature*, 224, p. 659.

McLean, J. R. *et al.* (2011) ‘State of the APC/C: organization, function, and structure.’, *Critical reviews in biochemistry and molecular biology*. 46(2), pp. 118–136.

Meek, D. W. (2000) ‘The role of p53 in the response to mitotic spindle damage.’, *Pathologie-biologie*. 48(3), pp. 246–254.

Meiri, D. *et al.* (2012) ‘Mechanistic Insight into the Microtubule and Actin Cytoskeleton Coupling through Dynein-Dependent RhoGEF Inhibition’, *Molecular Cell*, 45(5), pp. 642–655.

Meling, G. I. *et al.* (1993) ‘The TP53 tumour suppressor gene in colorectal carcinomas. II. Relation to DNA ploidy pattern and clinicopathological variables.’, *British journal of cancer*. 67(1), pp. 93–98. Melkov, A. *et al.* (2015) ‘Dynamic microtubule organization and mitochondrial transport are regulated by distinct Kinesin-1 pathways’, *Biology Open*, pp. 1696–1706.

Mellone, B. G. (2009) ‘Structural and temporal regulation of centromeric chromatin.’, *Biochemistry and cell biology = Biochimie et biologie cellulaire*. 87(1), pp. 255–264.

Meraldi, P., Honda, R. and Nigg, E. A. (2002) ‘Aurora-A overexpression reveals tetraploidization as a major route to centrosome amplification in p53-/- cells.’, *The EMBO journal*. 21(4), pp. 483–492.

Meraldi, P., Draviam, V. M. and Sorger, P. K. (2004) ‘Timing and checkpoints in the regulation of mitotic progression.’, *Developmental cell*. 7(1), pp. 45–60.

Michel, L. S. *et al.* (2001) ‘MAD2 haplo-insufficiency causes premature anaphase and chromosome instability in mammalian cells.’, *Nature*. 409(6818), pp. 355–359.

Miki, H., Okada, Y. and Hirokawa, N. (2005) ‘Analysis of the kinesin superfamily: Insights into structure and function’, *Trends in Cell Biology*, pp. 467–476.

Milks, K. J., Moree, B. and Straight, A. F. (2009) ‘Dissection of CENP-C-directed centromere and kinetochore assembly.’, *Molecular biology of the cell*. 20(19), pp. 4246–4255.

Mills, J. C., Stone, N. L. and Pittman, R. N. (1999) ‘Extranuclear apoptosis. The role of the cytoplasm in the execution phase.’, *The Journal of cell biology*. 146(4), pp. 703–708.

Minestrini, G., Harley, A. S. and Glover, D. M. (2003) ‘Localization of Pavarotti-KLP in Living Drosophila Embryos Suggests Roles in Reorganizing the Cortical Cytoskeleton during the Mitotic Cycle’, *Molecular biology of the cell*, 14(October), pp. 4028–4038.

Mitchison, T. and Kirschner, M. (1984) ‘Dynamic instability of microtubule growth.’, *Nature*.312(5991), pp. 237–242.

Mitchison, T. *et al.* (1986) ‘Sites of microtubule assembly and disassembly in the mitotic spindle.’, *Cell*. 45(4), pp. 515–527.

Mitchison, T. J. (1993) ‘Localization of an exchangeable GTP binding site at the plus end of microtubules.’, *Science* 261(5124), pp. 1044–1047.

Mitelman F, Johansson B, M. F. (2013) *Database of Chromosome Aberrations and Gene Fusions in Cancer.*

Mohammed, H. *et al.* (2016) ‘Rapid immunoprecipitation mass spectrometry of endogenous proteins (RIME) for analysis of chromatin complexes.’, *Nature protocols*. 11(2), pp. 316–326.

Moree, B. *et al.* (2011) ‘CENP-C recruits M18BP1 to centromeres to promote CENP-A chromatin assembly.’, *The Journal of cell biology*. 194(6), pp. 855–871.

Morgan, D. O. (2007) *The cell cycle: principles of control*. London: New Science Press in association with Oxford University Press.

Morton, W. M., Ayscough, K. R. and McLaughlin, P. J. (2000) ‘Latrunculin alters the actin-monomer subunit interface to prevent polymerization.’, *Nature cell biology*, 2(6), pp. 376–378.

Moritz, M. *et al.* (1995) ‘Microtubule nucleation by gamma-tubulin-containing rings in the centrosome.’, *Nature*. 378(6557), pp. 638–640.

Moutinho-Pereira, S. *et al.* (2013) ‘Genes involved in centrosome-independent mitotic spindle assembly in Drosophila S2 cells.’, *Proceedings of the National Academy of Sciences of the United States of America*, 110(49), pp. 19808–13.

Mukherjee, K. *et al.* (2010) ‘Dopamine and cAMP regulated phosphoprotein MW 32 kDa is overexpressed in early stages of gastric tumorigenesis.’, *Surgery*. 148(2), pp. 354–363.

Muller, P. A. J., Vousden, K. H. and Norman, J. C. (2011) ‘p53 and its mutants in tumor cell migration and invasion.’, *The Journal of cell biology*. 192(2), pp. 209–218.

Murray, A. W., Solomon, M. J. and Kirschner, M. W. (1989) ‘The role of cyclin synthesis and degradation in the control of maturation promoting factor activity.’, *Nature*. 339(6222), pp. 280–286.

Murugaesu, N. *et al.* (2015) ‘Tracking the genomic evolution of esophageal adenocarcinoma through neoadjuvant chemotherapy.’, *Cancer discovery*. 5(8), pp. 821–831.

Musacchio, A. and Hardwick, K. G. (2002) ‘The spindle checkpoint: structural insights into dynamic signalling.’, *Nature reviews. Molecular cell biology*. 3(10), pp. 731–741.

Muzny DM, Bainbridge MN, Chang K, *et al.* (2012) Comprehensive molecular characterization of human colon and rectal cancer. *Nature*. 487(7407), pp. 330–337.

Nabha, S. M. *et al.* (2002) ‘Combretastatin-A4 prodrug induces mitotic catastrophe in chronic lymphocytic leukaemia cell line independent of caspase activation and poly(ADP-ribose) polymerase cleavage.’, *Clinical cancer research : an official journal of the American Association for Cancer Research*. 8(8), pp. 2735–2741.

Nachury, M. V *et al.* (2001) 'Importin beta is a mitotic target of the small GTPase Ran in spindle assembly.', *Cell*. 104(1), pp. 95–106.

Nekrasov, V. S. *et al.* (2003) 'Interactions between centromere complexes in Saccharomyces cerevisiae.', *Molecular biology of the cell*. 14(12), pp. 4931–4946.

Nguyen, H. G. *et al.* (2005) 'Mechanism of Aurora-B degradation and its dependency on intact KEN and A-boxes: identification of an aneuploidy-promoting property.', *Molecular and cellular biology*. 25(12), pp. 4977–4992.

Nicholson, J. M. *et al.* (2015) 'Chromosome mis-segregation and cytokinesis failure in trisomic human cells.', *eLife*. 4.

Nigg, E. A. (1991) 'The substrates of the cdc2 kinase.', *Seminars in cell biology*. 2(4), pp. 261–270.

Nigg, E. A. (1993) 'Cellular substrates of p34(cdc2) and its companion cyclin-dependent kinases.', *Trends in cell biology*. 3(9), pp. 296–301.

Nigg, E. A. (2002) 'Centrosome aberrations: cause or consequence of cancer progression?', *Nature reviews. Cancer*. 2(11), pp. 815–825.

Nik-Zainal, S. *et al.* (2012) 'Mutational processes molding the genomes of 21 breast cancers.', *Cell*. 149(5), pp. 979–993.

Nishihashi, A. *et al.* (2002) 'CENP-I is essential for centromere function in vertebrate cells.', *Developmental cell*. 2(4), pp. 463–476.

Nishino, T. *et al.* (2012) 'CENP-T-W-S-X forms a unique centromeric chromatin structure with a histone-like fold.', *Cell*. 148(3), pp. 487–501.

Nishino, T. *et al.* (2013) 'CENP-T provides a structural platform for outer kinetochore assembly.', *The EMBO journal*. 32(3), pp. 424–436.

Nones, K. *et al.* (2014) 'Genomic catastrophes frequently arise in esophageal adenocarcinoma and drive tumorigenesis.', *Nature communications*. 5, p. 5224.

Noton, E. and Diffley, J. F. (2000) 'CDK inactivation is the only essential function of the APC/C and the mitotic exit network proteins for origin resetting during mitosis.', *Molecular cell*. 5(1), pp. 85–95.

Obuse, C. *et al.* (2004) 'A conserved Mis12 centromere complex is linked to heterochromatic HP1 and outer kinetochore protein Zwint-1.', *Nature cell biology*. 6(11), pp. 1135–1141.

O'Connor, K. and Chen, M. (2013) 'Dynamic functions of RhoA in tumor cell migration and invasion.', *Small GTPases*, 4(3), pp. 141–147.

Ohba, T. *et al.* (1999) 'Self-organization of microtubule asters induced in Xenopus egg extracts by GTP-bound Ran.', *Science* 284(5418), pp. 1356–1358.

Ohashi, H. *et al.* (1994) 'A stable acentric marker chromosome: possible existence of an intercalary ancient centromere at distal 8p.', *American journal of human genetics*. 55(6), pp. 1202–1208.

Okada, M. *et al.* (2006) 'The CENP-H-I complex is required for the efficient incorporation of newly synthesized CENP-A into centromeres.', *Nature cell biology*. 8(5), pp. 446–457.

Ormsby, A. H. *et al.* (2000) 'The location and frequency of intestinal metaplasia at the esophagogastric junction in 223 consecutive autopsies: implications for patient treatment and preventive strategies in Barrett's esophagus.', *Modern pathology : an official journal of the United States and Canadian Academy of Pathology, Inc*. 13(6), pp. 614–620.

Orth, J. D. *et al.* (2008) 'Quantitative live imaging of cancer and normal cells treated with Kinesin-5 inhibitors indicates significant differences in phenotypic responses and cell fate.', *Molecular cancer therapeutics*. 7(11), pp. 3480–3489.

Ouderkirk, J. L. and Krendel, M. (2014) 'Non-muscle myosins in tumor progression, cancer cell invasion, and metastasis', *Cytoskeleton*, pp. 447–463.

Pagliuca, C. *et al.* (2009) 'Roles for the conserved spc105p/kre28p complex in kinetochore-microtubule binding and the spindle assembly checkpoint.', *PloS one*. 4(10), p. e7640.

Pagliuca, F. W., Collins, M. O. and Choudhary, J. S. (2011) 'Coordinating cell cycle progression via cyclin specificity.', *Cell cycle* pp. 4195–4196.

Palmer, D. K. *et al.* (1987) 'A 17-kD centromere protein (CENP-A) copurifies with nucleosome core particles and with histones.', *The Journal of cell biology*. 104(4), pp. 805–815.

Palmer, D. K. *et al.* (1991) 'Purification of the centromere-specific protein CENP-A and demonstration that it is a distinctive histone.', *Proceedings of the National Academy of Sciences of the United States of America*.

88(9), pp. 3734–3738.

Pereira, G. and Schiebel, E. (1997) 'Centrosome-microtubule nucleation.', *Journal of cell science*. 110 Pt 3, pp. 295–300.

Perera, D. *et al.* (2007) 'Bub1 maintains centromeric cohesion by activation of the spindle checkpoint.', *Developmental cell*. 13(4), pp. 566–579.

Perez de Castro, I., de Cárcer, G. and Malumbres, M. (2007) 'A census of mitotic cancer genes: new insights into tumor cell biology and cancer therapy.', *Carcinogenesis*. 28(5), pp. 899–912.

Perpelescu, M. and Fukagawa, T. (2011) 'The ABCs of CENPs.', *Chromosoma*. 120(5), pp. 425–446.

Peters, J. M. *et al.* (1996) 'Identification of BIME as a subunit of the anaphase-promoting complex.', *Science (New York, N.Y.)*. 274(5290), pp. 1199–1201.

Peters, J.-M., Tedeschi, A. and Schmitz, J. (2008) 'The cohesin complex and its roles in chromosome biology.', *Genes & development*. 22(22), pp. 3089–3114.

Petrovic, A. *et al.* (2010) 'The MIS12 complex is a protein interaction hub for outer kinetochore assembly.', *The Journal of cell biology*. 190(5), pp. 835–852.

Phoa, K. N. *et al.* (2014) 'Radiofrequency ablation vs endoscopic surveillance for patients with Barrett esophagus and low-grade dysplasia: a randomized clinical trial.', *JAMA*. 311(12), pp. 1209–1217.

Pines, J. (2011) 'Cubism and the cell cycle: the many faces of the APC/C.', *Nature reviews. Molecular cell biology*. pp. 427–438.

Pluta, A. F. *et al.* (1992) 'Identification of a subdomain of CENP-B that is necessary and sufficient for localization to the human centromere.', *The Journal of cell biology*. 116(5), pp. 1081–1093.

Posch, M., Khoudoli, G. A., Swift, S., King, E. M., Deluca, J. G., & Swedlow, J. R. (2010) 'Sds22 regulates aurora B activity and microtubule-kinetochore interactions at mitosis.', *The Journal of cell biology*, 191(1), pp. 61–74.

Prabhu, V. V *et al.* (2012) 'Therapeutic targeting of the p53 pathway in cancer stem cells.', *Expert opinion on therapeutic targets*. 16(12), pp. 1161–1174.

Przewloka, M. R. *et al.* (2007) 'Molecular analysis of core kinetochore composition and assembly in Drosophila melanogaster.', *PloS one*. 2(5), p. e478.

Przewloka, M. R. and Glover, D. M. (2009) 'The kinetochore and the centromere: a working long distance relationship.', *Annual review of genetics*. 43, pp. 439–465.

Przewloka, M. R. *et al.* (2011) 'CENP-C is a structural platform for kinetochore assembly.', *Current biology* 21(5), pp. 399–405.

Quintyne, N. J. *et al.* (2005) 'Spindle multipolarity is prevented by centrosomal clustering.', *Science (New York, N.Y.)*., 307(5706), pp. 127–129.

Raaijmakers, J. A. *et al.* (2009) 'RAMA1 is a novel kinetochore protein involved in kinetochore-microtubule attachment.', *Journal of cell science*. 122(Pt 14), pp. 2436–2445.

Rastogi, A. *et al.* (2008) 'Incidence of esophageal adenocarcinoma in patients with Barrett's esophagus and high-grade dysplasia: a meta-analysis.', *Gastrointestinal endoscopy*., 67(3), pp. 394–398.

Reber, S. and Hyman, A. A. (2015) 'Emergent Properties of the Metaphase Spindle.', *Cold Spring Harbor perspectives in biology*. 7(7), p. a015784.

Regnier, V. *et al.* (2005) 'CENP-A is required for accurate chromosome segregation and sustained kinetochore association of BubR1.', *Molecular and cellular biology*. 25(10), pp. 3967–3981.

Reid, B. J. *et al.* (1996) 'Barrett's esophagus: ordering the events that lead to cancer.', *European journal of cancer prevention : the official journal of the European Cancer Prevention Organisation (ECP)*5 Suppl 2, pp. 57–65.

Rieder, C. L. (1982) 'The formation, structure, and composition of the mammalian kinetochore and kinetochore fiber.', *International review of cytology*. 79, pp. 1–58.

Rieder, C. L. and Alexander, S. P. (1990) 'Kinetochores are transported poleward along a single astral microtubule during chromosome attachment to the spindle in newt lung cells.', *The Journal of cell biology*. 110(1), pp. 81–95.

Rieder, C. L. *et al.* (1994) 'Anaphase onset in vertebrate somatic cells is controlled by a checkpoint that monitors sister kinetochore attachment to the spindle.', *The Journal of cell biology*. 127(5), pp. 1301–1310.

Rieder, C. L. *et al.* (1995) 'The checkpoint delaying anaphase in response to chromosome monoorientation is mediated by an inhibitory signal produced by unattached kinetochores.', *The Journal of cell biology*. 130(4), pp. 941–948.

Rieder, C. L. and Salmon, E. D. (1998) 'The vertebrate cell kinetochore and its roles during mitosis.', *Trends in cell biology*. 8(8), pp. 310–318.

Ring, D., Hubble, R. and Kirschner, M. (1982) 'Mitosis in a cell with multiple centrioles.', *The Journal of cell biology*. 94(3), pp. 549–556.

Robles, A. I. and Harris, C. C. (2010) 'Clinical outcomes and correlates of TP53 mutations and cancer.', *Cold Spring Harbor perspectives in biology*. 2(3), p. a001016.

Ross-Innes, C. S. *et al.* (2015) 'Whole-genome sequencing provides new insights into the clonal architecture of Barrett's esophagus and esophageal adenocarcinoma.', *Nature genetics*, 47(9), pp. 1038–1046.

Rubenstein, P. A. and Wen, K. K. (2014) 'Insights into the effects of disease-causing mutations in human actins', *Cytoskeleton*, pp. 211–229.

Ruchaud, S., Carmena, M. and Earnshaw, W. C. (2007) 'Chromosomal passengers: conducting cell division.', *Nature reviews. Molecular cell biology*. 8(10), pp. 798–812.

Saitoh, H. *et al.* (1992) 'CENP-C, an autoantigen in scleroderma, is a component of the human inner kinetochore plate.', *Cell*. 70(1), pp. 115–125.

Sanchez, A. D., & Feldman, J. L. (2017). 'Microtubule-organizing centers: from the centrosome to non-centrosomal sites'. *Current opinion in cell biology*, *44*, 93–101.

Sansregret, L. and Swanton, C. (2017) 'The Role of Aneuploidy in Cancer Evolution.', *Cold Spring Harbor perspectives in medicine*. 7(1).

Sansregret, L. *et al.* (2017) 'APC/C Dysfunction Limits Excessive Cancer Chromosomal Instability.', *Cancer discovery*. 7(2), pp. 218–233.

Sapkota, H. *et al.* (2018) 'Multiple determinants and consequences of cohesion fatigue in mammalian cells.', *Molecular biology of the cell*.29(15), pp. 1811–1824.

Sarpal, R. *et al.* (2003) 'Drosophila KAP Interacts with the Kinesin II Motor Subunit KLP64D to Assemble Chordotonal Sensory Cilia, but Not Sperm Tails', *Current Biology*, 13(19), pp. 1687–1696.

Sato, N. *et al.* (2001) ‘Correlation between centrosome abnormalities and chromosomal instability in human pancreatic cancer cells’, *Cancer Genetics and Cytogenetics*. Elsevier, 126(1), pp. 13–19.

Saunders, W. S. *et al.* (2000) ‘Chromosomal instability and cytoskeletal defects in oral cancer cells’, *Proceedings of the National Academy of Sciences*, 97(1), pp. 303 LP – 308.

Scaërou, F. *et al.* (1999) ‘The rough deal protein is a new kinetochore component required for accurate chromosome segregation in Drosophila.’, *Journal of cell science*. 112 (Pt 21), pp. 3757–3768.

Scaërou, F. *et al.* (2001) ‘The ZW10 and Rough Deal checkpoint proteins function together in a large, evolutionarily conserved complex targeted to the kinetochore.’, *Journal of cell science*. 114(Pt 17), pp. 3103–3114.

Schaar, B. T. *et al.* (1997) ‘CENP-E function at kinetochores is essential for chromosome alignment.’, *The Journal of cell biology*. 139(6), pp. 1373–1382.

Schjolberg, A. R. *et al.* (2009) ‘Aneuploidy is associated with TP53 expression but not with BRCA1 or TERT expression in sporadic colorectal cancer.’, *Anticancer research*. , 29(11), pp. 4381–4387.

Schmidt, J. C. *et al.* (2012) ‘The kinetochore-bound Ska1 complex tracks depolymerizing microtubules and binds to curved protofilaments.’, *Developmental cell*. 23(5), pp. 968–980.

Scholey, J. M., Brust-Mascher, I. and Mogilner, A. (2003) ‘Cell division.’, *Nature*. 422(6933), pp. 746–752.

Schittenhelm, R. B., Chaleckis, R. and Lehner, C. F. (2009) ‘Intrakinetochore localization and essential functional domains of Drosophila Spc105.’, *The EMBO journal*. 28(16), pp. 2374–2386.

Schreiber, A. *et al.* (2011) ‘Structural basis for the subunit assembly of the anaphase-promoting complex.’, *Nature*.470(7333), pp. 227–232.

Schuh, M., Lehner, C. F. and Heidmann, S. (2007) ‘Incorporation of Drosophila CID/CENP-A and CENP-C into centromeres during early embryonic anaphase.’, *Current biology* 17(3), pp. 237–243.

Schwab, M., Lutum, A. S. and Seufert, W. (1997) ‘Yeast Hct1 is a regulator of Clb2 cyclin proteolysis.’, *Cell*. 90(4), pp. 683–693.

Screpanti, E. *et al.* (2011) ‘Direct binding of Cenp-C to the Mis12 complex joins the inner and outer kinetochore.’, *Current biology* 21(5), pp. 391–398.

Sepp, K. J. *et al.* (2008) ‘Identification of neural outgrowth genes using genome-wide RNAi’, *PLoS Genetics*, 4(7).

Shaheen, N. J. *et al.* (2009) ‘Radiofrequency ablation in Barrett’s esophagus with dysplasia.’, *The New England journal of medicine*. 360(22), pp. 2277–2288.

Shaheen, N. J. *et al.* (2016) ‘ACG Clinical Guideline: Diagnosis and Management of Barrett’s Esophagus.’, *The American journal of gastroenterology*. 111(1), pp. 30–50; quiz 51.

Shannon, K. B., Canman, J. C. and Salmon, E. D. (2002) ‘Mad2 and BubR1 function in a single checkpoint pathway that responds to a loss of tension.’, *Molecular biology of the cell*. 13(10), pp. 3706–3719.

Sharma, P. *et al.* (1997) ‘Dysplasia in short-segment Barrett’s esophagus: a prospective 3-year follow-up.’, *The American journal of gastroenterology*. 92(11), pp. 2012–2016.

Sharp, D. J. *et al.* (2000) ‘Functional coordination of three mitotic motors in Drosophila embryos.’, *Molecular biology of the cell*, 11(1), pp. 241–53.

Sharp-Baker, H. and Chen, R. H. (2001) ‘Spindle checkpoint protein Bub1 is required for kinetochore localization of Mad1, Mad2, Bub3, and CENP-E, independently of its kinase activity.’, *The Journal of cell biology*. 153(6), pp. 1239–1250. .

Shirayama, M. *et al.* (1999) ‘APC(Cdc20) promotes exit from mitosis by destroying the anaphase inhibitor Pds1 and cyclin Clb5.’, *Nature*. 402(6758), pp. 203–207.

Shrestha, R. L. and Draviam, V. M. (2013) ‘Lateral to end-on conversion of chromosome-microtubule attachment requires kinesins CENP-E and MCAK.’, *Current biology* 23(16), pp. 1514–1526.

Shrestha, R. L. *et al.* (2017) ‘Aurora-B kinase pathway controls the lateral to end-on conversion of kinetochore-microtubule attachments in human cells.’, *Nature communications*. 8(1), p. 150.

Silkworth, W. T. *et al.* (2009) ‘Multipolar spindle pole coalescence is a major source of kinetochore mis-attachment and chromosome mis-segregation in cancer cells.’, *PloS one*. 4(8), p. e6564.

Sironi, L. *et al.* (2002) ‘Crystal structure of the tetrameric Mad1-Mad2 core complex: implications of a “safety belt” binding mechanism for the spindle checkpoint.’, *The EMBO journal*. 21(10), pp. 2496–2506.

Sivakumar, S. *et al.* (2016) ‘The human SKA complex drives the metaphase-anaphase cell cycle transition by recruiting protein phosphatase 1 to kinetochores.’, *eLife*. 5.

Skibbens, R. V, Skeen, V. P. and Salmon, E. D. (1993) ‘Directional instability of kinetochore motility during chromosome congression and segregation in mitotic newt lung cells: a push-pull mechanism.’, *The Journal of cell biology*. 122(4), pp. 859–875.

Smith, D. A., Baker, B. S. and Gatti, M. (1985) ‘Mutations in genes encoding essential mitotic functions in Drosophila melanogaster.’, *Genetics*., 110(4), pp. 647–670.

Song, K. *et al.* (2002) ‘Mutational analysis of the central centromere targeting domain of human centromere protein C, (CENP-C).’, *Experimental cell research*. 275(1), pp. 81–91.

Song, H., Hollstein, M. and Xu, Y. (2007) ‘p53 gain-of-function cancer mutants induce genetic instability by inactivating ATM.’, *Nature cell biology*. 9(5), pp. 573–580.

Sotillo, R. *et al.* (2007) 'Mad2 overexpression promotes aneuploidy and tumorigenesis in mice.', *Cancer cell*. 11(1), pp. 9–23.

Soto, A. M. and Sonnenschein, C. (2004) 'The somatic mutation theory of cancer: growing problems with the paradigm?', *BioEssays : news and reviews in molecular, cellular and developmental biology*. 26(10), pp. 1097–1107

Spechler, S. J. (2013) 'Barrett esophagus and risk of esophageal cancer: a clinical review.', *JAMA* 310(6), pp. 627–636.

Spector I, Shochet NR, Kashman Y, G. A. *et al.* (1983) 'Latrunculins: novel marine toxins that disrupt microfilament organization in cultured cells', *Science* , 5932(February), pp. 493–495.

Stachler, M. D. *et al.* (2015) 'Paired exome analysis of Barrett's esophagus and adenocarcinoma.', *Nature genetics*. 47(9), pp. 1047–1055.

Starr, D. A. *et al.* (1997) 'Conservation of the centromere/kinetochore protein ZW10.', *The Journal of cell biology*. 138(6), pp. 1289–1301.

Starr, D. A. *et al.* (1998) 'ZW10 helps recruit dynactin and dynein to the kinetochore.', *The Journal of cell biology*. 142(3), pp. 763–774.

Stemmann, O. *et al.* (2001) 'Dual inhibition of sister chromatid separation at metaphase.', *Cell*. 107(6), pp. 715–726.

Stephens, P. J. *et al.* (2011) 'Massive genomic rearrangement acquired in a single catastrophic event during cancer development.', *Cell*. 144(1), pp. 27–40.

Stevens, D. *et al.* (2011) 'Uncoordinated loss of chromatid cohesion is a common outcome of extended metaphase arrest.', *PloS one*. 6(8), p. e22969.

Storchova, Z. and Kuffer, C. (2008) 'The consequences of tetraploidy and aneuploidy.', *Journal of cell science*. 121(Pt 23), pp. 3859–3866.

Storchova, Z. and Pellman, D. (2004) 'From polyploidy to aneuploidy, genome instability and cancer.', *Nature reviews. Molecular cell biology*. 5(1), pp. 45–54.

Stroud, M. J. *et al.* (2014) 'Linker of nucleoskeleton and cytoskeleton complex proteins in cardiac structure, function, and disease', *Circulation Research*, pp. 538–548.

Su, L. K. *et al.* (1995) 'APC binds to the novel protein EB1.', *Cancer research*. 55(14), pp. 2972–2977.

Su, K. C., Takaki, T. and Petronczki, M. (2011) 'Targeting of the RhoGEF Ect2 to the Equatorial Membrane Controls Cleavage Furrow Formation during Cytokinesis', *Developmental Cell*, 21(6), pp. 1104–1115.

Sudakin, V., Chan, G. K. and Yen, T. J. (2001) 'Checkpoint inhibition of the APC/C in HeLa cells is mediated by a complex of BUBR1, BUB3, CDC20, andMAD2.', *The Journal of cell biology*. 154(5), pp. 925–936.

Suijkerbuijk, S. J. E. *et al.* (2012) 'Integration of kinase and phosphatase activities by BUBR1 ensures formation of stable kinetochore-microtubule attachments.', *Developmental cell*. 23(4), pp. 745–755.

Sullivan, K. F. and Glass, C. A. (1991) ‘CENP-B is a highly conserved mammalian centromere protein with homology to the helix-loop-helix family of proteins.’, *Chromosoma*. 100(6), pp. 360–370.

Sullivan, K. F., Hechenberger, M. and Masri, K. (1994) ‘Human CENP-A contains a histone H3 related histone fold domain that is required for targeting to the centromere.’, *The Journal of cell biology*. 127(3), pp. 581–592.

Sumara, I. *et al.* (2007) ‘A Cul3-based E3 ligase removes Aurora B from mitotic chromosomes, regulating mitotic progression and completion of cytokinesis in human cells.’, *Developmental cell*. 12(6), pp. 887–900.

Suzuki, A. *et al.* (2011) ‘Spindle microtubules generate tension-dependent changes in the distribution of inner kinetochore proteins.’, *The Journal of cell biology*. 193(1), pp. 125–140.

Swanton, C. *et al.* (2009) ‘Chromosomal instability determines taxane response.’, *Proceedings of the National Academy of Sciences of the United States of America*. 106(21), pp. 8671–8676.

Tadeu, A. M. B. *et al.* (2008) ‘CENP-V is required for centromere organization, chromosome alignment and cytokinesis.’, *The EMBO journal*. 27(19), pp. 2510–2522.

Takeuchi, K. and Fukagawa, T. (2012) ‘Molecular architecture of vertebrate kinetochores.’, *Experimental cell research*. 318(12), pp. 1367–1374.

Talapatra, S. K. *et al.* (2013) ‘Mitotic kinesin Eg5 overcomes inhibition to the phase I/II clinical candidate SB743921 by an allosteric resistance mechanism.’, *Journal of medicinal chemistry*. 56(16), pp. 6317–6329.

Tanaka, T. U. *et al.* (2002) ‘Evidence that the Ipl1-Sli15 (Aurora kinase-INCENP) complex promotes chromosome bi-orientation by altering kinetochore-spindle pole connections.’, *Cell*. 108(3), pp. 317–329.

Tanaka, K. *et al.* (2009) ‘CENP-C functions as a scaffold for effectors with essential kinetochore functions in mitosis and meiosis.’, *Developmental cell*. 17(3), pp. 334–343.

Tang, Z. *et al.* (2001) ‘APC2 Cullin protein and APC11 RING protein comprise the minimal ubiquitin ligase module of the anaphase-promoting complex.’, *Molecular biology of the cell*. 12(12), pp. 3839–3851

Taylor, J. B. and Rubenstein, J. H. (2010) ‘Meta-analyses of the effect of symptoms of gastroesophageal reflux on the risk of Barrett’s esophagus.’, *The American journal of gastroenterology*. 105(8), pp. 1729, 1730–7; quiz 1738.

Thein, K. H. *et al.* (2007) ‘Astrin is required for the maintenance of sister chromatid cohesion and centrosome integrity.’, *The Journal of cell biology*. 178(3), pp. 345–354.

Theis, M. *et al.* (2009) ‘Comparative profiling identifies C13orf3 as a component of the Ska complex required for mammalian cell division.’, *The EMBO journal*. 28(10), pp. 1453–1465.

Thompson, S. L. and Compton, D. A. (2008) ‘Examining the link between chromosomal instability and aneuploidy in human cells.’, *The Journal of cell biology*. 180(4), pp. 665–672.

Thompson, S. L. and Compton, D. A. (2011) ‘Chromosomes and cancer cells.’, *Chromosome research : an international journal on the molecular, supramolecular and evolutionary aspects of chromosome biology*. 19(3), pp. 433–444.

Tipton, A. R. *et al.* (2011) ‘BUBR1 and closed MAD2 (C-MAD2) interact directly to assemble a functional mitotic checkpoint complex.’, *The Journal of biological chemistry*. 286(24), pp. 21173–21179.

Tomkiel, J. *et al.* (1994) ‘CENP-C is required for maintaining proper kinetochore size and for a timely transition to anaphase.’, *The Journal of cell biology*. 125(3), pp. 531–545.

Topham, C. H. and Taylor, S. S. (2013) ‘Mitosis and apoptosis: how is the balance set?’, *Current opinion in cell biology*. 25(6), pp. 780–785.

Vangamudi, B. *et al.* (2010) ‘t-DARPP regulates phosphatidylinositol-3-kinase-dependent cell growth in breast cancer.’, *Molecular cancer*. 9, p. 240.

van Zon, W. *et al.* (2010) ‘The APC/C recruits cyclin B1-Cdk1-Cks in prometaphase before D box recognition to control mitotic exit.’, *The Journal of cell biology*. 190(4), pp. 587–602.

Varetti, G., Pellman, D. and Gordon, D. J. (2014) ‘Aurea mediocritas: the importance of a balanced genome.’, *Cold Spring Harbor perspectives in biology*. 6(11), p. a015842.

Vigneron, S. *et al.* (2004) ‘Kinetochore localization of spindle checkpoint proteins: who controls whom?’, *Molecular biology of the cell*. 15(10), pp. 4584–4596.

Visintin, R., Prinz, S. and Amon, A. (1997) ‘CDC20 and CDH1: a family of substrate-specific activators of APC-dependent proteolysis.’, *Science* 278(5337), pp. 460–463.

Vogelstein, B. and Kinzler, K. W. (2004) ‘Cancer genes and the pathways they control.’, *Nature medicine*. 10(8), pp. 789–799.

Vorozhko, V. V *et al.* (2008) ‘Multiple mechanisms of chromosome movement in vertebrate cells mediated through the Ndc80 complex and dynein/dynactin.’, *Chromosoma*. 117(2), pp. 169–179.

Voullaire, L. E. *et al.* (1993) ‘A functional marker centromere with no detectable alpha-satellite, satellite III, or CENP-B protein: activation of a latent centromere?’, *American journal of human genetics*. 52(6), pp. 1153–1163.

Vousden, K. H. and Ryan, K. M. (2009) ‘p53 and metabolism.’, *Nature reviews. Cancer*. 9(10), pp. 691–700.

Wainman, A. *et al.* (2012) ‘The Drosophila RZZ complex - roles in membrane trafficking and cytokinesis.’, *Journal of cell science*.125(Pt 17), pp. 4014–4025.

Wang, M. S. J. *et al.* (2005) ‘Overexpression of DARPP-32 in colorectal adenocarcinoma.’, *International journal of clinical practice*. 59(1), pp. 58–61.

Wang, X. *et al.* (2006) ‘Overexpression of aurora kinase A in mouse mammary epithelium induces genetic instability preceding mammary tumor formation.’, *Oncogene*. 25(54), pp. 7148–7158.

Wang, F. *et al.* (2010) ‘Histone H3 Thr-3 phosphorylation by Haspin positions Aurora B at centromeres in mitosis.’, *Science (New York, N.Y.)*330(6001), pp. 231–235.

Wang, F. *et al.* (2011) ‘A positive feedback loop involving Haspin and Aurora B promotes CPC accumulation at centromeres in mitosis.’, *Current biology* 21(12), pp. 1061–1069.

Wang, K. K. *et al.* (2012) ‘Medical and endoscopic management of high-grade dysplasia in Barrett’s esophagus.’, *Diseases of the esophagus : official journal of the International Society for Diseases of the Esophagus*. 25(4), pp. 349–355.

Wasch, R. and Cross, F. R. (2002) ‘APC-dependent proteolysis of the mitotic cyclin Clb2 is essential for mitotic exit.’, *Nature*.418(6897), pp. 556–562.

Waters, J. C. *et al.* (1998) ‘Localization of Mad2 to kinetochores depends on microtubule attachment, not tension.’, *The Journal of cell biology*. 141(5), pp. 1181–1191.

Warth, A. *et al.* (2009) ‘Chromosomal instability is more frequent in metastasized than in non-metastasized pulmonary carcinoids but is not a reliable predictor of metastatic potential.’, *Experimental & molecular medicine*. 41(5), pp. 349–353.

Weaver, B. A. A. and Cleveland, D. W. (2006) ‘Does aneuploidy cause cancer?’, *Current opinion in cell biology*. 18(6), pp. 658–667.

Weaver, B. A. A. *et al.* (2007) ‘Aneuploidy acts both oncogenically and as a tumor suppressor.’, *Cancer cell*.11(1), pp. 25–36.

Weaver, J. M. J. *et al.* (2014) ‘Ordering of mutations in preinvasive disease stages of esophageal carcinogenesis.’, *Nature genetics*. 46(8), pp. 837–843.

Wei, R. R., Sorger, P. K. and Harrison, S. C. (2005) ‘Molecular organization of the Ndc80 complex, an essential kinetochore component.’, *Proceedings of the National Academy of Sciences of the United States of America*. 102(15), pp. 5363–5367.

Welburn, J. P. I. *et al.* (2009) ‘The human kinetochore Ska1 complex facilitates microtubule depolymerization-coupled motility.’, *Developmental cell*. 16(3), pp. 374–385.

Wells, W. A. (1996) ‘The spindle-assembly checkpoint: aiming for a perfect mitosis, every time.’, *Trends in cell biology*. 6(6), pp. 228–234.

Westhorpe, F. G. and Straight, A. F. (2014) ‘The centromere: epigenetic control of chromosome segregation during mitosis.’, *Cold Spring Harbor perspectives in biology*. 7(1), p. a015818.

Westhorpe, F. G., Fuller, C. J. and Straight, A. F. (2015) 'A cell-free CENP-A assembly system defines the chromatin requirements for centromere maintenance.', *The Journal of cell biology*. 209(6), pp. 789–801.

White, E. A. and Glotzer, M. (2012) 'Centralspindlin: At the heart of cytokinesis', *Cytoskeleton*, pp. 882–892.

Wiese, C. and Zheng, Y. (2000) 'A new function for the gamma-tubulin ring complex as a microtubule minus-end cap.', *Nature cell biology*.2(6), pp. 358–364.

Wigge, P. A. *et al.* (1998) 'Analysis of the Saccharomyces spindle pole by matrix-assisted laser desorption/ionization (MALDI) mass spectrometry.', *The Journal of cell biology*. 141(4), pp. 967–977.

Wigge, P. A. and Kilmartin, J. V (2001) 'The Ndc80p complex from Saccharomyces cerevisiae contains conserved centromere components and has a function in chromosome segregation.', *The Journal of cell biology*. 152(2), pp. 349–360. Williams, B. C. and Goldberg, M. L. (1994) 'Determinants of Drosophila zw10 protein localization and function.', *Journal of cell science*. (Pt 4), pp. 785–798.

Williams, B. C. *et al.* (2003) 'Zwilch, a new component of the ZW10/ROD complex required for kinetochore functions.', *Molecular biology of the cell*. 14(4), pp. 1379–1391.

Williams, B. *et al.* (2007) 'Mitch a rapidly evolving component of the Ndc80 kinetochore complex required for correct chromosome segregation in Drosophila.', *Journal of cell science*. 120(Pt 20), pp. 3522–3533.

Willis, A. *et al.* (2004) 'Mutant p53 exerts a dominant negative effect by preventing wild-type p53 from binding to the promoter of its target genes.', *Oncogene*. 23(13), pp. 2330–2338.

Wittmann, T., Hyman, A. and Desai, A. (2001) 'The spindle: a dynamic assembly of microtubules and motors.', *Nature cell biology*. 3(1), pp. E28-34.

Wood, K. W. *et al.* (1997) 'CENP-E is a plus end-directed kinetochore motor required for metaphase chromosome alignment.', *Cell*. 91(3), pp. 357–366.

Wojcik, E. *et al.* (2001) 'Kinetochore dynein: its dynamics and role in the transport of the Rough deal checkpoint protein.', *Nature cell biology*.3(11), pp. 1001–1007.

Wolthuis, R. *et al.* (2008) 'Cdc20 and Cks direct the spindle checkpoint-independent destruction of cyclin A.', *Molecular cell*. 30(3), pp. 290–302.

Wong, D. J. *et al.* (2001) 'p16(INK4a) lesions are common, early abnormalities that undergo clonal expansion in Barrett's metaplastic epithelium.', *Cancer research*. 61(22), pp. 8284–8289.

Wynne, D. J. and Funabiki, H. (2015) 'Kinetochore function is controlled by a phospho-dependent coexpansion of inner and outer components.', *The Journal of cell biology*. 210(6), pp. 899–916.

Wynne, D. J. and Funabiki, H. (2016) 'Heterogeneous architecture of vertebrate kinetochores revealed by three-dimensional superresolution fluorescence microscopy.', *Molecular biology of the cell*.27(22), pp. 3395–3404.

Yamagishi, Y. *et al.* (2010) 'Two histone marks establish the inner centromere and chromosome bi-orientation.', *Science* 330(6001), pp. 239–243.

Yamazaki, H. *et al.* (1995) 'KIF3A/B: A heterodimeric kinesin superfamily protein that works as a microtubule plus end-directed motor for membrane organelle transport', *Journal of Cell Biology*130(6), pp. 1387–1399.

Yamamoto, T. G. *et al.* (2008) 'SPDL-1 functions as a kinetochore receptor for MDF-1 in Caenorhabditis elegans.', *The Journal of cell biology*. 183(2), pp. 187–194.

Yanagida, M. (2014) 'The role of model organisms in the history of mitosis research.', *Cold Spring Harbor perspectives in biology*. 6(9),

Yang, C. H. *et al.* (1996) 'Identification of overlapping DNA-binding and centromere-targeting domains in the human kinetochore protein CENP-C.', *Molecular and cellular biology*. 16(7), pp. 3576–3586.

Yang, Z. *et al.* (2007) 'Kinetochore dynein is required for chromosome motion and congression independent of the spindle checkpoint.', *Current biology* 17(11), pp. 973–980.

Yao, X. *et al.* (2000) 'CENP-E forms a link between attachment of spindle microtubules to kinetochores and the mitotic checkpoint.', *Nature cell biology*. 2(8), pp. 484–491

Yu, H. *et al.* (1998) 'Identification of a cullin homology region in a subunit of the anaphase-promoting complex.', *Science* 279(5354), pp. 1219–1222.

Yu, Z. *et al.* (2015) 'Dynamic phosphorylation of CENP-A at Ser68 orchestrates its cell-cycle-dependent deposition at centromeres.', *Developmental cell*. 32(1), pp. 68–81

Yüce, Piekny, A. and Glotzer, M. (2005) 'An ECT2-centralspindlin complex regulates the localization and function of RhoA', *Journal of Cell Biology*, 170(4), pp. 571–582.

Yucel, J. K. *et al.* (2000) 'CENP-meta, an essential kinetochore kinesin required for the maintenance of metaphase chromosome alignment in Drosophila.', *The Journal of cell biology*. 150(1), pp. 1–11.

Yuen, K. W. Y., Montpetit, B. and Hieter, P. (2005) 'The kinetochore and cancer: what's the connection?', *Current opinion in cell biology*. 17(6), pp. 576–582.

Zachariae, W. *et al.* (1998) 'Control of cyclin ubiquitination by CDK-regulated binding of Hct1 to the anaphase promoting complex.', *Science* 282(5394), pp. 1721–1724.

Zack, T. I. *et al.* (2013) 'Pan-cancer patterns of somatic copy number alteration.', *Nature genetics*.45(10), pp. 1134–1140.

Zhai, Y., Kronebusch, P. J. and Borisy, G. G. (1995) 'Kinetochore microtubule dynamics and the metaphase-anaphase transition.', *The Journal of cell biology*. 131(3), pp. 721–734.

Zhang, J. and Xu, M. (2002) 'Apoptotic DNA fragmentation and tissue homeostasis.', *Trends in cell biology*. 12(2), pp. 84–89.

Zhang, G. *et al.* (2012) ‘The Ndc80 internal loop is required for recruitment of the Ska complex to establish end-on microtubule attachment to kinetochores.’, *Journal of cell science*. 125(Pt 13), pp. 3243–3253.

Zheng, Y. *et al.* (1995) ‘Nucleation of microtubule assembly by a gamma-tubulin-containing ring complex.’, *Nature*. 378(6557), pp. 578–583.

zur Hausen, H. (2006) ‘Streptococcus bovis: causal or incidental involvement in cancer of the colon?’, *International journal of cancer*. pp. xi–xii.